NUREG-????

Technical Basis for Revision of the Pressurized Thermal Shock (PTS) Screening Criteria in the PTS Rule (10CFR50.61)

This document satisfies RES OpPlan Milesone 1A1ABDD and NRR User Need NRR-2002-025 entitled *"Complete analyses and transmit draft technical basis for revision of PTS rule to NRR. Final document transmitted to NRR."*

Manuscript Completed: December 2002
Date Published: ???? 2003

Prepared by

Mark Kirk
Shah Malik
Tanny Santos
Terry Dickson
Claud Pugh
Richard Bass
Paul Williams
Roy Woods
Nathan Siu
Lance Kim
Alan Kolaczkowski
Donnie Whitehead
Dave Bessette
Bill Arcieri
Robert Beaton
Don Fletcher
Ali Mosleh
James Chang

DRAFT

Division of Engineering
Office of Nuclear Regulatory Research
U.S. Nuclear Regulatory Commission
Washington, DC 20555-0001

Executive Summary

Background

One potentially significant challenge to the structural integrity of the reactor pressure vessel (RPV) in a pressurized water reactor (PWR) is posed by a pressurized thermal shock (PTS) event wherein severe cooling of the core occurs together with, or followed by, pressurization. A number of abnormal events and postulated accidents can thermally shock the vessel (either with or without significant internal pressure); these include a break of the main steam line, a rupture of a steam generator tube, a loss of coolant accident (LOCA), and extended injection of high-pressure water to name just a few.

In the early 1980s the nuclear industry and the NRC staff performed a number of investigations aimed at assessing the risk of vessel failure posed by PTS, and on establishing the operational limits needed to ensure that the likelihood of RPV failures caused by PTS transients be kept to a low level. These efforts led to the publication by the staff of a document [SECY-82-465] that provided the technical basis for subsequent development of what has come to be known as the "PTS Rule" [10CFR50.61]. The document included a number of probabilistic calculations performed to assess the influence of both contributory and mitigating factors (e.g. plant design, operator actions, operator training, material toughness, flaw population, and so on) to the outcome (vessel failure or non-failure) of a PTS event. These calculations established a relationship between the probability of a through wall crack developing in the RPV and the index temperature, RT_{NDT}, of the RPV steel. This result, combined with the judgment that a mean yearly probability $5x10^{-6}$ of developing a through wall crack is acceptable [RG 1.154], led to the establishment of +270°F (for axial welds, plates, and forgings) and +300°F (for circumferential welds) as the "screening limits," or maximum values of RT_{NDT}, permitted at or before the end of license (EOL) [10CFR50.61]. 10CFR50.61 defines RT_{PTS} to be the value of RT_{NDT} projected to exist at EOL.

As PWRs approach the end of their original 40-year operating licenses, and licensees consider requesting a 20 year license renewal, compliance with the PTS Rule [10CFR50.61] can become a factor that limits the operational life of the plant. Addressing this issue on a plant-specific basis has consumed considerable resources within both the NRC and industry. Additionally, it is now widely recognized that state of knowledge and data limitations in the early 1980's necessitated a conservative treatment of several key parameters and models used in the probabilistic calculations that provide the technical basis [SECY-82-465] of the current PTS rule [10CFR50.61]. The most prominent of these conservatisms include the following:

- The highly simplified treatment of plant transients (very coarse grouping of many operational sequences (order of 10^5) into very few groups (≈10) necessitated by limitations in the computational resources needed to perform multiple thermal hydraulic calculations,
- The lack of any significant credit for operator action,
- Characterization of fracture toughness using RT_{NDT}, which has an intentional conservative bias [ASME NB2331],
- The use of a flaw distribution that placed *all* of the flaws on the interior surface of the RPV, and, in general,

contains larger flaws than those usually detected in service,

- The modeling approach that treated the RPV as if it were made entirely from the most brittle of its constituent materials (welds, plates, or forgings), and
- The modeling approach that assessed embrittlement using the peak fluence over the entire interior surface of the RPV.

The cost associated with demonstrating and checking compliance with the current PTS screening criteria, the conservatisms known to underlie the screening criteria, and the considerable technical advancements that have occurred in the 20 years since the technical basis for the PTS Rule was established all combined to motivate the NRC Office of Nuclear Regulatory Research to undertake a project aimed at developing the technical basis to support a fundamental revision of the PTS rule and the associated PTS screening criteria. Additionally, although the PTS rule has provided a sound regulatory basis for PTS in a generic sense, plant-specific experience with the associated regulatory guide (1.154) in evaluating the Yankee Rowe pressure vessel led the Commission to direct the staff to revise the regulatory guide to address several shortcomings.

In this report we summarize the technical results of our activities and use them to illustrate a potential revision to the PTS screening criteria.

Approach

The PTS Re-Evaluation Project was initiated in 1999. In this project probabilistic calculations were performed to establish the technical basis for a potential revision to the PTS rule within an integrated systems analysis framework [Woods 01]. Our approach considers all of the factors that influence the risk of vessel failure during a PTS event while accounting for uncertainties in these factors in a consistent manner across a breadth of technical disciplines. Two central features of this approach are a focus on the use of realistic input values and models (wherever possible), and an *explicit* treatment of uncertainties (using currently available uncertainty analysis tools and techniques). Thus, our current approach improves upon that employed in the development of SECY-82-465 wherein intentional and un-quantified conservatisms were included in the many aspects of the analysis, and where uncertainties were treated *implicitly* by incorporating them into the models.

The combination of the following three main models allows us to estimate the yearly frequency of through-wall cracking in a RPV:

1. PRA/HRA: An event-tree analysis is performed to define the sequences of events that are likely to produce a PTS challenge to RPV integrity and to estimate the frequency with which such events can be expected to occur.
2. Thermal Hydraulics: The sequence definitions from Step 1 are passed to a thermal-hydraulic (TH) model that estimates the temporal variation of temperature, pressure, and heat-transfer coefficient in the RPV downcomer characteristic of each of the sequence definitions.
3. Probabilistic Fracture Mechanics: A probabilistic fracture mechanics (PFM) model uses these pressure, temperature, and heat transfer coefficient histories along with other information concerning plant design and materials of construction to estimate the probability that a particular sequence of events will produce a crack all the way through the RPV wall were that sequence of events to actually occur.

The final step in the analysis involves a simple matrix multiplication of the probabilities of through-wall cracking (from Step 3) with the frequency at which a particular event sequence is expected to occur (as defined from Step 1). This multiplication establishes an estimate of the yearly frequency of through wall cracking that can be expected for a particular plant after a particular period of operation. Performance of such analyses for various operating lifetimes provides an estimate of how the yearly through

wall cracking frequency can be expected to vary over the lifetime of the plant.

Findings and Considerations for Rulemaking

Our calculations demonstrate that the risk of vessel failure resulting from PTS is very low, suggesting that operating plants are even safer than they were previously believed to be. Improvements across a wide spectrum of areas have contributed to a more realistic characterization of PTS risk. These improvements include the following:

- Our understanding of the operative failure mechanisms under PTS,
- The data available to characterize these failure mechanisms,
- The ability to perform scientific computations that consider the complex interactions that could give rise to PTS failure, and
- Our understating of the frequency with which the operational sequences that give rise to PTS events occur.

These improvements have led to approximately equivalent reductions (relative to the SECY-82-465 and IPTS studies of the 1980s) in the values that characterize the frequency with which PTS events occur and in the values that characterize the effect of these events on the RPV should they occur. Specifically, we estimate that even after 60 years of operation the risk of through wall cracking posed by PTS challenges is between $1x10^{-9}$ and $5x10^{-8}$ events per reactor operating year. If the embrittlement in these plants is artificially advanced to the 10CFR50.61 RT_{PTS} screening limit the estimated yearly TWCF at the mean and 95th percentile is $\approx 1x10^{-8}$. Thus, by any measure the risk of PTS failure is very low, falling considerably below the RG 1.154 risk limit of $5x10^{-6}$. Operationally, the events that dominate the through wall cracking frequency are all primary size failures, including both loss of coolant accidents (LOCAs) and stuck open safety relief valves. Secondary side events (e.g., main steam line break, stuck open atmospheric dump valves, etc.) do not contribute significantly to PTS risk because they do not as severely challenge the vessel as do primary side failures. From a materials viewpoint, the properties of the axial welds and plates exert dominant control over PTS risk, with the influence of circumferential welds providing a small, second order, contribution.
We believe that the significant differences between the values of through wall cracking frequency estimated in this project and the 10CFR50.61 PTS screening limits justify consideration of rulemaking.

While there are numerous factors that should be addressed in any change to 10CFR50.61, this research shows that a significant increase (80°F to 110°) in the PTS screening criteria can be justified. Such a change could be implemented without imposing on the licensees either new material testing requirements or new inspection programs. It should be noted that any change to 10CFR50.61 should be made simultaneously with changes to the embrittlement estimation procedures of Regulatory Guide 1.99 so that these two documents are consistent.

Contents

Page

Executive Summary ii
Contents 4
List of Tables **8**
List of Figures **10**
1 Background **1-14**
1.1 Description of Pressurized Thermal Shock 1-14
1.2 Past Investigations of PTS 1-14
1.3 Motivation for Re-Evaluating the Technical Basis of the PTS Rule 1-2
1.4 Operational Occurrence of PTS Events 1-3
1.5 The Current PTS Rule (10CFR50.61) 1-3
1.5.1 Index Temperature Characterization of Transition Fracture Toughness in Ferritic Steels 1-1
1.5.2 Irradiation Effects on Index Temperature 1-2
1.5.3 Provisions of the Current Rule 1-3
1.5.4 Evaluation of Operating Plants Relative to the Current PTS Screening Limits 1-3
1.6 PTS Rule Re-Evaluation Project 1-4
1.6.1 Guiding Principles 1-4
1.6.2 Approach 1-4
1.6.2.1 PTS-Induced RPV through Wall Cracking Frequency Estimates 1-5
1.6.2.2 Reactor Vessel Failure Frequency Acceptance Criterion 1-1
1.6.2.3 Screening Limit Development 1-1
1.6.3 Participating Organizations 1-1
1.7 Structure of this Report 1-2
2 Methodology Used to Establish Models and Address Uncertainty **3**
2.1 PRA 2-3
2.1.1 Step 1: Collect Information 2-1
2.1.1.1 General Information 2-1
2.1.1.1.1 LER Review 2-1
2.1.1.1.2 Initiator Frequency and Probability Data 2-1
2.1.1.2 Plant Specific Information 2-1
2.1.1.2.1 Previous PTS-PRA Analyses 2-1
2.1.1.2.2 Plant-Specific Information 2-2
2.1.2 Step 2: Identify the Scope and Features of the PRA Model 2-2
2.1.2.1 Types of sequences 2-1
2.1.2.2 Initiating Events 2-1
2.1.2.3 Functional/Equipment Considerations 2-1
2.1.2.4 Human Action Considerations 2-2
2.1.3 Step 3: Construct the PRA Models 2-2
2.1.3.1 PRA Modeling Differences Attributable to the Organization Constructing the Model 2-3
2.1.3.2 PRA Modeling Differences Attributable to the Order of Plant Analysis 2-3
2.1.4 Step 4: Quantify and Bin the PTS-PRA Modelled Sequences 2-2
2.1.5 Step 5: Revise PTS-PRA Models and Quantification 2-3
2.1.6 Step 6: Perform Uncertainty Analyses 2-4
2.1.6.1 Modeling of Representative Scenarios to Characterize Aleatory Uncertainty 2-4
2.1.6.2 Quantification of Scenario Frequencies to Characterize Epistemic Uncertainty 2-5

2.1.7 Step 7: Incorporation of Uncertainty and Finalization of Results 2-5
2.2 Thermal Hydraulics 2-7
2.2.1 Model Development 2-7
2.2.2 Model Initialization 2-8
2.2.3 Transient Event Simulations 2-9
2.2.3.1 Loss of Coolant Accidents 2-10
2.2.3.2 Reactor/Turbine Trips with Various Failures 2-10
2.2.3.3 Main Steam Line Break 2-11
2.2.3.4 Operator Actions 2-11
2.2.4 Containment Considerations 2-12
2.2.5 RELAP5 Numeric Issues 2-12
2.2.6 Uncertainty Analysis Results 2-13
2.2.6.1 Oconee NPP TH Uncertainty Analysis Results 2-13
2.2.6.2 Palisades NPP TH Uncertainty Analysis Results 2-14
2.2.6.3 Beaver Valley NPP TH Uncertainty Analysis Results 2-14
2.3 Probabilistic Fracture Mechanics 2-9
2.3.1 Toughness and Embrittlement Model 2-9
2.3.1.1 Use of Fracture Mechanics to Estimate the Response of the RPV to a Particular Thermal Hydraulic Challenge 2-9
2.3.1.2 Approach to Model Development and Uncertainty Characterization 2-2
2.3.1.3 Crack Initiation Model 2-2
2.3.1.4 Irradiation Model 2-4
2.3.1.5 Crack Arrest Model 2-5
2.3.1.6 Warm Pre-Stress Model 2-3
2.3.1.7 Complete Toughness and Embrittlement Model, and Major Differences from the Model Used to Support the Current PTS Screening Criteria 2-3
2.3.2 Flaw Distribution 2-4
2.3.2.1 Distribution of Buried Flaws in Welds 2-1
2.3.2.2 Distribution of Buried Flaws in Plates 2-3
2.3.2.3 Distribution of Surface Flaws in Welds and Plates 2-3
2.3.2.4 Summary 2-4
2.3.3 Fluence 2-5
2.3.4 FAVOR Implementation of the Complete PFM Model 2-6
3 Validation of Models 3-2
3.1 Thermal Hydraulics 3-2
3.1.1 Introduction 3-2
3.1.2 Separate Effects Tests 3-2
3.1.2.1 Marviken Test 3-2
3.1.2.2 MIT Pressurizer Test ST4 3-3
3.1.2.3 Upper Plenum Test Facility 3-4
3.1.2.4 Semi-scale Tests 3-4
3.1.3 Integral System Response 3-6
3.1.3.1 ROSA-IV Experiments 3-6
3.1.3.2 ROSA AP-600 Tests 3-9
3.1.3.3 APEX Tests 3-12
3.1.3.4 LOFT Test 3-13
3.1.3.5 MIST Test 3-15
3.1.4 Summary 3-20
3.2 Linear Elastic Fracture Mechanics 3-20
3.2.1 Introduction 3-20
3.2.2 Intermediate Test Vessel (ITV) Experiments 3-21

3.2.3 Thermal-Shock Experiments 3-2
3.2.4 Pressurized Thermal Shock Experiments 3-6
3.2.5 Conclusions based on Large-Scale Experiments 3-3
4 Plant Specific Estimates of Through Wall Cracking Frequency Caused by PTS 4-4
4.1 Introduction 4
4.2 Plant Specific Analysis Features and Inputs 4
4.2.1 Analysis Methodology 4
4.2.2 Input Information 2
4.2.2.1 PRA and Thermal Hydraulic 2
4.2.2.2 Probabilistic Fracture Mechanics 2
4.3 Results 8
4.3.1 Comparison of Through-Wall Cracking Frequencies for the Three Pilot Plants 8
4.3.1.1 Explanation of Skewness in the TWCF Distribution 10
4.3.1.2 Explanation of Large Spread in the TWCF Distribution 10
4.3.2 Dominant Contributors to Through-Wall Cracking Frequency 11
4.3.2.1 Dominant Transients 11
4.3.2.1.1 Secondary Side Breaks 4-13
4.3.2.1.2 Primary Side Breaks 4-2
4.3.2.1.2.1 Stuck Open Valves 4-2
4.3.2.1.2.2 LOCAs 4-4
4.3.2.2 Dominant Material Contributors 4-6
4.4 Applicability of these Results beyond the Three Study Plants 4-7
4.4.1 Consideration of External PTS Pre-Cursor Events 4-8
4.4.1.1 Approach 4-9
4.4.1.2 Preliminary Findings Based on the Reviews 4-9
4.4.1.3 Additional Analyses 4-10
4.4.1.3.1 Overview 4-10
4.4.1.3.2 An Example 4-10
4.4.1.4 Overall Findings 4-11
4.4.2 Generalization of These Results to All PWRs 4-11
4.4.2.1 Approach 4-1
4.4.2.1.1 Representative Plants for Comparison Study 4-1
4.4.2.1.2 Plant Features to be Compared 4-1
4.4.2.2 Results of Comparison Study 4-3
4.5 Summary of Findings 2
5 Risk-Informed Reactor Vessel Failure Frequency Acceptance Criterion 5
5.1 Introduction 5-5
5.2 Current Guidance on Risk-Informed Regulation 5-5
5.3 Containment Performance During PTS Accidents 5-2
5.3.1 Previous Research Results 5-3
5.3.2 Post-RPV Failure Scenarios Scoping Study 5-4
5.4 Acceptance Criteria Options 5-1
5.5 Conclusions 5-2
6 PTS Screening Limit 6-2
6.1 Introduction 6-2
6.2 Material Embrittlement Metrics 6-2
6.3 Possible Screening Limit 6-2
7 Findings and Considerations for Rulemaking 7-3
7.1 Findings 3
7.2 Considerations for Rulemaking 2
8 References 3

Appendix A – Toughness and Embrittlement Model.....9
Appendix B – Warm Pre-Stress Model 10
Appendix C – Transient List and Initiating Event Frequency Values 11
Appendix D – RELAP Results for all Three Plants 67
Appendix E – Uncertainty Analysis 68

List of Tables

Page

Table 1.1. Plants included in PTS re-evaluation study. 1-2
Table 1.2. Participating organizations. 1-2
Table 2.1. Comparison of PRA analyses used in this study with the PRA analyses that supported 10CFR50.61. 2-1
Table 2.2. General Classes of Human Failures Considered in the PTS Analyses. 3
Table 2.3. The nominal values of the key parameters and their variations with break size fixed. 2-2
Table 2.4. The sensitivity runs matrix of the Oconee-1 PTS study for primary side breach related scenarios. The values are the average downcomer temperature of the first 10,000 seconds in Kelvin. 2-3
Table 2.5. The TH uncertainty representative scenarios of the event category of 1.5" – 4" LOCA and their probabilities of the Oconee NPP. 2-3
Table 2.6. The TH uncertainty representative scenarios of the event category of 4" – 8" LOCA and their probabilities of the Oconee NPP. 2-3
Table 2.7. The TH uncertainty representative scenarios of the event category of greater than 8" LOCA and their probabilities of the Oconee NPP. 2-4
Table 2.8. The TH uncertainty representative scenarios of the event category of reactor trips during full power operation causing PZR SRV stuck open and remaining open and their probabilities of the Oconee NPP. 2-4
Table 2.9. The TH uncertainty representative scenarios of the event category of reactor trips during hot zero power operation causing PZR SRV stuck open and remaining open and their probabilities of the Oconee NPP. 2-4
Table 2.10. The TH uncertainty representative scenarios of the event category of reactor trips during full power operation causing PZR SRV stuck open and reseated later by itself and their probabilities of the Oconee NPP. 2-4
Table 2.11. The TH uncertainty representative scenarios of the event category of reactor trips during hot zero power operation causing PZR SRV stuck open and reseated later by itself and their probabilities of the Oconee NPP. 2-5
Table 2.12. The sensitivity runs matrix of the Palisade PTS study for primary side breach related scenarios. The values are the average downcomer temperature of the first 10,000 seconds in Kelvin. 2-5
Table 2.13. The TH uncertainty representative scenarios of the event category of 1.4" – 4" LOCA and their probabilities of the Palisade NPP. 2-5
Table 2.14. The TH uncertainty representative scenarios of the event category of 4" – 8" LOCA and their probabilities of the Palisade NPP. 2-6
Table 2.15. The TH uncertainty representative scenario of the event category greater than 8" LOCA of the Palisade NPP. 2-6
Table 2.16. The design and results of the sensitivity scenarios of the Beaver Valley NPP. The values inside parentheses are the average temperature of the first 10,000 seconds (unit in Kelvin). 2-6
Table 2.17. The TH uncertainty representative scenarios of the event category of 1.4" – 4" LOCA and their probabilities of the Beaver Valley NPP. 2-6

Table 2.18. The TH uncertainty representative scenarios of the event category of 4" – 8" LOCA and their probabilities of the Beaver Valley NPP. 2-7
Table 2.19. The TH uncertainty representative scenarios of the event category greater than 8" LOCA and their probabilities of the Beaver Valley NPP. 2-7
Table 2.20. The TH uncertainty representative scenarios of the event category of PZR valves stuck open without reseating and their probabilities of the Beaver Valley NPP....2-7
Table 2.21. The TH uncertainty representative scenarios of the event category of one PZR valve stuck open and reseated later by itself and their probabilities when reactor trips during full power operation of the Beaver Valley NPP. 2-7
Table 2.22. The TH uncertainty representative scenarios of the event category of one PZR valve stuck open and reseated later by itself and their probabilities when reactor trips during hot zero power operation of the Beaver Valley NPP. 2-8
Table 2.23. The TH uncertainty representative scenarios of the event category of two PZR valves stuck open and reseated later by itself and their probabilities when reactor trips during full power operation of the Beaver Valley NPP. 2-8
Table 2.24. The TH uncertainty representative scenarios of the event category of two PZR valves stuck open and reseated later by itself and their probabilities when reactor trips during hot zero power operation of the Beaver Valley NPP. 2-8
Table 2.25. Summary of sources of experimental data sources for the flaw distribution. 2-1
Table 3.1. Summary of Measured and Calculated Sequence of Events for ROSA-IV Test SB-CL-18. 3-7
Table 3.2. Summary of Measured and Calculated Sequence of Events for ROSA-IV Test SB-HL-06. 3-8
Table 3.3. Summary of Measured and Calculated Sequence of Events for ROSA-AP600 Test AP-CL-03....3-9
Table 3.4. Summary of Measured and Calculated Sequence of Events for ROSA-AP600 Test AP-CL-09....3-11
Table 3.5. Summary of Measured and Calculated Sequence of Events for APEX-CE-13 Test. 3-12
Table 3.6. Summary of Measured and Calculated Sequence of Events for LOFT L3-7 Test. 3-14
Table 3.7. Summary of Key Events for the MIST T360499 Feed and Bleed Test....3-16
Table 3.8. Summary of Key Events for the MIST 31099AA Test. 3-17
Table 3.9. Summary of Key Events for the MIST 4100B2 Test. 3-19
Table 3.10. ITV test sequence and test parameters. 3-22
Table 3.11. List of detailed reports on individual ITV experiments. 3-2
Table 3.12. Results from six ITV experiments using specimens without nozzles. 3-3
Table 3.13. Geometric Parameters of the PTSE-1 vessel. 3-8
Table 3.14. Conditions for PTSE-1A, -1B and -1C transients. 3-10
Table 4.1. Plant specific material values drawn from the RVID database [RVID]. 4
Table 4.2. Summary of vessel specific inputs for the flaw distribution. 5
Table 4.3. List of transients that dominate PTS risk. 11
Table 4.4. Results Summary for Small Pipe Break LOCA. 4-1
Table 4.5. Plant list for generalization study. 4-2
Table 5.1. Post-RPV Failure Technical Issues. 5-1
Table 5.2. Potentially Risk Significant Post-RPV Failure Accident Progression Scenarios. 5-1
Table 5.3. Key APET Scenarios. 5-1

List of Figures

Page

Figure 1.1. Relationship between through wall cracking frequency (vertical axis) and RT_{NDT} (horizontal axis) from SECY-82-465 used to establish the current 10CFR50.61 PTS screening criteria. 1-3
Figure 1.2. Figure 2.13 from SECY-82-465 depicting the final temperatures for 32 PTS precursor events experienced in commercial reactor service prior to 1982. Cooling rates associated with the most significant transients have been superimposed on this graph. 1-1
Figure 1.3. The empirical data used to establish the ASME K_{Ic} curve. 1-2
Figure 1.4. High-level illustration of the overall probabilistic model to estimate the yearly frequency of through wall cracking caused by PTS events.....1-5
Figure 1.5. Illustration of the relationship between RT_{PTS} at the end of a 40 year operating license and the 10CFR50.61 PTS screening limit for all of the 69 currently operating PWRs.....1-1
Figure 1.6. Schematic illustration of how a PTS screening criteria can be developed. 1-2
Figure 2.1. High-level illustration of the overall probabilistic model to estimate the yearly frequency of through wall cracking caused by PTS events.....2-3
Figure 2.2. Diagrammatic representation of PRA approach.....2-2
Figure 2.3. Functional Event Tree as the Basis for the PTS PRA Analyses. 2-2
Figure 2.4. Illustration of the interrelationships between PFM model and the TH and PRA models, and of the three principal sub-models that comprise the PFM model. 2-9
Figure 2.5. Illustration of a root cause diagram showing how uncertainties in input variables (E, F, G, and H) propagate through models (nodes), themselves potentially having uncertainty, to produce uncertainty in a resultant value (A).....2-3
Figure 2.6. Schematic illustrating the key components of the crack initiation model. 2-3
Figure 2.7. Illustration of the inconsistency with which RT_{NDT} positions a K_{Ic} curve relative to measured fracture toughness data.....2-5
Figure 2.8. Illustration of $DRT_{epistemic}$ cumulative distribution function. 2-5
Figure 2.9. K_{Ic} model constructed from K_{Ic} data for 18 heats of RPV plates, welds, and forgings. 2-5
Figure 2.10. Schematic illustrating the key component of the irradiation shift model. 2-5
Figure 2.11. Schematic illustrating the key component of the irradiation shift model. 2-2
Figure 2.12. Data for RPV and other steels showing how the temperature separation between the crack arrest and crack initiation transition curves (vertical axis) varies with the crack initiation transition temperature (horizontal axis). 2-2
Figure 2.13. K_{Ia} model recommended for use in the PTS re-evaluation effort. 2-3
Figure 2.14. Flow diagram illustrating the key features of the toughness and embrittlement model adopted in the PTS re-evaluation project. Input parameters are shown in red, and models discussed in Section 2.3.1 are indicated by equation number. Details of the model not discussed in Section 2.3.1 are detailed in Appendices C and D.....2-1
Figure 2.15. Densities of buried weld flaws (and uncertainties) for the Shoreham vessel that have been adopted to characterize the density of all buried weld flaws in the PTS re-evaluation project.....2-2
Figure 2.16. Flaw depth distribution for non-repair welds.....2-2
Figure 2.17. Flaw depth distribution for repair welds. 2-2
Figure 2.18. Flaw length distribution for non-repair welds.....2-2

Figure 2.19. Flaw length distribution for repair welds. 2-3
Figure 2.20. Flaw density and depth distribution for buried flaws in plates. 2-4
Figure 2.21. Density and depth distribution for surface breaking circumferential flaws in single layer stainless steel cladding. 2-4
Figure 2.22. Comparison of the new flaw distribution to the Marshall flaw distribution.....2-5
Figure 2.23. Azimuthal variation of fluence on the inner diameter of the Oconee 1 vessel at the axial location of the peak fluence. 2-6
Figure 2.24. Axial variation of fluence on the inner diameter of the Oconee 1 vessel at the azimuthal location of peak fluence. 2-6
Figure 2.25. FAVOR data streams flow through three modules: (1) FAVLoad, (2) FAVPFM, and (3) FAVPost. 2-6
Figure 2.26. Flow chart for improved PFM model implemented in FAVPFM showing the four primary nested loops – (1) *RPV Trial Loop*, (2) *Flaw Loop*, (3) *Transient Loop*, and (4) *Time Loop*. 2-1
Figure 3.1. Pressure in Top of Vessel - Marviken Test 24.....3-3
Figure 3.2. Mass Flow Rate at Nozzle Outlet - Marviken Test 24.....3-3
Figure 3.3. Comparison of Measured Pressure Rise - MIT Pressurizer Test ST4x.....3-3
Figure 3.4. Downcomer Pressure - UPTF Test 6 - Run 131.....3-4
Figure 3.5. Lower Plenum Liquid Level - UPTF Test 6 - Run 1. 3-4
Figure 3.6. Mass Flow Rate vs. Primary System Inventory - S-NC-2.....3-5
Figure 3.7. Cold Leg Mass Flow Area vs. SGU Tube Heat Transfer Area 3-6
Figure 3.8. Downcomer Fluid Temperature at Top of Core Elevation - ROSA-IV SB-CL-18.....3-7
Figure 3.9. Pressurizer Pressure Comparison - ROSA-IV SB-CL-18. 3-7
Figure 3.10. Break Flow - ROSA-IV SB-CL-18. 3-7
Figure 3.11. Downcomer Temperature at Top of Core Elevation - ROSA-IV SB-HL-06. 3-8
Figure 3.12. Pressurizer Pressure - ROSA-IV SB-HL-06. 3-8
Figure 3.13. Loop A Mass Flow Rate - ROSA-IV SB-HL-06x.....3-8
Figure 3.14. Downcomer Temperature At Top of Core Elevation (C Loop Side) - AP-CL-03. 3-10
Figure 3.15. Downcomer Temperature at Top of Core Elevation (P Loop Side) - AP-CL-03.....3-10
Figure 3.16. Pressurizer Pressure - AP-CL-03x. 3-10
Figure 3.17. Cold Leg Flow in the CMT Loop - AP-CL-03x. 3-11
Figure 3.18. Downcomer Temperature at Top of Core Elevation (C Loop Side) - AP-CL-09. 3-11
Figure 3.19. Downcomer Temperature at Top of Core Elevation (P Loop Side) – AP-CL-09x. 3-11
Figure 3.20. Pressurizer Pressure - AP-CL-09. 3-12
Figure 3.21. Downcomer Fluid Temperature - OSU-CE-13x 3-13
Figure 3.22. Pressurizer Pressure - APEX-CE-1x. 3-13
Figure 3.23. Downcomer Level - APEX-CE-13.....3-13
Figure 3.24. Upper Downcomer Temperature – LOFT Test L3-7x 3-14
Figure 3.25. Primary System Pressure - LOFT Test L3-7x.....3-14
Figure 3.26. Break Mass Flow Rate -LOFT Test L3-7.....3-15
Figure 3.27. HPI Volumetric Flow - LOFT Test L3-6. 3-15
Figure 3.28. Upper Downcomer Temperature - MIST Test 360499x. 3-16
Figure 3.29. Primary System Pressure - MIST Test 360499x. 3-16
Figure 3.30. PORV Mass Flow Rate - MIST Test 360499. 3-16
Figure 3.31. HPI Mass Flow Rate - MIST 360499. 3-16
Figure 3.32. Downcomer Liquid Level - MIST Test 36049.....3-17
Figure 3.33. Downcomer Temperature - MIST Test 3109AA x. 3-18
Figure 3.34. Primary System Pressure - MIST Test 3109AA. 3-18
Figure 3.35. Break Flow Rate - MIST Test 3109AA 3-18
Figure 3.36. HPI Flow Rate - MIST Test 3109AA x. 3-18
Figure 3.37. Mass Flow Rate in Cold Legs (B Loop) - MIST Test 3109AA 3-18

Figure 3.38. Upper Downcomer Temperature - MIST Test 4100B2x. 3-19
Figure 3.39. Reactor Coolant System Pressure - MIST Test 4100B2. 3-19
Figure 3.40. Upper Downcomer Temperature - MIST Test 4100B2.Break Flow - MIST Test 4100B2.. 3-20
Figure 3.41. HPI Flow Rate - MIST Test 4100B2. 3-20
Figure 3.42. Upper Downcomer Temperature - MIST Test 4100B2x.LPI Flow Rate - MIST Test 4100B2. 3-20
Figure 3.43. Core Flood Tank Flow Rate - MIST Test 4100B2. 3-20
Figure 3.44. Schematic of ITV-7 test vessel. Dimensions were the same for each ITV vessel while the specifics of the flaw region and test material varied from test to test. 3-22
Figure 3.45. ITV test temperatures superimposed on a Charpy curve illustrate relative condition of the twelve ITV experiments. Also fracture surface is characterized for each test. 3-2
Figure 3.46. ITV-2 vessel was tested under high pressure and at a temperature (32°F) that was low in the Charpy transition region; fracture was by fast cleavage propagation. 3-2
Figure 3.47. ITV-6 test vessel was tested under pressure and at a temperature (190°F) that was well above onset of Charpy upper shelf; fracture was by ductile shear. 3-2
Figure 3.48. ITV-1 vessel was tested under pressure and at a temperature (130°F) that was high in the Charpy transition region; fracture was mixed cleavage and ductile behavior. 3-2
Figure 3.49. Plot of P_f/P_d (fracture pressure to design pressure ratio) for eight ITV experiments. 3-3
Figure 3.50. Typical instantaneous temperature, stress, fluence, stress-intensity factor, and fracture-toughness distributions through wall of PWR vessel during LBLOCA. 3-3
Figure 3.51. Critical-crack-depth curves for PWR vessel during LBLOCA. 3-3
Figure 3.52. TSE test cylinder like those used in TSE-5, -5A, -6, and -7.....3-4
Figure 3.53. Schematic of ORNL's thermal shock test facility used for TSE-5, 5A, 6, and 7.....3-4
Figure 3.54. Cross section of TSE-5 test cylinder showing the three long crack jumps that occurred during the thermal shock. 3-5
Figure 3.55. Comparison of laboratory-specimen and TSE large-specimen K_{Ic} data. 3-6
Figure 3.56. Comparison of laboratory-specimen and TSE large-specimen K_{Ia} data 3-6
Figure 3.57. Geometry of PTSE-1 test vessel.....3-8
Figure 3.58. Test vessel being lowered into outer containment vessel at HSST PTS test facility.....3-8
Figure 3.59. Essential features of the simple WPS cycle: (a) loading transient; (b) coordination of transient crack driving force with fracture toughness to induce simple WPS conditions. ..3-8
Figure 3.60. Idealized crack driving force transient for PTSE-1. 3-9
Figure 3.61. Pressure transients for PTSE-1A, -1B, and -1C. 3-10
Figure 3.62. Results of OCA analyses of PTSE-1 transients based on measured temperature, pressure, flaw depth, and time of the crack jump. 3-10
Figure 3.63. Comparison of curves representing small-specimen K_{Ic} and K_{Ia} data with ASME Section XI curves and results of PTSE-1 experiment. 3-2
Figure 3.64. Result of FAVOR re-analyses of PTSE-1 experiment: (a) predictions based on small-specimen data; (b) interpretation based on measured temperature, pressure, flaw depth, and time of the crack jump.....3-2
Figure 3.65. Comparison of PTSE-1 arrest toughness results with those for wide plate and thermal shock experiments, as well as with ASME Section XI curve. 3-3
Figure 4.1. Rollout diagram of beltline materials and representative fluence maps for Oconee. 3
Figure 4.2. Rollout diagram of beltline materials and representative fluence maps for Beaver Valley. ..3
Figure 4.3. Rollout diagram of beltline materials and representative fluence maps for Palisades. 4
Figure 4.4. Comparison estimated yearly through-wall cracking frequencies for Oconee, Beaver Valley, and Palisades. Median and 5th percentile value of TWCF that are zero are not plotted.....9
Figure 4.5. Typical distribution of through-wall cracking frequency (as calculated for Beaver Valley at 32 and 200 EFPY). 10

Figure 4.6. Percent contribution of various classes of transients to the total through wall cracking frequency. 13
Figure 4.7. Comparison of the driving force to fracture produced by LOCAs and by main MSLBs in Beaver Valley. 4-3
Figure 4.8. Comparison percentage contribution of both LOCAs and stuck open SRVs to both crack initiation and to through wall cracking frequency in Oconee. 4-4
Figure 4.9. Comparison of the driving force to fracture produced by loss of coolant accidents (top) and by stuck open safety release valves in Oconee. 4-4
Figure 4.10. Variation in the conditional probability of crack initiation and of through wall cracking with LOCA break size (dashed lines connect to values of CPI and CPTWC = 0). 4-5
Figure 4.11. Effect of LOCA break diameter on the time at which through wall cracking occurs in for Oconee and Palisades. 4-5
Figure 4.12. Variation of system pressure with LOCA break size for Beaver Valley. 4-6
Figure 4.13. Variation of pressure, temperature, and K values with time for a 5.66-in. diameter LOCA break size in Beaver Valley. 4-6
Figure 4.14. Contribution of axially oriented cracks to the total through wall cracking frequency (TWCF). The remainder of the TWCF contribution is entirely attributable to circumferentially oriented flaws. 4-7
Figure 4.15. Contribution of the different major material regions to the total through wall cracking frequency (TWCF). 4-8
Figure 5.1. Post RPV failure accident progression tree. 5-2
Figure 6.1. Plant-specific TWCF results combined with the Reg. Guide 1.99 Revision 2 / 10CFR50.61 embrittlement metric RT_{PTS}. 6-2
Figure 6.2. Variation of the mean through wall cracking frequency with RT_{NDT}* (see Eq. 6-1) for the three plants analyzed in this study. 6-2
Figure 6.3. A comparison of the 10CFR50.61 embrittlement metric (RT_{PTS}) and the embrittlement metric suggested by this study (RT_{NDT}*) for the three plants analyzed in this study illustrating that RT_{NDT}* is about 90°F lower than RT_{PTS}. 6-2

1 Background

1.1 Description of Pressurized Thermal Shock

One potentially significant challenge to the structural integrity of the reactor pressure vessel (RPV) in a pressurized water reactor (PWR) is posed by a pressurized thermal shock (PTS) event wherein severe cooling of the core occurs together with, or followed by, pressurization. A number of abnormal events and postulated accidents have the potential to thermally shock the vessel (either with or without significant internal pressure); these include a break of the main steam line, a rupture of a steam generator tube, a loss of coolant accident (LOCA), or extended injection of high-pressure water to name just a few. During these events, the water level drops due to the contraction produced by overcooling. In events involving a primary system breach (e.g., a LOCA) additional water level drop occurs due to leakage from the primary system. Automatic systems and operators must provide make-up water in the primary system to prevent overheating of the fuel in the core. The make-up water is much colder than that held in the primary system.

The temperature differential between the nominally ambient temperature make-up water and the operating temperature of a pressurized water reactor ($\Delta T = 550°F - 60°F = 490°F$) produces significant thermal stresses in the thick section steel wall of the RPV. For aged RPVs these stresses could be high enough to initiate a running cleavage crack, a crack that could propagate all the way through the vessel wall.

In the early 1980s attention was focused on the possibility that PTS events could challenge the integrity of the RPV wall for two reasons: operational experience suggested that overcooling events, while not common, did in fact occur, and the results of in-reactor materials surveillance programs suggested that the steels used in RPV construction were prone to loss of toughness over time as the result of neutron irradiation embrittlement.

1.2 Past Investigations of PTS

In the early 1980s the nuclear industry and the NRC staff performed a number of investigations aimed at assessing the risk of vessel failure posed by PTS, and on establishing the operational limits needed to ensure that the likelihood of RPV failures caused by PTS transients be kept to an acceptable level. These efforts led to the publication by the staff of a document [SECY-82-465] that provided the technical basis for subsequent development of what has come to be known as the "PTS Rule" [10CFR50.61]. The SECY document included a number of probabilistic calculations performed to assess the influence of both contributory and mitigating factors (e.g. plant design, operator actions, operator training, material toughness, flaw population, and so on) to the outcome (vessel failure or non-failure) of a PTS event. These calculations established a relationship between the probability of a through wall crack developing in the RPV and the RT_{NDT}[†] index temperature of the RPV steel (see Figure 1.1). This result, combined with the judgment that a

[†] The RT_{NDT} index temperature was intended to correlate with the fracture toughness transition temperatre of the material. Fracture toughness, and how it is reduced by neutron irradiation embrittlement, are key parameters controlling the resistance of the RPV to any loading challenge. Moreover, the ability to monitor the change in transition temperature with irradiation as part of 10CFR50 Appendix H mandated survellience programs makes it a useful parameter against which to correlate plant risk. In Section 1.5 we describe the RT_{NDT} index temperature and its use in 10CFR50.61 in greater detail.

$5x10^{-6}$ yearly probability of developing a through wall crack is acceptable [RG 1.154], led to the establishment of +270°F (for axial welds, plates, and forgings) and +300°F (for circumferential welds) as the "screening limits," or maximum values of RT_{NDT}, permitted during the operating life of the plant [10CFR50.61]. As illustrated in Figure 1.1, the +270°F screening criterion for axial cracks (in axial welds, plates, and forgings) was obtained from the results of the probabilistic calculations by adding a 2s "margin" term of 60°F to the mean value of RT_{NDT} to account for uncertainty in this transition temperature value. The +300°F screening criterion for circumferential cracks (in circumferential welds) was determined by adding 30°F to the +270°F value. This adjustment was based on the judgment that embrittlement of the circumferential welds did not pose as great a threat to the structural integrity of the RPV owing to the less severe driving force applied to circumferential cracks by PTS loading.

In the mid-1980s, the NRC conducted a number of follow-on studies concerning the risk associated with PTS events [ORNL 85a, 85b, 86]. These studies featured plant-specific analyses of Robinson, Calvert Cliffs, and Oconee, and demonstrated plants embrittled to the +270°F screening limit value invariably had a yearly probability of developing a through wall crack below $5x10^{-6}$ events/reactor year. Thus, these plant specific analyses demonstrated the conservatism of the generic analyses reported in SECY-82-465 that served as the basis for the provisions of 10CFR50.61

1.3 Motivation for Re-Evaluating the Technical Basis of the PTS Rule

As PWRs approach the end of their original 40-year operating licenses, and licensees consider requesting a 20 year license extension, compliance with the PTS Rule [10CFR50.61] can become a factor that limits the operational life of the plant. Addressing this issue on a plant-specific basis has consumed considerable resources within both the regulatory and operational communities. Additionally, it is now widely recognized that state of knowledge and data limitations in the early 1980's necessitated a conservative treatment of several key parameters and models used in the probabilistic calculations that provide the technical basis [SECY-82-465] of the current PTS rule [10CFR50.61]. The most prominent of these conservatisms include the following:

- The highly simplified treatment of plant transients (very coarse grouping of many operational sequences (order of 10^5) into very few groups (≈10)) necessitated by limitations in the computational resources needed to perform multiple thermal hydraulic calculations,
- The lack of any significant credit for operator action,
- Characterization of fracture toughness using RT_{NDT}, which has an intentional conservative bias [ASME NB2331],
- The use of a flaw distribution that placed *all* of the flaws on the interior surface of the RPV, and, in general, contains larger flaws than those usually detected in service,
- The modeling approach that treated the RPV as if it were made entirely from the most brittle of its constituent materials (welds, plates, or forgings), and
- The modeling approach that assessed RPV embrittlement using the peak fluence over the entire interior surface of the RPV.

The cost associated with demonstrating and checking compliance with the current PTS screening criteria, the conservatisms known to underlie the screening criteria, and the considerable technical advancements that have occurred in the 20 years since the technical basis for the PTS Rule was established all combined to motivate the NRC Office of Nuclear Regulatory Research to undertake a project aimed at developing the technical basis to support a potential revision of the PTS rule and the associated PTS screening criteria. Additionally, although the PTS rule has

provided a sound regulatory basis for PTS in a generic sense, plant-specific experience with the associated regulatory guide (1.154) in evaluating the Yankee Rowe pressure vessel led the Commission to direct the staff to revise the regulatory guide to address several shortcomings. In this report we summarize the technical results of this project and use them as the basis for identifying potential changes to the PTS screening criteria.

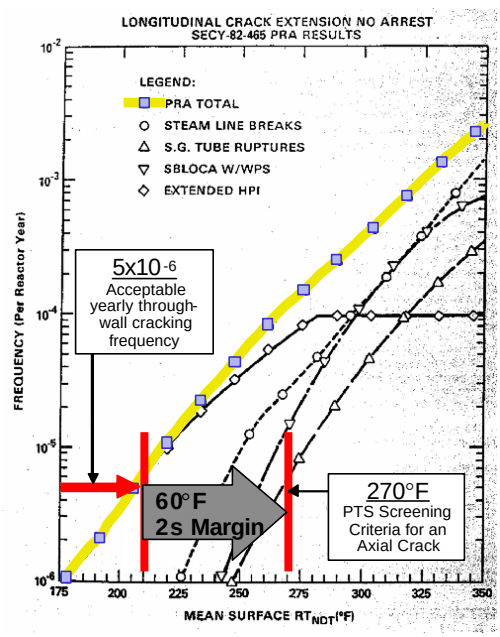

Figure 1.1. Relationship between through wall cracking frequency (vertical axis) and RT_{NDT} (horizontal axis) from SECY-82-465 used to establish the current 10CFR50.61 PTS screening criteria.

In this chapter we provide a context for the PTS problem by including a brief review of historically experienced overcooling events (Section 1.4). This is followed by a description of the current regulatory approach to ensuring RPV integrity when subjected to a PTS challenge (Section 1.5). We then discuss the PTS re-evaluation project (Section 1.6) focusing on a discussion of the guiding philosophy and a summary description of how the project was conducted. We conclude this chapter with a description of how the remainder of the report is structured (Section (1.7)).

1.4 Operational Occurrence of PTS Events

In the technical basis document written to support the current PTS rule [SECY-82-465] the staff summarized the operational events that had, to that date, presented PTS challenges to operating plants. These events are depicted in Figure 1.2, which illustrates the three key operational parameters influencing event severity: the final pressure of the RCS, the thermal gradients (*dT/dt*) caused by the event, and the existence (or not) of pressure. A more recent search of licensee event reports (LERs) submitted between 1980 and 2000 reveals the occurrence of 128 "potentially PTS significant" events. Approximately half of these LERs report the minimum temperature achieved by the RCS, and these data suggest that the most recent transients are nearly all benign, with all but one having minimum RCS temperatures above 500°F. Thus, while overcooling events have occurred, only rarely are they severe enough to pose any challenge to the structural integrity of the RPV

1.5 The Current PTS Rule (10CFR50.61)

As discussed in Section 1.2, 10CFR50.61 establishes "screening limits," or maximum values of RT_{NDT}, permitted during the operating life of the plant of +270°F (for axial welds, plates, and forgings) and +300°F (for circumferential welds). Here we discuss in greater detail the provisions of 10CFR50.61, including the following:

- Section ? : A discussion of why an index-temperature approach to the characterization of fracture toughness is adopted,
- Section 1.5.2: A description of how irradiation effects on the index temperature are characterized,
- Section 1.5.3: A discussion of the specific provisions of 10CFR50.61, and

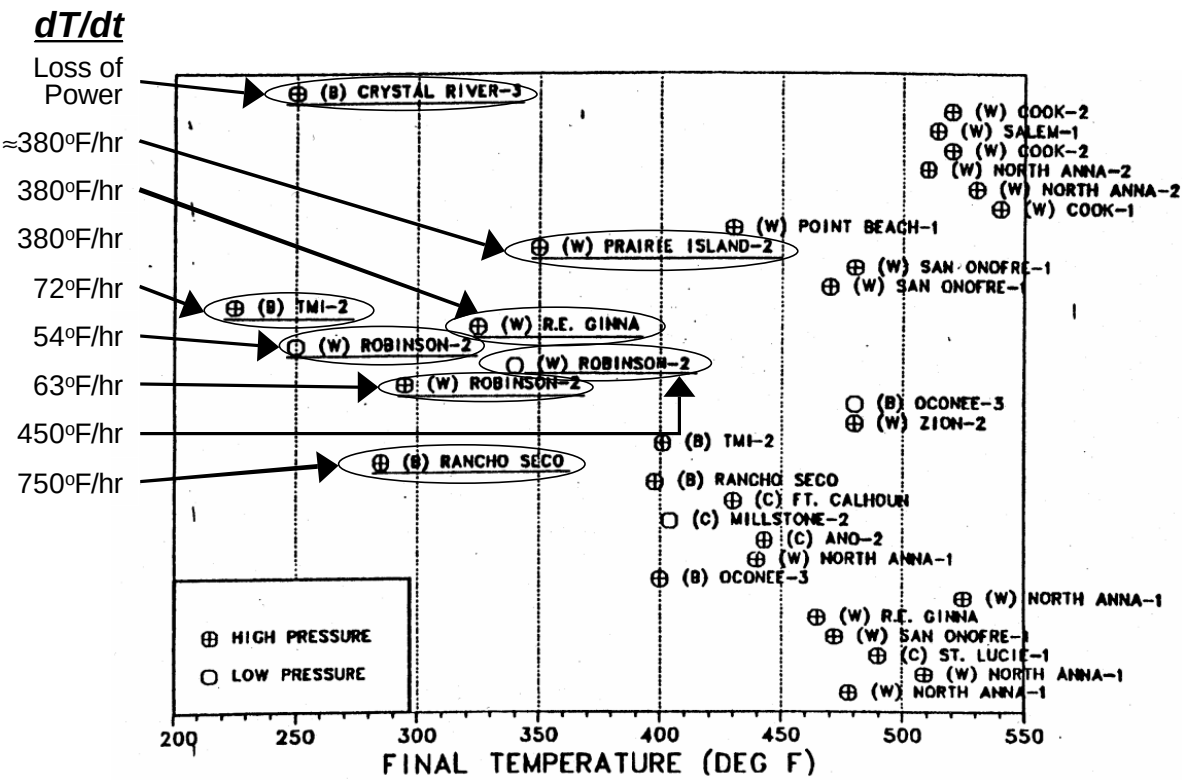

Figure 1.2. Figure 2.13 from SECY-82-465 depicting the final temperatures for 32 PTS precursor events experienced in commercial reactor service prior to 1982. Cooling rates associated with the most significant transients have been superimposed on this graph.

- Section 1.5.4: An evaluation of currently operating PWRs relative to the 10CFR50.61 PTS screening limits.

1.5.1 Index Temperature Characterization of Transition Fracture Toughness in Ferritic Steels

Both physical evidence as well as repeated and numerous experimental observations demonstrate that the temperature dependency of the cleavage initiation fracture toughness of ferritic steels (K_{Ic} or K_{Jc}) is invariant across a wide range of composition, heat treatment, material forming techniques (weld, plate, or forging), and irradiation conditions [Kirk 01a]. These factors all influence the position of the fracture toughness transition curve on the temperature axis, but not the variation of fracture toughness with temperature. This has led to widespread use of transition temperature approaches to characterize the cleavage fracture toughness of ferritic materials [WRC 175, Wallin 89]. These approaches employ empirical and/or physical evidence to establish the temperature dependency of fracture toughness that is common to all ferritic steels. Figure 1.3 shows the data used to establish the ASME K_{Ic} curve, one of the earliest transition temperature characterizations developed specifically using nuclear grade ferritic steels and weldments [WRC 175]. The formula for the curve in Figure 1.3 is as follows:

Eq. 1-1 $$K_{Ic} = 33.2 + 2.806 \cdot \exp[0.02 \cdot (T - RT_{NDT} + 100)]$$

where

RT_{NDT} is defined as per ASME NB-2331, i.e.
$$RT_{NDT} = MAX\{T_{NDT}, T_{35/50} - 60\},$$

T_{NDT} is the nil-ductility temperature determined by testing NDT specimens as per ASTM E208,

$T_{35,50}$ is the transition temperature at which Charpy-V notch (CVN) specimens tested as per ASTM E23 exhibit at least 35 mills lateral expansion and 50 ft-lbs absorbed energy.

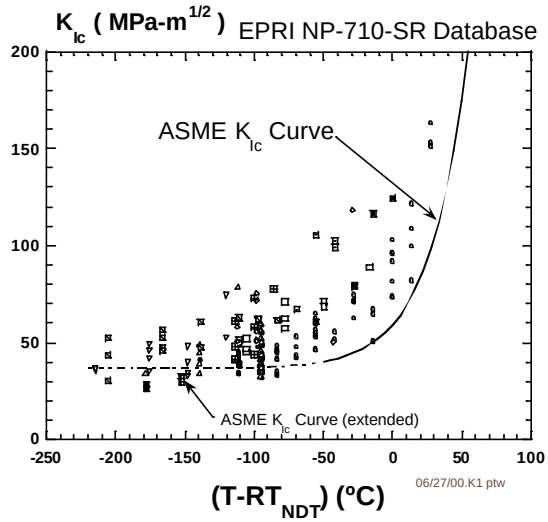

Figure 1.3. The empirical data used to establish the ASME K_{Ic} curve.

In Eq. 1-1 RT_{NDT} serves as an "index temperature," i.e., a single value that characterizes the combined effects of alloying heat treatment, irradiation, etc. on fracture toughness[‡]. Combining an index temperature with the (independently established) temperature dependency of fracture toughness (Eq. 1-1) defines the variation of toughness with temperature throughout the transition regime. The ease with which an index temperature can be experimentally established (relative to the much greater testing burden necessary to establish the complete toughness transition curve) makes transition temperature approaches attractive in applications where extensive material characterization is either economically infeasible or is, for practical reasons, impossible. The monitoring of neutron irradiation embrittlement falls into both categories due to both the expense associated with the testing of irradiated materials and due to the limited volumes of material that can be irradiated as part of a surveillance program.

1.5.2 Irradiation Effects on Index Temperature

As part of 10CFR50 Appendix H surveillance programs licensees attach surveillance capsules to the inner diameter of the RPV. These capsules, which contain Charpy V-notch (CVN) specimens [ASTM E23], are removed over the lifetime of the RPV [ASTM E185] and the CVN specimens are tested to establish the index temperature T_{30} (the temperature at which the energy consumed in fracturing the CVN specimen is 30 ft-lbs). The difference between T_{30} after some amount of irradiation and T_{30} before irradiation begins is called DT_{30}, a metric which has long been used to assess the degree of irradiation damage imparted to the steel (DT_{30} and the irradiation induced shift in the fracture toughness transition temperature are closely related, see Appendix A and [Kirk 01b]). These DT_{30} values from RPV surveillance programs provide the empirical basis to establish embrittlement trend curves that correlate the effect of irradiation exposure and chemical composition on DT_{30}. 10CFR50.61 adopts the following embrittlement trend curve [Randall 87]:

Eq. 1-2 $$\Delta T_{30} = (CF)\, f^{(0.28-0.1\log f)}$$

where

CF is a "chemistry factor" that characterizes the irradiation sensitivity of the steel. CF depends on copper content, nickel

‡ It should be noted that while RT_{NDT} is an index temperature that has customarily been used along with a fracture toughness transition curve (i.e., the ASME K_{Ic} curve), RT_{NDT} is ***not*** a *fracture toughness* index temperature. As specified by ASME NB-2331 (and as represented in Eq. 1-1) RT_{NDT} is defined based on non-fracture toughness tests that can, at best, be correlated with fracture toughness. In Section 2.3.1.3 we explore in greater detail the relationship between RT_{NDT} and fracture toughness, while Section 2.3.1.5 addresses RT_{NDT} and a transition curve for crack arrest toughness (K_{Ia}).

content, and product form. 10CFR50.61 includes tables of CF values.

f is the fast neutron fluence (E>1Mev) divided by 10^{19}.

1.5.3 Provisions of the Current Rule

10CFR50.61 uses the RT_{NDT} index temperature and the DT_{30} index temperature shift to estimate the effect of irradiation on RT_{NDT} using the following formula:

Eq. 1-3 $$RT_{NDT(f)} = RT_{NDT(u)} + \Re \cdot \Delta T_{30} + M$$

where

- $RT_{NDT(f)}$ is the estimated RT_{NDT} of the vessel material after irradiation to the fluence *f*. Toughness is determined from $RT_{NDT(f)}$ through its use as an index temperature for the ASME K_{Ic} and K_{IR} curves
- $RT_{NDT(u)}$ is the unirradiated RT_{NDT}. It can be determined based on either ASME NB-2331 or other, alternative, techniques can represent ***either*** of the following values:
- DT_{30} is defined by Eq. 1-2

Eq. 1-4 $$M = 2\sqrt{s_I^2 + s_\Delta^2}$$

where

- s_I is the standard deviation in the value of $RT_{NDT(u)}$
- s_D is the standard deviation in the value of DT_{30}

According to 10CFR50.61 the operator of a nuclear power plant is required to estimate the value of RT_{NDT} at EOL using Eq. 1-4 for all materials in the reactor vessel beltline region, These estimates are compared to the PTS screening limit specified by the rule of +300°F (for circumferential welds) or +270°F (for all other materials). If any of the beltline materials have a value of RT_{NDT} at EOL that is estimated to exceed the screening limit the licensee is required to either (a) implement flux reduction techniques to keep the value of RT_{NDT} at EOL below the screening limit, or (b) submit a safety analysis to the NRC demonstrating that the plant is safe to operate beyond the screening limit.

1.5.4 Evaluation of Operating Plants Relative to the Current PTS Screening Limits

In Figure 1.5 we compare RT_{NDT} values evaluated at the end of their originally licensed life (40 years) using Eq. 1-3 with the current 10CFR50.61 screening limits for all 69 currently operating PWRs. A number of points should be noted:

- No plants currently exceed the screening limit. However, since the operators of the Yankee Rowe nuclear power plant failed to persuade the staff to permit operation in excess of the screening limit using the probabilistic procedures outlined in Regulatory Guide 1.154, all plants that have predicted that they would exceed the screening limit before EOL have elected to remain in statutory compliance by either (a) implementing flux reduction, (b) pursuing new technological approaches coupled with exemption requests, or (c) a combination of the two approaches.
- Currently ten plants (Palisades, Beaver Valley 1, Fort Calhoun, Indian Point 3, TMI-1, Diablo Canyon 1, Point Beach 2, Salem 1, Watts Bar 1, and Calvert Cliffs 1) are projecting a RT_{NDT} at EOL ($\equiv RT_{PTS}$) within 20°F of the screening criteria.
- While the most embrittled region in one third of the operating PWRs is the circumferential weld, less than half of these plants (11 out of the 23) have their operation limited by the circumferential weld because of the higher PTS screening criteria (+300°F *vs*. the +270°F value used for axial welds, plates, and forgings) used currently to assess these plants.

1.6 PTS Rule Re-Evaluation Project

1.6.1 Guiding Principles

The PTS Re-Evaluation Project was initiated in 1999. In this project probabilistic calculations are performed to establish the technical basis for a revised PTS rule within an integrated systems analysis framework [Woods 01]. Our approach considers all of the factors that influence the likelihood of vessel failure during a PTS event while accounting for uncertainties in these factors in a consistent manner across a breadth of technical disciplines. Two central features of this approach are a focus on the use of realistic input values and models (wherever possible), and an *explicit* treatment of uncertainties (using currently available uncertainty analysis tools and techniques). Thus, our current approach improves upon that employed in the development of SECY-82-465 wherein intentional and un-quantified conservatisms were included in the many aspects of the analysis, and where uncertainties were treated *implicitly* by incorporating them into the models (see, for example, the discussion of RT_{NDT} later in Section 2.3.1).

Our probabilistic models distinguish between two types of uncertainties: aleatory and epistemic. Aleatory uncertainties arise due to the randomness inherent to a physical or human process, whereas epistemic uncertainties are caused by a limitation in our current state of knowledge (or understanding) of that process. A practical way to distinguish between aleatory and epistemic uncertainties is that epistemic uncertainties can, in principle, be reduced by an increased state of knowledge. Conversely, because aleatory uncertainties arise due to inherent randomness at a level below which a particular process is modeled, they are fundamentally irreducible. The distinction between aleatory and epistemic uncertainties is an important part of the PTS analysis because the mathematical procedures used to represent these different uncertainty types model them differently. For example, if the uncertainty in a variable is characterized as being epistemic, then, in a probabilistic simulation individual values of the variable are selected randomly from a distribution and propagated through the calculation. This procedure models the understanding that the "correct" value of the variable is knowable, at least in principal. Thus, for epistemic uncertainties individual simulation runs are deterministic while the totality of all simulation runs captures the uncertainty characteristic of the epistemic variable. Conversely, if the uncertainty in a variable is characterized as being aleatory then the entire distribution of the variable is carried through each simulation run. This procedure models the understanding that there is no single "correct" value of the variable.

In Chapter 2 we will discuss how we developed models and treated uncertainties in each of three major technical areas: event sequence analysis, thermal hydraulic (TH) analysis, and probabilistic fracture mechanics (PFM) analysis. Appendix E contains a detailed discussion of the principles behind our uncertainty analysis methodology.

1.6.2 Approach

Our approach involves the following three steps:

1. *PTS-Induced RPV Through Wall Cracking Frequency Estimates*: Estimate frequency of through wall cracking as due to a PTS event given the operating, design, and material conditions in a particular plant.
2. *Reactor Vessel Failure Definition and Frequency Acceptance Criterion*: Establish a value of reactor vessel failure frequency (RVFF) consistent with current guidance on risk-informed decision-making.
3. *Screening Limit Development*: Compare the results of the two preceding steps to determine if some simple, materials-based screening limit for PTS can be established. Conceptually, plants falling below the screening limit would be deemed adequately resistant to a PTS challenge and would not require further analysis. Conversely, more detailed, plant-specific, analysis would be needed to demonstrate

that plants beyond the screening limit can still be operated without posing an undue risk to public safety.

Chapters 4, 5, and 6 describe, respectively, our activities in these three areas. The general approach to each step is described in the following sub-sections.

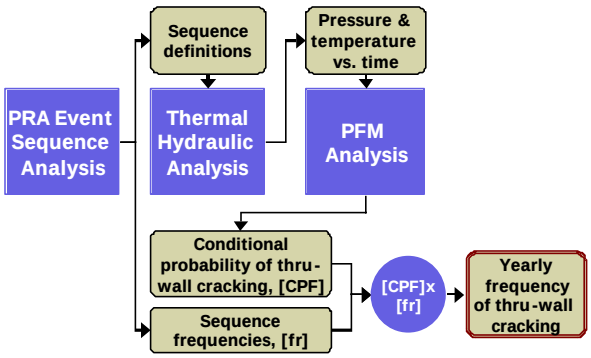

Figure 1.4. High-level illustration of the overall probabilistic model to estimate the yearly frequency of through wall cracking caused by PTS events.

1.6.2.1 PTS-Induced RPV through Wall Cracking Frequency Estimates

As illustrated in Figure 1.4 there are three main models (shown as blue boxes in the figure) that, together, allow us to estimate the yearly frequency of through-wall cracking in a RPV. First an event-tree analysis is performed to define the sequences of events that are likely to produce a PTS challenge to RPV integrity and to estimate the frequency with which such sequences can be expected to occur. The event sequence definitions are then passed to a thermal-hydraulic (TH) model that estimates the temporal variation of temperature, pressure, and heat-transfer coefficient in the RPV downcomer characteristic of each of the sequence definitions. These pressure, temperature, and heat transfer coefficient histories are passed to a probabilistic fracture mechanics (PFM) model. The PFM model uses the TH output along with other information concerning plant design and materials of construction to estimate the time variation of the driving force to fracture produced by a particular event sequence. The PFM model compares this estimate of fracture driving force to the fracture toughness, or fracture resistance, of the RPV steel. This comparison allows us to estimate the probability that a particular sequence of events will produce a crack all the way through the RPV wall were that sequence of events to actually occur. The final step in the analysis involves a simple matrix multiplication of the probability of through-wall cracking (from the PFM analysis) with the frequency at which a particular event sequence is expected to occur (as defined by the event-tree analysis). This multiplication establishes an estimate of the yearly frequency of through wall cracking that can be expected for a particular plant after a particular period of operation when subjected to a particular sequence of events. The yearly frequency of through wall cracking is then summed for all event sequences to estimate the total yearly frequency of through wall cracking for the vessel. Performance of such analyses for various operating lifetimes provides an estimate of how the yearly through wall cracking frequency can be expected to vary over the lifetime of the plant.

This step involves both development of the methodology to perform calculations for each of the models illustrated in Figure 1.4 as well as performance of these calculations for three operating PWRs. Chapters 2 and 3 describe, respectively, model development and validation, complete with a treatment of uncertainties following the framework described in [Woods 01] (see Section 1.6.1). Following model development we performed computations on three PWRs: Oconee 1, Beaver Valley 1, and Palisades. This group of plants was selected for the following reasons:

- The management and technical staff of these plants actively supported the NRC in this effort by providing access to plant personnel, plant simulators, records of construction, and other important information.

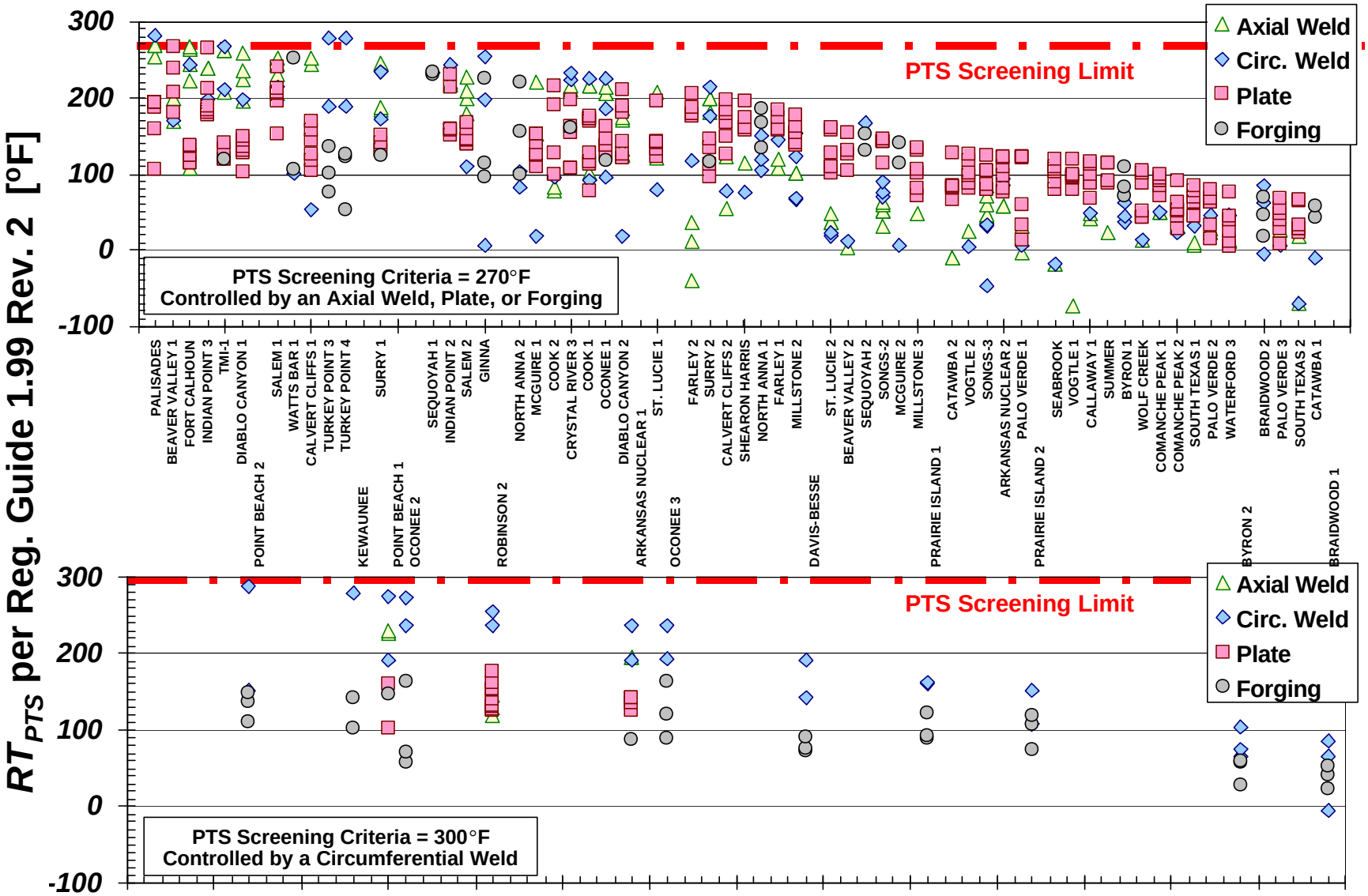

Figure 1.5. Illustration of the relationship between RT_{PTS} at the end of a 40 year operating license and the 10CFR50.61 PTS screening limit for all of the 69 currently operating PWRs.

- Oconee 1 was included in the IPTS studies [ORNL 86] that reinforced the conclusions and insights drawn from earlier analyses performed to support the development of 10CFR50.61. We judged it desirable to include these plants in our re-evaluation activities to provide a linkage to past efforts.
- Two of the plants (Palisades and Beaver Valley 1) are the closest of currently operating PWRs to the 10CFR50.61 screening limits (see Figure 1.5). Participation of these plants was deemed crucial since, based on our current state of knowledge, they are believed to be most "at risk."

Together the three plants sample of a wide range of design and construction methods. Additionally, the most embrittled constituents of the RPV in these three plants represent the key constituents of interest. Table 1.1 summarizes these plant characteristics.

1.6.2.2 Reactor Vessel Failure Frequency Acceptance Criterion

Since the issuance of SECY-82-465 and the publication of the original PTS Rule, the NRC has established a considerable amount of guidance on the use of risk metrics and risk information in regulation (e.g., the Safety Goal Policy Statement, the PRA Policy Statement, and RG 1.174). To ensure consistency of the PTS Re-Evaluation Project with this guidance, the staff identified and assessed options for a risk-informed criterion for the RVFF (currently specified in RG 1.154 in terms of TWCF).

As described in [SECY-02-0092], the options developed involved qualitative concerns (the definition of RPV failure) and quantitative concerns (a numerical criterion for the reactor vessel failure frequency). The options reflected uncertainties in the margin between PTS-induced RPV failure, core damage, and large early release. The options also incorporated input received from the Advisory Committee on Reactor Safeguards (ACRS) [NRC LTR 02a], regarding concerns with the potential for large-scale oxidation of reactor fuel in an air environment.

Our assessment of the options involved identification of technical issues unique to PTS accident scenario development, development of an accident progression event tree to structure consideration of the issues, performance of a scoping study of the issue of containment performance during PTS accidents, and review of the options in light of this information. The scoping study involved the collection and evaluation of available information, the performance of a few limited-scope thermal hydraulic and structural calculations, and a semi-quantitative analysis of the likelihood of various accident progression scenarios.

1.6.2.3 Screening Limit Development

As illustrated schematically in Figure 1.6, a screening limit for PTS can be established based on a simple comparison of estimates of the reactor vessel failure frequency (*RVFF*) as a function of an appropriate measure of RPV embrittlement with the reactor vessel failure frequency acceptance criterion (or *RVFF**, determined as described in Section 1.6.2.2). Beyond the work needed to establish both *the RVFF vs.* embrittlement curve and *RVFF** values, it is also necessary to establish a suitable vessel damage metric that, ideally, allows different conditions in different materials at different plants to be normalized. From a practical standpoint, "suitable" implies that the metric needs to be based only on information regarding plant operation and materials that is readily available. In Chapter 6 we identify a potentially useful metric that differs from the RT_{PTS} metric used in 10CFR50.61.

1.6.3 Participating Organizations

This project could not have succeeded were it not for the cooperation of a large number of individuals both inside and outside of the NRC. From its inception the commercial nuclear power industry, working under the auspices of EPRI, has been a key participant in this project.

Table 1.2 summarizes the key organizations, individuals, and their contributions to this project.

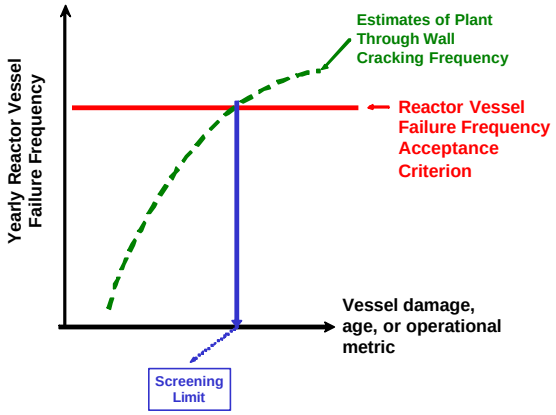

Figure 1.6. Schematic illustration of how a PTS screening criteria can be developed.

1.7 Structure of this Report

The remainder of the report is divided into six Chapters, as follows:

Chapter 2 details the models used and the treatment of uncertainty adopted in each of the three major technical areas: event sequence analysis, TH, and PFM.

Chapter 3 provides a discussion of how the models described in Chapter 2 were validated.

Chapter 4 summarizes the yearly frequency of through wall cracking estimated in our analysis of three operating PWRs. In this Chapter we discuss these results. Additionally, we discuss consideration given to events external to the plant controls that could initiate PTS events, and we describe how the results from three plant-specific analyses can be taken as representative of the entire population of operating PWRs for the purposes of establishing a screening PTS criteria.

Chapter 5 establishes a potential definition and numerical value for *RVFF**.

Chapter 6 discusses a potential PTS screening criterion.

Chapter 7 summarizes the major findings of this study.

Table 1.1. Plants included in PTS re-evaluation study.

Plant	Designed by	Constructed by	Materials	
			Most Limiting per 10CFR50.61	Most Embrittled
Oconee 1	Babcock & Wilcox		Axial Weld	Circumferential Weld
Beaver Valley 1	Westinghouse	Combustion Engineering	Plate	
Palisades	Combustion Engineering		Axial Weld	Circumferential Weld

Table 1.2. Participating organizations.

Sponsor / Organization		Individuals	Responsibilities
NRC	RES/DET/MEB	Mark Kirk, Shah Malik, Tanny Santos, Debbie Jackson	Project management, materials, fracture mechanics
	RES/DRAA/PRAB	Roy Woods, Nathan Siu, Lance Kim	PRA, human factors, event sequence analysis, risk goal
	RES/DSARE/SMSAB	Dave Bessette	Thermal hydraulics analysis
	Oak Ridge National Laboratory	Terry Dickson, Richard Bass, Paul Williams	PFM Code FAVOR
	Pacific Northwest National Laboratory	Fred Simonen, Steve Doctor, George Schuster	Flaw distribution
	Brookhaven National Laboratory	John Carew	Fluence
	Sandia National Laboratories	Donnie Whitehead, John Forester, Vincent Dandini	PRA, human factors, event sequence analysis, external events analysis, generalization task
	SAIC	Alan Kolaczkowski, Susan Cooper, Dana Kelly	PRA, human factors, event sequence analysis, external events analysis, generalization task
	University of Maryland	Mohammad Modarres, Ali Mosleh, Fei Li, James Chang	Uncertainty analysis of PFM and TH
	The Wreathwood Group	John Wreathall	Human factors
	Buttonwood Consulting	Dennis Bley	Human factors
	INEEL	William Galyean	PRA, event sequence analysis
	ISL	Bill Arcieri, Robert Beaton, Don Fletcher	Thermal hydraulic calculations using RELAP

Table 1.3 (cont.). Participating organizations.

Sponsor / Organization		Individuals	Responsibilities
EPRI	EPRI	Stan Rosinski	Program Management
	EPRI Materials Reliability Program (MRP) RPV Integrity Issue Task Group	Robert O. Hardies	ITG Chairman – Constellation Nuclear
	Westinghouse Electric Company	Ted Meyer, Bruce Bishop, Randy Lott, Steve Byrne, Robert Lutz, Barry Sloan, Eric Frantz	PRA, risk goal, PFM Code FAVOR, Fracture mechanics, materials, uncertainty analysis of PFM and TH
	Framatome ANP	Ken Yoon	Materials, fracture mechanics
	Sartrex Corporation	Ron Gamble	PRA, risk goal, PFM Code FAVOR
	Phoenix Engineering Associates	Marjorie Natishan	Uncertainty analysis of PFM, fracture mechanics
	ATI Consulting	William Server	Fracture mechanics, materials, PFM
	Constellation Nuclear – Calvert Cliffs	Robert O. Hardies	Plant-specific PTS
	First Energy – Beaver Valley	Dennis Weakland	Plant-specific PTS
	Duke Energy – Oconee	Jeff Gilreath	Plant-specific PTS
	Nuclear Management Company – Palisades	John Kneeland, Brian Brogan, Christer Dahlgren, Gary Pratt	Plant-specific PTS
	Applied Reliability Engineering	Dave Blanchard	Palisades PRA

2 Methodology Used to Establish Models and Address Uncertainty

As illustrated previously in Figure 1.4 (repeated here as Figure 2.2 for clarity), our estimate of the yearly frequency of through wall cracking in a PWR includes evaluation of three models, as follows:

1. PRA: The Probabilistic Risk Assessment model includes an event-tree analysis that defines both the sequences of events that are likely to produce a PTS challenge to RPV integrity and the frequency with which such sequences can be expected to occur.
2. TH: The Thermal Hydraulic model estimates the temporal variation of temperature, pressure, and heat-transfer coefficient in the down-comer characteristic for each of the sequences of plant events defiled by the PRA model.
3. PFM: The Probabilistic Fracture Mechanics model uses the thermal hydraulics output along with other information concerning plant design and materials of construction to estimate the probability that a particular sequence of events will produce a crack all the way through the reactor pressure vessel wall were that sequence of events to actually occur.

The final step in the analysis involves a simple matrix multiplication of the probability of through-wall cracking (from the PFM analysis) with the frequency at which a particular event sequence is expected to occur (as defined by the event-tree analysis). This multiplication establishes an estimate of the yearly frequency of through wall cracking that can be expected for a particular plant after a particular period of operation when subjected to a particular sequence of events. The yearly frequency of through wall cracking is then summed for all event sequences to estimate the total yearly frequency of through wall cracking for the vessel.

Each of the PRA, TH, and PFM models includes a myriad of sub models and parameters. In this Chapter we describe how we established these sub-models, how they connect to each other, and how the main PRA, TH, and PFM models connect to each other. Having defined the models and sub models we then describe how both parameter and model uncertainties were treated in a manner consistent with that described in Section 1.6.1. Sections 2.1, 2.2, and 2.3 describe, respectively, our approach to PRA, TH, and PFM model development and uncertainty treatment.

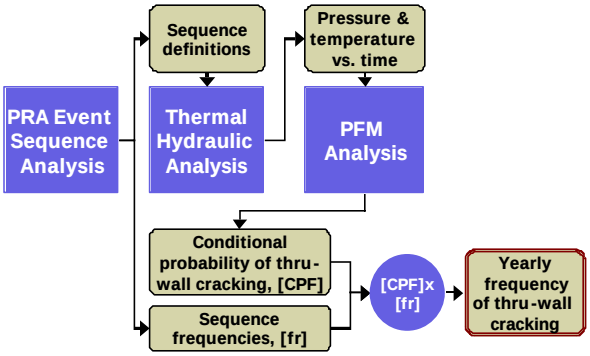

Figure 2.1. High-level illustration of the overall probabilistic model to estimate the yearly frequency of through wall cracking caused by PTS events.

2.1 PRA

Figure 2.2 depicts the steps followed both to define the sequences of events that may lead to PTS (for input to the TH model) and to define the frequencies with which these sequences are expected to occur (for combination with the PFM results to estimate the yearly frequency of through wall cracking). Although the approach is illustrated in a serial fashion, its

implementation involved multiple iterative passes through the various steps as the analyses evolved and the mathematical representation of each plant evolved. Also, each of the individual plant analyses included certain unique features; these are detailed later (in Section 4.1) when specific plant analyses are discussed. In the following Sections we describe the seven steps that together comprise the PRA analysis.

Step 1. (Section 2.1.1) Collect information
Step 2. (Section 2.1.2) Identify the scope and features of the PRA model
Step 3. (Section 2.1.3) Construct the PRA models
Step 4. (Section 2.1.4) Quantify and bin the PRA modeled sequences
Step 5. (Section 2.1.5) Revise PRA models and quantification
Step 6. (Section 2.1.6) Perform uncertainty analysis
Step 7. (Section 2.1.7) Incorporation of uncertainty and finalization of results

As discussed previously in Chapter 1, the reader should recognize that the PRA models described in this Section (2.1) consider *only* so-called PRA "internal event initiators" (e.g. LOCAs, loss of main feedwater, reactor trip, etc.) as possible PTS pre-cursors. This approach is consistent with that adopted when the PTS rule was first established. In principal, so-called PRA "external event initiators" (e.g., fires, floods, etc.) can also provide PTS pre-cursors. However, in the SECY-82-465 analysis the calculated yearly through wall cracking frequency caused by internal initiators alone was sufficiently large that any additional contribution resulting from external initiators was judged to be so small as to be justifiably ignored. However, early analyses in this effort revealed that the estimated frequencies of through wall cracking due to internal initiators were sufficiently low that the contribution of external initiators could no longer be summarily dismissed as "too small to count." For this reason we undertook a scooping study aimed at assessing the frequency and the consequences of external initiating events. The results of this external events study are detailed in Section 4.4.1; in this Section (2.1) we address only internal initiating events.

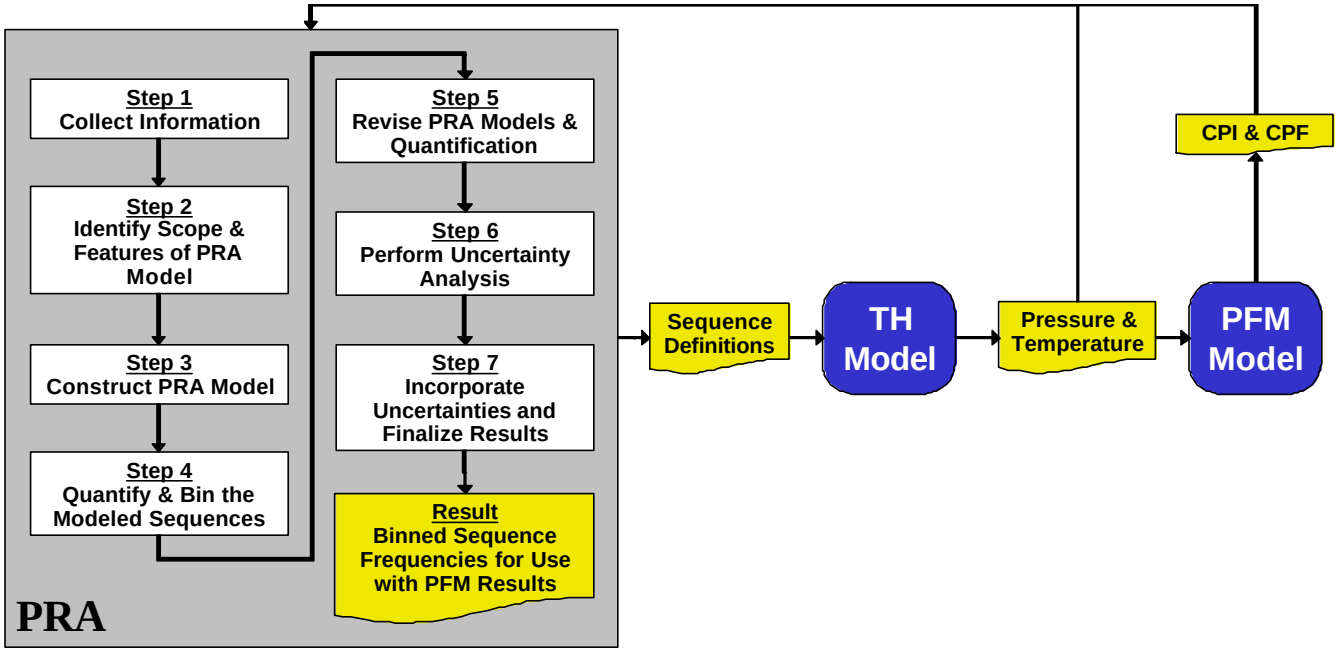

Figure 2.2. Diagrammatic representation of PRA approach.

2.1.1 Step 1: Collect Information

During the initial phase of the PTS project, significant resources were expended to collect information regarding PTS in general, and regarding each plant in particular. General information gathering activities included a review of the basis for the current PTS rule [10CFR50.61], and a licensee event report (LER) search for the years 1980 through 2000 to gain an understanding of the frequency and severity of real overcooling events [INEEL 00a]. Plant specific information sources included a review of the 1980s PRA analyses performed in support of the IPTS studies and the current PTS rule [ORNL 85a, 85b, 86], as well as plant-specific design and operational information. Familiarity with all of this information provided the bases upon which the PRA analysis of each plant was conducted.

2.1.1.1 General Information

2.1.1.1.1 LER Review

A total of 128 events of some significance were identified from the LER review, demonstrating that overcooling events, or at least their pre-cursors, do occur from time-to-time. These events are dominated by failure to properly control/throttle feed, a pre-cursor that leads to relatively minor over-cooling. Still, a few events have been associated with actual or potential loss of portions of secondary pressure control. Equipment failures in these events predominantly involve the main feedwater, feed-steam control, and main steam systems. These events demonstrate that both active and passive human actions play a role as many of the equipment failures were caused by improper maintenance or testing. Additionally, equipment in non-normal configurations can be an aggravating factor because contributing equipment faults have occurred that operators must identify and compensate for to prevent over-cooling.

2.1.1.1.2 Initiator Frequency and Probability Data

Initiator frequency and probability failure data are needed for initiating events, systems, and components as input to the PRA model. Since the goal of the PTS re-evaluation project is to provide a PTS risk perspective for the operating fleet of PWRs, it was judged appropriate to apply industry-wide data for initiator frequencies and equipment failure probabilities in our plant specific analyses. Hence, while the PRA model structure and its represented operational considerations were based on plant-specific information, initiator frequencies and equipment failure probability data were generally based on industry-wide experience. The generic data came from NUREG/CR-5750, which summarizes industry-wide experience for the years 1987 through 1995 [INEEL 00b]. This information was updated twice: first in an unpublished (at the time) addendum to NUREG/CR-5750 that extended the experience base through 1998, and later based on NRC staff input intended to account for time depended material aging mechanisms not included in the experiential data [NRC LTR 02b][§].

2.1.1.2 Plant Specific Information

2.1.1.2.1 Previous PTS-PRA Analyses

Review of the PRA analyses performed in support of the IPTS studies and the current PTS rule was another important input to our analyses. Of particular relevance were NUREG/CR-3770 [ORNL 86] and WCAP-15156 [Westinghouse 99] (a more recent 1999 study) since these are past analyses of two of the plants covered in this

---

[§] As will be detailed in Chapter 4, generic initiator frequency information (as described in Section 2.1.1.1.2) was used for Oconee 1 and Beaver Valley, whereas the plant-specific PRA conducted by Consumers' Energy personnel (for Palisades) ostensibly incorporated plant-specific initiator frequency information. However, the numerical differences between these generic and plant-specific initiator frequencies were, in practice, insignificant.

work, Oconee and Beaver Valley respectively. Information in NUREG/CR-4183 [ORNL 85b] concerning H.B. Robinson and NUREG/CR-4022 [ORNL 85a] concerning Calvert Cliffs plant was also considered. Review of these past analyses and the conduct of our current analyses ensured that at least one type of plant from each domestic PWR nuclear steam supply system vendors (Babcock and Wilcox, Westinghouse, and Combustion Engineering) was considered.

2.1.1.2.2 Plant-Specific Information

At the outset of each plant-specific analysis, a letter was sent to the licensee requesting information pertaining to plant design, procedures, training, and other aspects of plant operation relevant to building a PRA model. Information provided in response to these letters was supplemented by information gained during plant visits and by ongoing interactions (verbal, written, and e-mail exchanges) with each licensee as the analyses evolved. In total, plant specific information derived from the following sources:

- Summaries of any recent past actual overcooling events
- Current PRA models and associated documentation
- FSAR sections
- P&IDs / electrical drawings
- Emergency and Abnormal Operating Procedures
- Miscellaneous system design basis information and related material
- PTS-relevant training material
- Operational aspects associated with hot shutdown conditions
- Observed multiple simulator exercises at each plant involving overcooling events that were set-up and run based on a collaborative effort between each licensee and the NRC Contractor PRA analysts
- Periodic interactions with each licensee regarding modeling details as our analysis evolved
- Feedback from each licensee as our analysis evolved.

2.1.2 Step 2: Identify the Scope and Features of the PRA Model

The format, structure, and details considered by our current analyses draw considerably from the earlier PRA analyses of PTS. Besides recognition of the results and the reasons for the results from these past analyses, limitations and conservatism associated with the past studies were identified and, to the greatest extent possible, alleviated. Other improvements were adopted with the intent of increasing both the accuracy and comprehensiveness of the PRA representation of the plants. Table 2.1 summarizes the differences between our current PRA and that used to support the current PTS rule; these falling into the following three major categories:

1. Greater refinement / detail in the current PRA
2. More realistic treatment of operator actions in the current PRA
3. Use of the latest available data on initiating event frequencies and equipment failure probabilities (see also Section 2.1.1.1.2)

As noted in the table, since these improvements were made with the intent of increasing both the accuracy and comprehensiveness of the PRA representation of the plants, they neither systematically increase nor reduce the estimated risk for PTS.

In addition to identifying the areas for improvement of our PRA models that we noted in Table 2.1, our review of past PRA analysis of PTS provided information in four other areas:

1. It helped us to identify the types of sequences that need to be included in the PRA
2. It helped us to identify what types of initiating events should be included
3. It helped us to identify what functions and equipment status needed to be included, and
4. It helped us to identify what human actions needed to be considered.

Table 2.1. Comparison of PRA analyses used in this study with the PRA analyses that supported 10CFR50.61.

Difference Between Current PRA Analyses and the PRA Analyses that Supported 10CFR50.61			Effect on Calculated Risk	Comments
1	Refinement of / Detail Considered by the Analysis	Slight expansion of the types of sequences and initiators considered	Increase	
2		Slightly expanded consideration of support systems both as initiators and as dependencies affecting equipment response	Increase	
3		Less gross binning of TH sequences because there are more "case" sequences into which to bin individual TH runs	Reduce	Current work features 50-100 cases per plant whereas previous studies only consider about a dozen cases (e.g., small steamline breaks and the opening of 1-2 secondary valves were previously binned with a large guillotine steamline break, thereby treated the cooling effects of the smaller scenarios much too conservatively).
4		External initiating events considered as potential PTS pre-cursors	Increase	See Section 4.4.1
5	Treatment of Operator Actions	Credit for operator actions is based on detailed consideration of numerous contextual factors associated with the modeled sequences, on multiple simulator observations at each plant, on the latest procedures and relevant training, and on numerous discussions with operating and training staffs. Detrimental acts of commission are also considered based on these same inputs, including procedural steps that call for operator actions that can exacerbate overcooling in certain situations.	Both Increase and Reduce	
6		A greater number of discrete operator action times are considered.	Reduce	Previous studies considered success or failure of operator action generally at 1 time after the start of the event. Currently we consider up to 3 discrete times for operator action.
7	Use of New Data	Includes the latest industry-wide (and some plant-specific) data for initiating event frequencies, equipment failure probabilities, and common cause considerations.	Reduce	Largest factor is the significant drop in the initiator frequencies as a result of the decrease in scram rates resulting from institutional programs executed in the ‘80s and ‘90s.

The following four sub-sections describe the general features of our PRA models in each area. These features of our PRA models were established by a team approach involving analysts skilled in both system/sequence considerations and HRA considerations. Thus, our process for building the PRA models involved integrated consideration of both system/sequence and human reliability factors.

2.1.2.1 Types of sequences

The following list details the types of sequences that are included in our PRA models:

- Overcooling scenarios
  - At full/nominal power operation
  - At hot shutdown conditions
- Loss of reactor coolant system (RCS) pressure scenarios,
- Virtually sustained RCS pressure scenarios,
- Late re-pressurization scenarios,
- Scenarios that provide immediate overcooling as well as those that begin as loss of cooling scenarios (i.e., under-cooling) and subsequently become overcooling scenarios.

Two types of scenarios commonly modeled in PRAs are not included in our PTS models: anticipated transients without scram (ATWS) scenarios, and interfacing system LOCA scenarios. These scenarios were not included for two reasons. First, such events generally begin with severe under-cooling. Numerous subsequent failures of other systems (in combination) are needed to produce overcooling, making this outcome extremely unlikely. Second, the initiating event frequencies for typical ATWS and sizeable (not just small leaks) interfacing system LOCAs are $\approx 10^{-5}$ to 10^{-6} at most. Considering these low frequencies (other scenarios have initiator frequencies in the 1 to 10^{-3} range) coupled with the need for other failures to occur produce overcooling, ATWS and interfacing LOCA sequences are not expected to contribute significantly to PTS risk.

2.1.2.2 Initiating Events

The following internal initiating events were included in our PRA models:

- Small, medium, and large break loss of coolant accidents (LOCAs): pipe sizes range from 1- to 22-in.
- Transients commonly modeled in PRA analyses, including:
  - Reactor-turbine trip;
  - Loss of main feedwater;
  - Loss of main condenser; loss of offsite power (including station blackout);
  - Loss of support systems such as AC or DC buses,
  - Loss of instrument air, and
  - Loss of various cooling water systems
- Steam generator tube rupture (SGTR)
- Small and large steamline breaks with and without subsequent isolation.

2.1.2.3 Functional/Equipment Considerations

The event trees in our PRA models that depict potential overcooling sequences are based on the status and interactions of four plant functions and associated plant equipment. Figure 2.3 presents a function-level event tree depicting the four functions and resultant general types of sequences treated in the PRA models. Each plant analysis features much more detailed event trees constructed at the initiator and equipment response level that incorporate the plant specific design and operational features. These four functions (i.e., primary integrity, secondary pressure, secondary feed, and primary flow / pressure) are important to treat in the PTS analyses for the following reasons:

- <u>Primary integrity</u>: The status of this function influences the potential RCS pressure, which in turn influences the rate of cooldown (in some situations), the injection source capability, and the incoming and outgoing flowrates. All of these factors influence the vessel downcomer temperature.

- Secondary pressure: The status of this function influences the pressure and temperature in the RCS since the RCS and the secondary side of the plant are thermal-hydraulically coupled in most scenarios. For example, a rapid drop in secondary pressure can cause rapid cooling of the RCS affecting both the downcomer temperature and, potentially, the RCS pressure (depending on subsequent RCS injection flow and heat removal).

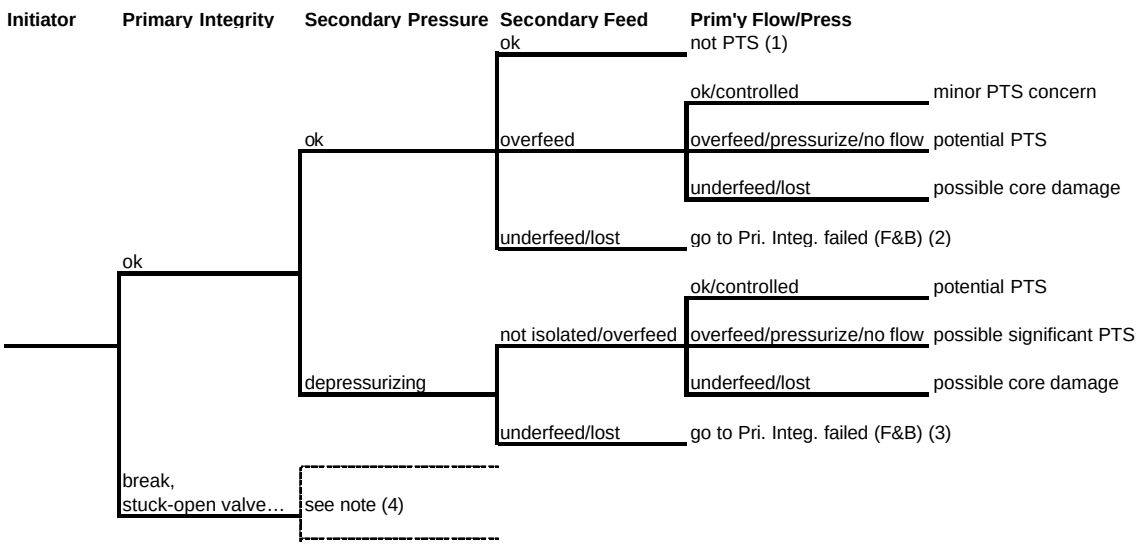

(1) not considered a PTS concern regardless of primary flow/pressure
(2) loss of feed to both SGs; procedures call for feed & bleed (F&B) which is equivalent to entering tree at Primary Integrity "failed"
(3) like (2) above except secondary depressurization has further lowered reactor coolant system (RCS) temperature
(4) logic is identical to rest of tree above except choices also exist for Primary Flow/Pressure even for Secondary Pressure and Feed "ok" state and PTS potential is generally greater for all scenarios

Figure 2.3. Functional Event Tree as the Basis for the PTS PRA Analyses.

- Secondary feed: The status of this function influences the pressure and temperature in the RCS since the RCS and the secondary side of the plant are thermal-hydraulically coupled in most scenarios. For example, overfeed can contribute to enhanced cooling of the RCS affecting both the downcomer temperature and, potentially, the RCS pressure (depending on subsequent RCS injection flow and heat removal).
- Primary pressure/flow: The status of this combination of conditions influences the RCS pressure and flow conditions (forced flow or natural circulation) during the overcooling event as well as the nature of the injection that can add cooling to the vessel wall. The flow characteristics either exacerbate or mitigate flow stagnation which can also affect the downcomer temperature.

In the plant event trees, the status of equipment relevant to each function are modeled in each PRA. This means that for each plant, the status of equipment relevant to each function is identified and included in the sequence modeling. For illustrative purposes, the following list summarizes the equipment associated with each function in the PRA models.

- Primary integrity: Status of - pipe breaks, pressurizer power-operated relief valves (PORVs) and associated block valves, pressurizer safety relief valves (SRVs), and pressurizer heaters and spray considerations where appropriate.

- Secondary pressure: Status of - steamline breaks, main steam isolation valves (MSIVs) and associated non-return valves as well as related bypass and drain valve considerations where appropriate, turbine throttle and governor valves, steam dump/turbine bypass valves and associated isolation valves (if any), atmospheric dump and associated isolation valves, and secondary steam relief valves (SSRVs).
- Secondary feed: Status of - main feedwater (MFW), condensate, and auxiliary/emergency feedwater (AFW/EFW) systems.
- Primary pressure/flow: Status of - high head safety injection, charging pumps and letdown considerations, accumulators/safety injection tanks, low head safety injection, reactor coolant pumps (RCPs).

The status of other equipment relevant because of interactions with the equipment in this list is also modeled as appropriate. Such equipment includes the saturation and protection/isolation circuitry associated with the equipment in the preceding list, and support systems including cooling water, instrument air, and electric power and instrumentation. Heating and ventilation equipment was not considered in the analyses due to the slow effects of such a loss and since such a loss can often be easily identified and recovered.

2.1.2.4 Human Action Considerations

Plant records of overcooling events that have actually occurred demonstrate that operator actions and inactions can significantly influence the degree of overcooling and the RCS pressure for many types of overcooling events. Consequently, operator action directly influences, in both beneficial and detrimental ways, the potential for many types of event sequences to become a serious PTS challenge. For example, early operator action to isolate the feed to a faulted (depressurizing or already depressurized) steam generator, directly affects the amount of overcooling that occurs and/or how long such cooling is sustained. Consequently, any "realistic" PTS analysis needs to consider operator actions and inactions that influence overcooling sequences. Therefore, consistent with the guiding principals of this project to adopt best-estimate models and treat uncertainties explicitly whenever practicable (see Section 1.6.1), we have included a rigorous treatment of human actions in PRA models. Our process to identify, model, and probabilistically quantify human factors derives largely from NUREG-1624, Revision 1 [NUREG 1624R1], which uses an expert elicitation approach. In our study the experts included both NRC contractors and licensees. These individuals considered both errors of omission and acts of commission. This process identified several general classes of human failures (see Table 2.2); we have incorporated these into our PRA models.

Table 2.2 also details which of the four primary functions identified in Section 2.1.2.3 and Figure 2.3 these failures most affect.

2.1.3 Step 3: Construct the PRA Models

We adopted the well-known and well-established event tree-fault tree PRA methodology as the basis for all plant specific analyses. However, our modeling approach varied somewhat from plant to plant because of the order in which the plants were analyzed (lessons learned in the Oconee analysis impacted the Beaver Valley and Palisades modeling approach, for example). Additionally, the availability of information from TH and PFM at the time PRA modeling initiated influenced how the PRA model evolved. Here we provide a

summary of the modeling approach for each of Oconee, Beaver Valley, and Palisades.

Table 2.2. General Classes of Human Failures Considered in the PTS Analyses.

Primary Integrity Control	Secondary Pressure Control	Secondary Feed Control	Primary Pressure/Flow Control
I. Operator fails to isolate an isolable LOCA in a timely manner (e.g., close a block valve to a stuck-open PORV) II. Operator induces a LOCA (e.g., opens a PORV) that induces/enhances a cooldown	I. Operator fails to isolate a depressurization condition in a timely manner II. Operator isolates when not needed (may create a new depressurization challenge, lose heat sink...) III. Operator isolates wrong path/SG (depressurization continues) IV. Operator creates an excess steam demand such as opening turbine bypass/atmospheric dump valves	I. Operator fails to stop/throttle or properly align feed in a timely manner (overcooling enhanced or continues) II. Operator feeds wrong (affected) SG (overcooling continues) III. Operator stops/throttles feed when inappropriate (causes underfeed, may have to go to feed and bleed & possible overcooling that way)	I. Operator does not properly control cooling and throttle/terminate injection to control RCS pressure II. Operator trips reactor coolant pumps (RCPs) when not suppose to and/or fails to restore them when desirable III. Operator does not provide sufficient injection or fails to trip RCPs appropriately (modeled as leading to core damage rather than a PTS concern)

2.1.3.1 PRA Modeling Differences Attributable to the Organization Constructing the Model

Both Oconee and Beaver Valley analyses use the same large event tree - small fault tree modeling format adopted by the PRAs that formed the technical basis for the current PTS rule. This approach makes best use of the earlier work in constructing updated PRA models. Since the desired outputs do not require the explicit component faults for some of the systems included in the model, very simple system fault trees were used with corresponding system-level failure data to represent the failure or unavailability of these systems.

In contrast, a plant-specific PRA model developed by the licensee [PAL-PRA] provides the starting point for the PRA model of the Palisades plant used in this project. The licensee's PRA includes more detailed component-level fault trees for all the systems included in the PTS-PRA model. However, in all three analyses, the level of resolution in the results is sufficient for the purposes of assessing the PTS risk.

2.1.3.2 PRA Modeling Differences Attributable to the Order of Plant Analysis

We constructed the PRA model of Oconee first at a time when feedback information from the TH analysis and from the PFM analysis was not

yet available. Consequently, it was not possible to screen out of the model overcooling sequences having a benign TH response or very low estimated conditional probabilities of through wall cracking (from the PFM analysis). Consequently, the Oconee PRA model contains virtually all the possible overcooling sequences with virtually no *a priori* screening out of "low significance" sequences. Subsequent feedback from both TH and PFM verified that many of the sequences included in the Oconee model could have been justifiably omitted from the PRA model.

Work on the Beaver Valley PRA model initiated after the Oconee model had been constructed at a time when the Oconee analysis results, while still evolving, were generally well understood. Also, as we began to construct the Beaver Valley PRA model some advanced TH and PFM results were already available for Beaver Valley sequences. Consideration of this TH/PFM information on Beaver Valley together with the "lessons learned" from the Oconee analysis permitted *a priori* screening of the following general categories of sequences from the Beaver Valley PRA model:

- Sequences involving certain combinations of stuck-open pressurizer PORVs or SRVs were not modeled
- Sequences involving certain combinations of secondary valve and simultaneous pressurizer PORV/SRV stuck-open events were not modeled
- Sequences involving only secondary valve (single or multiple) stuck-open events were not modeled
- Sequences involving only a single SG overfeed from AFW were not modeled
- Sources of secondary depressurization downstream of the MSIVs were not explicitly modeled
- Steam generator tube rupture (SGTR) sequences were not modeled including even those involving lack of proper feed control and even with RCPs shutdown (possibly inducing RCS loop stagnation)
- Other sequences were screened from modeling on a case-by-case basis if the sequence frequency could be conservatively estimated at lower than ~10^{-8}/yr since when coupled with even the highest CPFs being calculated for any type of sequence (in the 10^{-3} range) would yield a thru-wall crack frequency of $<10^{-11}$/yr range (thus would clearly not be important to the overall PTS results since some other sequences were known to involve thru-wall crack frequencies in the 10^{-8}/yr range or higher).

Because the Palisades model was built starting with an already established licensee component-level PRA model with overcooling sequences, it is the most detailed model of the three. This pre-existing Palisades model was added to by the licensee on the basis of NRC Contractor review and input to include possible scenarios and other factors not already in the pre-existing model. Consequently, the "lessons learned" from the Oconee PRA influenced the Palisades PRA model as well. In general, the Palisades PRA model addresses the same types of initiators, sequences, and functions and equipment and operator action relationships as do the Oconee and Beaver Valley models, but for Palisades-specific design and operational features using initiating event frequency and equipment failure probability data that is plant specific to Palisades.

2.1.4 Step 4: Quantify and Bin the PTS-PRA Modelled Sequences

For each plant, two conditions were modeled: full operating power and hot zero power (HZP). As identified in Section 2.1.3.2, little information was available to screen out potential PTS sequences for Oconee. Thus, because of a SAPHIRE code [SAPHIRE] limitation (i.e., the inability to store more than 100,000 sequences in a data base), it became necessary to produce separate SAPHIRE models for power and for HZP. Once the models (i.e., the event trees and fault trees) were constructed, the SAPHIRE code was used to generate the sequence logic for each event tree, and to solve the resulting sequences (90,629 sequences for each model) with no truncation due to frequency.

Given the number of potential PTS sequences for Oconee (181,258), it was necessary to group (i.e., bin) sequences with like characteristics into representative T-H cases that could be analyzed with the RELAP TH Code [RELAP]. Initial bins were constructed by developing event tree partitioning rules in SAPHIRE and then applying these rules to produce the T-H bins. Development of the partitioning rules required the analysts to examine the T-H information available from preliminary analyses to identify the characteristics that defined the preliminary analyses. Using this information, the analysts then made judgments as to whether existing T-H characteristics could be used to represent new groups of sequences. If the analysts judged that existing characteristics were appropriate, either because they matched the examined sequences exactly or because the T-H conditions from the new sequences were expected to be similar to but not be worse than the conditions from the existing analysis, then the uniquely-defining characteristics associated with the existing T-H analyses were written in rule form for application in SAPHIRE. For those cases where the analysts were sufficiently unsure as to the appropriateness of using existing characteristics, new T-H characteristics were identified. These new sets of characteristics were discussed with the T-H analysts. If after discussion with the T-H analysts, it was concluded that the expected T-H conditions could be sufficiently different from prior T-H analyses and that the frequency of occurrence of the conditions was such that it could not be "added" to some existing T-H bin without being unnecessarily conservative, then a new T-H calculation was identified and the T-H characteristics associated with this new calculation were written in rule form for subsequent application in SAPHIRE. This iterative process continued until all accident sequence cut sets were associated with one T-H analysis; thus, the final application of the developed rules involved the examination of each sequence cut set to determine which rule the cut set met, the subsequent "tagging" of the cut set, and the gathering of like-tagged cut sets into initial T-H bins. Once all cut sets were gathered into the initial T-H bins, the bins were re-quantified using a truncation limit of 1E-10.

For Beaver Valley, essentially the same process was followed. The major difference between the Oconee and Beaver Valley analyses was in the number of sequences developed and solved (a total of 8,298 sequences for power and HZP). As discussed in the previous subsection, knowledge about what was and was not important in the Oconee analysis was used with preliminary sequence frequency estimates and CPFs results from early Beaver Valley T-H and PFM calculations to minimize the number of sequences actually modeled in the corresponding SAPHIRE data bases. Given the significantly fewer number of sequences, no truncation was performed on the initial T-H bins.

For Palisades, the process was somewhat different in that the SAPHIRE model included both power and HZP sequences in the same data base (only 3425 sequences total) and the sequences were solved using a 1E-9 truncation value, a truncation limit approximately seven orders of magnitude less than the total sequence frequency. Another difference between the Palisades and Oconee or Beaver Valley analyses was how the T-H bins were created. In the Palisades analysis, each sequence end state was defined to a specific T-H bin and all resulting cut sets were placed in the defined bin. (Note: use of this binning process rather than the one used in the Oconee or Beaver Valley analyses should not have any impact on the results.)

More information with regard to the T-H bins that were created can be found in Section 2.2.

2.1.5 Step 5: Revise PTS-PRA Models and Quantification

With preliminary results available, reviews by both licensee and internal project staff were conducted. This allowed for formal feedback from the licensee with regard to the PTS-PRA models, inputs, assumptions, and results; and a time for analysts' self-review of the PRA to date. The purposes of the reviews were:

- to determine whether inaccuracies existed in the models, and whether additional potential PTS sequences needed to be modeled,

- to determine whether additional T-H bins should be created to reduce unnecessary conservatism based on new or updated information obtained from preliminary CPF calculations or needs identified by the uncertainty analysis,
- to determine which human actions were associated with the important T-H bins,
- to determine which of these human actions should be reexamined to produce even more realistic (i.e., less conservative) human error probabilities (HEPs), and
- To determine what combination of the above that could be accomplished within the constraints of the project.

For Oconee, the reviews identified the need:

- to add one more type of potential PTS sequence,
- for additional T-H bins to address uncertainty issues and to reduce conservatism, and
- To reexamine some human actions to produce updated HEPs to account for more specific conditions.

The Beaver Valley reviews identified the need:

- for additional T-H bins to address uncertainty issues and to reduce conservatism, and
- To reexamine a few human actions to produce updated HEPs to account for more specific conditions.

Because the Palisades analysis was being performed by the utility, the results of the review described here dealt only with issues identified by the NRC review of the licensee's PTS model. The review identified the need:

- to add additional break sizes to the LOCA class of initiating events and
- For additional T-H bins to address uncertainty issues.

It should be mentioned that while there were formal reviews set up, such as during the second plant visit at both Oconee and Beaver Valley, informal periodic review was conducted via the written and verbal communications among the licensees and project staff on a frequent basis. Appropriately, the models were revised and re-quantification was performed on the basis of these licensee inputs and as a result of self-evaluations by the project staff.

2.1.6 Step 6: Perform Uncertainty Analyses

The primary objective of the PRA portion of the PTS analyses is to produce frequencies of the set of representative plant responses to plant upsets (i.e., scenarios). These scenarios involve mitigating equipment successes and failures as well as operator actions that result in various degrees of overcooling of the internal reactor vessel downcomer wall. The major areas of uncertainty associated with the PRA can be grouped into two broad categories:

- modeling of the representative plant scenarios, and
- Estimation of the frequency of each modeled scenario.

These areas of uncertainty and the techniques used to deal with the uncertainties are discussed in the following two subsections.

2.1.6.1 Modeling of Representative Scenarios to Characterize Aleatory Uncertainty

Each scenario in the PRA is represented by a collection of events described by the logic of the event tree and relevant fault trees for each initiating event identified in the analysis. The model initially assumed binary logic (e.g., valve fully re-closes or sticks wide open; no in-between states) for the events. The only explicit modeling of event timing involved the timing of operator actions (i.e., failure to take an action is modeled as failure to take that action in multiple discrete times– for example, by 10 min, by 20 min–each with a probability). Most uncertainties with regard to the model structure (e.g., completeness, in-between states) are not quantified. However, where judged potentially

important, a few modeling uncertainties were addressed by purposely changing the model and assigning a probability to the applicability to that model. Each of these changes potentially becomes a different scenario (T-H bin) with an associated frequency (e.g., area associated with a stuck open SRV reduced 30%, timing of reclosure of a stuck open SRV–3000 sec vs. 6000 sec, actual break size of small and medium LOCAs). Since it is unknown which scenario will occur next, the complete set of scenarios characterize a large part of the aleatory uncertainty associated with the occurrence of a PTS challenge. The more important of these uncertainties that were handled explicitly in the analyses are addressed further in the next step; Step 7.

In addition, there is the overall general uncertainty as to the completeness issue (i.e., have all scenarios that potentially lead to PTS conditions been identified and modeled). This uncertainty issue was addressed non-quantitatively by having both internal (i.e., NRC and its contractors) and external (i.e., licensee) review of the PRA model. As a result of this peer review process, the models are expected to produce a sufficiently complete set of potential PTS sequences and thus any incompleteness in the model is expected to have a small effect on the results.

2.1.6.2 Quantification of Scenario Frequencies to Characterize Epistemic Uncertainty

Each scenario from the set of modeled scenarios is the interaction of what is treated as random events:

- initiating event (plant upset),
- series of mitigating equipment successes/failures (e.g., MFW trips, AFW starts, ADVs are challenged and one sticks open…), and
- Operator actions (e.g., fails to close ADV isolation valve by 20 minutes after the ADV sticks open).

Thus, the occurrence of each scenario is random, and the frequency of each scenario is obtained by:

Eq. 2-1

$$f_{scenario} = f_{initiating-event} \cdot \Pr_{equipment-response} \cdot \Pr_{Operator-Actions(s)}$$

Each of the variables used to obtain the scenario frequency have an epistemic uncertainty described by a distribution. The source of this information came primarily from the input data used in the analysis; i.e., the addendum to NUREG/CR-5750[Ref later] for Oconee and Beaver Valley, and the plant-specific data used in the Palisades analysis. For a few specific model inputs, other data sources were also used to derive these uncertainty estimates. For the HEPs, both best estimate values and uncertainty ranges and distributions were derived through the expert elicitation processes carried out in the human reliability analyses. Latin Hypercube sampling techniques were used to propagate these epistemic uncertainties to generate a probability distribution for each scenario frequency. Thus, the frequencies provided by the PRA analysts to the PFM analysts were described by histograms representing the resulting frequency distributions. In this way, these PRA uncertainty distributions were propagated through and combined with the PFM uncertainties to ultimately derive uncertainty distributions in the estimated thru-wall crack frequencies.

2.1.7 Step 7: Incorporation of Uncertainty and Finalization of Results

This section discusses important uncertainties (largely aleatory in nature) accounted for in the PRA and describes how each was handled. As described in the previous subsection, epistemic uncertainty in the frequency for each of the final thermal-hydraulic bins was estimated using Latin Hypercube sampling techniques and will not be described in this subsection.

The uncertainties below were dealt with quantitatively; however, the degree of resolution associated with each specific uncertainty was limited. These uncertainties include:

- size of the LOCA within a LOCA category plus other factors (e.g., initial injection water temperature),
- size of the opening associated with a single or multiple stuck open SRV(s),
- time at which a stuck open SRV recloses, and
- Time at which operators take or fail to take action.

These uncertainties were highlighted for specific treatment in the analysis based on (a) the dominating types of scenarios found to be most important to the PTS results, and (b) a series of uncertainty analyses performed by the University of Maryland (UMD) project team members on many of the inputs and parameters potentially affecting the PTS results to see which uncertainties would most affect those results. More on the specific UMD analyses is discussed in Section 2.2.6. The results of that work concluded that the above uncertainties are sufficiently important that they needed to be explicitly treated in the PRA model. These uncertainties and how they were addressed are discussed in the following paragraphs.

The actual break size of a LOCA for a specific LOCA class (i.e., small, medium, or large) can be any point on the spectrum of sizes defined by the two end points for that class. In addition, other factors (e.g., initial injection water temperature, break location, and injection flow rate) can contribute to the overall PTS model uncertainty since these factors along with the specific break size affects the rate of cooling and subsequent plant response. Numerical probability results from the UMD uncertainty analysis (see Section 2.2.6 for a discussion of what was considered) were used to model and estimate the importance of the various modeling uncertainties examined in the UMD analysis including the possibilities of break sizes within a given class (which was assumed to be uniformly distributed). These numerical analyses provide a spectrum of different plant thermal-hydraulic responses arising from uncertainties in these key parameters including break size. This spectrum of results was then represented by a number of discrete cases to cover the total spectrum of results. Each case was assigned a probability by the UMD analysts based on how much of the total spectrum the discrete case represents (see Section 2.2.6 for more detail). Each discrete case was assigned a new T-H case number with corresponding T-H curves, and the frequency of each new case was adjusted by the UMD assigned probability for that case. This was accomplished by gathering all cut sets from all sequences generated for a specific LOCA class into one bin. The cut sets were then reproduced a specified number of times corresponding to the number of discrete cases defined to represent the spectrum of results. Each set of reproduced cut sets was then modified to include the probability assigned that discrete case. Thus, the new modified cut sets account for the uncertainty associated with various parameters examined in the UMD analysis, including possible variation of break sizes within a given LOCA class.

Just as with the LOCAs, the size of the opening associated with a stuck open SRV can vary from a size that is not PTS significant all the way to the valve being fully stuck open. To deal with this issue and other relevant issues examined in the UMD analysis, the cut sets (and their associated frequencies) from stuck open SRV sequences were modified to include a fraction that represented the uncertainty from the UMD work. In this case, again it was assumed that the SRV opening size is uniformly distributed (any specific opening is equally likely) and the resulting fraction was included in the sequence frequency estimates to account for that fraction of possible SRV size openings that would be sufficient from a cooling perspective to be potentially important.

The time at which a stuck open SRV recloses is unknown and can occur at any point after the valve sticks open. To approximate this, the frequencies associated with stuck open SRV sequences with subsequent closure of the SRV were divided equally between two specific SRV

reclosure times (i.e., 3000 sec and 6000 sec). These two time points were chosen after reviewing stuck open SRV thermal-hydraulic conditions. The 6000 sec point was chosen to coincide with the point where the change in downcomer wall temperature had "flattened out." The 3000 sec point was chosen to coincide with the point where sufficient cooling has occurred to the downcomer wall such that PTS could become an issue. Use of these two time points provides a mechanism for determining some measure of the uncertainty associated with reclosure of stuck open SRVs. Each case was assigned a 50% chance of occurring.

Just as the time at which a stuck open SRV recloses is unknown, so too is the times at which operators perform actions. To address this issue, the times at which selected operator actions (i.e., those believed to be relatively important to PTS) were performed was varied. Typically, two or three different time points were chosen to represent the uncertainty in when the action would be performed. Once the time points were defined, typically as early as could be expected, as late as possible that would still affect the outcome, and for some actions some intermediate time point, the probability of failing to perform the action by the specified time was developed. Use of these operator action time points provides a means of estimating the uncertainty associated with when operators actually perform actions.

For the Oconee analysis, all issues identified above were incorporated into the analysis. For the Beaver Valley and Palisades analyses, results from the UMD analysis indicated that little uncertainty came from the sequences involving stuck open SRVs that remained stuck open; thus, no modifications were made to those types of sequences in the Beaver Valley and Palisades analyses. However, all other modifications were made for Beaver Valley and Palisades.

2.2 Thermal Hydraulics

This section describes the thermal-hydraulic analysis performed on the Oconee-1, Beaver Valley-1 and Palisades nuclear power plants. The Oconee-1 coolant system is a lowered-loop, Babcock & Wilcox design with two steam generators, two hot legs and four cold legs. The Beaver Valley-1 coolant system is a Westinghouse design with three steam generators, three hot legs and three cold legs. The Palisades coolant system is a Combustion Engineering design with two steam generators, two hot legs and four cold legs.

The RELAP5/MOD3.2.2 gamma computer code released in June 1999 was used for this analysis. The RELAP5 code was developed for best-estimate transient simulation of light water reactor coolant systems during postulated accidents and transients. The code models the coupled behavior of the reactor coolant system, core, and secondary side system for loss-of-coolant accidents and operational transients such as anticipated transients without scram, loss of offsite power, loss of feedwater, and loss of flow. With RELAP5, a generic modeling approach is used that permits simulating a variety of thermal-hydraulic systems. Control system and secondary system components are included to permit modeling of plant controls, turbines, condensers, and secondary feedwater and steam systems.

The thermal-hydraulic analyses were performed to generate the time histories for key parameters for use in the fracture mechanics analysis code, FAVOR. The parameter responses passed to the FAVOR code are the reactor vessel downcomer fluid temperature, pressure and heat transfer coefficient on the inside of the vessel wall. A wide variety of transients that could contribute to the risk of vessel failure were analyzed. These transients include reactor system overcooling due to a LOCA, a component failure that results in an uncontrolled release of steam from the secondary side, or a control system failure that results in overfilling the steam generators. Combinations of failures, such as a LOCA with one or more stuck open safety valves, are also of concern and were analyzed.

2.2.1 Model Development

For all three of the plants examined, the thermal-hydraulic analysis methodology is similar. For each plant, the best available RELAP5 input model was used as the starting point. For Oconee, the base model was that used in the code scaling, applicability and uncertainty (CSAU) study. For Beaver Valley, the base model was the H.B. Robinson-2 model used in the original PTS study in the mid 1980s. This model was reviewed by Westinghouse and revised and updated based on the review comments to reflect the Beaver Valley plant configuration. For Palisades, the base model was obtained from CMS Energy Corporation, the operators of the Palisades plant. This model was originally developed and documented by Siemens Power Corporation to support analysis of the loss of electrical load event for Palisades.

The RELAP5 models are detailed representations of the power plants and include all major components for both the primary and secondary plant systems. RELAP5 heat structures are used throughout the models to represent structures such as the fuel, vessel wall, vessel internals, and steam generator tubes. The reactor vessel nodalization includes the downcomer, lower plenum, core inlet, core, core bypass, upper plenum and upper head regions. Plant-specific features, such as the Oconee reactor vessel vent valves, are included as appropriate.

The downcomer model used in each plant was revised to use a two-dimensional nodalization. This approach was used to capture the possible temperature variation in the downcomer due to the injection of cold ECCS water into each of the cold legs. Capturing this temperature variation in the downcomer is not possible with the original one-dimensional downcomer. In the revised models, the downcomer is divided into six azimuthal regions for each plant. The reason for choosing six azimuthal regions is so that water from each of the cold legs would flow into a separate downcomer node.

The safety injection systems modeled for the Oconee, Palisades, and Beaver Valley plants include high pressure injection (HPI), low pressure injection (LPI), other ECCS components (e.g. accumulators, core flood tanks (CFTs), safety injection tanks (SITs) depending on the plant designation), and makeup/letdown as appropriate.

The secondary coolant system models include steam generators, main and auxiliary/emergency feedwater, steam lines, safety valves, main steam isolation valves (as appropriate) and turbine bypass and stop valves.

Each of the models was updated to reflect the current plant configuration including updating system setpoints (to best estimate values) and modifying control logic to reflect current operating procedures. Other changes to the models include the addition of control blocks to calculate parameters for convenience or information only (e.g., items such as minimum downcomer temperature).

Detailed information regarding the specific individual RELAP5 input models for the Oconee, Beaver Valley and Palisades plants can be found in [Beaton 02a, Beaton 02b, Fletcher 84, Fletcher 02a, Fletcher 22b, Fletcher 02c].

2.2.2 Model Initialization

The model for each plant was initialized to steady state full power conditions. An 8,000 second period was chosen to provide a starting point for the accident and transient event calculations. Null transient runs (with no transient event initiators but with various transient model features activated) were made (rather than "steady state" runs) to assure that the models hold the steady condition without the aid of steady state controllers. Results from the null transient calculations were compared to desired plant values for steady-state full power operation to assure valid starting conditions.

Because of the need to analyze transients from hot zero power (HZP), the Palisades and Beaver Valley models were also initialized to HZP conditions. For these analyses, HZP is defined as the plant conditions existing one month after shutdown from full power, with a core decay power is 0.2% of the rated thermal power, which corresponds to about 5 MW. Under these

conditions, heat delivered to the reactor coolant system is mostly RCP pump heat (15 MW) as opposed to decay heat from the core. Again, an 8,000 second period was chosen to achieve a steady state. Because decay heat is small, nearly uniform fluid temperatures will exist throughout all portions of the reactor coolant system (cold legs, hot legs and reactor vessel) and the steam generator (SG) secondary system.

The primary side fluid temperature defines the HZP secondary system pressure since the secondary side will be at the saturation pressure corresponding to the reactor coolant system temperature. The steam dump valve controllers in the plant and model modulate the steam dump valve to maintain this SG pressure and RCS average temperature. The turbine stop valves are closed. Feedwater is delivered at a very low rate, consistent with the low RCS heat load. Because the feedwater train heaters depend on turbine extraction steam for operation, feedwater is delivered to the steam generators at condenser temperature, rather than the elevated temperature associated with main feedwater at full power operation. The reduced steam generator heat load at HZP results in much less steam production and voiding in the SG boiler sections than at full power. Therefore, SG water mass is significantly higher for HZP operation than for HFP operation for the U-tube steam generator designs.

Hot zero power analyses for Oconee were performed by reducing the decay heat power to correspond to 0.3 percent of full core power. This low decay heat assumption was based on the observation that at one month, the decay heat load is approximately 0.3 percent of the full power output. The decay heat after one hour is about 1 percent of full power. The judgment was made to apply a multiplier of 0.3 to the full power decay heat curve for the HZP power cases. It was decided to use this approach early in the Oconee analysis to estimate the impact of transient initiation at low power operation on downcomer temperature and a significant number of calculations were performed using this assumption.

A key aspect of hot zero power operation from the perspective of thermal-hydraulic conditions is the change in the mass of water in the steam generator between full power and HZP operation. In a U-tube steam generator, the water mass decreases by about 50 percent between HZP and full power operation. Using the Palisades steam generator as an example, the mass of water is about 64,545 kg (142,000 lbm) at full power and 82,670 kg (210,000 lbm) at hot zero power. Conversely, in the once-through steam generator, the mass of water is much less during HZP operation compared to HFP operation. Using Oconee as an example, the mass of water is about 18,180 kg (40,000 lbm) during HFP operation and about 5,000 kg (11,000 lbm) during HZP operation. The amount of heat removed from the primary side due to initial secondary side water flashing during a steam line break will be less during hot zero power than during full power based on the difference in the water mass at Oconee. Other factors such as continuing feedwater flow to the affected steam generator will have a significant impact on the downcomer temperature and system pressure than differences in plant operating state and SG water mass between full power and hot zero power for Oconee. It was on this basis that the low decay heat assumption was retained. However, it is recognized that reinitializing the model for HZP operation for any plant is the preferable approach.

2.2.3 Transient Event Simulations

The transient event simulations were run as RELAP5 restart calculations, beginning from the end of the null transient calculations. Some of the early Oconee analyses were run for 10,000 sec after transient initiation. It was then decided to extend the transient time to 15,000 sec to ensure that the range of interest from the perspective of possible vessel failure was covered.

Transient events were selected for evaluation based on Probabilistic Risk Assessment (PRA) analysis (see Section 2.1). Since each plant possesses unique thermal-hydraulic, hardware failure, and operational characteristics, there was variation in the course of the transients events

analyzed for the three plants. Examples of plant-to-plant differences important for PTS that affect transient selection include variations in: shutoff heads for HPI pumps; initial pressure and temperature conditions in the accumulator (SIT, CFT); initial ECCS fluid temperature and allowed range; initial SG water masses; sizes and configurations of various valves, automatic controllers; and different operating procedures.

The development of the transient case list for each plant was an evolutionary and iterative process. Generally, transients were selected that would maximize the rate of primary system cooldown after transient initiation. Most transient event cases simulated generally fell into the categories of loss-of-coolant accidents (LOCAs), reactor/turbine trips with various complicating hardware and operator failures. Scenarios included stuck-open relief valves that either remain open or subsequently reclose later in the transient, system failures that cause steam generator overfeed, and main steam line breaks. Evaluations were also performed for other types of events, such as steam generator tube rupture, recovery from a loss of all feedwater event, and feed-and-bleed recovery from a LOCA with HPI failure.

2.2.3.1 Loss of Coolant Accidents

The smallest LOCA break size evaluated was 2.54 cm (1.0 inch) in diameter. Larger break sizes were also evaluated where the break flow area was progressively doubled up to 57.47 cm (22.63 in) diameter. Break sizes considered in the analysis therefore range over the full break spectrum. The breaks for most LOCA cases are assumed to be on the hot side of the RCS (in the pressurizer surge line for smaller breaks and in the hot leg for larger breaks). The hot leg break location was selected for most evaluations because it results in the greatest RCS depressurization and largest primary system cooldown rate. ECCS injection rates will also be maximized. Limited evaluation of cold leg break LOCAs was also performed.

For all LOCA cases, the discharge and flow loss coefficients used for break junctions are assumed to be equivalent to those used in AP600 analyses [??]. While these coefficients may not be appropriate for a specific break, the wide spectrum of break sizes accounts for any differences in loss coefficients.

2.2.3.2 Reactor/Turbine Trips with Various Failures

The majority of the cases analyzed are initiated by a reactor/turbine trip with various primary or secondary side failures. These include relief valve failures, steam generator level control failures, among others. In the RELAP5 model for all cases, the reactor trip is treated as coincident with a turbine trip.

There are numerous cases where stuck open valves (pressurizer or steam generator PORV, safety relief valves, etc.) are modeled as failures following a reactor/turbine trip. In these cases, the valve is assumed to spuriously open at time zero. Primary side stuck valves (pressurizer SRV or PORVs) are LOCAs where the "break" is located at the top of the pressurizer, rather than the surge line, hot leg or cold leg. RELAP5 used a single valve component to model several valves in parallel. For example, in Beaver Valley, there are three pressurizer PORVs modeled with a single RELAP5 valve component. To simulate a single PORV fail by sticking open, the RELAP5 valve component is opened to 1/3 full flow area.

In a number of cases, the valve which stuck open was assumed to reclose at some later time. The time of reclosure was defined as either 3000 seconds or 6000 seconds depending on the transient definition from the PRA analysis (occasionally a different time was chosen). Various times were chosen since it would not be known when the valve would re-close (if it were to re-close). The 6000 second reclosure time was selected as a point far enough out in time where the primary pressure and temperature reached a minimum.

Another set of failures is overfeeding of the steam generators. As with other cases, the initiating event is the reactor/turbine trip. These cases will result in an overcooling event. The fault could be anything from component failure,

control failure, or operator error. Cases were run where a single steam generator is filled to the top, and the water level is maintained at that level. There were cases where multiple steam generators are filled to the top. Cases were run where the steam generator(s) were filled to the top, then feedwater was stopped and the steam generator was allowed to boil dry.

2.2.3.3 Main Steam Line Break

Main steam line break cases were selected because they cause a rapid depressurization of the steam generator. The rapid depressurization is one of the most limiting overcooling transients from a single failure on the secondary side. Large breaks considered were modeled as double-ended guillotine breaks. These breaks were assumed to occur at the connection of the steam line to the steam generator (upstream of the main steam isolation valves). Smaller steam line breaks were simulated with stuck secondary side valves (SRVs, ADVs, TBVs) in plants with main steam isolation valves, some of these stuck valves (breaks) were isolated by closing the MSIVs.

2.2.3.4 Operator Actions

Various operator actions are considered in the RELAP5 analyses based on the transient definition from the PRA analysis. For the cases involving a primary system LOCA, the operator is assumed to take no action since automatic systems are presumed to operate and provide the core and primary system cooling. In these situations, the primary operator function is to monitor system conditions. For various transients involving reactor/turbine trips combined with component failures that lead to primary system overcooling, operator actions were modeled. Generally, two categories of operator actions are considered: 1) the operator correctly diagnoses the plant situation and performs the correct actions based on the Emergency Operating Procedures, and 2) the operator fails to correctly diagnose the situation or takes the incorrect action.

A significant operator action for the plants analyzed is HPI control/throttling. Depending on the transient scenario, continued HPI injection can cause the system to re-fill and repressurize to the HPI pump shutoff head pressure and/or the pressurizer PORV setpoint. An example of a transient where system repressurization can occur is a stuck open primary safety valve that recloses after the system has depressurized. Continued HPI will cause the primary system to repressurize in this case unless the operator recognized that the faulted valve has reclosed and takes action to control HPI injection.

Different plants have different methods of HPI control. In Oconee, the operator can throttle HPI flow to obtain a desired flowrate and maintain a certain pressurizer water level. In Beaver Valley, however, the operator can either have a pump running or not. There is no "throttling"; rather a pump gets turned off if conditions are met. In Palisades, the operator can throttle HPI if auxiliary feedwater is operating with the steam generator wide-range level > -84% and the reactor coolant system subcooling greater than 25°F. In this case, HPI is throttled to maintain pressurizer level between 40 and 60 percent.

HPI control is a contributor to the overall PTS risk. An event where there is no HPI control can be PTS significant, while the same event with HPI control will not be a PTS concern. One significant variable in the HPI control is the operator timing. Since the time that the operator will take control of the HPI is variable depending on the transient situation, several times are analyzed based on PRA input to determine the variation in overall system (downcomer) conditions. As an example, for Beaver Valley, cases were run where the operator does not control HPI, controls HPI 1 minute after the criteria for control are met, and operator controls HPI 10 minutes after the criteria are met.

Another example of an operator action is the control of the reactor coolant pumps. The different plants use different criteria for tripping the reactor coolant pumps (RCP). At Oconee, the operator is assumed to trip the RCPs on low subcooling. The Beaver Valley, the reactor

coolant pump trip criteria is based on the difference between steam generator and pressurizer pressures. At Palisades, RCP trip criteria are based on primary system pressure and subcooling margin. In some events, the RCPs were not predicted to trip; however, various operating procedures could have caused the operators to trip the pumps. Therefore, in some cases, the RCPs were set to trip as an operator action. An additional note about RCPs is that they will be tripped if there are "bad" containment conditions (i.e., main steam line break). Since the RELAP5 models used do not include the containment, the pumps were tripped manually if it was deemed necessary.

Failure of the operator to correctly diagnose the situation and take the correct action was also considered in the transient analysis. Failure to isolate the auxiliary/emergency feedwater to a faulted steam generator during a steam line break is an example of an operator failure considered in this analysis. This failure will result in an overcooling event where the faulted generator continues to remove heat, thus, lowering the primary temperature. Timing of operator action was also analyzed. As an example, analyses were performed assuming that the operator stops AFW/EFW to the faulted generator (at 30 minutes for Beaver Valley). Time of operator action was determined by PRA analysis.

2.2.4 Containment Considerations

The RELAP5 model does not include an explicit containment model. Discharge to the containment due to a break or valve failure is to a volume held at constant atmospheric pressure. Note that this assumption also applies to steam line breaks.

The RELAP5 analysis considers the increase in injection water temperature due to switchover of the ECCS suction from the refueling water storage tank (RWST) to the containment sump. This switchover occurs when the water inventory in the RWST is depleted due to the combined pumping of the ECCS and containment spray pumps. After switchover, the ECCS and containment sprays operate in a recirculation mode, taking suction from the containment sump. At the point of suction switchover, ECCS injection water temperature will increase from a typical range of 283 to 305 K (50 to 90°F) to 325 to 335 K (120 to 140°F) or higher. Increase in ECCS injection temperature will have a significant impact on the predicted risk of vessel failure.

In the PTS analysis performed in the 1980's, the ECCS suction switchover to the containment sump was not considered. It is believed that it was ignored because the RELAP5 analyses were typically terminated after a few thousand seconds due to computer costs. Results were then extrapolated to longer times. Depending on the transient, the ECCS suction may not have switched to the containment sump. Since computer technology has advanced significantly over the past 20+ years, cases are now run out to 10,000 or 15,000 seconds and, in this time period, the ECCS suction will switch to the containment sump.

There are two factors involved in the sump recirculation mode; time of switchover to sump and sump fluid temperature. Since this information is transient specific, plant specific assumptions were made. These modeling assumptions are discussed in References 5.2-1 through 5.2-5.

2.2.5 RELAP5 Numeric Issues

After simulating numerous LOCA cases for the Oconee plant, it was discovered that there was a flow recirculation problem in the cold legs. In LOCAs with a break diameter of more than 3.59 cm (1.414 in) the operators are assumed to trip the RCP due to loss of subcooling margin. The loop flow is then driven by natural circulation and stagnation may occur depending on conditions. RELAP5 predicts a recirculation flow pattern at that point where the flow becomes negative in one cold leg (in a given loop), and positive in the other cold leg. The magnitude of the flow is on the order of 200 kg/sec (440 lb/sec). This flow pattern occurs in 2x4 plants like Oconee and Palisades where two cold legs are connected to each steam generator. This pattern is not observed in Beaver Valley

which has only one cold leg connected to each steam generator. It should be noted that occurrence of the cold leg recirculation flow pattern is not new and was seen in the original PTS analysis (Ref. 5.2-7). The recirculation flow is believed to be numerically driven and not realistic. The root cause of this problem in the RELAP5 code was being investigated at the time this report was prepared.

Cold leg recirculation causes an unrealistic increase in the downcomer fluid temperature due to overprediction of the amount of mixing between ECC injection and downcomer water. This increase can be on the order of 30°F or more and can have a significant impact on the vessel failure probability. To avoid this recirculation problem, a high reverse loss coefficient was added in the cold leg near the RCP in the Oconee and Palisades models for the LOCA cases. Addition of this coefficient prevents negative flow in the cold legs, thereby inhibiting cold leg recirculation.

Recirculating flow patterns were also observed in the RELAP5 results in the two-dimensional downcomer for Palisades for LOCAs with a break diameter of more than 5.08 cm (2.0 in). In this case, the recirculation occurred in the axial direction in parallel flow channels in the two-dimensional downcomer. The magnitude of the flow was on the order of thousands of pounds per second or more. The cause of the recirculation was traced to application of the momentum flux model in RELAP5 particularly in the connection between the downcomer and the lower plenum. The root cause of this problem in the RELAP5 code was being investigated at the time this report was prepared. Numerics issues are discussed further in Section 2.2.5.

2.2.6 Uncertainty Analysis Results

This section discusses the identification of the TH uncertainty representative scenarios of the Oconee, Palisades, and Beaver Valley nuclear power plants in PTS context. Based on the PRA assessment, the primary side breach events, including LOCA and PZR SRV stuck open events, are the dominant PTS scenarios for all three plants. Due to the plant different design, the list of key PTS contributing parameters is slightly different. Focusing on the dominant PTS contributing scenarios, the key PTS contributing parameters and their uncertainty ranges of the Oconee, Palisades, and Beaver Valley NPPs are discussed in Sections 2.2.6.1, 2.2.6.2, and 2.2.6.3, respectively, and their TH uncertainty representative scenarios are identified.

The first 10,000 seconds downcomer average temperature is used as the primary PTS sensitivity indicator. For each key PTS contributing parameters, typically three representative values representing lower bound, nominal, and upper bound with corresponding pre-determined probabilities are used for the assessment of their impacts on the sensitivity indicator. The assessment is based on the RELAP5 calculation. The sensitivity results are applied on PTS representative scenarios identification.

2.2.6.1 Oconee NPP TH Uncertainty Analysis Results

The Oconee is a B&W type NPP, which has a plant-specific design, reactor vessel vent valve, connecting the upper plenum and downcomer. The representative values and corresponding probabilities of the key PTS contributing parameters, classified into parameter uncertainty related and model uncertainty related, and shown in Table 2.3. The sensitivity results calculated by RELAP5 are shown in Table 2.4.

The primary system breach event is classified into several groups for TH uncertainty analysis. These groups and their representative scenarios are:

- Table 2.5: LOCA between 1.5-inch and 4-inch
- Table 2.6: LOCA between 4-inch and 8-inch
-

Table 2.7: LOCA greater than 8-inch
- Table 2.8: Reactor trip plus PZR SRV suck open without reseating during full power operation
- Table 2.9: Reactor trip plus PZR SRV suck open without reseating during hot zero power operation
- Table 2.10: Reactor trip plus PZR SRV suck open during full power operation. The PZR SRV is reseated later automatically
- Table 2.11: Reactor trip plus PZR SRV suck open during hot zero power operation. The PZR SRV is reseated later automatically

2.2.6.2 Palisades NPP TH Uncertainty Analysis Results

The Palisades NPP has low HPI pump head thus the RCS repressurization, one of the important PTS contributing factor for the Oconee NPP, is not a factor for the Palisade NPP. The initiating events of the reactor trips with PZR SRV stuck open are not PTS concern thus the TH uncertainty analysis focuses on the LOCA. The break size is divided into three groups for the analysis:

- Table 2.13: Between 1.4-inch and 4-inch in diameter LOCA
- Table 2.14: Between 4-inch and 8-inch in diameter LOCA
- Table 2.15: Greater than 8-inch in diameter LOCA

2.2.6.3 Beaver Valley NPP TH Uncertainty Analysis Results

Same as the Oconee NPP, the LOCA and the PZR PORV and PZR SRV stuck open events are the primary PTS concern for the Beaver Valley NPP. The Beaver Valley NPP is designed with large capacities of PZR PORVs and PZR SRVs. Both the PZR PORV and SRV stuck open events are PTS concern. PRA analysis identifies that the simultaneous two PZR valves stuck open events have reasonable likelihood to be PTS concern. The one or two PZR valves stuck open events are explicitly represented in the PRA model. The probabilities calculation of the TH representative scenarios of the PZR valves stuck open is relative complex. It is not discussed in this section. Only the results of binned PRA probabilities are presented. The detail probability calculation can be seen in the TH uncertainty individual report.

The sensitivity results calculated by RELAP5 are shown in Table 2.16. The TH uncertainty analysis divides the primary breach events into several groups, consisting with PRA classification, for the TH representative scenarios identification:

- LOCA:
  1. Table 2.17: LOCA between 1.4-inch and 4-inch
  2. Table 2.18: LOCA between 4-inch and 8-inch
  3. Table 2.19: LOCA larger than 8-inch
- PZR Valves Stuck Open
  1. Table 2.20: Valves stuck open and remain open or two valves stuck open simultaneously with one remaining open and the other reseated later by itself
  2. Table 2.21: One SRV stuck open and reseated; reactor trips at full power operation
  3. Table 2.22: One SRV stuck open and reseated; reactor trips at hot zero power operation
  4. Table 2.23: Two valves stuck open and reseated; reactor trips at full power operation
  5. Table 2.24: Two valves stuck open and reseated; reactor trips at hot zero power operation

Table 2.3. The nominal values of the key parameters and their variations with break size fixed.

	Factors	Value 1 (lower Bound)	Value 2 (Nominal)	Value 3 (Upper Bound)
		Probability	Probability	Probability
Parametric (Boundary Condition) Uncertainty	Break Size	N number of representative break sizes	--	--
		1/N	--	--
	Break Location	Hot Leg	Cold Leg	--
		0.5	0.5	--
	*Decay Heat	Nominal	HZP	--
		0.98	0.02	--
	**Season	Winter	Spring/Fall	Summer
		0.25	0.5	0.25
	High Pressure Injection System Flow Rate	90%	Nominal	110%
		0.1	0.8	0.1
	Core Flood Tanks Pressure	50 psi less	Nominal	50 psi more
		0.1	0.8	0.1
	Sump recirculation	If break size > ~ 4”	If break size < ~4”	
		1.0	0.0	
RELAP5 Code Model Uncertainty	Reactor Vessel Vent Valves State	Fully close	Nominal	Fully open
		0.25	0.5	0.25
	Component Heat Transfer Rate	70%	Nominal	130%
		0.1	0.8	0.1
	Flow Resistance	100% more	Nominal	--
		0.1	0.9	--
	Break Flow Rate (Break Area)	70%	Nominal	130%
		0.25	0.5	0.25
	Numerical “Mixing”	High cold legs reverse flow resistance	--	--
		1.0	--	--

*Applied only on LOCA. PRA method treats HZP explicitly in the initiating events of reactor trip with PZR SRV stuck open.
**In winter, t(HPI) = 4.4 ºC (40 ºF), t(CFT) = 21.1 ºC (70 ºF), and t(LPI) = 4.4 ºC(40 ºF);
**in summer, t(HPI)= 29.4 ºC (85 ºF), t(CFT) = 37.8 ºC (100 ºF), and t(LPI) = 29.4 ºC (85 ºF);
**in spring and fall, t(HPI) = 21.1 ºC (70 ºF), t(CFT) = 26.7 ºC (80 ºF), and t(LPI) = 21.1 ºC (70 ºF)

Table 2.4. The sensitivity runs matrix of the Oconee-1 PTS study for primary side breach related scenarios. The values are the average downcomer temperature of the first 10,000 seconds in Kelvin.

Break Size [m^*2] / Parameter	[0.001] (1.5")	[0.002] (2")	[0.004] (2.828")	[0.008] (4")	[0.016] (5.656")	[0.032] (8")
Nominal	416	393	390	363	330	313
Winter	405		370		317	297
Summer			392		336	323
P(CFT) += 50 psi			387			
P(CFT) –= 50 psi			390			
110% m(HPI)	401		381			
90% m(HPI)	419		401			
HZP	400		349		314	311
Vent Valve Fully Close			361	346		
Vent Valve Fully Open			416	369		
High Cold Leg Reverse Flow Resistance	400	373	377	355		310
130% Components Heat Transfer Coefficient	421	398	396		330	311
70% Components Heat Transfer Coefficient	407	396	380		326	
200% Loop Flow Resistance		394	387			
Cold Leg LOCA		457	415	377	345	328

Table 2.5. The TH uncertainty representative scenarios of the event category of 1.5" – 4" LOCA and their probabilities of the Oconee NPP.

ID	Frequency**	Mean CPF*	Brief Scenario Description
145	1.34E-4	0	1.5" surge line LOCA *= 130% break area + Hi CL Rev. K
141	1.06E-4	1.11E-5	2.8" surge line LOCA *= 130% break area + Hi CL Rev. K
142	1.06E-4	9.12E-7	2.8" surge line LOCA *= 70% break area + Hi CL Rev. K
172	1.06E-4		4" cold leg LOCA + Hi CL Rev. K + Sump recirculation (modification of #143)
154	1.34E-4	4.98E-6	4" surge line LOCA *= 70% + VV Closed + Hi CL Rev. K + Sump recirculation

*FAVOR (v02.2 1/2) results, OCNPFM.doc, May 24, 2002
**PRA results, O-new-m.xls, Oct. 8, 2002

Table 2.6. The TH uncertainty representative scenarios of the event category of 4" – 8" LOCA and their probabilities of the Oconee NPP.

ID	Frequency**	Mean CPF*	Brief Scenario Description
178	1.34E-4	4.98E-6	4" surge line LOCA + Hi CL Rev. K + Sump recirculation
160	1.82E-5	8.93E-5	5.7" surge line LOCA + Hi CL Rev. K + Sump recirculation
164	2.12E-5	1.14E-4	8" surge line LOCA + Hi CL Rev. K + Sump recirculation

*FAVOR (v02.2 1/2) results, OCNPFM.doc, May 24, 2002
**PRA results, O-new-m.xls, Oct. 8, 2002

Table 2.7. The TH uncertainty representative scenarios of the event category of greater than 8" LOCA and their probabilities of the Oconee NPP.

ID	Frequency**	Mean CPF*	Brief Scenario Description
156	7.03E-6	1.50E-4	16" surge line LOCA + Hi CL Rev. K + Sump recirculation

*FAVOR (v02.2 1/2) results, OCNPFM.doc, May 24, 2002
**PRA results, O-new-m.xls, Oct. 8, 2002

Table 2.8. The TH uncertainty representative scenarios of the event category of reactor trips during full power operation causing PZR SRV stuck open and remaining open and their probabilities of the Oconee NPP.

ID	Frequency**	Mean CPF*	Brief Scenario Description
146	4.23E-5	1.12E-7	SRV open area *= 70% + summer + VV Close
147	3.63E-5	2.68E-7	Summer
148	4.23E-5	0	SRV open area = 1.5" + Comp. HTC *= 130%, RCPs trip

*FAVOR (v02.2 1/2) results, OCNPFM.doc, May 24, 2002
**PRA results, O-new-m.xls, Oct. 8, 2002

Table 2.9. The TH uncertainty representative scenarios of the event category of reactor trips during hot zero power operation causing PZR SRV stuck open and remaining open and their probabilities of the Oconee NPP.

ID	Frequency**	Mean CPF*	Brief Scenario Description
169	7.33E-6	1.73E-6	SRV open area *= 70% + summer + VV Close + HZP
170	6.28E-6		Summer + HZP
171	7.33E-6		SRV open area = 1.5" + Comp. HTC *= 130%, RCPs trip + HZP

*FAVOR (v02.2 1/2) results, OCNPFM.doc, May 24, 2002
**PRA results, O-new-m.xls, Oct. 8, 2002

Table 2.10. The TH uncertainty representative scenarios of the event category of reactor trips during full power operation causing PZR SRV stuck open and reseated later by itself and their probabilities of the Oconee NPP.

ID	Frequency**	Mean CPF*	Brief Scenario Description
112	1.25E-4	4.45E-7	SRV reseated @ 100 min; HPI throttle @ 1 minute after it can be throttled
113	5.07E-5	7.69E-5	SRV reseated @ 100 min; HPI throttle @ 10 minute after it can be throttled
109	9.58E-6	7.23E-5	SRV reseated @ 100 min; HPI is not throttled
114	1.25E-4	3.92E-12	SRV reseated @ 50 min; HPI throttle @ 1 minute after it can be throttled
115	5.07E-5	1.55E-8	SRV reseated @ 50 min; HPI throttle @ 10 minute after it can be throttled
149	9.58E-6	3.48E-7	represents SRV reseated @ 50 min; HPI is not throttled

*FAVOR (v02.2 1/2) results, OCNPFM.doc, May 24, 2002
**PRA results, O-new-m.xls, Oct. 8, 2002

Table 2.11. The TH uncertainty representative scenarios of the event category of reactor trips during hot zero power operation causing PZR SRV stuck open and reseated later by itself and their probabilities of the Oconee NPP.

ID	Frequency**	Mean CPF*	Brief Scenario Description
121	2.28E-5	3.03E-6	SRV reseated @ 100 min; HPI throttle @ 1 minute after it can be throttled + HZP
122	7.57E-6	1.78E-4	SRV reseated @ 100 min; HPI throttle @ 10 minute after it can be throttled + HZP
165	1.76E-6	2.71E-4	SRV reseated @ 100 min; HPI is not throttled + HZP
123	2.28E-5	6.53E-7	SRV reseated @ 50 min; HPI throttle @ 1 minute after it can be throttled + HZP
124	7.57E-6	5.26E-5	SRV reseated @ 50 min; HPI throttle @ 10 minute after it can be throttled + HZP
168	1.76E-6	5.43E-5	represents SRV reseated @ 50 min; HPI is not throttled + HZP

*FAVOR (v02.2 1/2) results, OCNPFM.doc, May 24, 2002
**PRA results, O-new-m.xls, Oct. 8, 2002

Table 2.12. The sensitivity runs matrix of the Palisade PTS study for primary side breach related scenarios. The values are the average downcomer temperature of the first 10,000 seconds in Kelvin.

Break Size (in inch diameter)	1.4	2	2.8	4	5.7	8
Nominal	482	427	391	350	320	310
Winter*	476	419	374	334	304	294
Summer*	490	437	404	364	333	325
110% m(HPI)	478	422	386			
90% m(HPI)	488	432	397			
100 % HPI Failed	550	532	501			
HZP (0.7%)	450	406	364	333	319	310
HZP (0.2%)	416	380	351	330	318	309
130% Components Heat Transfer Coefficient	486	433	402	355		
70% Components Heat Transfer Coefficient	479	425	389	346		
70% Break Area		440	415	370	334	313
130% Break Area		418	373	338	314	309
Cold Leg LOCA	491	465	430	373	352	332

*Winter [T(HPI)= 4.4 °C/40 °F, T(LPI)= 4.4 °C/40 °F]
*Summer [T(HPI)= 37.8 °C/100 °F, T(LPI)= 37.8 °C/100 °F]
*Spring/Fall [T(HPI)= 21.1 °C/70 °F, T(LPI)= 21.1 °C/70 °F]

Table 2.13. The TH uncertainty representative scenarios of the event category of 1.4" – 4" LOCA and their probabilities of the Palisade NPP.

ID	Frequency**	Mean CPF*	Brief Scenario Description
58	2.66E-4	4.25E-5	4" cold leg LOCA in winter
59	2.09E-4	8.55E-8	4" cold leg LOCA in summer
60	2.09E-4	7.79E-7	2" surge line LOCA in winter
61	2.09E-4		2.8" surge line LOCA in summer
2	2.66E-4		1.4" surge line LOCA

*FAVOR results based on 60 EPFY, Nov. 22, 2002
**PRA results M_M&M.exl, Oct. 31, 2002

Table 2.14. The TH uncertainty representative scenarios of the event category of 4" – 8" LOCA and their probabilities of the Palisade NPP.

ID	Frequency**	Mean CPF*	Brief Scenario Description
62	7.07E-6	2.21E-4	8" cold leg LOCA in winter
63	6.06E-6	1.12E-4	5.7" cold leg LOCA in winter
64	7.07E-6	6.20E-5	4" surge line LOCA in summer

*FAVOR results based on 60 EPFY, Nov. 22, 2002
**PRA results M_M&M.exl, Oct. 31, 2002

Table 2.15. The TH uncertainty representative scenario of the event category greater than 8" LOCA of the Palisade NPP.

ID	Frequency**	Mean CPF	Brief Scenario Description
40	3.22E-5	2.13E-5	16" surge line LOCA

**PRA results M_M&M.exl, Oct. 31, 2002

Table 2.16. The design and results of the sensitivity scenarios of the Beaver Valley NPP. The values inside parentheses are the average temperature of the first 10,000 seconds (unit in Kelvin).

Break Size (in inch diameter)	1.4	2	2.8	4	5.7	8	1 SRV	2 SRVs
Nominal	459	371	336	319	313	300	393	350
Winter*	457	366	333	318	316	297		
Summer*	460	371	344	331	319	303		
110% m(HPI)		362	334					
90% m(HPI)	466	373	341					
100 % HPI Failed	521	496	432					
HZP (0.7%)	360	348	325	312	304	299		
HZP (0.2%)	353	337	312	309	302	298		
130% Components Heat Transfer Coefficient	462	374	342	324		301		
70% Components Heat Transfer Coefficient	455	362	331	321				
130% Break Area		329	325	307	301	301		
70% Break Area		359	359	324	306	306		
Cold Leg LOCA	455	453	415	369	347	340		

*Water temperature during Summer: T(HPI)= 55°F, T(ACCU)= 105°F ,T(LPI)= 55°F
*Water temperature during Spring/fall: T(HPI)= 50°F, T(ACCU)= 90°F ,T(LPI)= 50°F
*Water temperature during winter: T(HPI)= 45°F, T(ACCU)= 75°F ,T(LPI)= 45°F

Table 2.17. The TH uncertainty representative scenarios of the event category of 1.4"– 4" LOCA and their probabilities of the Beaver Valley NPP.

ID	Frequency**	Mean CPF*	Brief Scenario Description
56	1.23E-4	3.97E-5	4" surge line LOCA in summer; reactor trips at hot zero power operation (0.7% of full power)
114	9.76E-5		2.8" surge line LOCA in summer; with 130% component heat transfer coefficient
3	9.76E-5		2" surge line LOCA; 90% of nominal HPI flow rate
115	9.76E-5		2.8" cold leg LOCA
2	1.23E-4		1.4" cold leg LOCA in winter

*FAVOR results based on 60 EPFY, Nov. 22, 2002
** PRA results, BV-m.xls, Oct. 8, 2002

Table 2.18. The TH uncertainty representative scenarios of the event category of 4" – 8" LOCA and their probabilities of the Beaver Valley NPP.

ID	Frequency**	Mean CPF*	Brief Scenario Description
7	2.11E-5	2.98E-5	8" surge line LOCA; with 30% reduced break area
116	1.81E-5		5.7" cold leg LOCA; with 30% reduced break area
117	2.11E-5		5.7" cold leg LOCA in summer

*FAVOR results based on 60 EPFY, Nov. 22, 2002
** PRA results, BV-m.xls, Oct. 8, 2002

Table 2.19. The TH uncertainty representative scenarios of the event category greater than 8" LOCA and their probabilities of the Beaver Valley NPP.

ID	Frequency**	Mean CPF*	Brief Scenario Description
9	6.99E-6	2.52E-5	16" surge line LOCA

*FAVOR results based on 60 EPFY, Nov. 22, 2002
** PRA results, BV-m.xls, Oct. 8, 2002

Table 2.20. The TH uncertainty representative scenarios of the event category of PZR valves stuck open without reseating and their probabilities of the Beaver Valley NPP.

ID	Frequency**	Mean CPF	Brief Scenario Description
14	2.23E-4		1 SRV SO and remaining open, full power
72	5.14E-7		1 SRV SO and remaining open, full power, no HPI
34	4.95E-7		2 SRVs SO and remaining open, full power
65	1.04E-9		2 SRVs SO and remaining open, full power, no HPI
66	1.18E-7		2 SRVs SO and one reseated at 50 minutes, full power
67	1.18E-7		2 SRVs SO and one reseated at 100 minutes, full power
83	3.51E-6		2 PORVs SO and remaining open, full power
78	3.25E-8		Open all ADVs after loss of MFW and AFW
31	3.10E-7		Open all PZR PORVs and HPI on with loss of feed water
75	2.95E-4		MFW overfed all SGs and SG remain as liquid solid
94	4.10E-5		1 SRV SO and remaining open, HZP
73	6.55E-8		1 SRV SO and remaining open, HZP, no HPI, all ADVs are open 5 minutes after HPI fails to start
64	8.67E-8		2 SRVs SO and remaining open, HZP
92	2.13E-7		2 SRVs SO and one reseated at 50 minutes, HZP
93	2.13E-7		2 SRVs SO and one reseated at 100 minutes, HZP
76	1.06E-4		2 PORVs SO and remaining open, HZP

** PRA results, BV-m.xls, Oct. 8, 2002

Table 2.21. The TH uncertainty representative scenarios of the event category of one PZR valve stuck open and reseated later by itself and their probabilities when reactor trips during full power operation of the Beaver Valley NPP.

ID	Frequency**	Mean CPF	Brief Scenario Description
59	3.46E-4		1 SRV stuck open; reseated at 50 minutes; HPI has not been throttled
95	1.34E-4		1 SRV stuck open; reseated at 100 minutes; HPI is throttled at 1 minute after it can be throttled
96	1.87E-4		1 SRV stuck open; reseated at 100 minutes; HPI is throttled at 10 minute after it can be throttled
60	2.15E-5		1 SRV stuck open; reseated at 100 minutes; HPI has not been throttled
82	1.51E-6		1 SRV stuck open, no HPI, all ADVs are open 5 minutes after HPI fails to start

** PRA results, BV-m.xls, Oct. 8, 2002
Notes: 1 SRV stuck open and reseated at 50 minutes and that HPI is throttled at 1 and 10 minutes are eliminated due to low event frequencies

Table 2.22. The TH uncertainty representative scenarios of the event category of one PZR valve stuck open and reseated later by itself and their probabilities when reactor trips during hot zero power operation of the Beaver Valley NPP.

ID	Frequency**	Mean CPF	Brief Scenario Description
99	2.59E-5		1 SRV stuck open; reseated at 50 minutes; HPI is throttled at 1 minute after it can be throttled; HZP
101	3.09E-5		1 SRV stuck open; reseated at 50 minutes; HPI is throttled at 10 minute after it can be throttled; HZP
97	3.74E-6	2.54E-5*	1 SRV stuck open; reseated at 50 minutes; HPI has not been throttled; HZP
98	2.59E-5		1 SRV stuck open; reseated at 100 minutes; HPI is throttled at 1 minute after it can be throttled; HZP
100	3.09E-5		1 SRV stuck open; reseated at 100 minutes; HPI is throttled at 10 minute after it can be throttled; HZP
71	3.74E-6		1 SRV stuck open; reseated at 100 minutes; HPI has not been throttled; HZP

*FAVOR results based on 60 EPFY, Nov. 22, 2002
** PRA results, BV-m.xls, Oct. 8, 2002

Table 2.23. The TH uncertainty representative scenarios of the event category of two PZR valves stuck open and reseated later by itself and their probabilities when reactor trips during full power operation of the Beaver Valley NPP.

ID	Frequency**	Mean CPF	Brief Scenario Description
61	1.79E-6		2 SRV stuck open; reseated at 50 minutes; HPI has not been throttled
86	6.84E-7		2 SRV stuck open; reseated at 100 minutes; HPI is throttled at 1 minute after it can be throttled
87	9.98E-7		2 SRV stuck open; reseated at 100 minutes; HPI is throttled at 10 minute after it can be throttled
62	1.08E-7		2 SRV stuck open; reseated at 100 minutes; HPI has not been throttled
68	1.33e-8		2 SRV stuck open; no HPI, all ADVs are open 5 minutes after HPI fails to start

** PRA results, BV-m.xls, Oct. 8, 2002
Notes: 2 SRV stuck open and reseated at 50 minutes and that HPI is throttled at 1 and 10 minutes is eliminated due to low event frequencies

Table 2.24. The TH uncertainty representative scenarios of the event category of two PZR valves stuck open and reseated later by itself and their probabilities when reactor trips during hot zero power operation of the Beaver Valley NPP.

ID	Frequency**	Mean CPF	Brief Scenario Description
88	1.33E-7		2 SRV stuck open; reseated at 50 minutes; HPI is throttled at 1 minute after it can be throttled; HZP
90	1.65E-7		2 SRV stuck open; reseated at 50 minutes; HPI is throttled at 10 minute after it can be throttled; HZP
69	2.09E-8		2 SRV stuck open; reseated at 50 minutes; HPI has not been throttled; HZP
89	1.33E-7		2 SRV stuck open; reseated at 100 minutes; HPI is throttled at 1 minute after it can be throttled; HZP
91	1.65E-7		2 SRV stuck open; reseated at 100 minutes; HPI is throttled at 10 minute after it can be throttled; HZP
70	2.09E-8		2 SRV stuck open; reseated at 100 minutes; HPI has not been throttled; HZP

** PRA results, BV-m.xls, Oct. 8, 2002

2.3 Probabilistic Fracture Mechanics

The PFM model estimates the probability of a through-wall crack developing in the RPV as the consequence of a particular thermal hydraulic challenge. Figure 2.4 illustrates how the PFM model connects to both the PRA and TH models discussed in Section 2.1 and 2.2, respectively.

The Figure also illustrates the sub-models that comprise the PFM model: a toughness and embrittlement model, a flaw distribution model, and a nucleonics model. These sub-models are described in Sections 2.3.1, 2.3.2, and 2.3.3, respectively. The computer code FAVOR (**F**racture **A**nalysis of **V**essels, **O**ak **R**idge) is the implementation of this model used in this investigation [FAVOR 02].

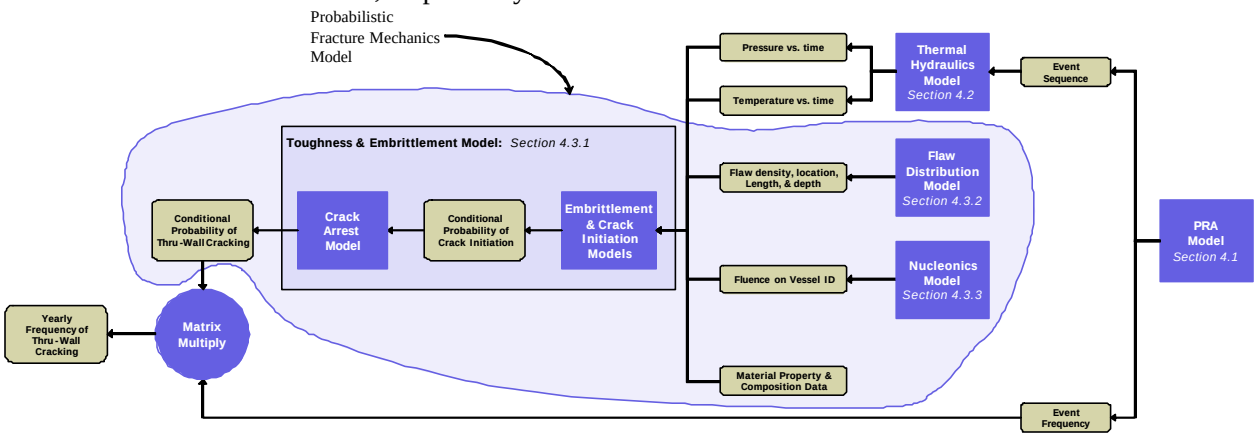

Figure 2.4. Illustration of the interrelationships between PFM model and the TH and PRA models, and of the three principal sub-models that comprise the PFM model.

2.3.1 Toughness and Embrittlement Model

A working party including representatives from both the NRC and from the commercial nuclear power industry completed a comprehensive *Evaluation and Characterization of Uncertainty in Fracture Toughness Models for Ferritic Reactor Pressure Vessel Steels*. The report of this working party [Natishan 02] provides the technical justification for a physically motivated toughness and embrittlement model, and also provides an assessment of uncertainties associated with this model. In Appendix A we summarize the findings arrived at by the working party, and use this information as the basis for recommending a treatment of uncertainties for incorporation into FAVOR that is consistent with PRA requirements expressed in Section 1.6.1. In this Section we begin (Section 2.3.1.1) with a discussion of how fracture mechanics is used to estimate the response of the RPV to a particular thermal-hydraulic challenge. This is followed with a description (Section 2.3.1.2) of how we developed the toughness and embrittlement models, and how we characterized uncertainties in these models. We then describe a few of the specifics of the crack initiation index toughness model (Section 2.3.1.3), the irradiation model (Section 2.3.1.4), the crack arrest toughness model (Section 2.3.1.5), and the warm pre-stress model (Section 2.3.1.6). Finally, in Section 2.3.1.7 we bring these individual models together to specify the complete toughness and embrittlement model used in the FAVOR code.

2.3.1.1 Use of Fracture Mechanics to Estimate the Response of the RPV to a Particular Thermal Hydraulic Challenge

The variation of temperature and pressure with time produced by a particular sequence of operational events establishes a time-dependent stress state in the wall of the RPV. Should flaws exist in the vessel wall, these stresses give rise to a time dependent *driving force to fracture* (K_I).

Should the applied value of K_I exceed the *initiation fracture toughness* (K_{Ic}) of the material the flaw will grow larger, and will continue to grow unless the applied K_I for the larger flaw falls below the *arrest fracture toughness* (K_{Ia}) of the material. The values of K_{Ic} and K_{Ia} depend on both the degree of irradiation damage the steel has experienced and on the temperature of the steel. Thus, to estimate the frequency with which a through wall crack can be expected to develop in the RPV wall as a consequence of a particular thermal hydraulic challenge models are needed for the initiation fracture toughness, for the arrest fracture toughness, and for the effect of irradiation and temperature on both K_{Ic} and K_{Ia}.

2.3.1.2 Approach to Model Development and Uncertainty Characterization

As discussed in Section 1.6.1, our approach requires an explicit identification of the type of uncertainty present (aleatory or epistemic) to enable the development of an appropriate mathematical model. To do this it is first necessary to establish an independent, physically motivated, model of crack initiation and arrest toughness that accounts for the effects of irradiation damage and temperature. The approach used by the NRC / Industry working party to achieve this goal is summarized below.

- Uncertainty Identification: The working party began by constructing a graphical description of the current toughness model. This description, called a "root cause diagram," is illustrated schematically in Figure 2.5. Diagrams of this type show *all* of the parameters (shaded boxes) and *all* of the relationships (nodes) used to estimate the fracture toughness for a particular set of conditions. Decomposing the toughness / embrittlement model in this way permitted identification of individual sources of uncertainty, both in the parameters and in the relationships assumed between the parameters.
- Uncertainty Classification: Uncertainties were classified through an understanding of the basic physical mechanisms responsible for crack initiation, for crack arrest, and for irradiation damage. Without this physical understanding, it was impossible to distinguish the irreducible (i.e. aleatory) uncertainties associated with variability of the material from reducible (i.e. epistemic) uncertainties caused by limited data, imperfect models, and so on.
- Uncertainty Quantification: The physical understanding developed to classify uncertainty types also played a pivotal role in uncertainty quantification because a model of fracture toughness that can be regarded as representing the true behavior of the material is needed to quantify the uncertainties present in any other model. Therefore, uncertainty quantification was achieved by comparing the RT_{NDT}-based toughness model developed for use in the PTS re-evaluation project to this best-estimate model.

To be consistent with LEFM principles, LEFM-valid K_{Ic} and K_{Ia} values were used by the working party to calibrate the parameters of this best estimate model. However, the best-estimate model cannot be constructed as a purely empirical fit to these K_{Ic} and K_{Ia} values. Without the insights available from a physically based understanding it was impossible to discern if the trends demonstrated by the laboratory data can be expected to apply to the material and loading conditions of interest in commercial pressurized water reactors. Consequently, the "best estimate models" developed by the working party each had a form motivated by the physical processes responsible for crack initiation, crack arrest, or irradiation damage.

2.3.1.3 Crack Initiation Model

As illustrated in Figure 2.6, the crack initiation model includes two major components. The first component is a model describing the scatter and temperature dependency of the resistance of the RPV steel to crack initiation in cleavage (K_{Ic}). As discussed at length in Appendix A, an understanding of the physical nature of cleavage fracture in ferritic steels demonstrates that the scatter in and temperature dependency of K_{Ic}

data are features *universal* to all RPV steels, features that within this class of materials are insensitive to all individual and combined effects of alloying, heat treatment (and other thermal processing), mechanical processing, and irradiation. These factors *only* influence the temperature range over which a particular steel experiences a transition from brittle behavior (at low temperatures) to ductile behavior (at higher temperatures). Thus, the second parameter of the crack initiation model is an index temperature value that is used to locate the K_{Ic} transition curve for a specific material condition (i.e., a specific combination of composition, heat treatment, and irradiation) on the temperature axis.

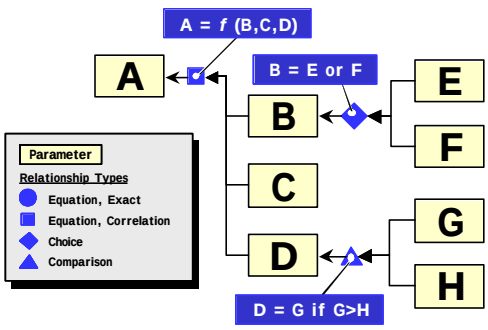

Figure 2.5. Illustration of a root cause diagram showing how uncertainties in input variables (E, F, G, and H) propagate through models (nodes), themselves potentially having uncertainty, to produce uncertainty in a resultant value (A).

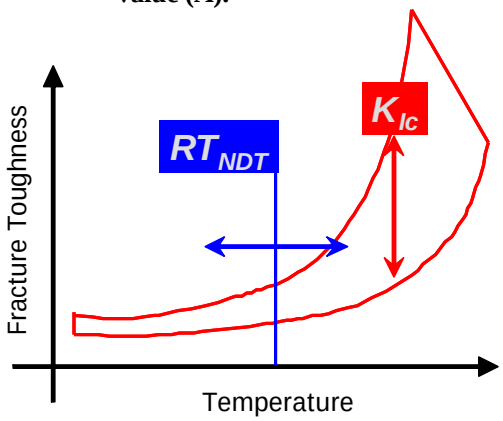

Figure 2.6. Schematic illustrating the key components of the crack initiation model.

To enable all commercial operators of pressurized water reactors to assess the state of their RPV relative to the new PTS screening criteria without the need to make new material property measurements, it was decided that the initiation fracture toughness of the RPV should to be estimated using the index temperature RT_{NDT} [ASME NB2331] because RT_{NDT} value have already been established for all steels in operating PWRs. The value of RT_{NDT}, which is defined by ASME NB-2331 based on the following model:

Eq. 2-2 $$RT_{NDT} = MAX\{T_{NDT}, T_{35/50} - 60\}$$

where

T_{NDT} is the nil-ductility temperature determined by testing NDT specimens as per ASTM E208,

$T_{35,50}$ is the transition temperature at which Charpy-V notch (CVN) specimens tested as per ASTM E23 exhibit at least 35 mills lateral expansion and 50 ft-lbs absorbed energy.

was intended to account for the combined effects of alloying, heat treatment (and other thermal processing), mechanical processing, and irradiation on the fracture toughness transition temperature, thereby allowing a single toughness transition curve to represent all RPV steels. However, neither NDT nor CVN tests actually measure fracture toughness, so RT_{NDT} can only be correlated with the fracture toughness transition temperature. As a consequence, RT_{NDT}-based models of fracture toughness have a known and intentional conservative bias that, as illustrated in Figure 2.7, is highly inconsistent from material to material. To quantify this bias the Working Party collected data sets for RPV steels from the literature that contained both enough K_{Ic} data at different temperatures to define the K_{Ic} transition curve as well as a NB-2331 valid estimate of RT_{NDT} to permit positioning of the ASME K_{Ic} curve. A parameter ? $RT_{epistemic}$ was defined as the temperature shift needed to make a NB-2331 RT_{NDT}-positioned K_{Ic} curve lower bound the K_{Ic} data. A cumulative distribution function constructed from ? $RT_{epistemic}$ values for 18 different heats of RPV plate, welds, and forgings

(see Figure 2.8) was proposed by the Working Party as a quantification of the epistemic uncertainty in RT_{NDT}. This model, when combined with the statistical fit to the K_{Ic} data for these 18 steels (see Figure 2.9) comprises the crack initiation model used in the PTS re-evaluation project**. Mathematically, this model is as follows:

Eq. 2-3 $$\Delta RT_{epistemic} = -40.02 + 124.88\left[-\ln(1-R)\right]^{0.51}$$

Eq. 2-4
$$K_{Ic}(\Delta T) = a_{K_{Ic}}(\Delta T) + b_{K_{Ic}}(\Delta T)\left[-\ln(1-P)\right]^{1/c_{K_{Ic}}} \quad \text{for } 0 \le P < 1$$

where

R	is a random number between 0 and 1
K_{Ic}	is in ksiÖin
T	is the temperature in °F,
ΔT	is T-(RT_{NDT}-$RT_{epistemic}$), in °F,
P	is the fracture probability, and

$$a_{K_{Ic}}(\Delta T) = 19.35 + 8.335\exp\left[0.02254(\Delta T)\right] \ [\text{ksi}\sqrt{\text{in.}}]$$
$$b_{K_{Ic}}(\Delta T) = 15.61 + 50.132\exp\left[0.008(\Delta T)\right] \ [\text{ksi}\sqrt{\text{in.}}]$$
$$c_{K_{Ic}} = 4$$
$$-250°\text{F} \le \Delta T \le +50°\text{F}$$

2.3.1.4 Irradiation Model

Because the effects of irradiation of RPV steel influence neither the temperature dependency nor the scatter in initiation fracture toughness, it is simply necessary to quantify the shift in the initiation fracture toughness index temperature produced by irradiation (see Figure 2.10). To enable all commercial operators of pressurized water reactors to assess the state of their RPV relative to the new PTS screening criteria without the need to make new material property measurements, it was decided that this index temperature shift should be estimated using only currently available data on composition (e.g. Cu, Ni, P) and irradiation conditions (e.g. flux, time, temperature, fluence). Unfortunately, the most comprehensive irradiation effects models available today relate these variables to the shift in CVN energy transition temperature (DT_{30}) rather than to shifts in the initiation toughness transition temperature. This focus on DT_{30} occurs due to the historical practices of measuring Charpy shift as part of RPV surveillance programs, and of using DT_{30} as an approximate measure of the effect of irradiation on the shift in the initiation fracture toughness transition temperature. Consequently, the working party proposed to combine a physically motivated Charpy shift model with a physically motivated, empirically calibrated conversion between Charpy-shift and initiation fracture toughness transition temperature shift. The embrittlement model used in the PTS re-evaluation project is as follows:

Eq. 2-5 $$\Delta T_{30} = A\exp\left(\frac{19310}{T_c + 460}\right)(1 + 110P)(ft)^{0.4601} + B\left(1 + 2.40Ni^{1.250}\right)f(Cu)g(ft) + Bias$$

where

$$A = \begin{Bmatrix} 8.86\text{x}10^{-17}, \text{ welds} \\ 9.30\text{x}10^{-17}, \text{ forgings} \\ 12.7\text{x}10^{-17}, \text{ plates} \end{Bmatrix},$$

$$B = \begin{Bmatrix} 230, \text{ welds} \\ 132, \text{ forgings} \\ 206, \text{ plates in CE vessels} \\ 156, \text{ other plates} \end{Bmatrix}$$

$$f(Cu) = \begin{Bmatrix} 0, Cu \le 0.072 \text{ wt\%} \\ (\text{Cu - }0.072)^{0.659}, Cu > 0.072 \text{ wt\%} \end{Bmatrix},$$

$$g(ft) = \frac{1}{2} + \frac{1}{2}\tanh\left[\frac{\log\left(ft + 4.579\text{x}10^{12}t_i\right) - 18.265}{0.713}\right]$$

$$Cu_{\max} = \begin{Bmatrix} 0.25, \text{ for welds with Linde 80 or Linde 0091 flux} \\ 0.305, \text{ for everything else} \end{Bmatrix}$$

$$Bias = \begin{Bmatrix} 0, t_i < 97000 \text{ h} \\ 9.4, t_i \ge 97000 \text{ h} \end{Bmatrix}$$

Eq. 2-6 $$\Delta RT_{NDT} = \alpha \cdot \Delta T_{30}$$

where α = 0.99 for welds and 1.10 for plates and forgings.

** Appendix xx provides justification for the appropriateness of applying the RT_{NDT} bias correction of Figure 2.8 and the K_{Ic} model of Figure 2.9 to all RPV steels.

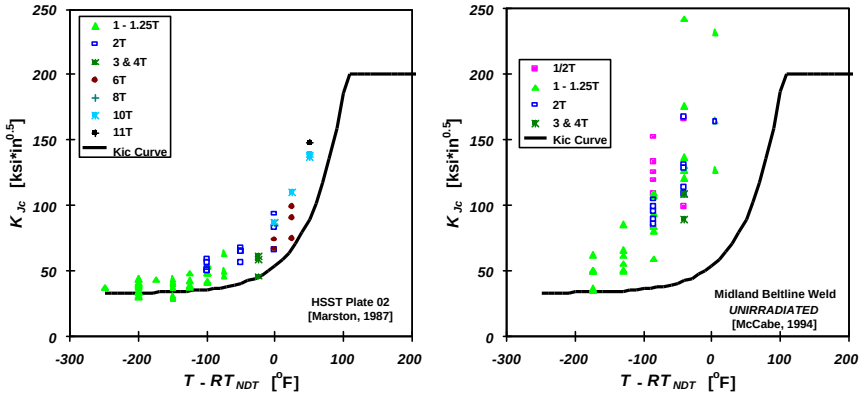

Figure 2.7. Illustration of the inconsistency with which RT_{NDT} positions a K_{Ic} curve relative to measured fracture toughness data.

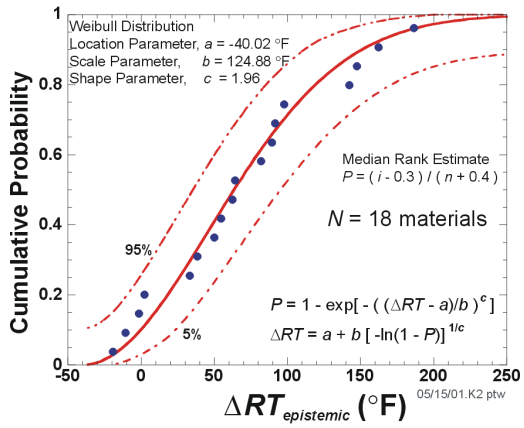

Figure 2.8. Illustration of $DRT_{epistemic}$ cumulative distribution function.

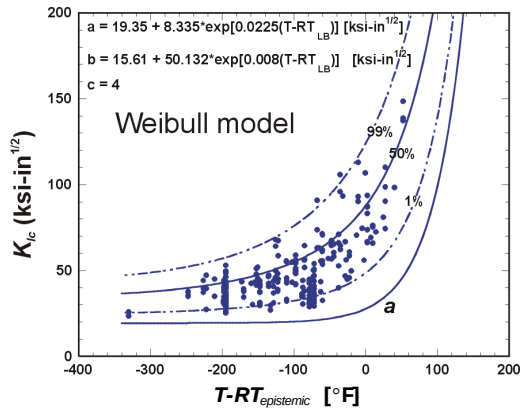

Figure 2.9. K_{Ic} model constructed from K_{Ic} data for 18 heats of RPV plates, welds, and forgings.

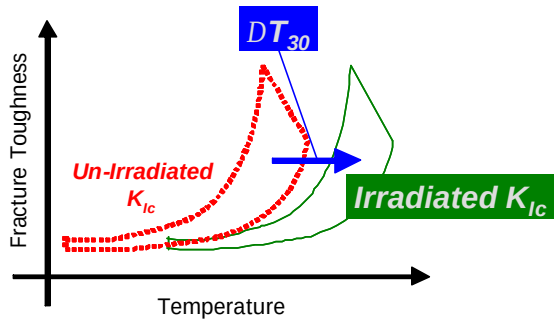

Figure 2.10. Schematic illustrating the key component of the irradiation shift model.

2.3.1.5 Crack Arrest Model

The information presented in Appendix A suggests that a K_{Ia} model can be defined from the following four elements:

1. A temperature dependency
2. A description of scatter in K_{Ia} data
3. An index temperature that defines the position of the K_{Ia} transition curve on the temperature axis, and
4. A relationship between the index temperatures for the initiation and arrest fracture toughness curves.

As was the case with the initiation fracture toughness model summarized in Section 2.3.1.3, the temperature dependency of K_{Ia} data is universal to all reactor pressure vessel steels. Within this class of materials the temperature dependency is insensitive to all individual and

combined effects of alloying, heat treatment (and other thermal processing), mechanical processing, and irradiation. These material variables only influence the temperature range over which a particular steel experiences a transition from brittle behavior (at low temperatures) to ductile behavior (at higher temperatures), this being quantified by a heat specific index temperature value called T_{KIa} that is defined from crack arrest toughness data. Furthermore, the information presented in Appendix A suggests that the relationship between the index temperatures for crack initiation and crack arrest toughness is also not expected to be influenced strongly by heat specific factors. Consequently, as illustrated schematically in Figure 2.11, the working party recommended that the crack arrest model be specified by the use of a shift between the crack initiation and crack arrest transition curves (DRT_{ARREST}) coupled with a crack arrest toughness transition curve. Figure 2.12 illustrates the model for DRT_{ARREST} derived from data on several dozen RPV steels while Figure 2.13 depicts the crack arrest toughness transition curve fit to data from three particularly well populated data sets[††]. This crack arrest model is specified mathematically as follows:

Eq. 2-7

$$\Delta RT_{ARREST} \equiv 44.1 \cdot \exp\left\{-0.006\frac{RT_{INIT} - 14.4 - 32}{1.8}\right\}$$

Eq. 2-8

$$m_{\ln(K_{Ia})}(\Delta T_{RELATIVE}) = \ln\left[\bar{K}_{Ia}(\Delta T_{RELATIVE})\right] - \frac{s^2_{\ln(K_{Ia})}}{2}$$

where

$$s_{\ln(K_{Ia})} = 0.18$$

$$\bar{K}_{Ia}(\Delta T_{RELATIVE}) = 27.302 + 69.962\exp\left[0.006057(\Delta T_{RELATIVE})\right] \quad [\text{ksi}\sqrt{\text{in.}}]$$

where

T = temperature [°F]
$RT_{INIT} = RT_{NDT} - DRT_{epistemic}$
$RT_{ARREST} = RT_{INIT} + 14.4 + DRT_{ARREST}$
$DT_{relative} = T - RT_{ARREST}$

[††] Appendix C provides justification for the appropriateness of applying this crack arrest model to all RPV steels.

It should be noted that no information beyond that used in the crack initiation model (Eq. 2-2 and Eq. 2-3) and in the irradiation model (Eq. 2-5 and Eq. 2-6) is used in Eq. 2-7. Thus, Eq. 2-7 can be evaluated without the need to make new material property measurements.

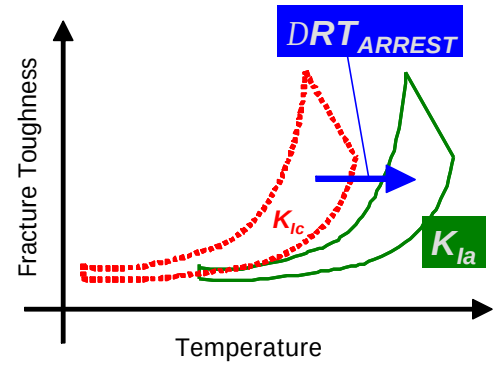

Figure 2.11. Schematic illustrating the key component of the irradiation shift model.

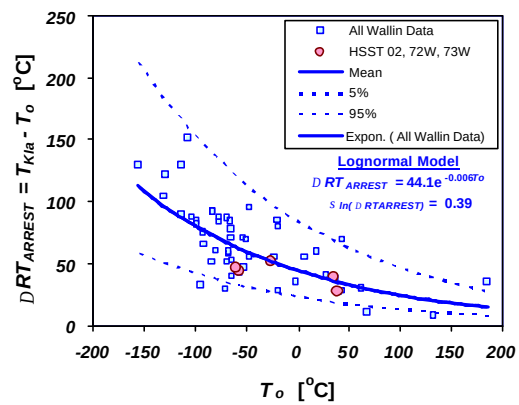

Figure 2.12. Data for RPV and other steels showing how the temperature separation between the crack arrest and crack initiation transition curves (vertical axis) varies with the crack initiation transition temperature (horizontal axis).

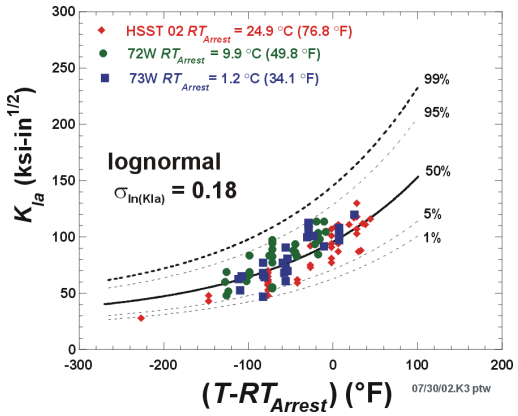

Figure 2.13. K_{Ia} model recommended for use in the PTS re-evaluation effort.

2.3.1.6 Warm Pre-Stress Model

Warm pre-stress (WPS) effects were first noted in the literature in 1963 [Brothers 63]. These investigators reported (as have many since them) that the apparent fracture toughness of a ferritic steel can be elevated in the fracture mode transition regime if the specimen is first "pre-stressed" at an elevated temperature. Once a specimen is subjected to a certain $K_{applied}$ and has not failed, the temperature can be reduced and the specimen will remain intact despite the fact that the process of reducing the temperature has also reduced the initiation fracture toughness (K_{Ic} or K_{Jc}) to values smaller than $K_{applied}$. In the past four decades, the physical mechanisms responsible for the WPS effect have been identified, studied extensively, and validated.

The types of loading that produce PTS challenges are characterized (generally) by a rapid cooldown on the inside of the RPV. This type of loading produces values of $K_{applied}$ that initially increase but later decrease as the transient progresses. Thus, depending upon the specifics of the transient (temperature gradients, flaw location, and so on) WPS may be effective, thereby preventing initiation of a cleavage crack even though $K_{applied}$ exceeds K_{Ic}. Nevertheless, to date PFM performed to assess the challenge to RPV integrity posed by pressurized thermal shock events have not included WPS as part of the PFM model [SECY-82-465, ORNL 85a, ORNL 85b, ORNL 86] for two reasons:

1. TH transients were previously represented as smooth variations of both pressure and temperature with time. However, data taken from operating nuclear plants demonstrates that actual TH transients are not always so well behaved. This created the possibility that, due to short duration fluctuations of pressure and/or temperature with time, the criteria for WPS might be satisfied by the idealized transient, but not by the real transient it was intended to represent.
2. In the past, the probabilistic risk assessment (PRA) models of human reliability (HR) were not sufficiently sophisticated to capture the potential for plant operators to re-pressurize the primary system as part of their response to a reactor vessel integrity challenge. Since such a re-pressurization would largely nullify the benefit of WPS, it was viewed as non-conservative to account for the benefit produced by WPS within a model that may also ignore the potentially deleterious effects of operator actions.

This re-evaluation PTS rule features both more realistic representations of the TH transients as well as much more sophisticated PRA/HR models that consider explicitly both acts of omission and commission on the part of plant operators. Consequently, on the basis of the information presented in Appendix B the staff has deemed it appropriate to incorporate WPS effects into the PFM model. Thus, in this model the following two requirements must ***BOTH*** be met for a crack to initiate:

Eq. 2-9 $$K_{applied} \geq K_{Ic(min)}$$
$$dK_{applied}/dt > 0$$

2.3.1.7 Complete Toughness and Embrittlement Model, and Major Differences from the Model Used to Support the Current PTS Screening Criteria

Figure 2.14 provides a diagrammatic representation of how FAVOR V02.4 implements the toughness and embrittlement model described in the preceding sections. Certain features of this model represent significant departures from PFM models used previously in evaluations of PTS risk, departures that are justified based the significantly increased state of knowledge regarding material deformation and fracture that has developed since the early 1980s (see Appendices C and D for supporting information). Specifically, the following features of the model depicted in Figure 2.14 differ from the PFM model used to support the current PTS screening criteria:

- The RT_{NDT} bias correction of Eq. 2-3 and Figure 2.8
- The K_{Ic} → K_{Ia} curve separation model of Eq. 2-7 and Figure 2.12
- The warm pre-stress model of Eq. 2-9

While there are many other differences between this model and that used to establish the current PTS screening criteria (again, see Appendices C and D for full details), these three differences are expected to have the most significant impact on the calculated values of through wall cracking frequency.

2.3.2 Flaw Distribution

One of the major unknowns / uncertainties identified in the last comprehensive evaluation of PTS [SECY-82-465] was the distribution of flaws assumed to exist in the RPV wall. This study used flaw models based on the Marshall study that included data from a limited population of nuclear vessels, and from many non-nuclear vessels [Marshall 82]. These flaw measurements were part of routine pre-service NDE examinations performed 25 or more years ago at vessel fabrication shops. Due to limitations of the NDE technology available at the time, the Marshall flaw distribution provides a reasonable representation only for flaws having depth dimensions larger than ≈1-in. The Marshall distribution was nevertheless applied in SECY-82-465 and in the IPTS studies [ORNL 85a, 85b, 86] by extrapolating fits to the data to the much smaller flaws of concern in PTS calculations (less than ≈¼-in.). Additionally, all flaws in the Marshall distribution were assumed to break the inner-diameter surface of the RPV despite the fact that the observations rarely, if ever, revealed surface breaking flaws in nuclear grade construction.

To improve on this very limited state of knowledge concerning the population of flaws likely to exist in nuclear grade construction, the NRC's Office of Nuclear Regulatory Research has sponsored a multi-year research project at the Pacific Northwest National Laboratory (PNNL) focused on making detailed destructive and non-destructive measurements of fabrication flaws in nuclear grade RPV welds and plates. A major product of this research has been recommendations for the flaw distributions to use in a probabilistic assessment of the resistance of a nuclear RPV to a PTS challenge [Simonen 02]. In this section we summarize the recommendations made in this document.

The recommendations of [Simonen 02] are based on a combination of experimental evidence, physical models, and expert opinions. However, whenever possible experimental evidence has either been used exclusively, or given the greatest "weight" in establishing the recommended flaw distributions. Table 2.25 summarizes the various sources of experimental data used in this study. As reflected in the table, the focus to date of this investigation has primarily been the definition of a flaw distribution for welds. Welds have been focused on because they typically exhibit larger flaws than plates or forgings, and because welds are typically more embrittled than either plates or forgings[‡‡].

[‡‡] To date no data has been collected on forgings. For the purposes of this study the plate flaw distributions are assumed to apply to the one forging in Oconee (none of the other three plants contain forgings). In follow-on work we will address forging flaw distributions including, specifically, consideration of the potential for under-clad cracking.

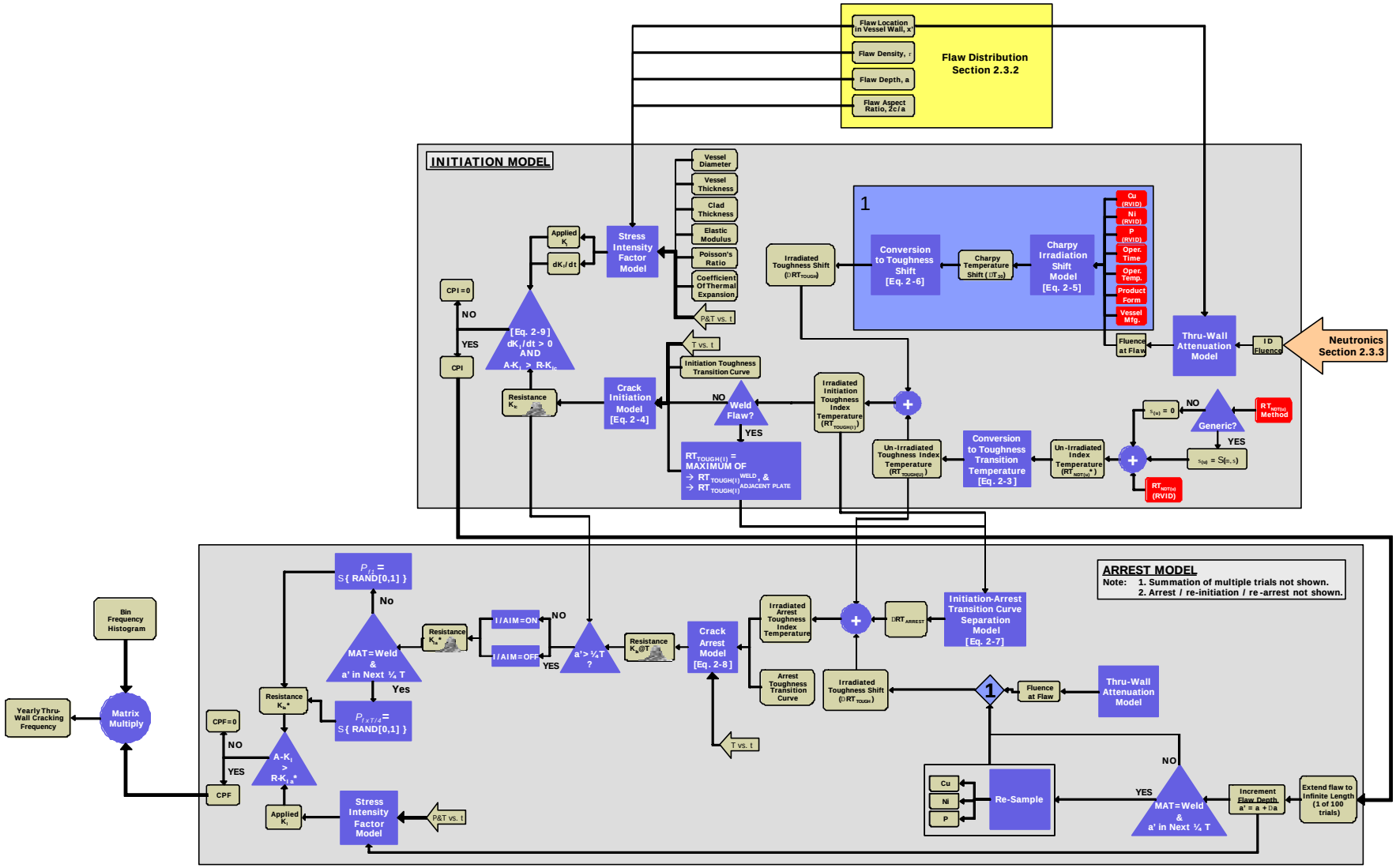

Figure 2.14. Flow diagram illustrating the key features of the toughness and embrittlement model adopted in the PTS re-evaluation project. Input parameters are shown in red, and models discussed in Section 2.3.1 are indicated by equation number. Details of the model not discussed in Section 2.3.1 are detailed in Appendices C and D.

In the following sections we summarize the findings of this study, and the recommended flaw distributions for buried flaws in welds (Section 2.3.2.1), for buried flaws in plates (Section 2.3.2.2), and for surface flaws in both plates and welds (Section 2.3.2.3).

Table 2.25. Summary of sources of experimental data sources for the flaw distribution.

Vessel	Weld	Plate	Clad
PVRUF	9150	855	1650
Shoreham	10375	975	--
Hope Creek	245	550	--
River Bend	2440	1465	--
Table entries represent volume of material examined in in^3.			

2.3.2.1 Distribution of Buried Flaws in Welds

The Simonen study made several observations regarding weld flaws:

1. Flaws in welds are distributed uniformly through the thickness of the RPV weld. There is no significant tendency for a greater density of flaws to occur either near the root or cap passes.
2. No surface breaking flaws were identified in all of the weld material examined, nor was a credible mechanism for surface flaw generation identified. Consequently, the flaw distributions recommended to characterize welds in the PTS re-evaluation study contain *only* buried flaws. This is a significant change from the Marshall flaw distribution used in the probabilistic calculations that established the current PTS rule, which contained *only* surface breaking flaws.
3. Virtually all non-volumetric flaws found in welds were lack of side-wall fusion defects that exist on the fusion line between the deposited weld metal and the plate or forging being joined. Consequently, the number of flaws in a particular weld can be expected to scale in proportion to the fusion line area of the weld. Additionally, this observation implies that axial welds contain *only* axially oriented flaws whereas circumferential welds contain *only* circumferentially oriented flaws.
4. Flaw densities exhibited statistically significant differences depending upon the welding process used (SAW, SMAW, GMAW, or repair weld). However, it is difficult in practice to ascertain from records precisely where different weld processes were used, or where repair welds were made. For this reason it was decided that the flaw distributions used in FAVOR PFM calculations would represent blended combinations of the SAW, SMAW, and REPAIR flaw distributions. Percentages of SAW and SMAW were established on a vessel specific basis. The percentage of repair weld was assumed to be 2% for all vessels analyzed. A repair weld volume of 2% exceeds slightly the repair percentage of 1.5% that was observed by PNNL for both the Shoreham and PVRUF vessels.
5. Flaw densities exhibited statistically significant differences depending upon the vessel examined (PVRUF or Shoreham). Since the results of the NRC RES investigation have to date not established a model capable of explaining why the density and size of flaws can be expected to vary from vessel to vessel, it was decided to adopt for FAVOR calculations flaw densities based only on observations of the Shoreham vessel because the Shoreham welds had a higher flaw density than the PVRUF welds.
6. Flaw depth dimensions did not exhibit statistically significant differences for the different welding process and vessels examined, and in this case the data from the different processes and vessels were pooled to obtain more statistically robust distributions. There were however clear differences in the distributions of flaws length depending on the welding processes and vessels examined, and the flaw length distributions were established on a case-by-case basis.

The following figures depict the information used as input to generate flaw distributions for

use in the probabilistic fracture mechanics calculations performed by FAVOR V02.4. The uncertainty bounds on these data reflect the statistical uncertainty in these data sets.

- Figure 2.15 depicts the flaw density distribution
- Figure 2.16 depicts the flaw depth distribution for non-repair welds
- Figure 2.17 depicts the flaw depth distribution for repair welds
- Figure 2.18 depicts the flaw length distribution for non-repair welds
- Figure 2.19 depicts the flaw length distribution for repair welds

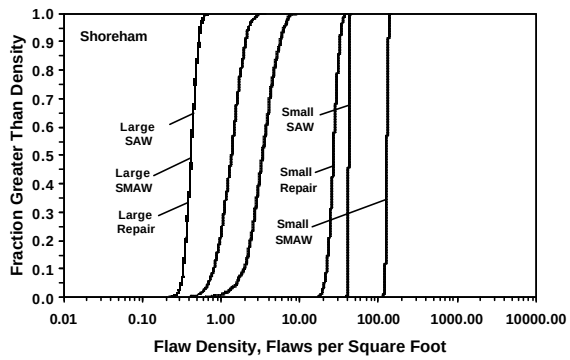

Figure 2.15. Densities of buried weld flaws (and uncertainties) for the Shoreham vessel that have been adopted to characterize the density of all buried weld flaws in the PTS re-evaluation project.

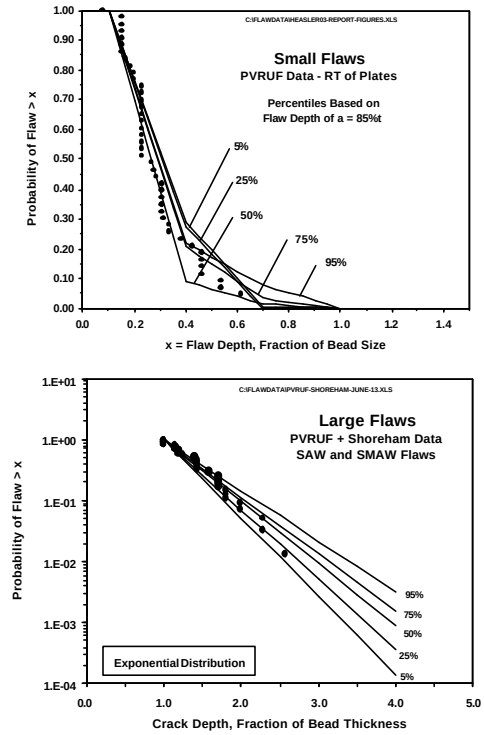

Figure 2.16. Flaw depth distribution for non-repair welds.

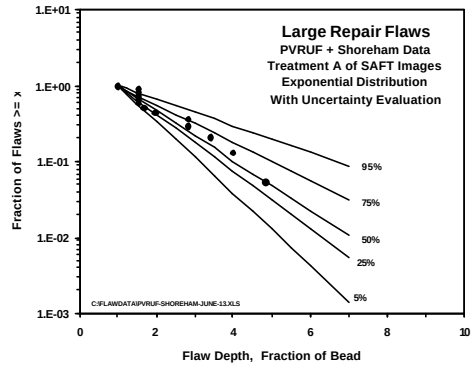

Figure 2.17. Flaw depth distribution for repair welds.

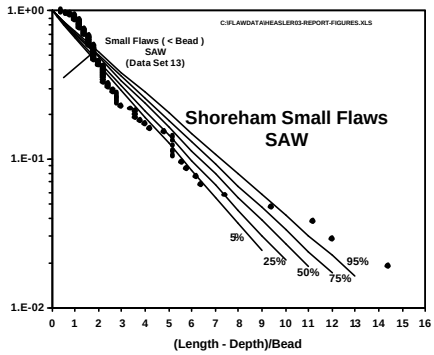

Figure 2.18. Flaw length distribution for non-repair welds.

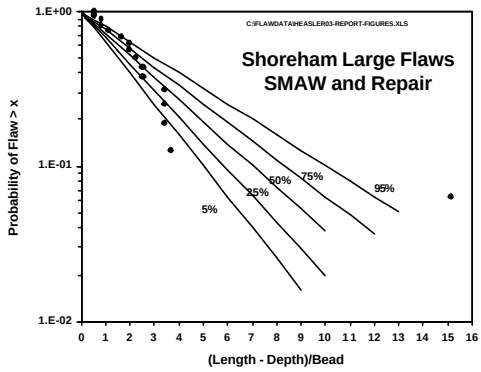

Figure 2.19. Flaw length distribution for repair welds.

In closing it should be noted that the empirical data in Figure 2.15 through Figure 2.19 do not, and cannot, provide any information about the maximum size a flaw can be. For this reason it was decided to truncate the non-repair flaw distribution at 1-in., and the repair flaw distribution at 2-in. In both cases the truncation limit selected exceeds by a factor of two times the maximum observed flaw size. We performed a sensitivity study with FAVOR and ascertained that, within reasonable bounds on truncation limit dimension, the estimated through wall cracking frequency is not influenced in any significant way by the truncation limit.

2.3.2.2 Distribution of Buried Flaws in Plates

As reflected by the information in Table 2.25, the empirical evidence available to support a plate flaw distribution is much more limited than the available information for welds. These data on flaw rates and sizes in plates are summarized in Figure 2.20 (see individual symbols), along with two flaw distributions for plates derived by applying flaw density adjustment factors to weld flaw distributions (see lines). These adjustment factors, which were proposed by a group of experts [Jackson 00], are as follows:

- The density of plate flaws of depth less than 6 mm is 10% of that for weld flaws
- The density of plate flaws of depth above 6 mm is 2.5% of that for weld flaws.

Since there is reasonable agreement between the limited experimental data on plate flaws and the adjusted weld distributions it was decided to use the adjusted weld distributions as input to FAVOR. As was the case with weld flaws, the truncation limit of 0.43-in. in Figure 2.20 was selected because it exceeds by a factor of two the largest observed plate flaw. Again, a FAVOR sensitivity study has revealed that this truncation limit does not influence significantly the estimated through wall cracking frequency.

In closing, two other points should be noted:

- In FAVOR the uncertainty bounds on the plate flaw distribution (Figure 2.20) is derived from the statistical uncertainty bounds for weld flaws (Figure 2.15 through Figure 2.19).
- The experimental studies conducted at PNNL failed to reveal any preferred orientation for plate flaws. To represent this finding in FAVOR in the most accurate way possible without needing to do mixed-mode fracture calculations it was decided that half of the simulated plate flaws will be orientated axially while the remaining half will be oriented circumferentially in the vessel.

2.3.2.3 Distribution of Surface Flaws in Welds and Plates

The entire inner-diameter of a nuclear RPV is clad with a thin layer of stainless steel to prevent corrosion of the underlying ferritic steel. Lack of inter-run fusion can occur between adjacent weld beads, resulting in circumferentially oriented cracks (all cladding in RPVs was deposited circumferentially). Figure 2.21 shows data on circumferential flaws in cladding collected by PNNL. These data agree closely with results of the weld flaw simulation code PRODIGAL, which are also shown on Figure 2.21.

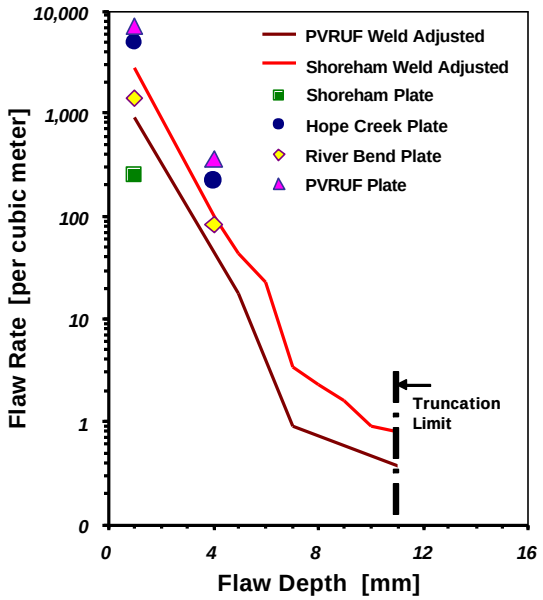

Figure 2.20. Flaw density and depth distribution for buried flaws in plates.

It should be noted that none of the experimental evidence in Figure 2.21 reveal a flaw that has completely compromised the clad layer. Only flaws that completely penetrate the clad layer are expected to challenge the integrity of the RPV during PTS loading because it is only in this situation that the crack is relatively large and has its tip residing in the ferritic RPV steel that is subject to neutron irradiation embrittlement. Despite the lack of empirical evidence supporting surface flaws that fully penetrate the clad layer, it was not believed to be appropriate to completely exclude such flaws from the FAVOR analysis owing to the limited amount of clad material examined. For this reason we developed a distribution for small buried cladding flaws illustrated in Figure 2.21 based on a combination of expert judgment and the predictions of the weld flaw simulation code PRODIGAL. This distribution was used to estimate the small number of the clad flaws that penetrate a sufficient fraction of the clad thickness that they may contribute to the through wall cracking frequency. We estimated that only 1/1000th of the observed density of clad flaws would act as a surface breaking flaw penetrating the full clad thickness. This factor was used to generate the distribution of circumferential flaws in single layer cladding in FAVOR. Multi-layer cladding was assumed to have no surface breaking flaws because the likelihood of two lack of inter-run fusion defects aligning in two different weld layers is quite remote indeed.

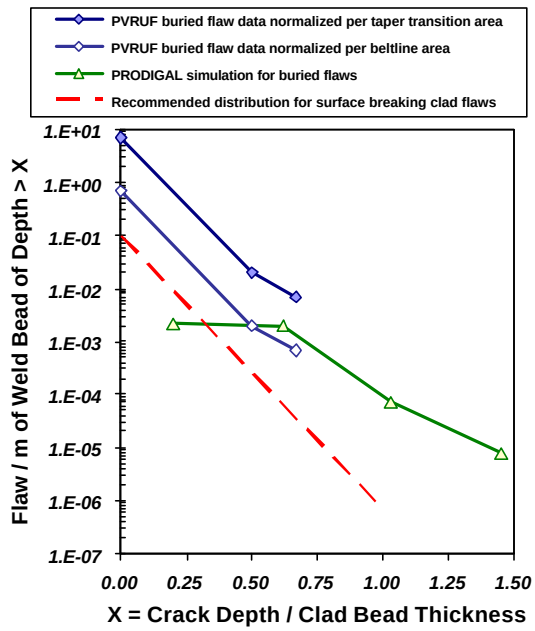

Figure 2.21. Density and depth distribution for surface breaking circumferential flaws in single layer stainless steel cladding.

2.3.2.4 Summary

As mentioned previously, the information presented in this section is intended to only synopsize that presented in the NUREG/CR report by Simonen and co-workers; full details and justification of the information presented herein can be found in that report. The uncertainties represented on the Figures in this Section represent only statistical uncertainty bounds on the available empirical data, they neither include nor attempt to characterize any model uncertainties associated with application of these experimentally derived flaw distributions to situations of interest in service. These uncertainties are represented to the PFM code FAVOR by generating an input file of 1,000 candidate flaw distributions randomly selected from within the uncertainty bounds

illustrated in the figures for each of buried flaws in welds, buried flaws in plates and forgings, and surface flaws in both plates and forgings. Again, the NUREG/CR report by Simonen and co-workers describes in detail the procedure for generating these flaw data files that are read as input by FAVOR.

Figure 2.22 provides a comparison of the Marshall flaw distribution that was used to establish the current PTS rule with the three components of the overall vessel flaw distribution. In general the following observations can be made:

- In general the individual contributions to the flaw distribution contain more flaws than the Marshall distribution, but the flaws are considerably smaller in size.
- Only at larger flaws depths (~ 1.0 inch) which are relevant to the data available to the Marshall study does the present distribution appear to be consistent with the Marshall distribution.
- While all of the flaws in the Marshall distribution were surface breaking, only flaws associated with the cladding are surface breaking in our new distributions, and these comprise only a small percentage of the total. Also, these surface flaws in the new distribution are all oriented circumferentially in the vessel.
- The Marshall distribution focused on flaws in welds and did not distinguish between flaws in different product forms. The new distribution does, and it demonstrates that flaws in base metal are very much smaller than flaws in welds.

In a recently published sensitivity study, Dixon and Simonen report that the estimated through wall cracking frequency reduces by between a factor of 20 and 70 when the new flaw distribution is adopted instead of the Marshall distribution [Dixon 02a].

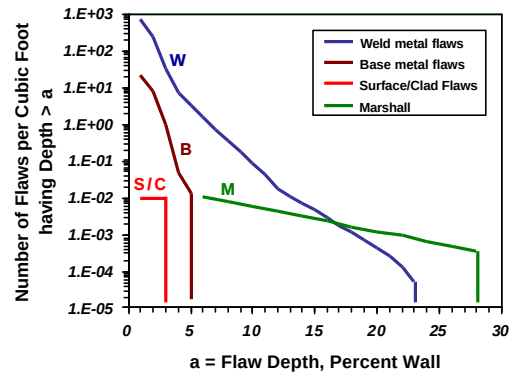

Figure 2.22. Comparison of the new flaw distribution to the Marshall flaw distribution.

2.3.3 Fluence

A series of neutron fluence transport calculations was performed to determine the neutron fluence on the inner-wall of four PWR vessels. The modeling procedures were based on the guidance provided in the NRC Regulatory Guide 1.190 [RG 1.190], "Calculational and Dosimetry Methods for Determining Pressure Vessel Neutron Fluence." The calculations were performed in (r, θ) and (r, z) geometry using the DORT [DORT] discrete ordinates transport code and the BUGLE-93 [BUGLE] forty-seven neutron group ENDF/B-VI nuclear cross sections and fission spectra. The calculations employed an S_8 angular quadrature set and the scattering cross sections were represented using a P_3 Legendre expansion.

The calculational models extended radially from the core out to the primary (concrete) biological shield and over an axial height from one-foot below to one-foot above the active fuel. The model retained the octant core symmetry and represented a 45° azimuthal sector of the geometry. The calculations included a detailed representation of the core/internals/vessel materials and geometry based on plant-specific information provided by the licensee and/or fuel vendor. The models incorporated the dimensions and region-specific material compositions of the core, barrel, thermal shield, vessel and biological shield. The downcomer water density was determined using the inlet and outlet coolant temperatures and system pressure.

The calculations included a detailed modeling of the core neutron source using the MESH code [MESH] which accounted for the reduced power in the fuel pins close to the core reflector, and the increased number and higher energy of the neutrons produced in the high burnup fuel assemblies. The source was based on the plant-specific operating data; i.e., (1) the core thermal power operating history (2) the fuel assembly-wise power, burnup and axial power distribution and (3) the peripheral fuel assembly pin-wise power distribution.

The E > 1MeV fluence was calculated as a function of azimuthal and axial location on the vessel inner-wall. The fluence was extrapolated from the current state-point to 32 and 40 Effective Full Power Years (EFPYs) assuming a linear extrapolation of the most recent operating cycles. Figure 2.23 illustrates the azimuthal variation of fluence on the vessel inner-wall at the axial location having the peak fluence is for Oconee at both the 32 EFPY and 40 EFPY state-points. The maximum fluence occurs at an azimuth of ≈12° where the core-to-vessel separation is a minimum. Figure 2.24 illustrates the axial fluence on the inner-wall of this vessel for these state-points. The axial fluence decreases rapidly at elevations above and below the active fuel and includes small oscillations due to the presence of the baffle former plates.

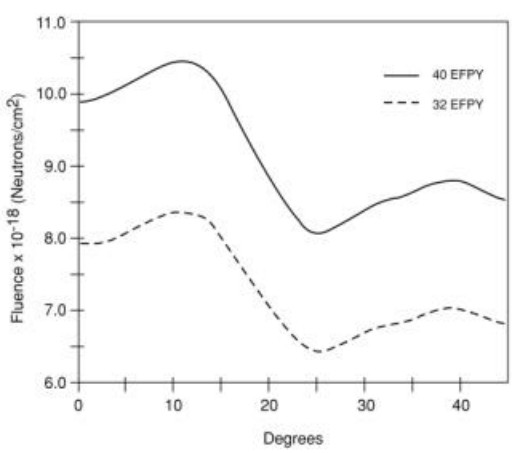

Figure 2.23. Azimuthal variation of fluence on the inner diameter of the Oconee 1 vessel at the axial location of the peak fluence.

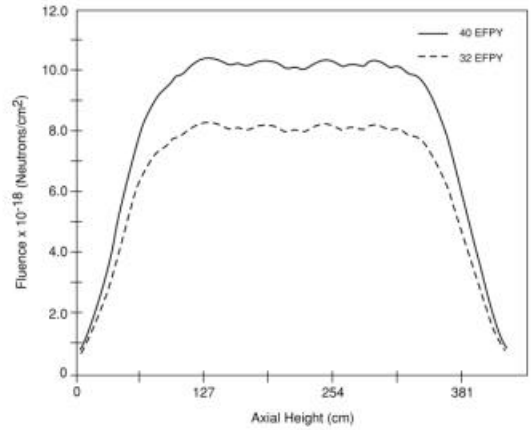

Figure 2.24. Axial variation of fluence on the inner diameter of the Oconee 1 vessel at the azimuthal location of peak fluence.

2.3.4 FAVOR Implementation of the Complete PFM Model

As shown in Figure 2.25, FAVOR is composed of three computational modules: (1) a deterministic load generator (**FAVLoad**), (2) a Monte Carlo PFM module (**FAVPFM**), and (3) a post-processor (**FAVPost**). Figure 2.25 also indicates the nature of the data streams that flow through these modules.

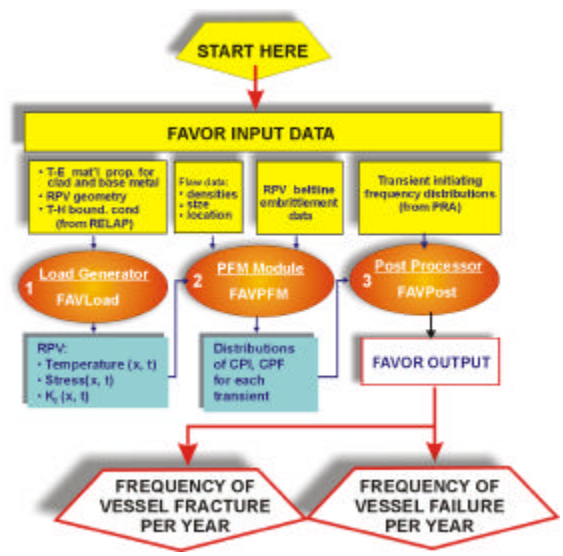

Figure 2.25. FAVOR data streams flow through three modules: (1) FAVLoad, (2) FAVPFM, and (3) FAVPost.

FAVLoad takes as input the time histories of temperature, and heat transfer coefficient defined by the RELAP thermal-hydraulic analysis. These inputs are used along with a 1D transient heat conduction equation to estimate the time dependent variation of temperature through the vessel wall. These time dependent temperature profiles are used, along with the RELAP pressure history, in a linear elastic stress analysis to estimate the time history of applied-K_I, which is passed to FAVPFM for further analysis.

The FAVPFM module implements the logical specification of the PFM model illustrated in Figure 2.14 within a series of nested loops illustrated in Figure 2.26. These loops step through the TH time history and implement the Monte-Carlo trials necessary to estimate the conditional probabilities of crack initiation and of though wall cracking. The probabilities estimated by FAVOR (complete with uncertainties) are *conditional* in the sense that, within the FAVPFM module, the TH transients are assumed to occur.

The FAVPFM module provides the capability to model the variation of radiation damage in the *beltline region* of an RPV with as much detail as the analyst considers necessary. Only that portion of the beltline that is proximate to the active core need be modeled because the fast-neutron flux, and thus the radiation damage, drops to nearly zero within a foot beyond the fuel region. Within this region (active core ± 1-ft.) the vessel is represented as a combination of "major regions," with each major region representing a different plate, weld, or forging each having (potentially) a unique combination of mean copper content, mean nickel content, mean phosphorus content, unirradiated RT_{NDT}. Each major region may be divided into as many "sub-regions" as the analyst feels is necessary to accurately represent both the axial and azimuthal variation of fluence. Sufficient discretization is adopted so that each sub-region is effectively iso-fluence. In this way the complex variation of embrittlement throughout the vessel wall that is caused by variations in both material and radiological conditions is represented to the model. It should be noted that this material / radiological model is a considerably more accurate representation of reality than the models adopted in the calculations performed to support SECY-82-465 and the IPTS studies. In these preceding calculations the entire vessel was presumed to be made out of the most irradiation sensitive material, and all of this material was assumed to be subjected to the peak fluence that occurred anywhere in the vessel.

The last FAVOR module, FAVPost, combines the conditional initiation and through-wall cracking probabilities and combines these, through a matrix multiplication, with the initiating event frequency histograms for each TH sequence provided by the PRA analyses. In this way the complete distribution of through wall cracking frequency (per operating year) is estimated.

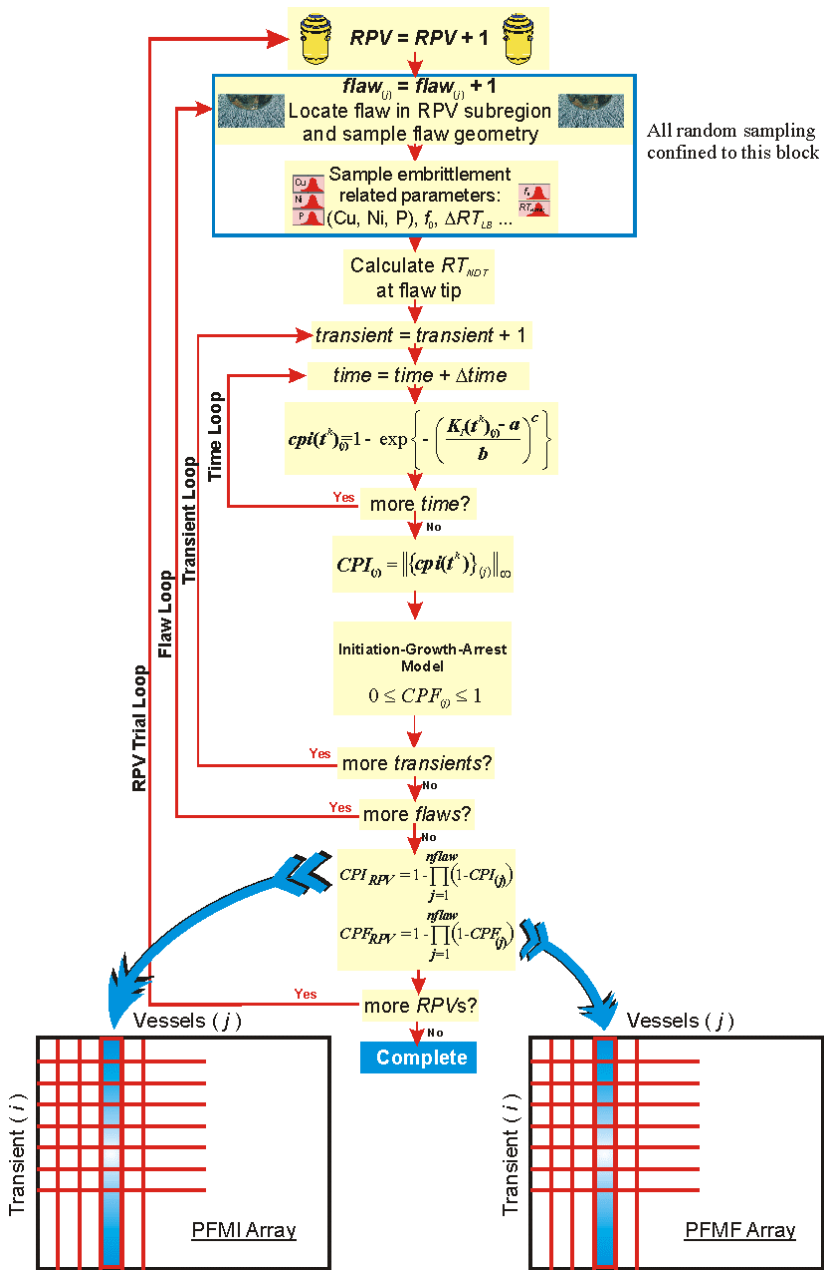

Figure 2.26. Flow chart for improved PFM model implemented in FAVPFM showing the four primary nested loops – (1) *RPV Trial Loop*, (2) *Flaw Loop*, (3) *Transient Loop*, and (4) *Time Loop*.

3 Validation of Models

3.1 Thermal Hydraulics

3.1.1 Introduction

In this section, assessments of RELAP5 are presented that demonstrate the suitability of the code for analyzing PTS transients. This assessment consists of performing analysis on a particular experimental facility for a given transient and comparing the results of that analysis to measurements made at that facility.

RELAP5/Mod 3.2.2 Gamma assessment was performed to establish the suitability of RELAP5 for the analysis of transients that may be significant risk contributors to PTS events. This version of RELAP5 is the same that is used for the plant PTS calculations.

Assessment of RELAP5 has been performed for a wide variety of transients over the 20-year development history of the code. Many of these assessments focused on LOCA where the purpose of the analysis is to demonstrate core integrity during postulated licensing basis transients. For LOCAs, conditions in the core region are of principal interest. In contrast, for PTS related transients, the focus is on the temperature and pressure conditions in the reactor vessel downcomer. Hence, assessment focuses on comparing RELAP5 results to experimental data for conditions in the downcomer. Note that LOCA can be an important risk contributor to PTS and so assessments using LOCA tests are relevant.

PTS risk significant transients primarily involve a period of relatively rapid energy removal from the primary system followed by a relatively quiescent period where pressure and temperature conditions do not rapidly change. During the period of energy removal, the primary system cools down significantly. Depending on the type of transient, this cooldown can be due to the combined effect of loss of high energy coolant (through a break or valve), excessive heat removal by the secondary, and injection of low temperature coolant from the ECCS. In some transients, late repressurization can occur due to an event such as reclosure of a stuck-open relief valve or from simply refilling the system. Many events will have single phase flow in the primary loops once the quiescent period is reached. For some events, notably events where no break in the primary system is postulated, single phase flow conditions will exist in the primary loops throughout the event, so that complex two-phase flow phenomena will play no role. However, thermal hydraulic conditions are quite variable during PTS risk significant transients, depending on the nature of the transient. Some phenomena such as cold leg thermal stratification cannot be modeled by a one-dimensional code such as RELAP5. However, these phenomena were found to have a minimal effect on the downcomer temperature and system pressure.

Because of the wide variation in thermal hydraulic conditions that can occur in PTS transients, assessment is presented with emphasis on the following phenomena:

- Break flow
- Re-pressurization
- Natural circulation/flow stagnation
- Boiling-condensation mode / Reflux condensation (B&W)
- Mixing in downcomer
- Condensation mixing and stratification in the cold leg
- Integral system response

These phenomena were selected because of their primary or secondary importance for the PTS figures of merit (downcomer fluid temperature in the reactor vessel, pressure, and wall heat transfer coefficient). Three phenomena of most importance to PTS significant transients were identified. Natural circulation/flow stagnation is particularly significant because if loop flow continues, warm (average coolant system temperature) fluid is delivered to the reactor vessel downcomer, while if it stagnates the effects of cold ECCS water are seen immediately and directly in the downcomer. Integral system response is important because the ECCS injection behavior (flow rates, timings, and to some extent temperatures) are functions of the overall system behavior (mainly pressure, but also various levels and temperatures). Pressurization is itself a primary figure of merit in the PTS analyses. The other phenomena were selected because of their influence on the main phenomena or because they represent potentially significant downcomer localized effects.

Assessments performed for these phenomena are discussed in the following sections.

3.1.2 Separate Effects Tests

RELAP5 was assessed against several separate-effects tests to evaluate key aspects of the RELAP5 results against experimental data. These tests included Marviken tests for critical flow model assessment, MIT Pressurizer facility tests for steam condensation rate and critical heat transfer, and UPTF facility tests for condensation and steam-water flow phenomena. These assessments are presented in this section.

3.1.2.1 Marviken Test

Critical flow assessments were performed based on data obtained from experiments conducted at the Marviken facility. Marviken is a full-scale critical flow test fabricated from the pressure vessel that was part of the Marviken nuclear power plant. The RELAP5 code utilizes the Henry-Fauske critical flow model to determine break flow during periods when critical flow occurs. This test is part of the separate-effects problems included in the RELAP5 Developmental Assessment. See Reference 6.1-1 for further information on this test.

The RELAP5 results are assessed against two Marviken tests identified as Run 22 and Run 24. In the tests, the vessel is pressurized, the desired temperatures are established and the break is opened, allowing vessel blowdown to occur. The main difference between the two tests is that the length of the discharge pipe was changed. In both cases, the diameter of the discharge pipe is 500 mm (1.64 ft). In Run 24, the L/D ratio is 0.33, so that the discharge pipe length is 165 mm (0.54 ft). In Run 22, the L/D ratio is 1.5, so that the discharge pipe length is 750 mm (2.46 ft). The Marviken vessel has an inside diameter of 5.22 m (17.12 ft) and an overall length of 24.55 m (80.5 ft). The net internal volume is 420 m^3 (14830 ft^3).

The initial test conditions for Run 24 and Run 22 were the same. The vessel was filled with water to an elevation of 16.7 m (54.8 ft). A warm-up process was utilized to produce a temperature profile in the vessel water pool. The steam dome above the water was pressurized to saturation conditions at 4.96 MPa (720 psia). The corresponding temperature is about 533 K (500°F), In the water pool, there was a saturated liquid region to a depth of about 2 meters (6.56 ft) and a transition region where the temperature dropped to 504 K (447°F). The fluid at the bottom the vessel was about 32 K (58°F) subcooled relative to the steam dome temperature.

A comparison of the vessel pressure and mass flow rate at the nozzle outlet between RELAP5 predictions and Marviken data is presented in Figure 3.1 and Figure 3.2 for Test 24. The RELAP5 code under predicts the measured pressure somewhat in the first 20 seconds of the transient, but is in good agreement after that time. The comparison of mass flow rate shows excellent agreement between RELAP5 and the results of the Marviken test. The results for Test 22 are similar.

It should be noted that a RELAP5 analysis of a spectrum of breaks was performed for each plant

included in the PTS study. Break diameters of 2.54 cm (1 in) to 57.5 cm (22.63 in) in equal flow area increments were analyzed. As a result, the effects of any uncertainty in the break flow model on the PTS calculated results are significantly reduced, since a whole spectrum of break sizes was analyzed.

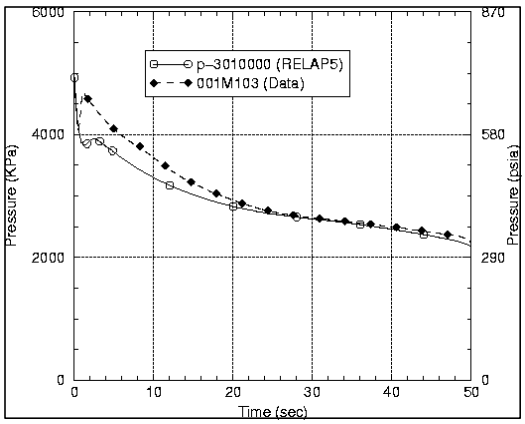

Figure 3.1. Pressure in Top of Vessel - Marviken Test 24.

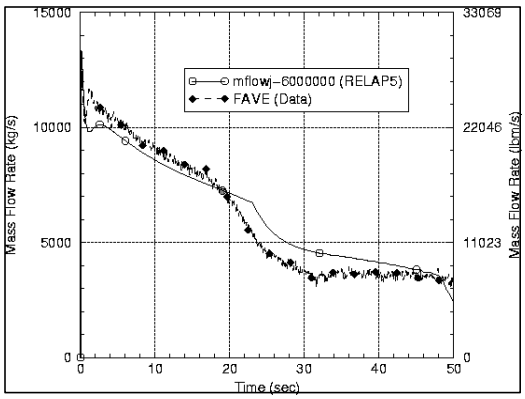

Figure 3.2. Mass Flow Rate at Nozzle Outlet - Marviken Test 24**.**

3.1.2.2 MIT Pressurizer Test ST4

The RELAP5 calculations of the steam condensation rate and the interfacial heat transfer between the stratified liquid and the vapor above the liquid were tested using comparisons to test data from MIT Pressurizer Test ST4. Mixing of incoming cold water with hot water present in the system will affect the system pressure prediction and is a potentially important phenomenon. This test is part of the separate-effects problems included in the RELAP5 Developmental Assessment. See Reference 6.1-1 for further information on this test.

The MIT Pressurizer Test ST4 was a small-scale, low-pressure representation of a pressurizer. The vessel representing the pressurizer was 1.14 m (3.74 ft) tall with an inner diameter of 0.203 m (0.667 ft) and is insulated. Test ST4 was initialized with 0.432 m (1.41 ft) of saturated water at a pressure of 0.493 MPa (71.5 psia) under quiescent conditions. Subcooled water was injected into the tank for 41 sec, increasing the water level of the tank by about 1 cm/sec (0.394 in/sec). The initial subcooling of the injected water was 129 K (232°F).

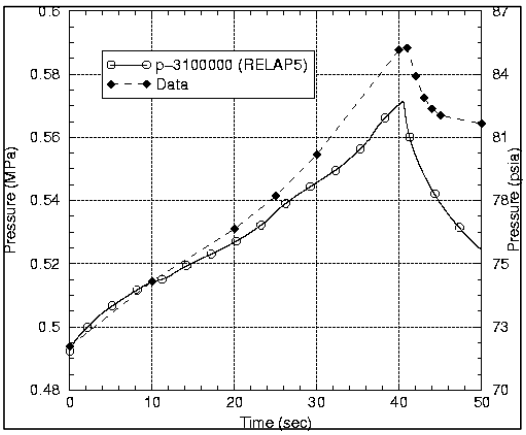

Figure 3.3. Comparison of Measured Pressure Rise - MIT Pressurizer Test ST4**x.**

A comparison of the measured pressure rise to the RELAP5-calculated value is shown in Figure 3.3. Initially, pressure increased due to compression of the steam volume above the water surface. As the pressure increased, the saturation temperature also increased. During this period, RELAP5 over predicts the wall condensation and, as a result, under predicts the pressure. However, overall, RELAP5 did capture the overall trend displayed by the test data. It should be noted that this test was conducted at low pressure conditions about 30 times lower than the operating pressure of a PWR plant.

3.1.2.3 Upper Plenum Test Facility

The Upper Plenum Test Facility (UPTF) is a full-scale model of a four-loop 1300 MWe PWR. Components included in this facility are the reactor vessel, downcomer, lower plenum, core simulation, upper plenum, and four loops with pump and steam generator simulation. The test vessel, core barrel, and interiors are a full-size representation of a PWR with four full-scale hot and cold legs simulating three intact loops and a broken loop. Further information on this test is found in Reference 6.1-2.

RELAP5 assessment was performed for Run 131 of UPTF Test 6. This test is a separate-effects test to investigate the steam-water phenomenon in the lower plenum and downcomer during the end-of-blowdown and refill portions of a large-cold leg break LOCA.

Run 131 of UPTF Test 6 was started by injecting steam through the core and steam generator simulators. The steam flowed upward through the downcomer toward the broken cold leg. The steam flow was kept constant in the test. After the steam flow came to an almost steady condition, slightly subcooled emergency core cooling water was injected into the cold leg of the three intact loops. The same injection flow rate, 482 kg/sec (1060 lbm/sec) was injected into each loop. The test was started at an initial vessel pressure of 0.258 MPa (37.4 psia) at a temperature of 458 K (364°F). The emergency core cooling accumulator pressure was 1.95 MPa (283 psia). The emergency core cooling water temperature is 392 K (246°F).

Figure 3.4 shows a comparison of the calculated and measured pressure in the downcomer for Run 131 of UPTF Test 6 and RELAP5. These results show good agreement the code and test results. A comparison of the lower plenum liquid level between RELAP5 and the test is shown in Figure 3.5. Here, there is fairly good agreement between the test results and the code prediction.

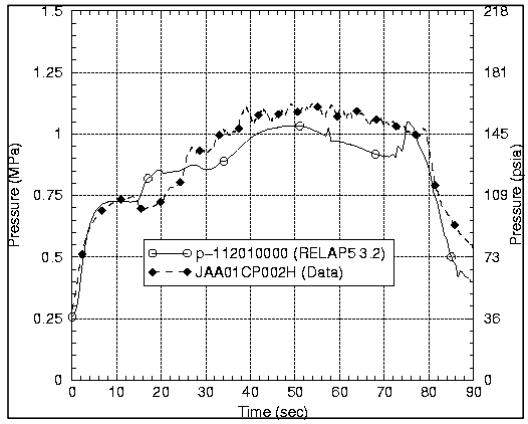

Figure 3.4. Downcomer Pressure - UPTF Test 6 - Run 131.

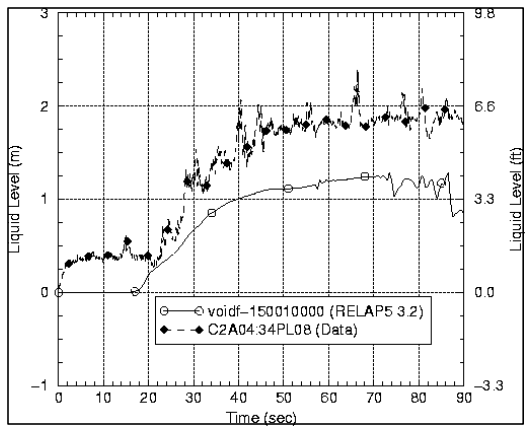

Figure 3.5. Lower Plenum Liquid Level- UPTF Test 6 - Run 1.

Overall, it is concluded that the RELAP5 predictions are fairly close to the UPTF experimental results.

3.1.2.4 Semi-scale Tests

Experiments were performed in the Semi-scale Mod-2A test facility to evaluate single-phase, two-phase, and reflux steady state phenomena and also primary side two-phase natural circulation behavior. This facility was a small-scale model of the primary system of a four-loop PWR plant. The scaling factor is 1:1705. The facility incorporated the major components of a PWR, including, steam generators, vessel, downcomer, pumps, pressurizer, and loop piping. The natural circulation experiments

conducted at the facility utilized a single-loop configuration where the intact loop pump was replaced with a spool piece containing an orifice that simulated the hydraulic resistance of a locked pump rotor. The vessel was also modified to ensure a uniform heatup of the entire system and to avoid condensation in the upper head structures.

Two tests were used in the RELAP5 assessment, which are Test S-NC-2 and Test S-NC-3. Steady-state loop natural circulation flow rate as a function of primary side mass inventory was measured during Test S-NC-2. Single-phase, two-phase, and reflux steady-state modes were examined in this test by varying the primary side system mass while holding the steam generator secondary side conditions constant. A total of 17 separate steady-state conditions with different primary side inventories ranging from 100 % to 61.2% of the full or maximum inventory were used for Test S-NC-2.

Figure 3.6 presents a plot of the mass flow rate as a function of primary coolant system inventory that compares the RELAP5 result to Test S-NC-2 data. The calculated results compare well with the points in the 97% to 100% mass inventory range, which was during single-phase conditions. During two-phase conditions, which occurred between 70% and 94% of the maximum primary system inventory, the mass flow rate predicted by RELAP5 increased relative to the test results. This increase is attributed to boiling in the core causing a larger density difference between the core and steam generator in the RELAP5 predictions. Further reduction in the mass inventory caused void formation in the steam generator (down side of the U-tubes) and subsequently the mass flow rate decreased due to the smaller density difference between the core and the steam generator. The mass flow rate predicted by RELAP5 is lower that the test result, which is attributed to the interphase drag model. In this case, the interphase drag model caused more liquid to be carried into the hot leg relative to the test, affecting the density head difference and resulting in lower mass flow rate. The calculated cold leg flow rate response is reasonable during reflux conditions, which occurred between 60% and 70% of the maximum primary system inventory. It is noted that the calculated mass flow was oscillatory in the reflux mode, so that the average value is shown. In general, the overall RELAP5 prediction of the average loop flow is reasonable.

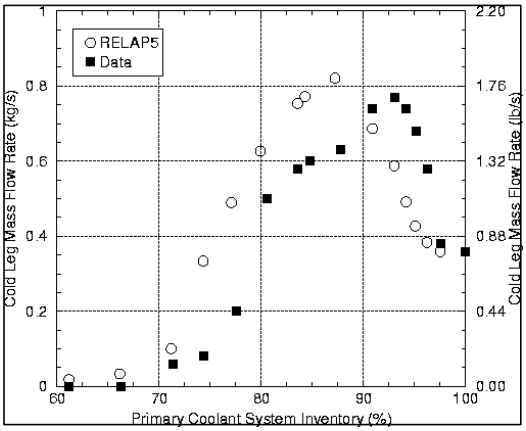

Figure 3.6. Mass Flow Rate vs. Primary System Inventory - S-NC-2.

Test S-NC-3 examined primary side two-phase natural circulation behavior under varying steam generator secondary side mass inventory. A core power of 62 kW was used for the test. The steady-state loop natural circulation flow rate as a function of steam generator heat transfer area was measured.

Figure 3.7 shows the mass flow rate as a function of steam generator tube heat transfer area. There is good agreement in the calculated mass flow rate at effective heat transfer areas above 55%. As the heat transfer area was reduced, the heat removal capability of the steam generator was also reduced. Consequently, the driving potential (density difference between the core and the steam generator) was diminished and the mass flow rate slowed.

Overall, RELAP5 simulated the Semi-scale natural circulation tests reasonably well for the higher primary coolant system mass inventories. Also, at the higher steam generator mass inventories, the code calculations are in good agreement with the measured data.

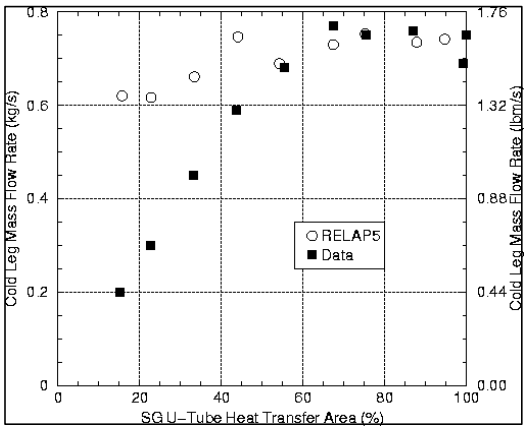

Figure 3.7. Cold Leg Mass Flow Area vs. SGU Tube Heat Transfer Area .

3.1.3 Integral System Response

RELAP5 was assessed against several integral tests to evaluate key aspects of the RELAP5 results against experimental data. These tests included ROSA-IV, ROSA-AP600, Semi-scale, OSU-APEX, LOFT and MIST Tests. These assessments are presented in this section.

3.1.3.1 ROSA-IV Experiments

The ROSA-IV facility is a 1/48 volume scaled, full-pressure representation of a Westinghouse-type 3423 MWth four-loop PWR. The facility utilizes a full-height electrically heated core. Four PWR coolant loops are represented with two equal-volume loops. Components that are included in the loops are the hot leg, steam generator, reactor coolant pump, cold leg, pressurizer (on intact loop) and ECCS systems (high pressure injection, low pressure injection and accumulators).

RELAP5 was assessed against the three ROSA IV experiments listed below:

- ROSA-IV SB-CL-18: 15.24 cm (6 in) diameter cold leg LOCA with HPI failure
- ROSA-IV SB-HL-06: 5.08 cm (2 in) diameter hot leg LOCA with HPI failure
- ROSA-IV ST-NC-09: loop natural circulation

The ROSA-IV SB-CL-18 test is a 5% 15.24 cm (6 in) equivalent diameter scaled break on the side of the cold leg with the reactor in full power operation. The high pressure injection and auxiliary feedwater are assumed to fail. Also, loss of offsite power is assumed at the time of reactor scram.

A tabulation of the measured and RELAP5 calculated sequence of events is presented in Table 3.1.

Figure 3.8 presents a comparison of the RELAP5 calculated downcomer temperature to the measured data from the ROSA-IV test. As seen from this plot, the RELAP5 temperature is substantially colder compared to the results. A comparison of RELAP5 calculated pressurizer pressure compared to the test result is presented in Figure 3.9. There is also a significant difference in the primary system pressure that causes a higher rate of emergency core cooling injection and earlier accumulator discharge. Figure 3.10 shows a break flow rate comparison between RELAP5 results and the test data. The break flow is somewhat over predicted, contributing to a lower calculated pressure.

Overprediction of condensation by RELAP5 is another contributor to the lower pressure in the primary system. This lower pressure increases the ECCS system flow rate, further increasing condensation. Another result of the more over prediction of the depressurization is that accumulator injection occurs earlier in the calculation. Overprediction of condensation is a known factor for RELAP5. Overprediction of the condensation rate affects only the larger breaks where there is mostly steam at the injection location.

The ROSA-IV SB-HL-06 test is a 0.5% 5.08 cm (2 in) equivalent diameter scaled break on the top of the hot leg with the reactor in full power operation. The high pressure injection and auxiliary feedwater are assumed to fail. Also, loss of offsite power is assumed at the time of reactor scram. Once core uncovery and heatup started, the pressurizer PORV was opened to depressurize the primary system and initiate accumulator injection.

Table 3.1. Summary of Measured and Calculated Sequence of Events for ROSA-IV Test SB-CL-18.

Event Description	Event Time (s)	
	Measured	RELAP5
Break opens	0	0
Scram signal	10	8.9
Safety injection signal	12	9.6
Steam line valve closes	14	8.9
Feedwater flow stops	16	10
First core uncovery begins	120-155	186
Loop seal clearing	140	180
Primary pressure falls below secondary	180	221
Reactor coolant pumps stop	265	270
Second core uncovery begins	420-540	239
Accumulator injection flow begins	455	355

A tabulation of the measured and RELAP5 calculated sequence of events is presented in Table 3.2.

Although the code-to-data comparisons show differences, the RELAP5 downcomer temperature results are conservative for PTS relative to the test results.

Figure 3.11 presents a comparison of the RELAP5 calculated downcomer temperature to the measured data from the ROSA-IV test. As seen from this plot, the RELAP5 temperature agrees reasonably well with the results with about a maximum of 30 K (54°F) difference. A comparison of RELAP5 calculated pressurizer pressure compared to the test result is presented in Figure 3.12. The calculated primary system pressure also agrees reasonably well with the test data.

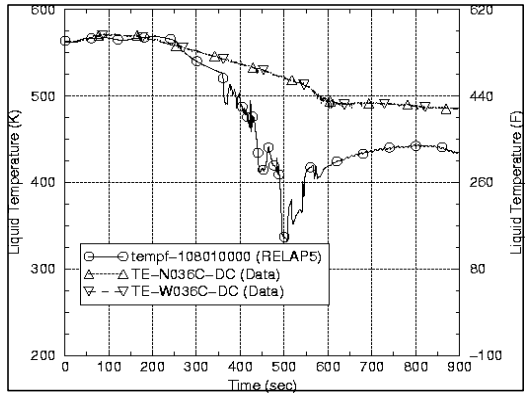

Figure 3.8. Downcomer Fluid Temperature at Top of Core Elevation - ROSA-IV SB-CL-18

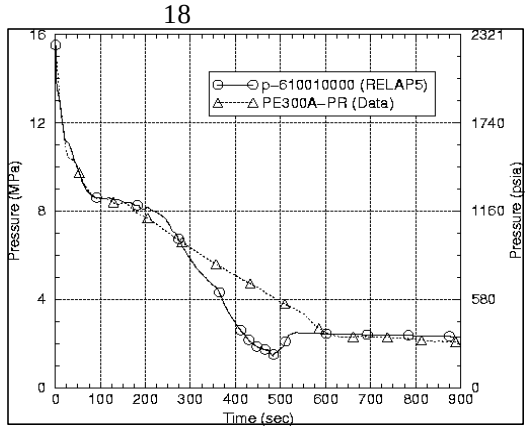

Figure 3.9. Pressurizer Pressure Comparison - ROSA-IV SB-CL-18.

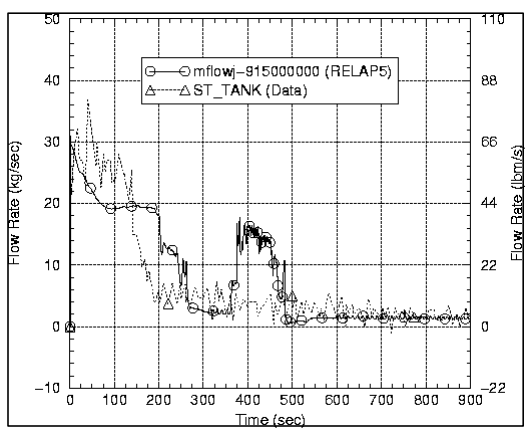

Figure 3.10. Break Flow - ROSA-IV SB-CL-18.

Table 3.2. Summary of Measured and Calculated Sequence of Events for ROSA-IV Test SB-HL-06.

Event Description	Event Time (s)	
	Measured	RELAP5
Break opens	0	0
Scram signal	87	94
Steam line valve closes	90	94
Feedwater flow stops	92	95
Initiation of core power decay	110	110
Vapor appears in hot legs	200	150
Reactor coolant pumps stop	341	350
Vapor appears in cold legs	800	840
Loop A natural circulation stops	1200	1700
Loop B natural circulation stops	1900	1700
Core heatup begins	5680	5200
Pressurizer PORV opened	5806	5806

Test ST-NC-09 is a natural circulation experiment under reflux condensation cooling conditions. Both coolant loops in the experimental facility were included in the test. The pressurizer was isolated. Basically, this experiment is a series of quasi-steady tests at secondary side pressures of 7, 3, and 1 MPa (1015, 435, and 145 psia). Primary coolant is discharged to induce the reflux cooling mode. At each of the three pressures, core power is varied in steps.

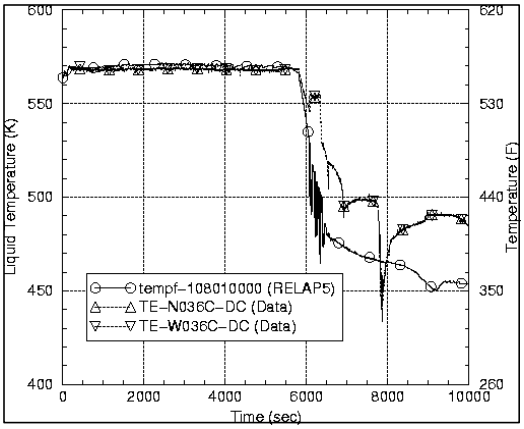

Figure 3.11. Downcomer Temperature at Top of Core Elevation - ROSA-IV SB-HL-06.

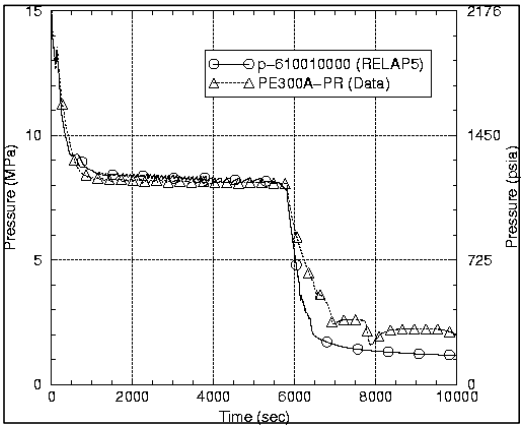

Figure 3.12. Pressurizer Pressure - ROSA-IV SB-HL-06.

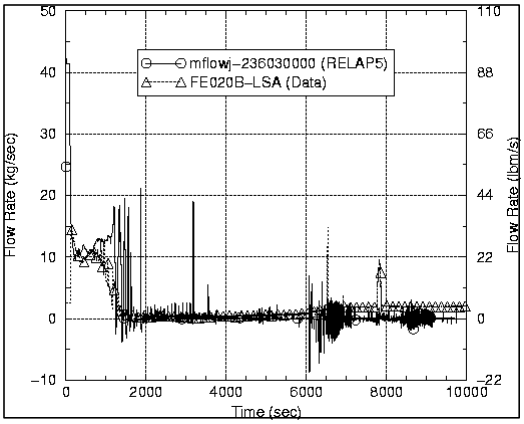

Figure 3.13. Loop A Mass Flow Rate - ROSA-IV SB-HL-06x.

The results of code-data comparisons for Test ST-NC-09 indicate that the code acceptably predicts the primary coolant system pressure.

The prediction of countercurrent flow in the hot legs and steam generator tubes is not well predicted. At the higher pressures and lower core powers, RELAP5 held up too much water in the steam generator tubes. At lower pressures and higher core powers, RELAP5 was shown to provide a limited predictive capability for the hot leg and steam generator tube countercurrent flow associated with reflux cooling.

3.1.3.2 ROSA AP-600 Tests

The ROSA-AP600 facility is a 1/30 volume scaled, full pressure representation of a Westinghouse AP600 PWR. The facility utilizes a full-height electrically heated core. The two AP600 coolant loops are represented with two equal-volume loops. Components that are included in the loops are the hot leg, steam generator, one reactor coolant pump (vs. two pumps in the plant design), one cold leg (vs. two in the plant design), pressurizer (on one loop), and core makeup tanks (CMTs) on the opposite loop. The passive residual heat removal system (PRHR), the automatic depressurization system (ADS), and the in-containment refueling water storage tank (IRWST) are also included.

RELAP5 was assessed against the two ROSA-AP600 experiments listed below:

ROSA-AP600 AP-CL-03: 2.54 cm (1 in) diameter cold leg LOCA

- ROSA-AP600 AP-CL-09: 2.54 cm (1 in) diameter cold leg LOCA with multiple passive safety system failures

Test AP-CL-03 is a 0.1% 2.54 cm (1 in) diameter scaled break on the bottom of the cold leg in the core makeup tank (CMT) loop. The reactor is operating at full power when the break opens. An additional failure, where one of the two ADS-4 valves on the CMT loop fails to open is also assumed.

A tabulation of the measured and RELAP5 calculated sequence of events is presented in Table 3.3.

Table 3.3. Summary of Measured and Calculated Sequence of Events for ROSA-AP600 Test AP-CL-03.

Event Description	Event Time (s)	
	Measured	RELAP5
Break opens	0	0
CMT recirculation begins	158	137
PRHR flow begins	159	137
Reactor scram, reactor coolant pumps tripped	178	152
S signal	203	163
Loss of natural circulation in pressurizer loop	463	470
Loss of natural circulation in CMT loop	1115	1080
Accumulator injection begins	1934	1900
CMT draining begins	2198	2196
ADS-1 valve opened	3533	3055
ADS-4 valves opened	4450	3853
IRWST injection begins	4978	4246

Figure 3.14 and Figure 3.15 present comparisons of the RELAP5 calculated downcomer temperature to the measured data from the ROSA-AP600 test at the elevation of the top of the core. Two positions are shown which are the "P" or pressurizer loop side and the "C" or CMT loop side.

Despite the fact that the positions are on opposite sides of the downcomer, there is little difference in the results. These results indicate that the effect of extreme cold-leg thermal stratification (observed in this test due to PRHR injection into the "P" loop) on downcomer temperature is minimal.

A comparison of RELAP5 calculated and measured pressurizer pressures is presented in Figure 3.16. This comparison shows that the calculated primary system pressure agrees well with the test data.

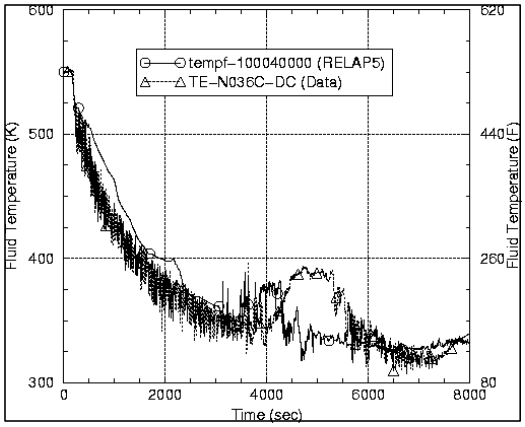

Figure 3.14. Downcomer Temperature At Top of Core Elevation (C Loop Side) - AP-CL-03.

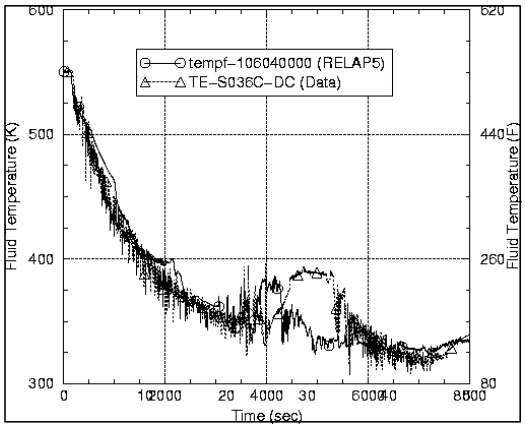

Figure 3.15. Downcomer Temperature at Top of Core Elevation (P Loop Side) - AP-CL-03.

Figure 3.17 presents a comparison of the calculated and measured cold leg flow rates in the CMT loop. As seen from this figure, the RELAP5 calculated flow is in good agreement with the measured data. The results are similar in the pressurizer loop.

Overall, this test comparison shows that complex system behavior and timing are well predicted with RELAP5. The RELAP5 prediction of coolant loop flow stagnation and draining are in good agreement with the test data. Also, from the above results, this test shows that the effect of cold leg thermal stratification on the downcomer liquid temperature is minimal.

Test AP-CL-09 is a 0.1% 2.54 cm (1 in) diameter scaled break on the bottom of the cold leg in the core makeup tank (CMT) loop. The reactor is operating at full power when the failure occurs. In this test, failure of several passive safety systems was simulated. These systems are listed below:

- Both CMT discharge valves fail closed.
- Half of the valves in each ADS stage fail closed.
- ADS (normally activated on low CMT level) activated 30 minutes after low-low pressurizer pressure signal occurs
- Check valve in accumulator discharge line on the CMT loop assumed to fail
- Check valve in the IRWST discharge line on the CMT loop assumed to fail closed
- Only one-half of the PRHR heat exchanger tubes used

This test was intended to demonstrate the robustness of the AP600 design for safe shutdown. It is analyzed here since it has some similarity to PTS significant events.

A tabulation of the measured and RELAP5 calculated sequence of events is presented in Table 3.4.

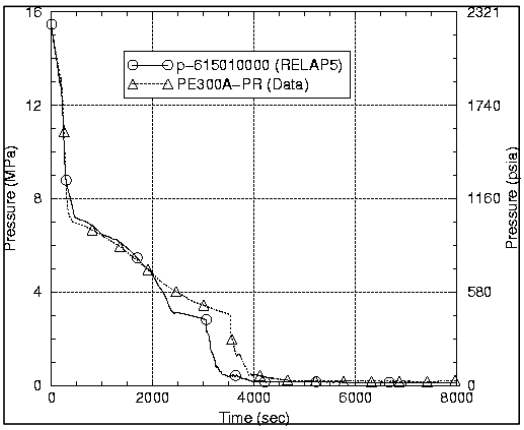

Figure 3.16. Pressurizer Pressure - AP-CL-03x.

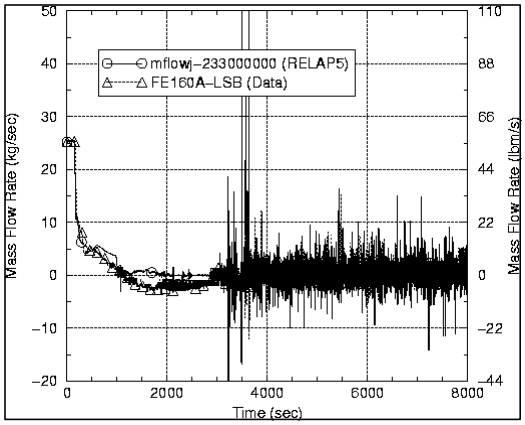

Figure 3.17. Cold Leg Flow in the CMT Loop - AP-CL-03x.

Table 3.4. Summary of Measured and Calculated Sequence of Events for ROSA-AP600 Test AP-CL-09.

Event Description	Event Time (s)	
	Measured	RELAP5
Break opens	0	0
Reactor scram, steam line valve closes, reactor coolant pumps tripped, PRHR activated, CVCS pump injection begins	183	173
S signal	203	173
Loss of natural circulation in the CMT loop	500	1972
Loss of natural circulation in the pressurizer loop	1650	740
ADS-1 valve opened	1985	1950
Accumulator injection begins	2190	2056
ADS-4 valves opened	3486	3150
IRWST injection begins	3990	4000

Figure 3.18 and Figure 3.19 present a comparison of the RELAP5 calculated downcomer temperature to the measured data from the ROSA-AP600 test at the elevation of the top of the core. Two positions are shown the "P" or pressurizer loop side and the "C" or CMT loop side. The comparisons show good agreement between the code prediction and the test data.

A comparison of RELAP5 calculated and measured pressurizer pressure is presented in Figure 3.20. This comparison shows that the primary system pressure agrees well with the test data.

Overall, this test comparison shows that complex system behavior and timing are well predicted with RELAP5. The RELAP5 prediction of coolant loop flow stagnation and draining are in good agreement with the test data. However, there was disagreement between the calculated and measured loop flow behavior regarding which loop stagnated first. This difference was found to affect the cooldown rate comparisons over the first 2000 sec, as seen in Figure 3.18 and Figure 3.19.

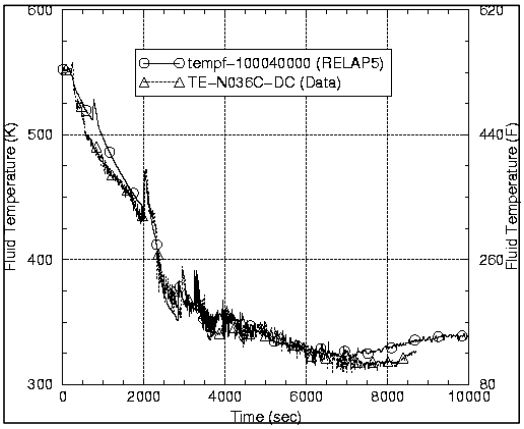

Figure 3.18. Downcomer Temperature at Top of Core Elevation (C Loop Side) - AP-CL-09.

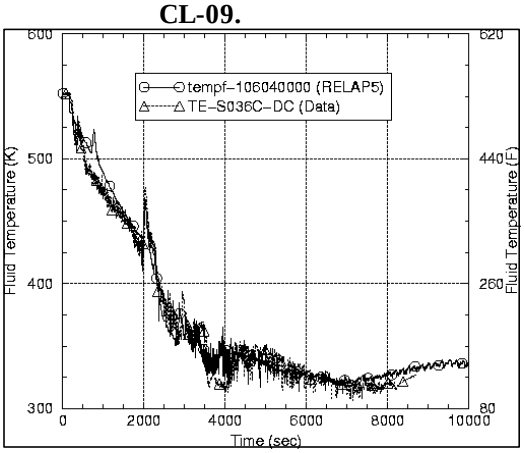

Figure 3.19. Downcomer Temperature at Top of Core Elevation (P Loop Side) – AP-CL-09x.

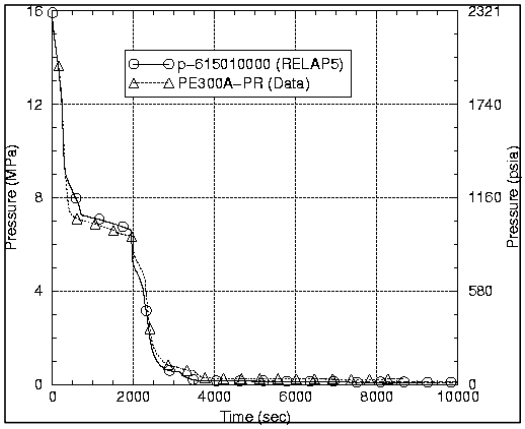

Figure 3.20. Pressurizer Pressure - AP-CL-09**.**

3.1.3.3 APEX Tests

A series of tests specific to CE plants was conducted at the APEX facility operated by Oregon State University. The APEX facility is a ¼ height scale low pressure integral systems facility that has been configured to model the thermal hydraulic phenomena of CE plants. The purpose of these tests was to investigate mixing of high pressure injection fluid in the cold leg and the downcomer. In particular, it was necessary to ensure that strong plumes did not persist into the downcomer region adjacent to the core in order to support the adequacy of the 1-D treatment of the temperature boundary condition in the probabilistic fracture mechanics code FAVOR. A second goal was to elucidate the onset of loop flow stagnation, which is generally necessary to achieve low temperatures in the downcomer.

Test APEX-CE-13 simulates a stuck open safety relief valve from full power with subsequent reclosure. This transient is a typical PTS event and can be an important risk contributor due to the repressurization by continued high pressure injection operation after plant cooldown has occurred. This test was initiated from full power steady-state conditions. The ADS-2 valve was opened at the start of the transient to simulate the stuck open pressurizer safety relief valve. Simultaneously, two of the reactor coolant pumps were tripped, the high-pressure injection was actuated and reactor core power was shifted to decay heat mode. The ADS-2 valve was kept open for an hour and then was closed. The test was terminated about 20 minutes later after the system had refilled.

Test APEX-CE-13 was initialized at a reactor coolant system pressure of 2.65 MPa (385 psia). The core power was 610 kW. Cold leg temperature was initially 480 K (403°F). Pressure and level in both steam generators was 38.6 cm (15.2 in) of water at a pressure of 1.71 MPa (249 psia). The pressurizer level was 53.8 cm (21.2 in).

A summary of the measured and calculated sequence of events is presented in Table 3.5. Note that the events listed in Table 3.5 are all manual actions, which is why the agreement between RELAP5 and the test is exact.

Table 3.5. Summary of Measured and Calculated Sequence of Events for APEX-CE-13 Test.

Event Description	Event Time (s)	
	Measured	RELAP5
Pressurizer SRV opened	0	0
Scram signal (core power decay)	0	0
HPI flow starts	0	0
RCP #1 and #4 tripped	4.2	4.2
RCP #2 and #3 tripped	20.8	20.8
Turbine stop valves closed	18.0	18.0
Pressurizer SRV closed	3589.1	3589.1
Simulation ended.	4800	4800

Figure 3.21 shows a comparison of the downcomer temperature between the RELAP5 results and the APEX-CE-10 measurements. Two adjacent downcomer locations are shown. Downcomer temperature is determined in several locations in both the RELAP5 results and the test measurements. A review of the temperature results at various positions shows little dependence on position in both the RELAP5 results and the APEX measurements, as illustrated in Figure 3.21.

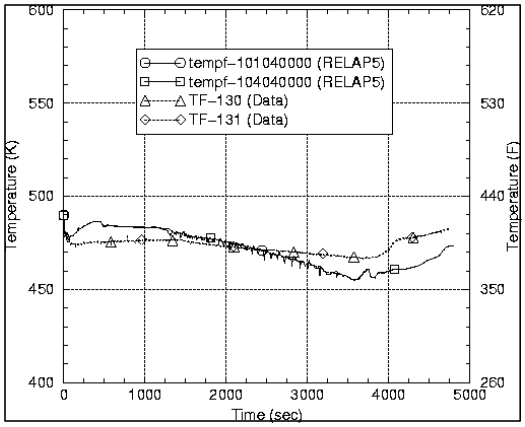

Figure 3.21. Downcomer Fluid Temperature - OSU-CE-13**x** **.**

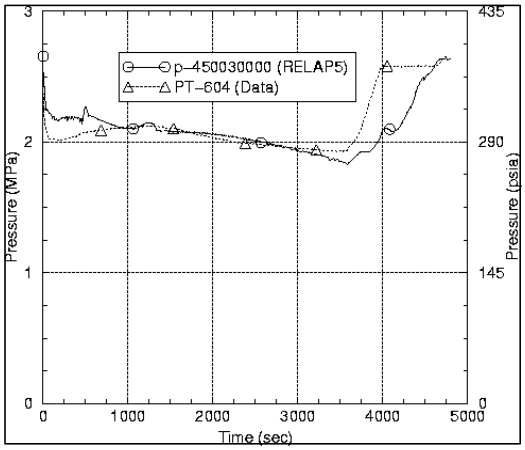

Figure 3.22. Pressurizer Pressure - APEX-CE-1x.

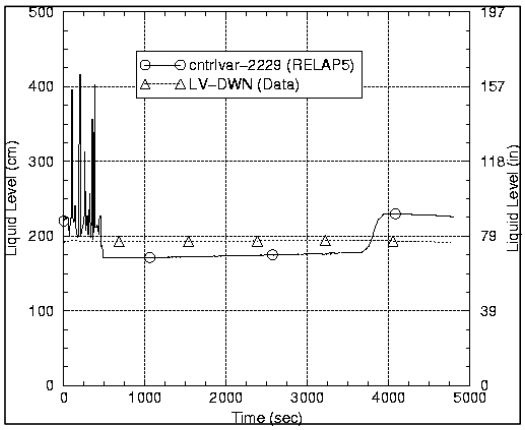

Figure 3.23. Downcomer Level - APEX-CE-13

Figure 3.22 shows a comparison of the primary system pressure calculated by RELAP5 to the measured data. The rise in pressure at about 3500 sec is due to the valve reclosure. The RELAP5 result shows repressurization at a somewhat lower rate than the measured data. The downcomer level is shown in Figure 3.23. Good agreement is seen between the RELAP5 results and the APEX measurements.

Overall, it is concluded that RELAP5 prediction is a reasonable simulation of the APEX-CE-13 test data. The downcomer temperature is predicted with reasonable accuracy. Temperature shows little dependence on azimuthal position in both the RELAP5 results and the APEX measurements. The RELAP5 results shows repressurization at a somewhat lower rate than the measured data, but the eventual peak pressure is slightly higher.

3.1.3.4 LOFT Test

The Loss of Fluid Test (LOFT) Facility was a 50 MWth volumetrically scaled PWR system. The LOFT facility was designed to obtain data on the performance of the engineered safety features of a commercial PWR system for postulated accidents including LOCAs.

The LOFT nuclear core was approximately 1.68 m (5.51 ft) and 0.61 m (2 ft) in diameter and was composed of nine fuel assemblies containing 1300 fuel rods of representative PWR design. Three intact loops were simulated using a volume/power ratio scaled by the single circulating (intact) loop in the LOFT primary system. The broken loop was simulated by the scaled LOFT blowdown loop.

An emergency core cooling system was provided to simulate the engineered safety features in PWRs. A high-pressure injection system centrifugal pump and a nitrogen-pressurized accumulator supplied emergency core cooling. The low pressure injection system and accumulator discharge lines were orificed as required to simulate the delivery characteristics of various PWR emergency core cooling systems. Further information on LOFT can be found in Reference 6.1-1.

RELAP5 assessment was performed using LOFT Test L3-7 that is part of the developmental assessment test suite. The primary purpose of this test was to establish a break flow approximately equal to high pressure injection flow when the primary system pressure was approximately 6.9 MPa (1000 psia) and to isolate the break and stabilize the plant at cold shutdown conditions. Prior to transient initiation, the core was operating at a power of 49 MW. Other significant initial conditions for Test L3-7 were a system pressure at 14.90 MPa (2160 psia), a core outlet temperature of 576.1 K (577.3°F), and an intact loop flow rate of 481.3 kg/sec (1059 lbm/sec).

The measured and calculated sequence of events for the LOFT L3-7 test is presented in Table 3.6. Test L3-7 was initiated and the reactor scrammed on a low system pressure signal. At 10 seconds after scram, the reactor coolant pumps were manually tripped and coasted down. Pump coastdown was followed by the inception of loop natural circulation flow. Between 1800 and 5974 seconds, the high pressure injection system was turned off to hasten the loss of fluid inventory and to establish the conditions favorable for reflux flow in the primary loop. Later in the test, at 7302 seconds, the blowdown isolation valve was closed which isolated the break. The RELAP5 simulation was ended at this point since cold leg break closure is not included in the PTS event sequences.

Figure 3.24 shows a comparison of the downcomer temperature results between RELAP5 and Test L3-6 data. The system pressure comparison is shown in Figure 3.25. Both figures show excellent agreement between RELAP5 and the LOFT results.

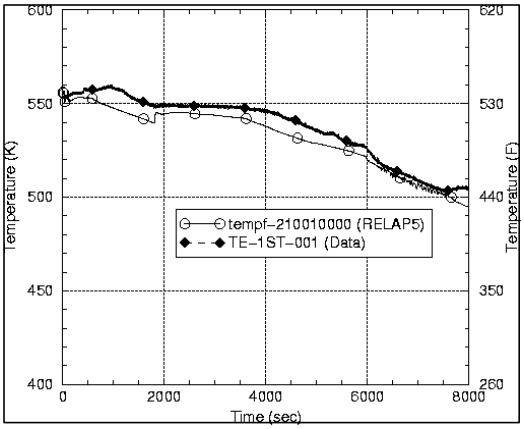

Figure 3.24. Upper Downcomer Temperature – LOFT Test L3-7x .

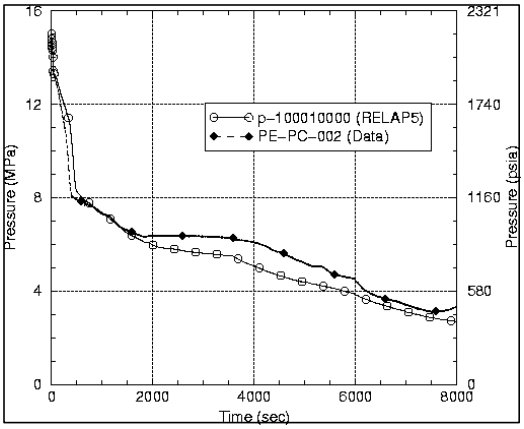

Figure 3.25. Primary System Pressure - LOFT Test L3-7**x.**

Table 3.6. Summary of Measured and Calculated Sequence of Events for LOFT L3-7 Test.

Event Description	Event Time (s)	
	Measured	RELAP5
Break valve opened	0	0
Scram signal (p < 14.193 MPa (2058 psia))	36	28
Reactor coolant pumps tripped manually at scram	39	28
HPI flow begins (p < 13.159 MPa (1908 psia))	65.4	80.1
HPI flow turned off	1800	1800
HPI flow turned on	5974	5974
Simulation ended.	7302	7300

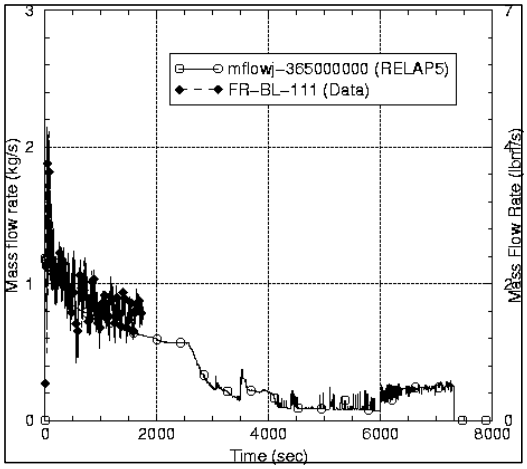

Figure 3.26. Break Mass Flow Rate -LOFT Test L3-7.

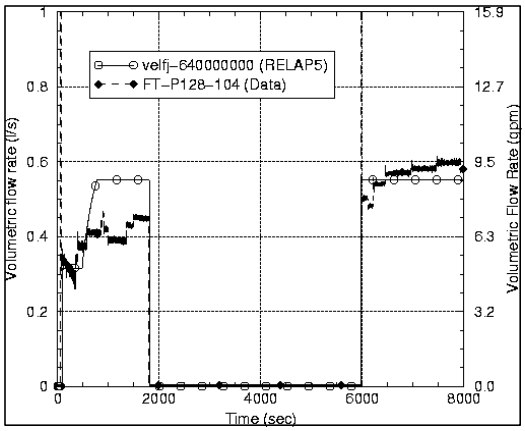

Figure 3.27. HPI Volumetric Flow - LOFT Test L3-6.

The break mass flow rate comparison is shown in Figure 3.26. The HPI flow rate comparison is shown in Figure 3.27.

The RELAP5 prediction of the break flow and the HPI flow are in good agreement with the LOFT results. Given that the primary system pressure comparison is also good indicates that good modeling of the break flow and HPI flow will yield good results for the pressure.

3.1.3.5 MIST Test

The MIST (Multi-loop Integral System Test) is a scaled, full-pressure experimental facility that represents the B&W lowered loop plant design with two hot legs and four cold legs. The plant to facility power scaling factor is 817 and the plant to facility volume scaling factor is 620 for the total primary system volume, excluding the core flood tanks. Major components include two once-through steam generators with full length tubes, two hot leg pipe segments, four cold leg pipe segments, four coolant pumps, a reactor vessel with an external downcomer, a pressurizer with spray and PORV connections, and one core flood tank. Boundary systems provided simulation of the HPI, auxiliary feedwater, and various types of failures such as steam generator tube ruptures and LOCAs. Reference 6.1-3 provides further information on the MIST facility.

RELAP5 assessment was performed for three MIST test cases, which are: 1) Test 360499 which is a HPI-PORV feed and bleed simulation, 2) Test 3109AA – a 10 cm^2 (0.0108 ft^2) cold leg break LOCA, and 3) Test 4100B2 which is a 100 cm^2 (0.1076 ft^2) cold leg break LOCA.

Test T360499 is a high pressure injection – power operated relief valve (HPI-PORV) feed and bleed simulation. The MIST facility was initially operating at full reactor coolant pump flow and 10% scaled power. The primary system pressure was 14.82 MPa (2150 psia) and the core exit subcooling margin was 47.2 K (85°F). The feed and bleed event is initiated by interrupting feed to both steam generators followed by isolation of both steam generators. Core decay power was initiated at 9 seconds into the transient. A summary of key events is presented in Table 3.7.

The key parameters of interest for assessing RELAP5 are the overall pressure and temperature response during the test. Figure 3.28 and Figure 3.29 present comparisons of the downcomer temperature and reactor coolant system pressure between RELAP5 and Test 360499, which show excellent agreement between the RELAP5 code and the test. The flow from the reactor coolant system through the PORV and the flow into the system from HPI show good agreement as seen from Figure 3.30 and Figure 3.31. Good agreement is also seen in the liquid level as shown in Figure 3.32. Reasons for the drop in level at about 6000 sec

and again at about 15000 sec are being investigated.

Table 3.7. Summary of Key Events for the MIST T360499 Feed and Bleed Test.

Event	Event Time (s)	
	Measured	RELAP5
Stop AFW pumps and isolate SGs	0	0
Scram signal (core power decay)	9	9
Pressurizer sprays actuated	48	141
PORV locked open	282	240
HPI flow begins	286	286
Reactor coolant pumps tripped	338	280
Liquid flow at PORV begins	516	251
Flow stagnation in loop A	6,963	N/A
Flow stagnation in loop B	4,285	6,232
HPI flow throttled	8,728	9,701
High point vents opened (simulation ended)	28,800	28,800

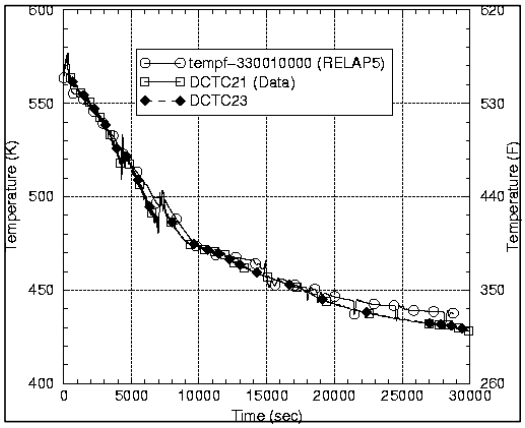

Figure 3.28. Upper Downcomer Temperature - MIST Test 360499x.

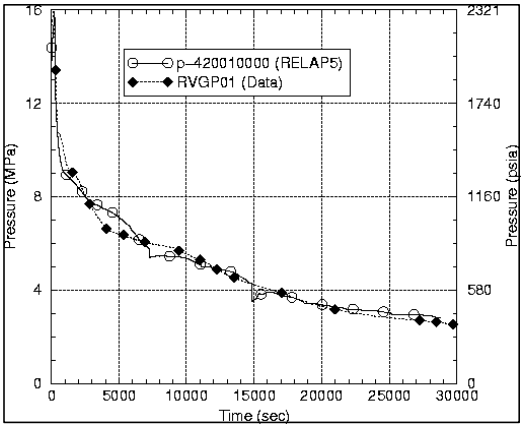

Figure 3.29. Primary System Pressure - MIST Test 360499**x.**

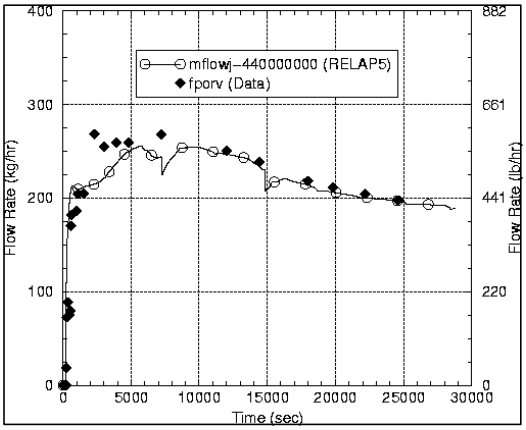

Figure 3.30. PORV Mass Flow Rate - MIST Test 360499**.**

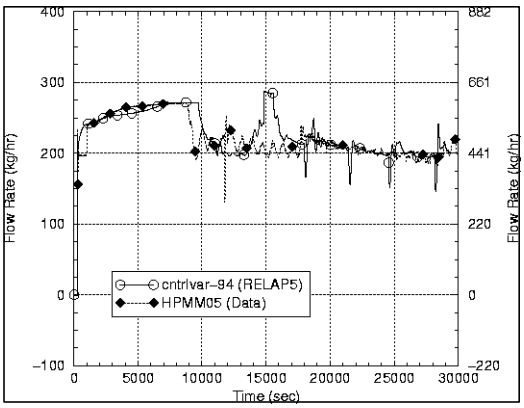

Figure 3.31. HPI Mass Flow Rate - MIST 360499**.**

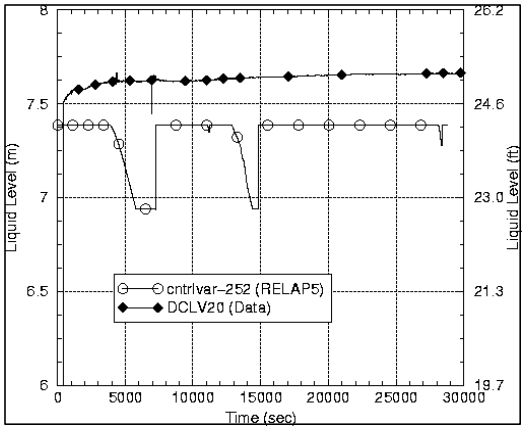

Figure 3.32. Downcomer Liquid Level - MIST Test 36049

Overall, the RELAP5 results show good agreement to MIST Test 360499. Although this test is characterized as a "feed and bleed", it resembles a stuck-open PORV with continued HPI injection and HPI throttling to control subcooling margin. Transients with stuck-open PORVs with continued HPI injection are expected to be significant contributors to the risk of vessel failure, particularly for those transients where the valve is postulated to reclose. As such, the ability of RELAP5 to reproduce the test results demonstrates that the code is suitable for characterizing the thermal hydraulic response of transients involving stuck open primary safety valves.

The second MIST test considered is Test 3109AA. This test is a 10 cm^2 cold leg break in the reactor coolant discharge section of the cold leg. This break size scales to a 3.59 cm (1.4 in) diameter break in the plant. At the start of the test, the facility was operating under natural circulation conditions with the reactor coolant pumps in a locked rotor position. The primary system pressure was 11.9 MPa (1739 psia), the secondary side pressure was 7.0 MPa (1015 psia), and the hot leg subcooling was 12.8 K (23.1°F). The core exit temperature was 584.5 K (592.4°F) and the total core mass flow rate was 0.86 kg/sec (1.9 lbm/sec). Pressurizer collapsed liquid level was 7.06 m (23.17 ft). When the pressurizer level dropped 25.4 cm (12 in) after about 1 minute, the following actions were initiated: 1) SG level setpoint was increased from 2.94 m (9.63 ft) to 9.63 m (31.6 ft), 2) the HPI was started, and 3) core decay power was initiated. A summary of key events is presented in Table 3.8.

Table 3.8. Summary of Key Events for the MIST 31099AA Test.

Event	Event Time (s)	
	Measured	RELAP5
Break opened	0	0
Low pressurizer level – initiate HPI and power decay	126	55
Hot leg A flow interruption	228	143
SG level reaches 31.6 ft setpoint level	552	532
Hot leg B flow interruption	1,020	1,362
Complete loss of loop natural circulation flow	1,560	1,373
Flow reversal in loop B	1,606	1,515
Flow reversal in loop A	2,662	4,447
Simulation ended	4,800	4,800

The key parameters of interest for RELAP5 assessment are the overall pressure and temperature response during the test. Figure 3.33 and Figure 3.34 present comparisons of the downcomer temperature and reactor coolant system pressure between RELAP5 and Test 3109AA data. The temperature comparisons show good agreement for the first 500-600 sec. Then RELAP5 is predicting a somewhat warmer (approximately 10K (18°F)) downcomer temperature. The pressure trend between RELAP5 and the test data is similar with the RELAP5 results being about 1 MPa (150 psia) higher, as seen in Figure 3.33. The measured and calculated break flow rate and the HPI flow rate are in good agreement as seen from Figure 3.35 and Figure 3.36.

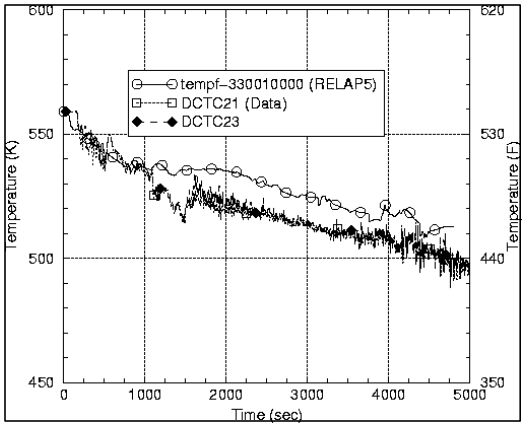

Figure 3.33. Downcomer Temperature - MIST Test 3109AA **x.**

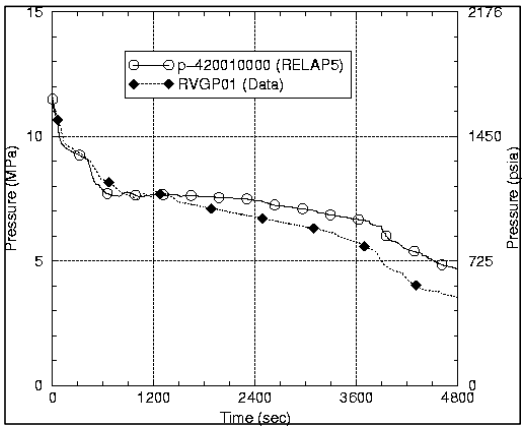

Figure 3.34. Primary System Pressure - MIST Test 3109AA.

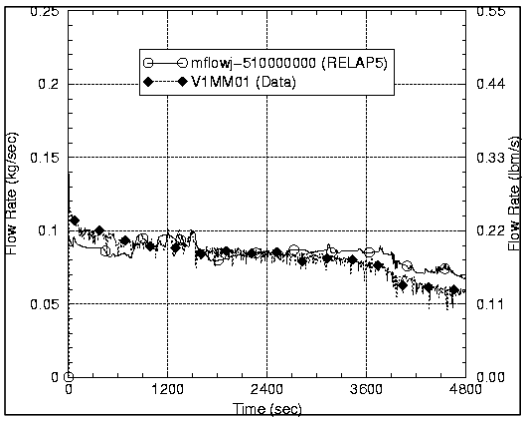

Figure 3.35. Break Flow Rate - MIST Test 3109AA

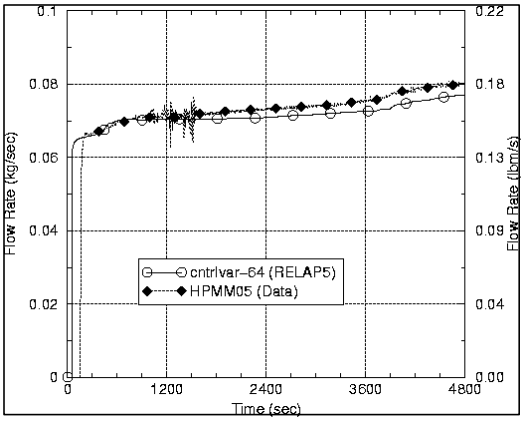

Figure 3.36. HPI Flow Rate - MIST Test 3109AA **x.**

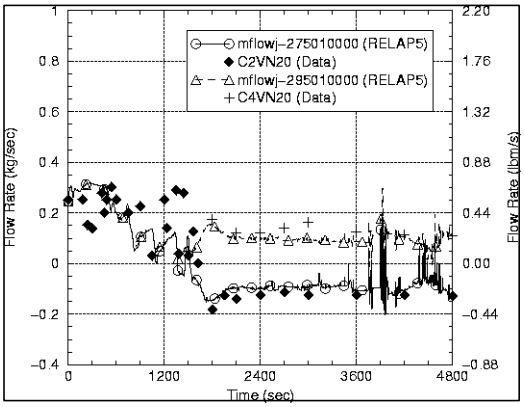

Figure 3.37. Mass Flow Rate in Cold Legs (B Loop) - MIST Test 3109AA .

An interesting aspect of the results of MIST test 3109AA is the cold leg flow rate. A recirculating pattern where the flow is positive in one cold leg and negative in the other cold leg in the same loop was observed. This behavior starts at about 1500 sec as seen in Figure 3.37. The Loop A results also showed a recirculating flow behavior. It is interesting that RELAP5 predicts the same type of flow pattern and is in reasonable agreement with the data. This result was evaluated and it was concluded that no justification exists for these results. It is possible that some aspect of the facility design, possibly an imbalance in heat losses, caused the cold leg flow recirculation. Also, it is believed that the RELAP5 prediction is coincidental and does not justify the comparison. Flow recirculation will cause more mixing to occur in the downcomer, resulting in higher temperatures, which is not correct. In the plant

analysis, high reverse loss coefficients were utilized in the loops near the reactor coolant pump to inhibit recirculating flows.

The third MIST test considered in the assessment is Test 4100B2. This test is a 100 cm^2 (4.4 in diameter) cold leg break in the reactor coolant discharge section of the cold leg. Core power decay is initiated after the pressurizer drains. High pressure injection and emergency feedwater are actuated increasing the level in the steam generator to the "constant level control" setpoint of 9.6 m (31.6 ft). The primary system pressure was 12.06 MPa (1750 psia), the secondary side pressure was 6.96 MPa (1010 psia), and the core exit subcooling was 12.2 K (22°F). Pressurizer collapsed liquid level was 7.0 m (23.0 ft). Table 3.9 presents a summary of key events for this test.

Table 3.9. Summary of Key Events for the MIST 4100B2 Test.

Event	Event Time (s)	
	Measured	RELAP5
Break opened	0	0
Initiate HPI and power decay	manual (within 20 sec)	0
Loss of loop natural circulation flow	~120	114
SG level reaches 31.6 ft setpoint level	~530	532
Accumulator injection begins	~1,000	991
LPI flow begins	2,043	2,093
HPI flow throttled on high subcooling	2,986	N/A
Simulation ended	4,800	4,800

As in the earlier tests, the key parameters of interest are the overall system pressure and downcomer temperature response. Figure 3.38 and Figure 3.39 present comparisons of the downcomer temperature and reactor coolant system pressure between RELAP5 and Test 4100B2. The temperature and pressure comparisons show good agreement throughout the test. The slight increase in temperature at approximately 3000 sec is due to HPI throttling during the test.

Figure 3.40 presents a comparison of the break flow between RELAP5 and Test 4100B2. There is good agreement for the first 2000 sec. After that time, RELAP5 displays an oscillatory behavior but represents the average reasonably well.

The high pressure injection, low pressure injection, and core flood tank flow rate is shown in Figure 3.41 to Figure 3.43. The drop in the HPI flow rate at about 3000 sec in the MIST test is due to HPI throttling. The differences in LPI and core flood tank are attributed to slight differences in the system pressure.

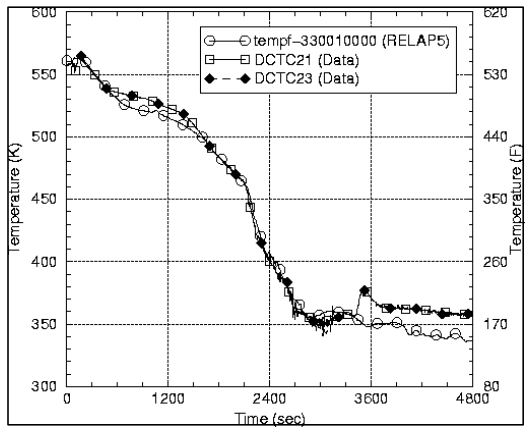

Figure 3.38. Upper Downcomer Temperature - MIST Test 4100B2**x.**

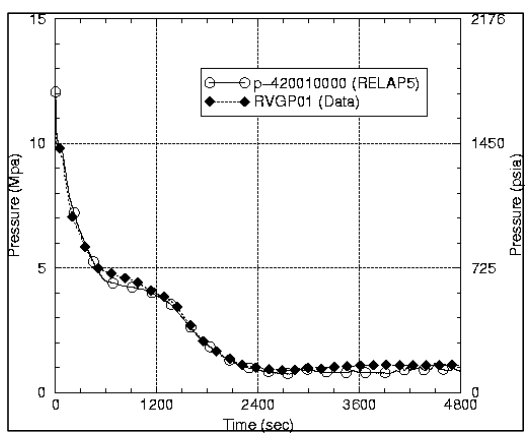

Figure 3.39. Reactor Coolant System Pressure - MIST Test 4100B2**.**

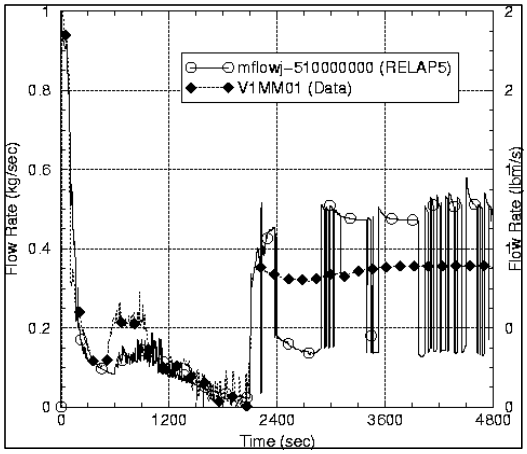

Figure 3.40. Upper Downcomer Temperature - MIST Test 4100B2.Break Flow - MIST Test 4100B2.

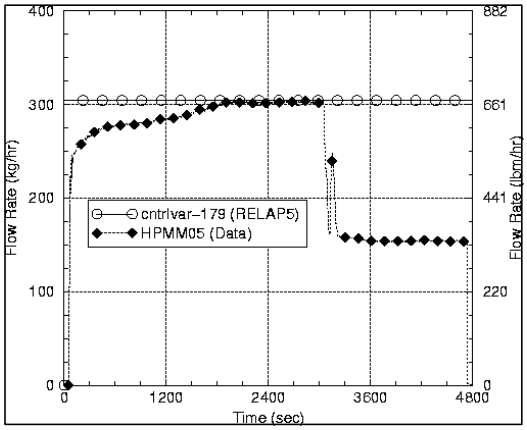

Figure 3.41. HPI Flow Rate - MIST Test 4100B2.

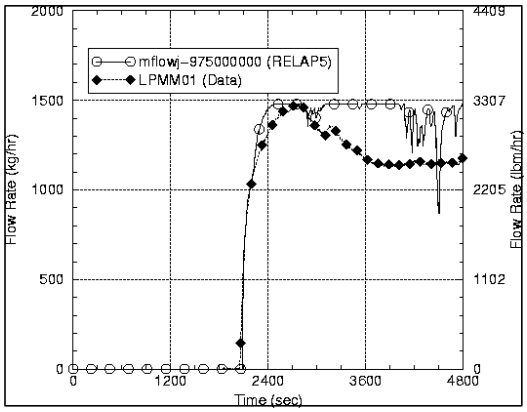

Figure 3.42. Upper Downcomer Temperature - MIST Test 4100B2**x.**LPI Flow Rate - MIST Test 4100B2**.**

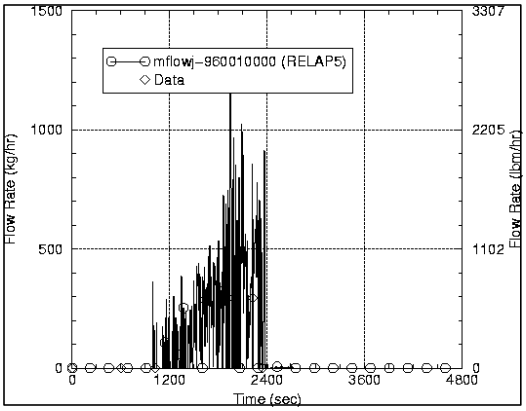

Figure 3.43. Core Flood Tank Flow Rate - MIST Test 4100B2**.**

3.1.4 Summary

Although RELAP5 has been the subject of extensive developmental and independent assessment, additional work was performed specific to the PTS re-evaluation project. This assessment included PTS-specific experiments at the Oregon State University APEX-CE facility. Additionally, this assessment included integral systems tests specific to the B&W geometry (MIST) and the Westinghouse/CE geometries (ROSA-IV). Separate effects assessment was performed to evaluate RELAP5's ability to estimate phenomena/processes judged to be of greatest importance to PTS analysis. The assessment results confirm the applicability of RELAP5 to analyze PTS transients and to establish the validity of uncertainty studies on the TH contributions to the overall PTS uncertainty.

3.2 Linear Elastic Fracture Mechanics

3.2.1 Introduction

The importance of structural integrity of RPVs has been recognized by all stake holders from the beginning of the nuclear power enterprise in the United States. Correspondingly, the NRC and the Atomic Energy Commission (AEC) before it have maintained a strong research program to evaluate and improve the technology available for use in RPV integrity assessments. The NRC/AEC research efforts have been

continuous and integrated with those of other stakeholders in the nuclear power enterprise. Those efforts began in the mid 1960s, and in the case of materials and structures technology, validation of the applicability of fracture mechanics methods to RPV analyses has been of utmost importance. One measure of the importance of the advancements that have been made is the fact that many ASTM standards (e.g. E-1820 for fracture-toughness measurement and E-1221 for crack-arrest test procedures) and much of the fracture mechanics methodology in Sections III and XI of the ASME Boiler and Pressure Vessel Code are derived from results of this research.
It has also been broadly understood that PTS events can present the most complex challenge to the structural integrity of an RPV. The NRC/AEC research efforts have methodically and sequentially addressed the various technical factors that influence loadings, material properties, and RPV response under credible scenarios including PTS situations. Therefore, the technology employed today in PTS analysis tools is the result of the progress made over the past three decades. This includes the methods, such as the FAVOR computer code, employed in current efforts to evaluate and potentially revise the PTS rule in 10CFR50.

Concerning the FAVOR computer code, fracture mechanics methodology is the most fundamental element in the overall model to compute probabilities of RPV failure. Although the FAVOR code performs probabilistic analyses, the fracture mechanics computations are made up of many deterministic analyses. The following paragraphs summarize important aspects of the NRC research that has contributed to validating the applicability of deterministic linear-elastic fracture mechanics (LEFM) to RPV analyses. The activities discussed were carried out at the Oak Ridge National Laboratory (ORNL) under the NRC-sponsored Heavy-Section Steel Technology (HSST) program. A comprehensive summary of the overall efforts of the HSST program's research through the mid 1980s is given by (Whitman 86).

That research has included detailed integrated experimental/analytical studies of RPV behavior and integrity through the use of specimens whose sizes have ranged from small to large. The studies of the fracture behavior of large-scale specimens are emphasized in the following paragraphs, and included three distinct phases of experiments that used thick-wall cylindrical specimens. Those phases sequentially addressed vessels exposed to (1) pressure loads, (2) thermal transient loads, and (3) concurrent pressure and thermal transients, and have been historically referred to as Intermediate Test Vessel (ITV) experiments, Thermal Shock Experiments (TSEs), and Pressurized Thermal Shock Experiments (PTSEs). Each of these three phases is discussed below in terms of fracture behavior and their roles in validating the applicability of LEFM to PTS analyses. A total of 22 thick-wall cylinder tests made up these phases, and they were carried out from the early 1970s to the mid 1980s.

3.2.2 Intermediate Test Vessel (ITV) Experiments

The ITV experiments were planned to demonstrate a capability to predict vessel transition behavior, which is a demarcation between ductile and frangible behavior, to verify methods of analysis that could be used to predict fracture behavior over a range of conditions in heavy-section thickness, and to examine the conservatism in the then current ASME design rules for RPVs. The ITV specimens were thick-wall pressure vessels that had a 6-in. wall thickness, an outer diameter of 39 in., and a test section length of 54 in. Each ITV was designed and fabricated consistent with the then current edition of the ASME Boiler and Pressure Code. Accordingly, each vessel had an ASME internal design pressure equal to 9.6 kips. After fabrication, ORNL intentionally flawed the vessels with cracks of prescribed geometries and tested the vessels to failure under internal pressure. ORNL analyses and extensive peer review determined that the 6-in. thickness would produce adequate constraint for fracture analysis validation experiments, and that the constraint and stress states would be representative of those which could occur in a full-scale RPV.

Ten ITV vessels were procured, and three were fabricated with cylindrical nozzles having features typical of light-water reactor vessel penetrations. As an example, Figure 3.44 shows a schematic of the vessel that was used in test ITV-7. Each ITV test vessel had the same dimensions except for the test area (flaw geometry).

A total of 12 tests were performed on 9 intermediate vessels over a period of 10 years. (One of the nozzle vessels remains untested.) Some of the vessels were used in more than one experiment by replacing the test section with different test materials. Preparation of the tests involved a great deal of engineering development and planning to deliberately fail the vessels within a given range of high internal pressures and with high priority given to test safety considerations. Table 3.10 lists the test dates, materials, test temperatures, flaw sizes, and material toughness values.

The 12 tests involved cases where the test region was RPV base metal and others where it was weld metal. The test temperatures traversed the Charpy energy curve from the low transition region to well above onset of the upper shelf region. Accordingly, the fracture behavior ranged from brittle fast fracture to total ductile tearing, respectively. This is illustrated by Figure 3.45, which shows the position of each test on the Charpy curve and indicates transition of fracture characteristics from cleavage to ductile propagation.

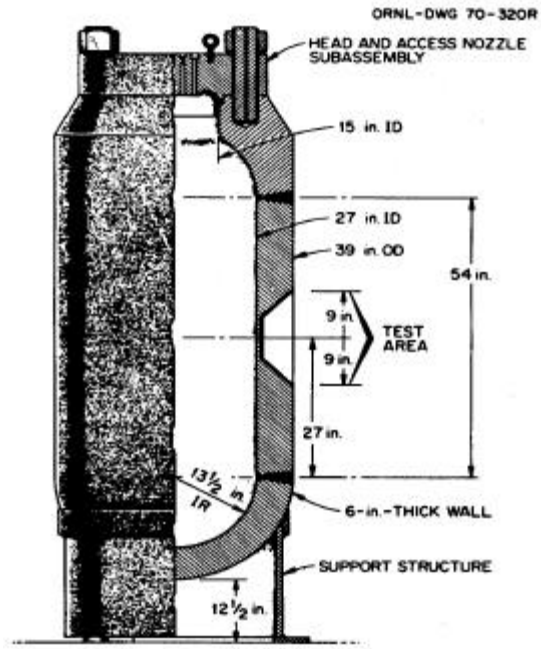

Figure 3.44. Schematic of ITV-7 test vessel. Dimensions were the same for each ITV vessel while the specifics of the flaw region and test material varied from test to test.

Table 3.10. ITV test sequence and test parameters.

Vessel No.	Test Date	Flaw Depth (in.)	Flaw Length (in.)	Test Temp. (°F)	Fracture Toughness (ksiÖin)	Test Material
1	6/30/72	2.56	8.25	130	311	A508-2
2	9/28/72	2.53	8.30	32	184	A508-2
3	11/8/72	2.11	8.50	130	325	Weld
4	12/20/72	3.00	8.25	75	160	Weld
6	7/7/73	1.87	5.25	190	369	Weld
5	2/13/74	1.20	Nozzle	190	241	A508-2
7	6/19/74	5.30	18.6	196	301	A533-B
9	8/28/74	1.20	Nozzle	75	150-275	A508-2
7A	6/18/76	5.30	18.6	196	301	A533-B
7B	7/14/77	5.30	18.6	196	199-329	Weld HAZ
8	7/26/78	2.50	8.10	-11	90	Weld
8A	8/11/82	2.75	11.0	300	200	LUS Weld

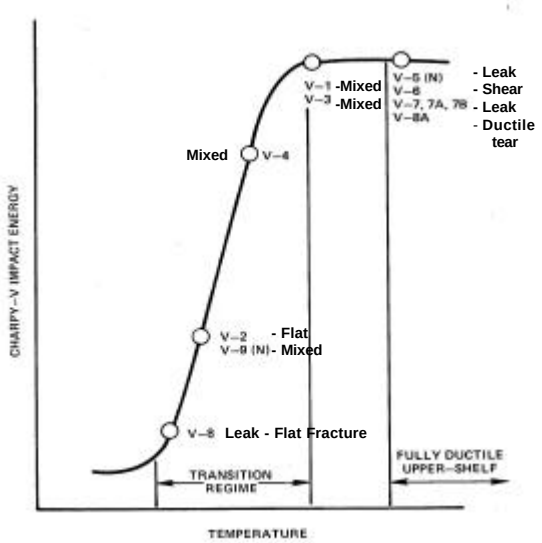

Figure 3.45. ITV test temperatures superimposed on a Charpy curve illustrate relative condition of the twelve ITV experiments. Also fracture surface is characterized for each test.

The first test, ITV-1, was performed to show that gross yielding of the vessel wall could be achieved with a large flaw present when the vessel was operating in the upper-shelf regime of toughness. The sequence of tests that followed covered the complete range of fracture failure behavior in relevant materials with varying flaw sizes to include complex stress states and residual stress effects. (Whitman, 86) provides a summary of the ITV experiments and other important parts of the HSST program through the mid 1980s, while Table 3.11 lists detailed reports that were prepared for individual ITV tests.

Figure 3.46 and Figure 3.47 show the posttest condition of the test vessels for ITV-2 and ITV-6. Because the temperature for ITV-2 was low in the Charpy transition range (just above NDT) and that for ITV-6 was well above onset of Charpy upper shelf region, the fracture modes are fully cleavage fast fracture and fully ductile shear, respectively. This range of fracture modes for the thick sections is consistent with fracture behavior observed from tests of smaller laboratory specimens.

Table 3.11. List of detailed reports on individual ITV experiments.

ITV Test Number	Report Reference	Report Number
ITV-1 and -2	(Derby 74)	ORNL-44895
ITV-3, -4, and -6	(Bryan 75)	ORNL-5069
ITV-5 and -6	(Merkle 77)	ORNL/NUREG-7
ITV-7	(Merkle 76)	ORNL-NUREG-1
ITV-7B	(Bryan 78a)	NUREG/CR-0309 (ORNL/NUREG-38)
ITV-8	(Bryan 79)	NUREG/CR-0675 (ORNL/NUREG-58)
ITV-8A	(Bryan 87b)	NUREG/CR-4760 (ORNL-6187)
ITV-7A	(Bryan 78b)	ORNL/NUREG-9

As was the case with each ITV vessel, the ITV-2 vessel contained a fabricated flaw, and because it had a test temperature (32°F) low in the Charpy transition range, it fractured by fast cleavage propagation. It was the only vessel in the ITV series where the crack branched to the point that fragments separated from the remainder of the vessel. All others ITV tests resulted in fracture surfaces whose deviations from flatness and bulging increased from very little to more pronounced (e.g., ITV-6) as the test temperature rose from low to high on the Charpy curve. The flaws that propagated by ductile tearing (e.g., ITV-6) arrested when the crack driving force began to decrease with depressurization due to the through-wall crack.

Figure 3.46. ITV-2 vessel was tested under high pressure and at a temperature (32°F) that was low in the Charpy transition region; fracture was by fast cleavage propagation.

Figure 3.47. ITV-6 test vessel was tested under pressure and at a temperature (190°F) that was well above onset of Charpy upper shelf; fracture was by ductile shear.

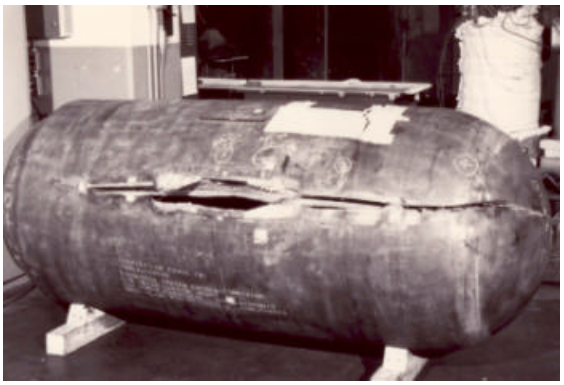

Figure 3.48. ITV-1 vessel was tested under pressure and at a temperature (130°F) that was high in the Charpy transition region; fracture was mixed cleavage and ductile behavior.

Most of the other ITV vessels showed mixed cleavage and ductile behavior and the post fracture vessels appeared similar to ITV-1, which is shown Figure 3.48. The fractures were generally flat, and there was limited gross bulging of the vessels.

From an overall point of view, the fracture mode results for these tests verified for the first time that thick sections of RPV steels exhibit a fracture mode transition with temperature consistent with that observed for small specimens. In that transition, the fracture goes from brittle cleavage fracture to ductile tearing as the temperature increases from the lower shelf region to the upper shelf region of the Charpy energy curve.

(Merkle 75) provides a thorough evaluation of ITV test results including interpretations relative to Section III, ASME-BPV code. As taken from (Merkle 75), Table 3.12 shows a summary of the test results for six ITV experiments that used vessels without nozzles.

Table 3.10 and Table 3.12 show that (in addition to temperature) flaw size and stress concentrations have a strong influence on the conditions at failure. This is illustrated best by comparing the results of tests ITV-6 and ITV-7. These experiments were conducted at similar temperatures, but ITV-7 had a much deeper flaw

(a = 5.3 in.) than did ITV-6 (a = 1.87 in.). One of the principal objectives of ITV-7 experiment was to demonstrate whether or not a vessel with a very deep flaw could sustain a pressure in excess of the design pressure prior to crack initiation. In fact, Table 3.12 shows the vessel sustained more than two times the design pressure before fracture occurred.

The data in Table 3.12 also show that each of the six vessels without nozzles did not exhibit fracture until the applied pressure exceeded the design pressure by a factor of about three. Figure 3.49 shows the ratio of failure pressure to design pressure for these six tests and two tests of ITV vessels that contained nozzles (ITV-5 and -9) ranged from 2.2 to 3.2.

While these experiments demonstrated the very good ability of LEFM methods to predict failure of thick wall vessels, they also provided excellent opportunities to compare loading conditions allowed by the ASME code with actual failure conditions of those pressure vessels. (Merkle 75) conducted a methodical study that illustrated the conservatism in LEFM methodology even when it was assumed that a flaw might exist with depth equal to the maximum allowed by Section XI, ASME BPV code. In that case, (Merkle 75) showed that the vessel would still experience gross yielding prior to reaching fracture initiation.

Table 3.12. Results from six ITV experiments using specimens without nozzles.

ITV Test No.	P_f Max. Test Pressure (ksi)	P_d ASME Design Pressure (ksi)	P_{LEFM} Predicted Max. Pressure (ksi)	Load Factor P_f/P_{LEFM}	Load Factor P_f/P_d
2	27.9	9.6	27.4	1.018	2.87
4	26.5	9.6	26.2	1.012	2.73
1	28.8	9.6	27.5	1.047	2.96
3	31.0	9.6	27.5	1.127	3.19
6	31.9	9.6	27.5	1.160	3.28
7	21.4	9.6	20.8	1.929	2.20

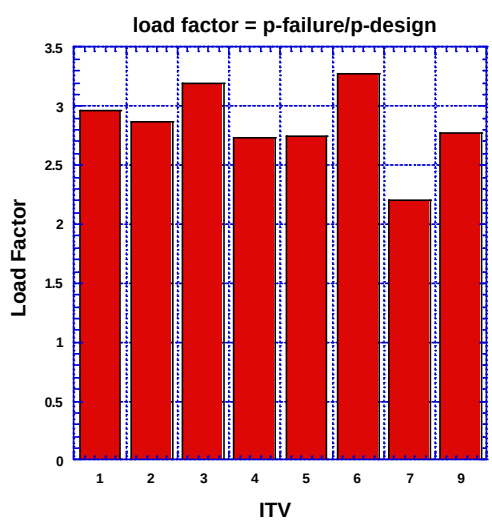

Figure 3.49. Plot of P_f/P_d (fracture pressure to design pressure ratio) for eight ITV experiments.

In summary, the principal observations and conclusions made from the ITV tests include (1) the transitional character of fracture-failure was verified using thick-section structures with appropriate temperatures and stress levels; (2) analyses based on LEFM very closely predicted actual fracture pressures for these thick-wall pressure vessels, (3) flawed vessels fractured at pressure levels significantly greater than the operating pressure allowed under the ASME Code; (4) methods for calculating fracture toughness from small specimens were successfully used in applications of fracture analysis of thick flawed vessels; and (5) the vessels were observed to generally sustain loads three times their design pressure, thus confirming the existence of the intended margin of safety for full-scale vessels.

3.2.3 Thermal-Shock Experiments

The second phase of HSST large-scale fracture experiments was carried out between 1975 and 1983 and was made up of a set of eight thermal-shock experiments (TSEs) that used thick cylinders made of RPV steel. The purpose of these experiments was to investigate the behavior of surface cracks under thermal shock conditions similar to those that in principle would be encountered during certain PWR postulated accident conditions, such as large-break loss of coolant accident (LBLOCA). It was known that the injection of cold water by the emergency core cooling system into a hot reactor vessel after a LOCA could produce conditions under which a preexisting small flaw might suddenly extend as a result of the low temperature and (higher) thermal stresses. The propensity for such an occurrence is strongly dependent on the degree of degradation in fracture toughness the vessel wall may undergo from radiation damage and the temperature of the cooling water. The HSST program was directed to address this issue to ensure that material properties and methods of analysis were developed to a degree that vessel integrity could be accurately assessed throughout the projected vessel lifetime. It was recognized that fracture mechanics analysis for thermal shock conditions involves several features that may not have been adequately examined experimentally, e.g., equal biaxial stresses, steep gradients in stress and toughness through the wall, variations in these parameters with time, crack arrest in a rising K_I field, and warm prestressing (WPS).

To aid in the definition of the TSEs, Figure 3.50 was constructed to illustrate through-wall conditions that would exist at a point in time during a thermal shock that would correspond to a LBLOCA. If a flaw of depth a existed on the inner surface of the vessel of wall thickness W, the high thermally-induced tensile stress will result in a significant stress-intensity factor at the tip of the flaw. The combined effect of this high K_I and low fracture toughness in the inner-surface region may result in propagation of the flaw. However, the steep positive gradient in the fracture toughness provides a mechanism for crack arrest. Figure 3.50 includes K_I, K_{Ic}, and K_{Ia} curves for this situation and shows that both shallow and deep flaws can initiate. A shallow flaw, which is more likely to exist as an initial flaw, can initiate and propagate through a significant distance (e.g., about 30 percent of the wall in this figure) before arresting. The deep flaws may be the result of an earlier initiation-arrest event, and at the time shown in this figure, will experience an additional initiation and arrest event (e.g., an additional 10 percent of the wall in this figure).
These curves illustrate that flaws of different depth could initiate at the same time into the transient and arrest at the same depth. They also illustrate that LEFM analyses predict that a given initial flaw can experience multiple run-arrest events. Similar to observations from Figure 3.50, Figure 3.51 illustrates that deep flaws that are subject to initiation may exist because it was a preexisting flaw or because it was created by a shallow flaw experiencing earlier run-arrest events. It is also seen that growth of a deep flaw can result in relatively long jumps.

Critical-crack-depth curves were also constructed as an additional aid in designing and interpreting the TSEs. Figure 3.51 illustrates such curves for the thermal shock addressed in Figure 3.50. The critical-crack-depth curves display the calculated behavior of a flaw during the transient by plotting the crack depths corresponding to initiation and arrest events ($K_I = K_{Ic}$ and $K_I = K_{Ia}$) and other conditions of interest as functions of time into the transient at which they occur. These calculations were based on LEFM models.

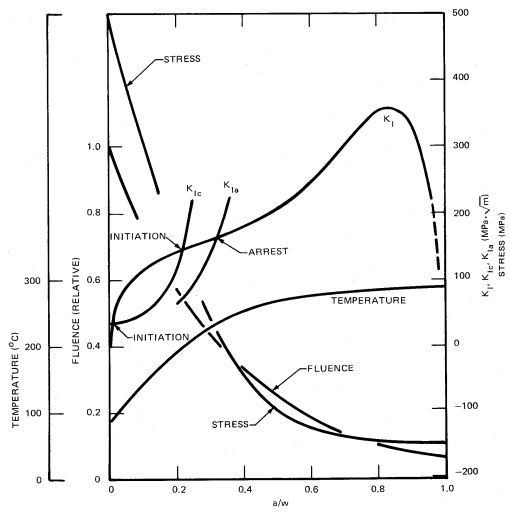

Figure 3.50. Typical instantaneous temperature, stress, fluence, stress-intensity factor, and fracture-toughness distributions through wall of PWR vessel during LBLOCA.

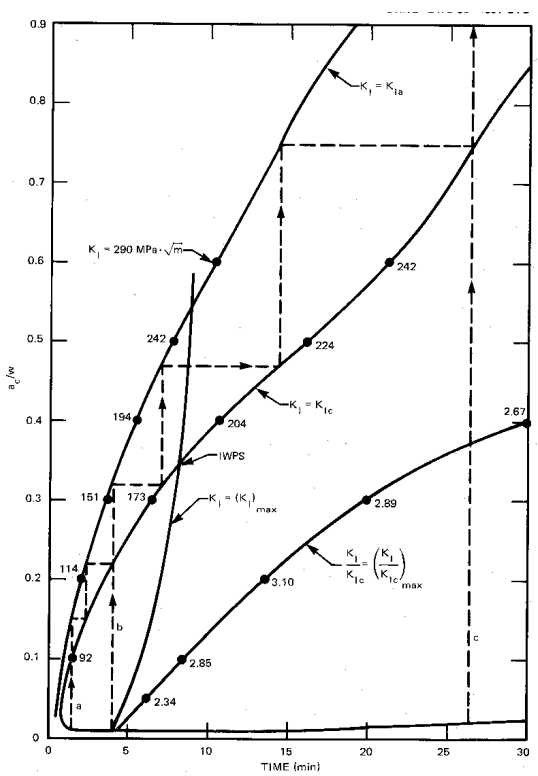

Figure 3.51. Critical-crack-depth curves for PWR vessel during LBLOCA.

The phenomenon known as warm prestressing (WPS) was recognized to be capable of preventing reinitiation at depths less than the final arrest depth indicated by Figure 3.51. The concept of WPS means that a flaw will not initiate when K_I is decreasing with time even though $K_I \geq K_{Ic}$. In the case of thermal shock loading conditions, a deep flaw can conceivably experience it maximum K_I value at a time before the crack tip temperature has decreased enough to make $K_I \geq K_{Ic}$. During the thermal shock, K_I for a given crack depth increases and then begins to decrease with the temperature gradient. However, K_{Ic} continues to decrease as long as the temperature continues to decrease. The curve in Figure 3.51 labeled $K_I = K_{I(max)}$ shows the times at which K_I reaches a maximum for various crack depths. Thus, for times less than indicated by this curve, K_I is always increasing, and for greater times, K_I is always decreasing. If WPS is effective, then crack initiation would be limited to times to the left of this curve. Another feature of the WPS effect would be that if K_I were to later begin to increase (e.g. due to repressurization), the material would exhibit an apparent elevated fracture toughness for temperatures below that for which K_{Ic} is approximately equal to the previously experienced $K_{I(max)}$.

All these observations contributed to the design of the TSE experiments. The TSE series included scenarios that involved both long and short crack jumps, as well as cases to examine fracture behavior where multiple crack initiation-arrest events would occur and potentially experience intervention by WPS effects. Eight TSE experiments were carried out in two phases that used different specimens and test conditions as summarized below.

The first four TSEs were conducted from September 1975 to January 1977 and used hollow cylindrical specimens fabricated from the trepanned cores taken from the ITV forgings (A508 class-2 steel). The test system used chilled water or water-alcohol mixtures (-23°C) to produce thermal stresses in the heated (288°C) test specimens containing a long internal surface flaw. These test cylinders had an OD of 530 mm (21 in.) and an ID of 240 mm (9.5 in.), and they were 910mm (36 in.) in

length. The flaws were shallow with a depth of either 11mm (0.42 in.) or 19 mm (.75 in.). As discussed by (Cheverton 76 and 77), the fracture results from these experiments were in very good agreement with predictions based on the LEFM analyses. This was valuable information as these initiations took place under the nonhomogeneous conditions produced by the thermal shocks, and the LEFM models made use of properties obtained from small laboratory specimens tested under homogeneous material and loading conditions. However, because of the specimen stiffness, deep crack penetrations could not be achieved. Therefore, from August 1979 to May 1983, the second set of four experiments (TSE-5, 5A, 6, and 7) was performed with larger specimens in which deeper crack advance could occur from greater bending, as would be the case in a PWR vessel.

The larger cylinders used for these tests were made of A508, Class 2 steel, and had an OD of 991mm (39 in.), ID of 682 mm (27 in.), and length of 1220 mm (48 in.). They were given a quench and temper heat treatment that led to higher (and more conventional) fracture toughness values than was the case for the first four TSE specimens (quench only heat treatment). Thus, a facility that could provide a more severe thermal shock was required for this second set of TSEs. Figure 3.53 shows a schematic of the liquid nitrogen facility that was constructed at ORNL for testing these larger specimens.

Figure 3.52 shows a TSE test cylinder prior to its instrumentation and installation into the TSE test facility. The heated (96°C) test cylinders that contained inner surface flaws were submerged into the liquid nitrogen tank (-196°C) to chill their inner surface to produce the desired level of temperatures and stresses at the crack tips.

The conditions of these tests are discussed in detail in (Cheverton 85a, 85b, and 86). The test cylinders for TSE-5, 5A, and 6 contained long surface flaws with depths a = 16, 11 , and 7.6 mm, respectively, while the TSE-7 specimen contained a finite length flaw that was 37 mm long and 14 mm deep.

Figure 3.52. TSE test cylinder like those used in TSE-5, -5A, -6, and -7.

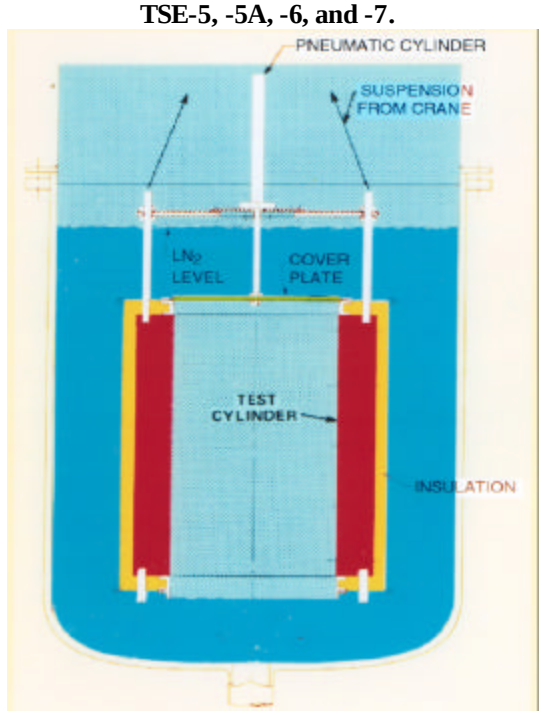

Figure 3.53. Schematic of ORNL's thermal shock test facility used for TSE-5, 5A, 6, and 7.

TSE-5 experienced a series of three initiation/arrest events with deep penetration (to 80 percent of the wall) of the two dimensional

flaw. The occurrence of the three events was entirely consistent with predictions based on LEFM analyses that included the generation of critical crack depth curves [Cheverton 85a]. The analyses predicted a final crack depth of a/W = 0.50 to 0.70 depending upon the effective of WPS effects. Figure 3.54 shows a posttest cross section of the TSE-5 cylinder that clearly shows the three phases of crack jumps that occurred in this test.

As reported by (Cheverton 86), TSE-5A experienced four initiation/arrest events with 50 percent penetration of the wall. Again this was consistent with pretest analyses based on LEFM methods. A fifth event was prevented by WPS effects and one of the arrest events took place with KI increasing with crack depth. After the WPS intervention, the K_I/K_{Ic} ratio reached a maximum value of 2.3 without crack initiation taking place.

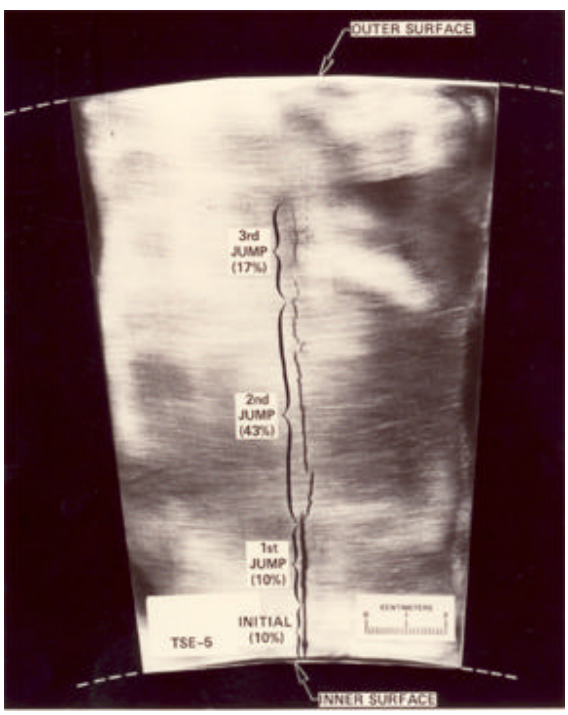

Figure 3.54. Cross section of TSE-5 test cylinder showing the three long crack jumps that occurred during the thermal shock.

The TSE-6 cylinder had a thinner wall (76 mm vs. 152 mm for the other tests) and introduced the potential for a single long crack jump to a depth greater than 90 percent of the wall thickness. There were actually two crack jumps in the test, the first being relatively short, and the total penetration of 93 percent. This test helped demonstrate the inability of a long flaw to fully penetrate the vessel wall under thermal-shock only loads. This test also demonstrated that there appeared to be negligible dynamic effects associated with arrest following a long crack jump, and the first arrest took place with K_I increasing with crack depth.

TSE-7 was intended to demonstrate the ability of a short and shallow flaw, in the absence of cladding, to extend on the surface to effectively become a long flaw. The initial flaw, which was oriented axially and was essentially semi-elliptical in shape, extended on the surface in a single event and bifurcated many times to produce an extensive cracking pattern [Cheverton 85b]. This event was followed by two crack initiation events that extended the complex flaw to a 55 mm depth in the central portion of the cylinder and to lesser depths toward the ends of the cylinder.

Critical values of K_I deduced from these TSE experiments and corresponding to the crack initiation and arrest events are compared with laboratory specimen data in Figure 3.55 and Figure 3.56, respectively. (Data from TSE-7 are omitted because of the uncertainty introduced by the complex three-dimensional consideration of the flaws.)

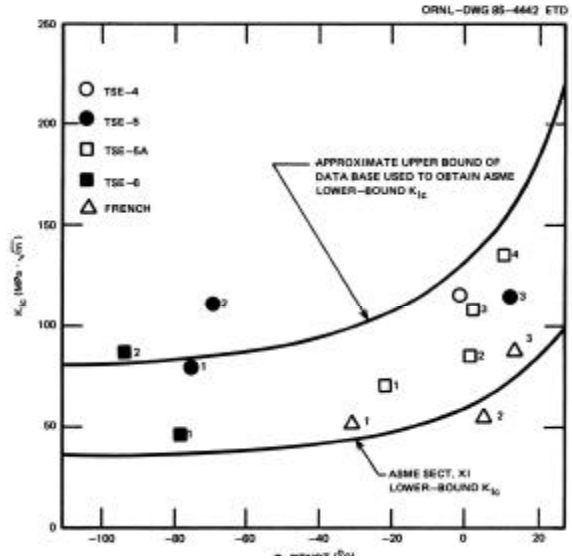

Figure 3.55. Comparison of laboratory-specimen and TSE large-specimen K_{Ic} data.

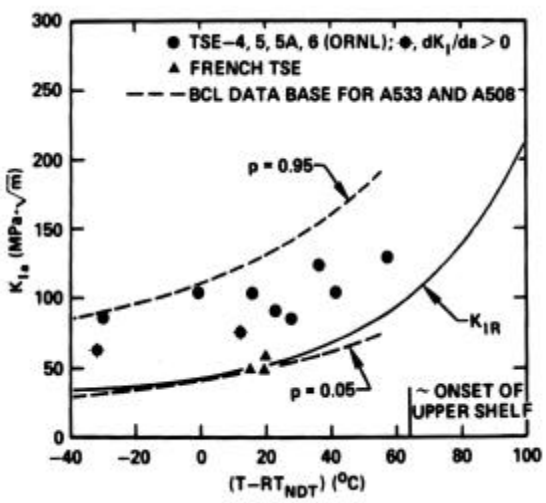

Figure 3.56. Comparison of laboratory-specimen and TSE large-specimen K_{Ia} data

(The data points (in Figure 3.55 and Figure 3.56) identified as FRENCH data should be ignored in this assessment as discussed by [Cheverton 85b]) The curves shown in these figures are the upper and lower-bound curves from small-specimen data. Overall the K_{Ic} and K_{Ia} values derived from TSE experiments shown in these two figures demonstrate that the behavior of these large-scale fracture situations can be adequately predicted by the use of LEFM methods and fracture properties obtained from tests of small laboratory specimens.

In summary, the objectives of the TSEs were successfully achieved and greatly enhanced the confidence that can be placed in predictive capabilities and the inherent integrity of RPVS. Specific conclusions reached included (1) multiple initiation-arrest events with deep penetration into the vessel wall were predicted and observed; (2) short, shallow flaws surface flaws could be made to grow long and deep; (3) warm prestressing limited crack extension through the wall under LOCA conditions; (4) flaws did not penetrate the outer vessel wall even after long crack jumps; (5) small-specimen fracture mechanics data could be interpreted for use in fracture mechanics analysis of the vessel; (6) crack arrest could be obtained in a rising stress field; and (7) dynamic effects were not significant in arrest calculations for the advances produced in the test structures.

In addition to these results, the OCA series of computer programs were developed under the thermal-shock project [Iskander 81, Cheverton 84] and the thermal-shock analysis was the forerunner and foundation for subsequent pressurized thermal shock tests and evaluations.

3.2.4 Pressurized Thermal Shock Experiments

The PTS experiments conducted by the HSST Program [Bryan 85; Bryan 87a] represent major milestones in the long succession of fracture-mechanics experiments that investigated important aspects of fracture behavior in nuclear RPVs. These experiments provided the means for confirming the application of theoretical models of fracture behavior to fracture analysis of vessels in nuclear plants. Principal issues of concern in the PTS experiments included

- warm-prestressing effects;
- crack propagation from brittle to ductile regions;
- nature of cleavage crack arrest at temperatures near or above the onset of the Charpy upper shelf;
- behavior of low upper-shelf energy steels.

The HSST program developed facilities for performing PTS experiments that challenged the predictions of analytical methods applicable to full-scale RPVs under combined thermal and pressure loadings. The scale of the tests was chosen to be large enough to attain full-scale constraint of the flawed region in the vessel. Test conditions and materials were selected to produce stress fields and gradients around the flaw that are characteristic of RPVs and to provide realistic fracture toughness conditions. The experiments were designed and analyzed using

- small-specimen fracture toughness data; and
- the OCA [Iskander 81, Cheverton 84] linear-elastic fracture mechanics (LEFM) code (a precursor to the FAVOR [FAVOR 02] code).

In this section, the focus of the discussion is on the first PTS experiment performed by HSST, i.e., PTSE-1 [Bryan 85]. That experiment incorporated a surface crack that was long, sharp and shallow, as assumed in regulatory assessments at the time of the test. The material properties were typical of those for an RPV subjected to moderate neutron embrittlement of the wall. Analytical studies confirmed that the stress levels and gradients around the outside surface flaw in the test vessel provide an acceptable approximation of those occurring in an RPV with a flaw on the inner surface during a postulated PTS event. Recently, the PTSE-1 experiment was re-analyzed using version 02.2 of FAVOR [FAVOR 02]. Results of that re-analysis, presented herein in a following section, provide confirmation that cleavage-crack behavior in large-scale thick-walled pressure vessels is reasonable described by LEFM methodology as embodied in the FAVOR code.

The geometry and dimensions of the ITV are shown in Figure 3.57 and in Table 3.13. A plug of specially tempered SA508, Class 2 steel was welded into the ITV V8-A vessel. A sharp outer-surface flaw (1m long) was implanted into the plug by cracking a shallow electron-beam weld under the influence of hydrogen charging. Extensive instrumentation was applied to the vessel to provide direct measurements of crack-mouth opening displacement, temperature profiles through the wall, and internal pressure during the transient. The flawed and instrumented vessel was inserted into an outer vessel, which was electrically heated to bring the vessel to the desired uniform initial temperature of about 290°C. (Figure 3.58 depicts an ITV being lowered into the outer containment vessel at the HSST test facility). The outer vessel also served as a shroud for the PTS transient. A thermal transient was initiated by suddenly injecting chilled water or a methanol-water mixture into the outer vessel. The annulus between the cylindrical surfaces of the two vessels was designed to permit coolant velocities that would produce the appropriate convective heat transfer from the outer surface of the test vessel for a period of about 10 min. Internal pressurization of the test vessel was controlled independently by a system capable of pressures up to about 100 MPa.

Extensive material properties characterization testing and fracture mechanics analyses were carried out during the design phase of the PTSE-1 experiment. Fracture initiation and arrest toughness data were generated from tests of 25 mm and 37 mm compact specimens. Those small-specimen data were employed to construct fracture toughness models for planning the test transient. The test plan for PTSE-1 was to achieve initiation and arrest of a fast-running crack, render the crack super-critical (i.e., $K_I > K_{Ic}$) while in a warm-prestressed (WPS) state, and then re-initiate the crack, driving it toward the completely ductile material deep into the wall. The transient was to be terminated at an appropriate point in time to avoid deliberately bursting the wall of the test vessel. Figure 3.59 depicts essential features of the simple WPS cycle envisioned for the PTSE-1 experiment. The loading factors of temperature and pressure [Figure 3.59 (a)] are coordinated to produce a crack driving force K_I that is decreasing with time ($dK_I/dt < 0$) when the flaw becomes critical [$K_I = K_{Ic}$ in Figure 3.59 (b)]. Crack propagation of the super-critical crack is inhibited by simple WPS during this period. Warm-prestressing is relieved by increasing the pressure and

rendering $dK_I/dt > 0$, thereby introducing the possibility of initiation for the super-critical crack.

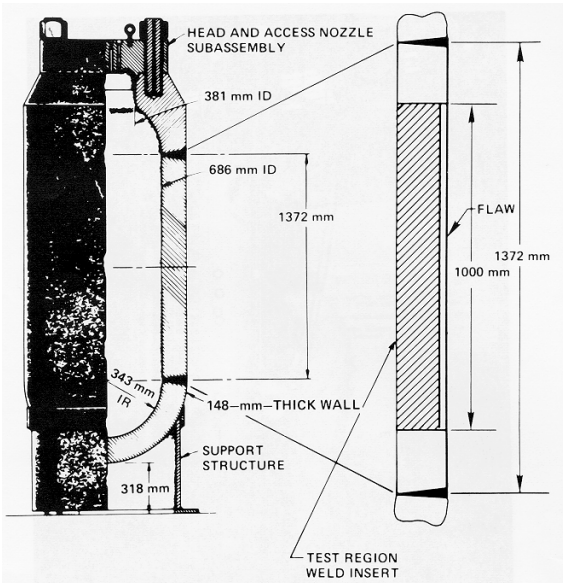

Figure 3.57. Geometry of PTSE-1 test vessel

Table 3.13. Geometric Parameters of the PTSE-1 vessel.

Parameter	Value
Inside radius, mm	343
Wall thickness (w), mm	147.6
Flaw length, mm	1000
Flaw depth (a), mm	12.2
a/w	0.083

Figure 3.58. Test vessel being lowered into outer containment vessel at HSST PTS test facility.

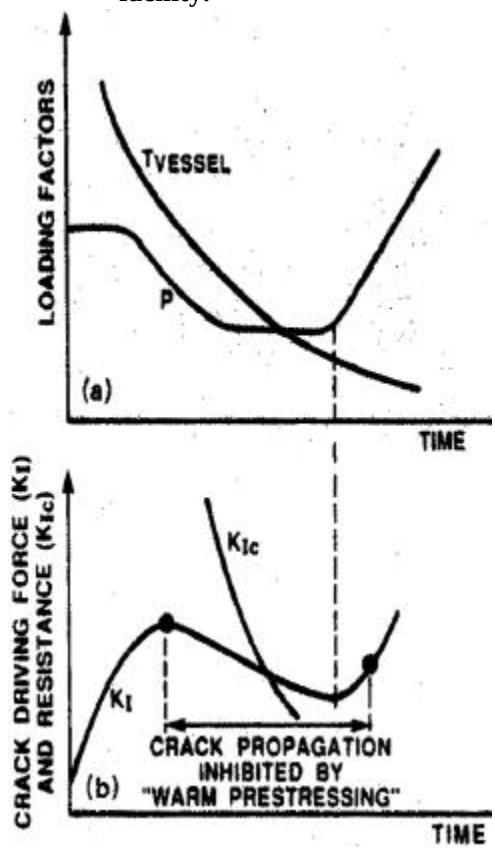

Figure 3.59. Essential features of the simple WPS cycle: (a) loading transient; (b) coordination of transient crack driving force with fracture toughness to induce simple WPS conditions.

The idealized transient originally designed for the PTSE-1 experiment is depicted in Figure 3.60. Referring to Figure 3.60, the specific objectives are defined in the following intervals.

- Interval A-B: initiation at A and arrest at B of a cleavage fracture;
- Interval B-C: continued loading of the arrested crack;
- Interval C-D-E: crack becomes critical at D, but cleavage initiation is inhibited by WPS;
- Interval E-F: WPS is relieved by increasing the pressure beginning at E;
- Interval F-G: cleavage re-initiation at F and arrest on ductile upper shelf at G;
- Beyond G: termination of transient to prevent through-wall failure.

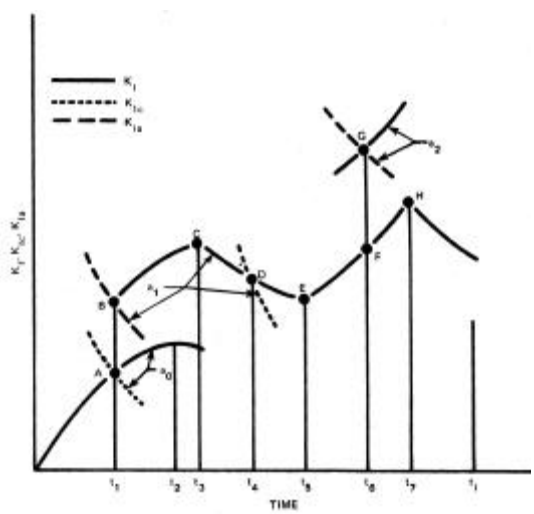

Figure 3.60. Idealized crack driving force transient for PTSE-1.

The actual PTSE-1 experiment was conducted in three transients, denoted as PTSE-1A, -1B, and –1C. Initial flaw depths and vessel/coolant temperatures for those transients are summarized in Table 3.14; time histories of the applied internal pressure are depicted in Figure 3.61. The KI trajectories constructed from experimental data recorded during the three transients are shown in Figure 3.62. Because temperature (on the abscissa) decreased monotonically with time, the temporal progression of the K_I trajectories is from right to left in Figure 3.62. In the A test, the actual pressure transient varied slightly from what was planned, the crack was slightly deeper than had been estimated, and the actual toughness was high than had been estimated. As a consequence, the crack did not propagate during the A transient. Inspection of the K_I trajectory for that test in Figure 3.62 reveals two episodes of simple WPS ($dK_I/dt < 0$), each followed by simple anti-WPS ($dK_I/dt > 0$) when K_I is greater than K_{Ic}. Termination of the transient produced a third episode of simple WPS.

Plans for the B and C transients were based on evidence from test A that the vessel had greater toughness than first estimated and that to overcome WPS, a higher K_I value would have to be attained. Thus, a small adjustment was made to the fracture toughness curve used in pretest analyses, lower coolant temperatures were selected for the thermal transient, and a transient utilizing higher pressure was defined. A two-step pressure transient was not performed during the B test because a second pressure increase of useful magnitude was not achievable with the pressurization system. The B transient produced a crack jump to a depth of 24.4 mm. The conditions of initiation and arrest are shown in Figure 3.62 and in Table 3.14. The arrested crack was subjected to a WPS event in the B transient. The third transient, PTSE-1C, was subjected to an even higher peak pressure transient, and resulted in a crack jump to a depth of 41 mm under the conditions presented in Figure 3.62. Conditions of initiation and arrest depicted in Figure 3.62 were determined from analyses performed using the OCA LEFM computer code.

Following completion of the experiment, the flawed region was removed from the test vessel and broken open to reveal the fracture surface. Fractographic examination of the surfaces and measurement of the flaw dimensions indicated that the initial flaw experienced slight tearing prior to the first cleavage event. That initial cleavage run-arrest event (i.e., B test) was essentially a pure cleavage fracture for the first half of the extension and primarily cleavage (approx. 90 percent) with finely dispersed ductile tearing in the remainder of propagation. In the second crack jump (i.e., C test), crack

extension was mixed mode throughout with approximately 85 percent cleavage. No regions of coherent ductile tearing were observed at the termini of the two crack extension, contrary to the pretest predictions of 2 and 11 mm for transients B and C, respectively.

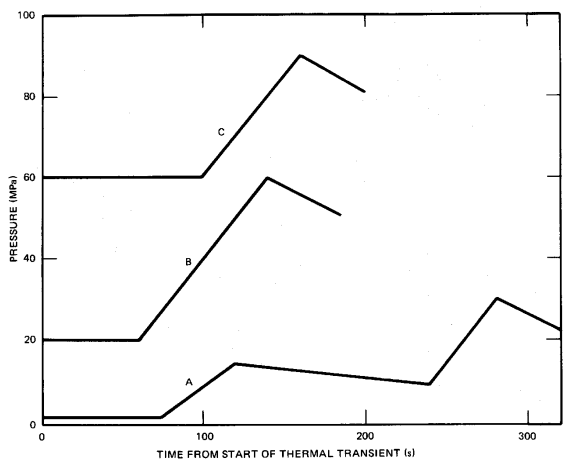

Figure 3.61. Pressure transients for PTSE-1A, -1B, and -1C.

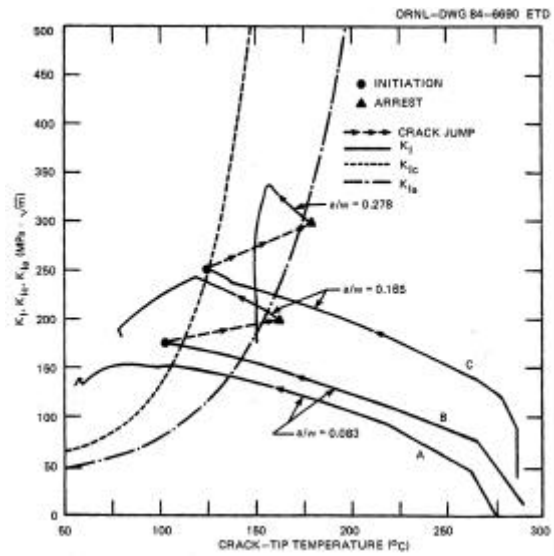

Figure 3.62. Results of OCA analyses of PTSE-1 transients based on measured temperature, pressure, flaw depth, and time of the crack jump.

Table 3.14. Conditions for PTSE-1A, -1B and -1C transients.

Transient	**PTSE-1A**	**PTSE-1B**	**PTSE-1C**
Initial vessel temperature (°C)	277.6	290.7	287.4
Coolant temperature (°C)	15 - 34#	-22 - 0#	-29 - 14#
heat-transfer coefficient $W.m^{-2} K^{-1}$	8000-6000#	5500-6500#	4000-5500#
Initial flaw depth *a*, mm	12.2	12.2	24.4
a/W	0.083	0.083	0.083

Initial and final (t ˜ 300s) values

At the time of the PTSE-1 experiment, pre- and post-test analyses were carried out using the OCA LEFM computer code; pre-test calculations were based on small-specimen data, while the post-test interpretations utilized data recorded during the experiment. In Figure 3.63 , K_{Ic} and K_{Ia} values inferred from the experiment are compared with the pre-test estimates and with the K_I and K_{Ia} relations from Section XI of the ASME Boiler and Pressure Vessel Code. The pre-test estimates of fracture toughness obtained from small specimen data are

reasonably close to the measured PTSE-1 values. Also, as expected, the fracture toughness relations from Section XI are conservative with respect to the measured data.

Recently, the PTSE-1 experiment was re-analyzed by ORNL using version 02.2 of the FAVOR code. Those results for the B transient are depicted in Figure 3.64. Analyses based on small-specimen data [see Figure 3.64 (a)] predict two crack propagation events, the first of which has the flaw initiating immediately after becoming critical (i.e., $K_I / K_{Ia} = 1$) and then arresting at a = 19 mm. As depicted in Figure 3.64 (b), the flaw actually initiated somewhat later in the transient, and arrested at a depth of a = 24 mm; the arrested flaw did not re-initiate after becoming critical just before the onset of WPS. These results are interpreted as a re-confirmation that cleavage-crack behavior in large-scale thick-walled pressure vessels is reasonable described by LEFM methodology as embodied in the FAVOR code.

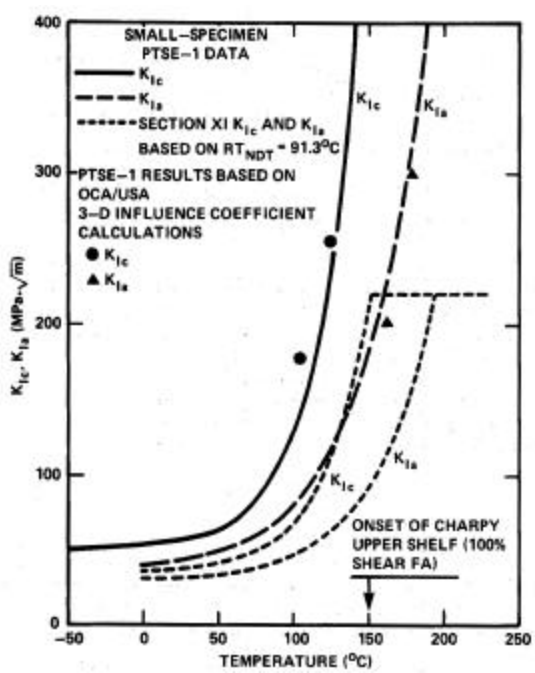

Figure 3.63. Comparison of curves representing small-specimen K_{Ic} and K_{Ia} data with ASME Section XI curves and results of PTSE-1 experiment.

Arrest toughness values measured in the experiment were substantially above the 220 MPa vm cutoff implied in ASME Section XI. Furthermore, Figure 3.65 illustrates that the PTSE-1 arrest data are consistent with (1) arrest measurements made in an international set of experiments that include wide-plate and thermal shock tests and (2) the ASME Section XI K_{IR} curve. The highest arrest value recorded in PTSE-1 occurred at a temperature approximately 30°C above the onset of the Charpy upper shelf. These results imply that the methods of LEFM are useful in fracture evaluations of vessels at high Charpy upper-shelf temperatures.

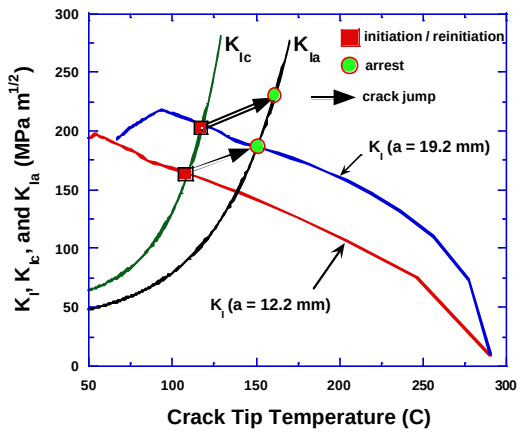

(a)

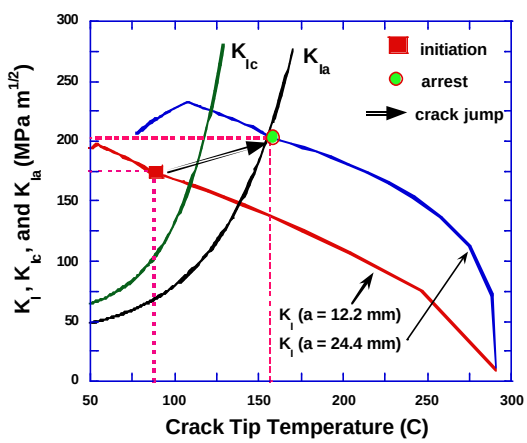

(b)

Figure 3.64. Result of FAVOR re-analyses of PTSE-1 experiment: (a) predictions based on small-specimen data; (b) interpretation based on measured temperature, pressure, flaw depth, and time of the crack jump.

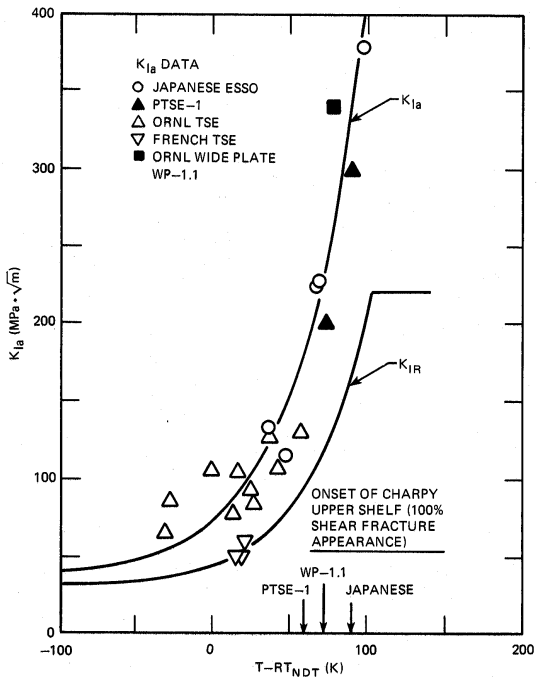

Figure 3.65. Comparison of PTSE-1 arrest toughness results with those for wide plate and thermal shock experiments, as well as with ASME Section XI curve.

Both the PTSE-1A and -1B transients demonstrated that simple WPS (i.e., $dK_I/dt < 0$) strongly inhibits cleavage crack initiation. In those transients, K_I exceeded K_{Ic} during WPS by 50 to 100 percent without initiation being achieved. In the PTSE-1A transient, simple anti-WPS (i.e., $dK_I/dt > 0$) prevailed during two periods of 40-s duration without cleavage initiation, even though K_I exceeded K_{Ic} by 60 to 100 percent. Thus, it can be concluded that simple anti-WPS is not a sufficient condition for overcoming the effects of WPS.

3.2.5 Conclusions based on Large-Scale Experiments

Accomplishments and conclusions supported by results from large-scale HSST experiments (i.e., ITVs, TSEs, and PTSEs) conducted over the past 30-plus years include the following points:

- Cleavage fracture was observed in these large-scale tests consistent with the implications of small-specimen data;
- The observed cleavage-crack behavior in these thick-section experiments has been well described by LEFM methodology as embodied in the OCA/FAVOR analysis codes;
- WPS inhibited cleavage-fracture initiation in these experiments where ($dK_I/dt < 0$);
- Simple anti-WPS ($dK_I/dt > 0$) is not a sufficient condition for overcoming the effects of WPS.

4 Plant Specific Estimates of Through Wall Cracking Frequency Caused by PTS

4.1 Introduction

In this Chapter we describe the results of our probabilistic calculations for each of Oconee, Beaver Valley, and Palisades. Section 4.2 details the plant specific features of each analysis, including both methodology and input variables. In Section 4.3 we present the results of our analysis, focusing on trends of increasing through wall cracking frequency with increasing plant age, and on the prime transients and material features responsible for these trends. In Section 4.4 we discuss the applicability of these results beyond the three study plants. The Chapter concludes with Section 4.5 where we summarize findings from this analysis key to constructing a proposal for a new PTS screening limit in Chapter 6.

4.2 Plant Specific Analysis Features and Inputs

4.2.1 Analysis Methodology

In the case of both the Oconee and Beaver Valley PRA analyses, the NRC Contractors were responsible for both the construction of the PRA models and for the *binning* of overcooling sequences into “case” sequences. The PRA models were constructed from scratch largely based on information learned from the 1980's PTS work but with numerous improvements. Additionally, the human reliability analysis (HRA) portion of the PRA was also initially performed by the NRC Contractors. The corresponding licensees provided information about each plant and answered both written and verbal questions as the PRA model and the PRA/HRA evolved. In each case, two plant visits took place; one early in the process to gather plant information, and a second when interim results were available to allow licensee review and input. Hence these two analyses were largely conducted by the NRC Contractors but with licensee review and input.

The Palisades analysis was conducted in a different fashion. Here, the PRA construction was largely founded on an existing licensee PRA model that already included overcooling sequences. The NRC Contractors provided comments on the existing PRA model, a model that was subsequently modified by the licensee in response to these comments. Once the revised PRA model was satisfactory to both the licensee and the NRC Contractors, the HRA portion of the analysis was conducted as a collaborative effort involving both licensee and NRC Contractor personnel. This HRA information was included in the Palisades PRA model and sequence *binning* and frequency estimates were subsequently performed primarily by the licensee with NRC Contractor review, input, and slight modification. Two plant visits were also conducted for the Palisades analysis; the first for initial project and plant familiarization, and the second for conducting the collaborative HRA. As was done for the other two plant analyses, numerous discussions were held between the Palisades staff and NRC Contractors as the PRA model and PRA/HRA evolved. Hence, while the same overall approach was followed, this analysis was based on more of a collaborative effort between the NRC Contractors and the licensee starting with an existing PTS-related PRA model of the plant.

4.2.2 Input Information

4.2.2.1 PRA and Thermal Hydraulic

The plant-specific PRAs described in Section 4.2.1 led ultimately to the definition of a master list of thermal-hydraulic transients. A sub-set of these transients from this list was defined as the "base case" for each plant, which represents our best mathematical description of the conditions at the plant that could produce a PTS challenge to vessel integrity. TH cases from the master list were eliminated from the base case for a number of reasons, including the following:

- Certain transients were binned together, making some TH runs redundant, or
- Sensitivity studies revealed that certain TH cases did not need to be passed on to, or
- Either the minimum temperature remained above 400°F within the first ≈170 minutes or the cooldown rate was slower than 100°F/hour. Experience gained from previous analysis of PTS has repeatedly demonstrated that transients need to be at least this severe to make any contribution at all to the calculated through wall cracking frequency. Later examination of TWCF estimates for all base case transients revealed that many transients having more severe cooldown rates and/or lower temperatures still made no contribution to TWCF, thus demonstrating the appropriateness of these screening criteria.

Appendix C the master list of transients for all three plants, and also lists the initiating event frequency values for the base-case transients. Appendix D provides a complete set of thermal hydraulic information for all of these transients.

4.2.2.2 Probabilistic Fracture Mechanics

Plant specific input values include mechanical and compositional properties specific to each of the individual plates, welds, and forgings in the vessel. Figure 4.1, Figure 4.2, and Figure 4.3, illustrate the spatial arrangement of the different welds, plates, and forgings in Oconee, Beaver Valley, and Palisades, respectively. These figures also illustrated limited information drawn from the plant-specific fluence maps. Table 4.1 lists the composition and unirradiated RT_{NDT} values for each of all of the welds, plates, and forgings in each of the three plants. The vessel-specific information used in constructing the flaw distributions is detailed in Table 4.2.

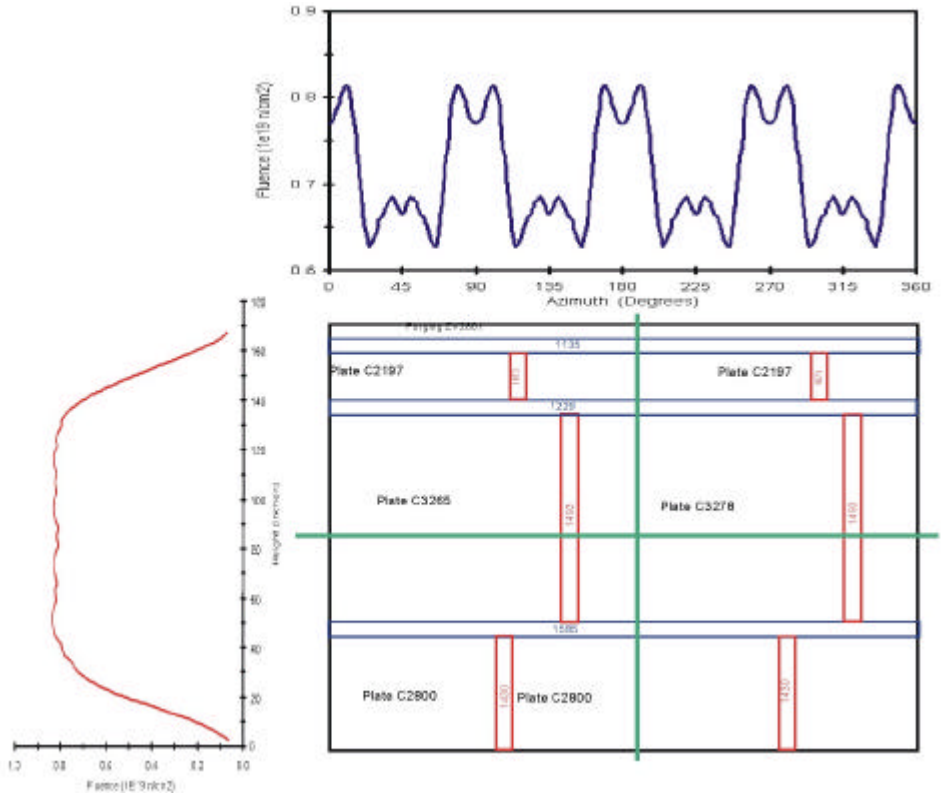

Figure 4.1. Rollout diagram of beltline materials and representative fluence maps for Oconee.

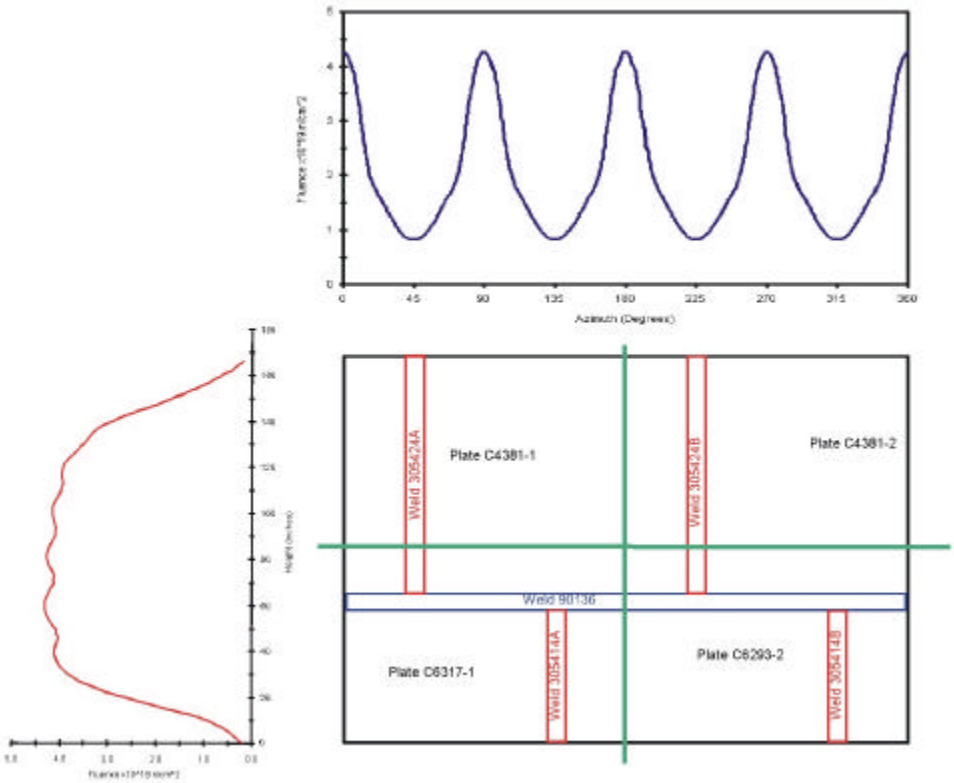

Figure 4.2. Rollout diagram of beltline materials and representative fluence maps for Beaver Valley.

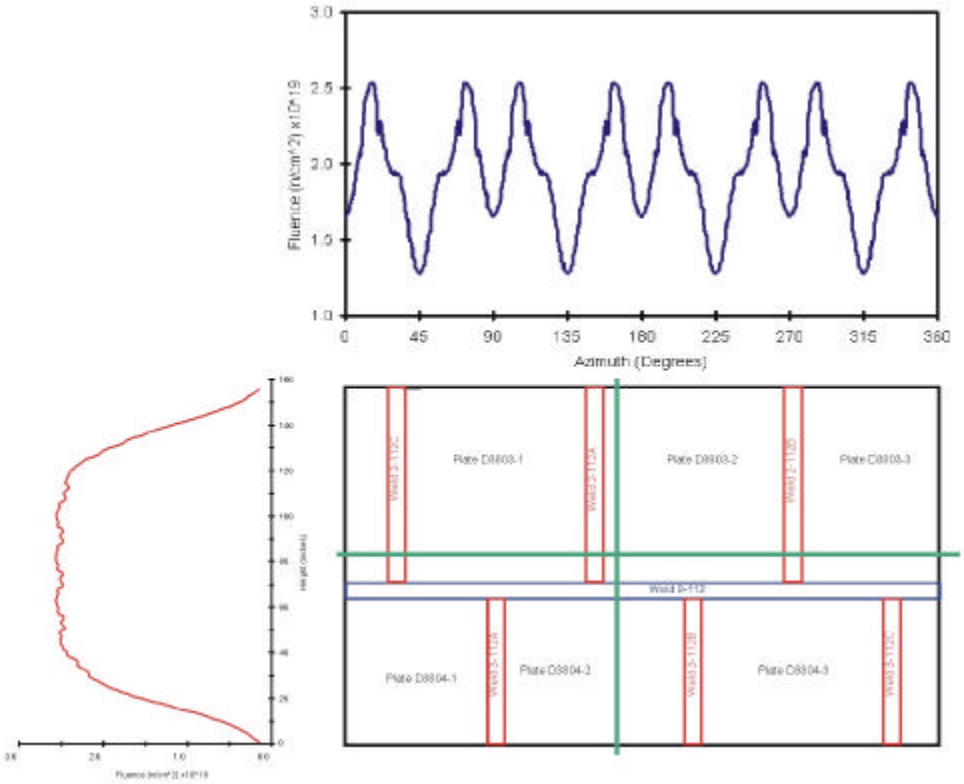

Figure 4.3. Rollout diagram of beltline materials and representative fluence maps for Palisades.

Table 4.1. Plant specific material values drawn from the RVID database [RVID].

Plant	Major Material Region Description				Cu [wt%]	Ni [wt%]	P [wt%]	Un-Irradiated RT_{NDT}	
	#	Type	Heat	Location				[°F]	Method
Oconee	1	Axial Weld	SA-1430	lower	0.190	0.570	0.017	-5	B&W Generic
	2	Axial Weld	SA-1493	intermediate	0.190	0.570	0.017	-5	B&W Generic
	3	Axial Weld	SA-1073	upper	0.210	0.640	0.025	-5	B&W Generic
	4	Circ Weld	SA-1585	lower	0.220	0.540	0.016	-5	B&W Generic
	5	Circ Weld	SA-1229	intermediate	0.230	0.590	0.021	10	ASME NB-2331
	6	Circ Weld	SA-1135	upper	0.230	0.520	0.011	-5	B&W Generic
	7	Plate	C-2800	lower	0.110	0.630	0.012	1	B&W Generic
	8	Plate	C3265-1	intermediate	0.100	0.500	0.015	1	B&W Generic
	9	Plate	C3278-1	intermediate	0.120	0.600	0.010	1	B&W Generic
	10	Plate	C2197-2	upper	0.150	0.500	0.008	1	B&W Generic
	11	Forging	ZV2861	upper	0.160	0.650	0.006	3	B&W Generic
Beaver	1	Axial Weld	305414A	lower	0.337	0.609	0.012	-56	Generic
	2	Axial Weld	305414B	lower	0.337	0.609	0.012	-56	Generic
	3	Axial Weld	305424A	upper	0.273	0.629	0.013	-56	Generic
	4	Axial Weld	305424B	upper	0.273	0.629	0.013	-56	Generic
	5	Circ Weld	90136	intermediate	0.269	0.070	0.013	-56	Generic
	6	Plate	C6317-1	lower	0.200	0.540	0.010	27	MTEB 5-2
	7	Plate	C6293-2	lower	0.140	0.570	0.015	20	MTEB 5-2
	8	Plate	C4381-2	upper	0.140	0.620	0.015	73	MTEB 5-2
	9	Plate	C4381-1	upper	0.140	0.620	0.015	43	MTEB 5-2

Palisades	1	Axial Weld	3-112A	lower	0.213	1.010	0.019	-56	Generic
	2	Axial Weld	3-112B	lower	0.213	1.010	0.019	-56	Generic
	3	Axial Weld	3-112C	lower	0.213	1.010	0.019	-56	Generic
	4	Axial Weld	2-112A	upper	0.213	1.010	0.019	-56	Generic
	5	Axial Weld	2-112B	upper	0.213	1.010	0.019	-56	Generic
	6	Axial Weld	2-112C	upper	0.213	1.010	0.019	-56	Generic
	7	Circ Weld	9-112	intermediate	0.203	1.018	0.013	-56	Generic
	8	Plate	D3804-1	lower	0.190	0.480	0.016	0	ASME NB-2331
	9	Plate	D3804-2	lower	0.190	0.500	0.015	-30	MTEB 5-2
	10	Plate	D3804-3	lower	0.120	0.550	0.010	-25	MTEB 5-2
	11	Plate	D3803-1	upper	0.240	0.510	0.009	-5	ASME NB-2331
	12	Plate	D3803-2	upper	0.240	0.520	0.010	-30	MTEB 5-2
	13	Plate	D3803-3	upper	0.240	0.500	0.011	-5	ASME NB-2331

Table 4.2. Summary of vessel specific inputs for the flaw distribution.

Variable		Oconee	Beaver Valley	Palisades	Calvert Cliffs	Notes
Inner Radius (to cladding)	[in]	85.5	78.5	86	86	Vessel specific info
Base Metal Thickness	[in]	8.438	7.875	8.5	8.675	Vessel specific info
Total Wall Thickness	[in]	8.626	8.031	8.75	8.988	Vessel specific info

Variable			Oconee	Beaver Valley	Palisades	Calvert Cliffs	Notes
SAW Weld	Volume fraction	[%]	97%				100% - SMAW% - REPAIR%
	Thru-Wall Bead Thickness	[in]	0.1875	0.1875	0.1875	0.1875	All plants report plant specific dimensions of 3/16-in.
	Truncation Limit	[in]	1				Judgment. Approx. 2X the size of the largest non-repair flaw observed in PVRUF & Shoreham.
	Buried or Surface	--	All flaws are buried				Observation
	Orientation	--	Circ flaws in circ welds, axial flaws in axial welds.				Observation: Virtually all of the weld flaws in PVRUF & Shoreham were aligned with the welding direction because they were lack of sidewall fusion defects.
	Density basis	--	Shoreham density				Highest of observations
	Aspect ratio basis	--	Shoreham & PVRUF observations				Statistically similar distributions from Shoreham and PVRUF were combined to provide more robust estimates, when based on judgment the amount data were limited and/or insufficient to identify different trends for aspect ratios for flaws in the two vessels.
	Depth basis	--	Shoreham & PVRUF observations				Statistically similar distributions combined to provide more robust estimates

Variable			Oconee	Beaver Valley	Palisades	Calvert Cliffs	Notes
SMAW Weld	Volume fraction	[%]	1%				Upper bound to all plant specific info provided by Steve Byrne (Westinghouse – Windsor).
	Thru-Wall Bead Thickness	[in]	0.21	0.20	0.22	0.25	Oconee is generic value based on average of all plants specific values (including Shoreham & PVRUF data). Other values are plant specific as reported by Steve Byrne.
	Truncation Limit	[in]	1				Judgment. Approx. 2X the size of the largest non-repair flaw observed in PVRUF & Shoreham.
	Buried or Surface	--	All flaws are buried				Observation
	Orientation	--	Circ flaws in circ welds, axial flaws in axial welds.				Observation: Virtually all of the weld flaws in PVRUF & Shoreham were aligned with the welding direction because they were lack of sidewall fusion defects.
	Density basis	--	Shoreham density				Highest of observations
	Aspect ratio basis	--	Shoreham & PVRUF observations				Statistically similar distributions from Shoreham and PVRUF were combined to provide more robust estimates, when based on judgment the amount data were limited and/or insufficient to identify different trends for aspect ratios for flaws in the two vessels.
	Depth basis	--	Shoreham & PVRUF observations				Statistically similar distributions combined to provide more robust estimates

Variable			Oconee	Beaver Valley	Palisades	Calvert Cliffs	Notes
Repair Weld	Volume fraction	[%]	2%				Judgment. A rounded integral percentage that exceeds the repaired volume observed for Shoreham and for PVRUF, which was 1.5%.
	Thru-Wall Bead Thickness	[in]	0.14				Generic value: As observed in PVRUF and Shoreham by PNNL.
	Truncation Limit	[in]	2				Judgment. Approx. 2X the largest repair flaw found in PVRUF & Shoreham. Also based on maximum expected width of repair cavity.
	Buried or Surface	--	All flaws are buried				Observation

	Orientation	--	Circ flaws in circ welds, axial flaws in axial welds.	The repair flaws had complex shapes and orientations that were not aligned with either the axial or circumferential welds; for consistency with the available treatments of flaws by the FAVOR code, a common treatment of orientations was adopted for flaws in SAW/SMAW and repair welds.
	Density basis	--	Shoreham density	Highest of observations
	Aspect ratio basis	--	Shoreham & PVRUF observations	Statistically similar distributions from Shoreham and PVRUF were combined to provide more robust estimates, when based on judgment the amount data were limited and/or insufficient to identify different trends for aspect ratios for flaws in the two vessels.
	Depth basis	--	Shoreham & PVRUF observations	Statistically similar distributions combined to provide more robust estimates

Variable			Oconee	Beaver Valley	Palisades	Calvert Cliffs	Notes
Cladding	Actual Thickness	[in]	0.188	0.156	0.25	0.313	Vessel specific info
	# of Layers	[#]	1	2	2	2	Vessel specific info
	Bead Width	[in]	1				Bead widths of 1 to 5-in. characteristic of machine deposited cladding. Bead widths down to ½-in. can occur over welds. Nominal dimension of 1-in. selected for all analyses because this parameter is not expected to influence significantly the predicted vessel failure probabilities. May need to refine this estimate later, particularly for Oconee who reported a 5-in bead width.
	Truncation Limit	[in]	Actual clad thickness rounded to the nearest 1/100th of the total vessel wall thickness				Judgment & computational convenience
	Surface flaw depth in FAVOR	[in]	0.259	0.161	0.263	0.360	
	Buried or Surface	--	All flaws are surface breaking				Judgment. Only flaws in cladding that would influence brittle fracture of the vessel are brittle. Material properties assigned to clad flaws are that of the underlying material, be it base or weld.

	Orientation	--	All circumferential.	Observation: All flaws observed in PVRUF & Shoreham were lack of inter-run fusion defects, and cladding is always deposited circumferentially
	Density basis	--	No surface flaws observed. Density is 1/1000 that of the observed buried flaws in cladding of vessels examined by PNNL. If there is more than one clad layer then there are no clad flaws.	Judgment
	Aspect ratio basis	--	Observations on buried flaws	Judgment
	Depth basis	--	Depth of all surface flaws is the actual clad thickness rounded up to the nearest 1/100th of the total vessel wall thickness.	Judgment.

Variable			Oconee	Beaver Valley	Palisades	Calvert Cliffs	Notes
Plate	Truncation Limit	[in]	0.433				Judgment. Twice the depth of the largest flaw observed in all PNNL plate inspections.
	Buried or Surface	--	All flaws are buried				Observation
	Orientation	--	Half of the simulated flaws are circumferential, half are axial.				Observation & Physics: No observed orientation preference, and no reason to suspect one (other than laminations which are benign.
	Density basis	--	1/10 of small weld flaw density, 1/40 of large weld flaw density of the PVRUF data				Judgment. Supported by limited data.
	Aspect ratio basis	--	Same as for PVRUF welds				Judgment
	Depth basis	--	Same as for PVRUF welds				Judgment. Supported by limited data.

4.3 Results

In this discussion of the results for Oconee, Beaver Valley, and Palisades we will address all three plants together rather than focus on individual discussion of each plant. We begin with the "highest level" result (i.e., the estimated values and distributions of through wall cracking frequency), and how these values and distributions change as the operating plant ages (Section 4.3.1). We then examine the results more closely to reveal both the transient (Section 4.3.2.1) and material regions (Section 4.3.2.2) that provide the dominant contributions to the TWCF values. The insights derived from this discussion sets the scene to use this information together with the risk goal (see Chapter 5) to establish a proposal for a revised PTS screening criteria, which will be discussed in Chapter 6.

4.3.1 Comparison of Through-Wall Cracking Frequencies for the Three Pilot Plants

In Figure 4.4 we compare the frequency of through wall cracking estimated by FAVOR V02.4 to occur per year of operation for Oconee, Beaver Valley, and Palisades. In this Figure we have used the number of effective full power years (EFPY) as a simple metric to reflect the plant's age. In Chapter 6 we will develop metrics that better reflect the combined effects of operational time, of the applied irradiation damage, and of the irradiation sensitivity of the material. Here it is relevant to note that the trends revealed in Figure 4.4, i.e.:

- A higher TWCF associated with both Palisades and Beaver Valley (relative to Oconee), and

- A more rapid rate of increase of TWCF with time associated with both Palisades and Beaver Valley (again relative to Oconee)

are completely expected because of the more irradiation sensitive materials in the Palisades and Beaver Valley RPVs. Restricting attention to the lower part of Figure 4.4, these results demonstrate that even at the end of license extension (60 operational years, or 48 EFPY at an 80% capacity factor) the upper end of the estimated TWCF distributions range between $1x10^{-9}$/yr and $5x10^{-8}$/yr. Considering that the Beaver Valley and Palisades RPVs are constructed from some of the most irradiation sensitive materials in commercial reactor service today, these results suggest that, provided operating practices do not change dramatically in the future, even after license extension the operating reactor fleet is in little danger of challenging the numerical risk expectation on TWCF of $5x10^{-6}$/yr expressed by Regulatory Guide 1.154.

The data in Figure 4.4 reveal TWCF distributions are both very broad (e.g., three or more orders of magnitude separate the 5th and 95th percentiles) and highly skewed (e.g., the arithmetic mean and the 95th percentile approximately coincide). Figure 4.5 provides data for Beaver Valley illustrative of the characteristics of the distributions from which the percentiles and mean values in Figure 4.4 are derived (the calculated distributions for all three plants exhibited identical characteristics). As described in the following sections, both the skewness and the spread in these results is expected, and results from the physics of cleavage fracture.

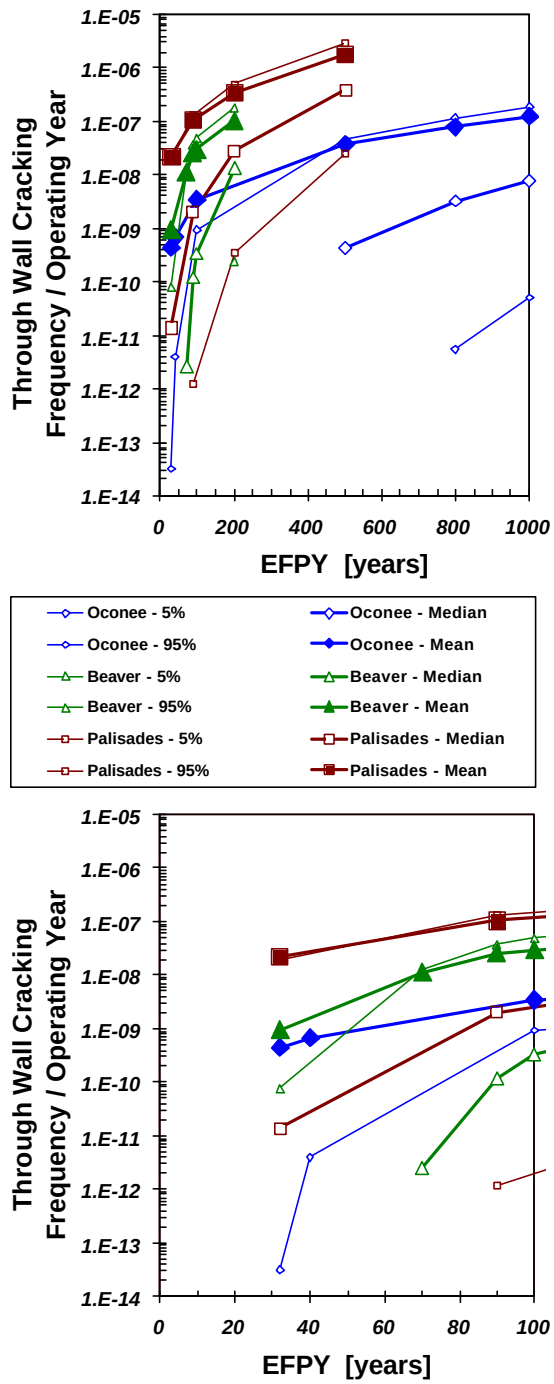

Figure 4.4. Comparison estimated yearly through-wall cracking frequencies for Oconee, Beaver Valley, and Palisades. Median and 5th percentile value of TWCF that are zero are not plotted.

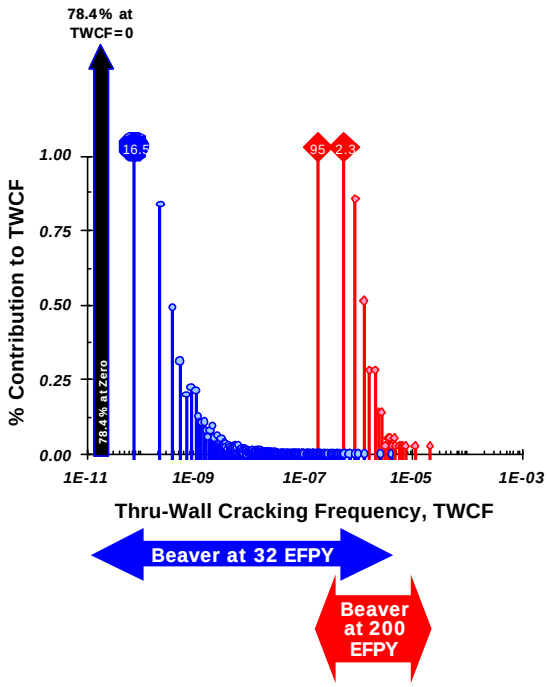

Figure 4.5. Typical distribution of through-wall cracking frequency (as calculated for Beaver Valley at 32 and 200 EFPY).

4.3.1.1 Explanation of Skewness in the TWCF Distribution

The skewness in the TWCF distributions illustrated in Figure 4.5 results directly from the physical nature of cleavage crack initiation and arrest. The crack initiation (K_{Ic}) and crack arrest (K_{Ia}) toughness distributions shown in Figure 2.9 and Figure 2.13 respectively both have finite lower bound values that are physically justified (see Appendix A). Thus, the following three mathematical conditions all lead to a likelihood of through wall cracking that is *by definition* zero (not just a very small number):

- If the applied-K_I value for a particular FAVOR simulation run (i.e., a particular crack in a particular location subjected to a particular TH transient) never exceeds the minimum K_{Ic}, then the crack has a probability of crack initiation of zero, and (consequently) a contribution to the through wall cracking frequency that is zero.
- If the applied-K_I value for a particular simulation run exceeds the minimum K_{Ic}, but exceeds it at a time when the applied-K_I value is dropping with time (i.e., dK_I/dt = 0), then warm pre-stress has occurred and the crack has a probability of crack initiation of zero, and (consequently) a contribution to the through wall cracking frequency that is zero.
- If the applied-K_I value for a particular simulation run exceeds the minimum K_{Ic} at a time when the applied-K_I value is increasing with time (i.e., $dK_I/dt > 0$) then the crack has a non-zero probability of crack initiation. However, if while the crack is propagating through the RPV wall the applied-K_I value falls below the minimum K_{Ia} value then the crack arrest must occur. Such a crack would provide no contribution to the through wall cracking frequency.

In practice these mathematical conditions are satisfied most of the time in the Monte Carlo simulations conducted by FAVOR because the simulated crack is small and the simulated toughness is high and the simulated TH transient does not produce a very severe stress state in the RPV wall. However, on rare occasions a larger crack will be simulated in a lower toughness material and subjected to a more severe transient. In these situations the likelihood of developing a through wall crack is higher. However, this combined sampling of the upper tails of many distributions happens only rarely.

4.3.1.2 Explanation of Large Spread in the TWCF Distribution

The TWCF distributions illustrated in Figure 4.5 are very broad, spanning three or mode orders of magnitude from minimum to maximum. This characteristic again relates to the physics of cleavage fracture. As discussed in Section 4.3.1.1, the absolute lower bounds associated with both the K_{Ic} and K_{Ia} distributions leads to a large number of the Monte Carlo simulations producing a through-wall cracking probability that is, *by definition*, zero. However, on rare occasions the upper tails of many distributions

are sampled in the same simulation run, resulting in a larger crack being simulated to occur in a lower toughness material and be subjected to a more severe transient. This combined possibility of both zero and higher probabilities of TWCF leads to TWCF distributions that are naturally broad. As illustrated in Figure 4.5, the TWCF distributions tend to compress as the plants age because the more embrittled materials in these plants are less likely to produce through wall cracking frequencies that are either very low, or zero.

4.3.2 Dominant Contributors to Through-Wall Cracking Frequency

4.3.2.1 Dominant Transients

Of the ≈50 to ≈150 thermal hydraulic cases that comprise the base case list for each plant, only ≈10 transients in each plant contribute significantly to the through wall cracking frequency. Table 4.3 lists all of the PRA bins that contribute 1% of the TWCF or greater. As reflected in the table, bins that represent a class of transients (small break LOCAs, for example) are represented by individual TH cases (a 4-in. surge line break, for example).

The dominant transients divide into the following four general classes of transients:

- Breaks in the primary system
  - Loss of coolant accidents (LOCA)
  - Stuck-open valves
- Breaks in the secondary system
  - Main steam line breaks (MSLB)
  - Stuck-open valves

Table 4.3. List of transients that dominate PTS risk.

Primary System - LOCAs			
PRA Bin Description	**Oconee**	**Beaver Valley**	**Palisades**
SBLOCA (1.4" – 4.0")	No dominant contributors	TH 56: 4" surge line break at HZP	TH 58: 4" cold leg break, winter conditions TH 59: 4" cold leg break, winter conditions TH 60: 2" surge line break, winter conditions
MBLOCA (4.0" – 8.0")	TH 160: 5.656" surge line break TH 164: 8" surge line break	TH 7: 8" surge line break	TH 62: 8" cold leg break, winter conditions TH 63: 5.656" cold leg break, winter conditions TH 64: 4" surge line break, summer conditions
LBLOCA (> 8.0")	TH 156: 16" hot leg break	TH 9: 16" hot leg break	TH 40: 16" hot leg break

Operator trips RCP's as appropriate. No other operator action is taken. Sump recirculation is included as appropriate.

Primary System – Stuck Open Valves			
PRA Bin Description	**Oconee**	**Beaver Valley**	**Palisades**
SRV stuck open / recloses	TH 109: Reactor/turbine trip with 1 stuck open pressurizer SRV that recloses at 6000 sec, no HPI throttling TH 113: Reactor/turbine trip with 1 stuck open pressurizer SRV that recloses at 6000 sec, operator throttles HPI 10	TH 97: Reactor/turbine trip with 1 stuck open pressurizer SRV that recloses at 3000 sec, at HZP, no HPI throttling	TH 65: Reactor/turbine trip with 1 stuck open pressurizer SRV that recloses at 6000 sec, at HZP, no HPI throttling or charging control

Primary System – Stuck Open Valves			
PRA Bin Description	**Oconee**	**Beaver Valley**	**Palisades**
	minutes after allowed3 TH 115: Reactor/turbine trip with 1 stuck open pressurizer SRV that recloses at 3000 secs, operator throttles HPI 10 minutes after allowed TH 122: Reactor/turbine trip with 1 stuck open pressurizer SRV that recloses at 6000 sec, at HZP, operator throttles HPI 10 minutes after allowed TH 124: Reactor/turbine trip with 1 stuck open pressurizer SRV that recloses at 3000 sec, at HZP, operator throttles HPI 10 minutes after allowed		

Operator trips RCP's as appropriate. Other operator actions are specifically noted.

Secondary System – Main Steam Line Break			
PRA Bin Description	**Oconee**	**Beaver Valley**	**Palisades**
Large Main Steam Line Breaks	No dominant contributors	TH 102: MSLB with AFW continuing to feed bad generator for 30 min and operator throttles HPI 30 min after allowed, break is assumed to occur inside containment so RCPs are tripped due to adverse containment conditions TH 103: MSLB with AFW continuing to feed bad generator for 30 min and operator throttles HPI 30 min after allowed, at HZP, break is assumed to occur inside containment so RCPs are tripped due to adverse containment conditions TH 104: MSLB with AFW continuing to feed bad generator for 30 min and operator throttles HPI 60 min after allowed, break is assumed to occur inside containment so RCPs are tripped due to adverse containment conditions TH 105: MSLB with AFW continuing to feed bad generator for 30 min and operator throttles HPI 60 min after allowed, at HZP, break is assumed to occur inside containment so RCPs are tripped due to adverse containment conditions	TH 54: MSLB with failure of both MSIVs to close, break is assumed to be inside containment causing containment spray actuation and RCP trip, operator does not isolate AFW on affected SG, operator does not throttle HPI or control charging

Secondary System – Stuck Open Valves			
PRA Bin Description	**Oconee**	**Beaver Valley**	**Palisades**
Secondary Side Stuck	No dominant contributors	No dominant contributors	TH 19: Reactor/turbine trip with 1 stuck open ADV, at HZP,

Secondary System – Stuck Open Valves			
PRA Bin Description	**Oconee**	**Beaver Valley**	**Palisades**
Open Valve			operator does not throttle HPI or control charging, AFW continues to feed bad generator TH 52: Reactor/turbine trip with 1 stuck open ADV, at HZP, operator does not throttle HPI or control charging, failure of both MSIVs to close, AFW continues to feed bad generator TH 55: Reactor/turbine trip with 2 stuck open ADVs, controller failure resulting in the flow from 2 AFW pumps into affected SG, operator starts second AFW pump, operator does not throttle HPI or control charging

Operator trips RCP's as appropriate.

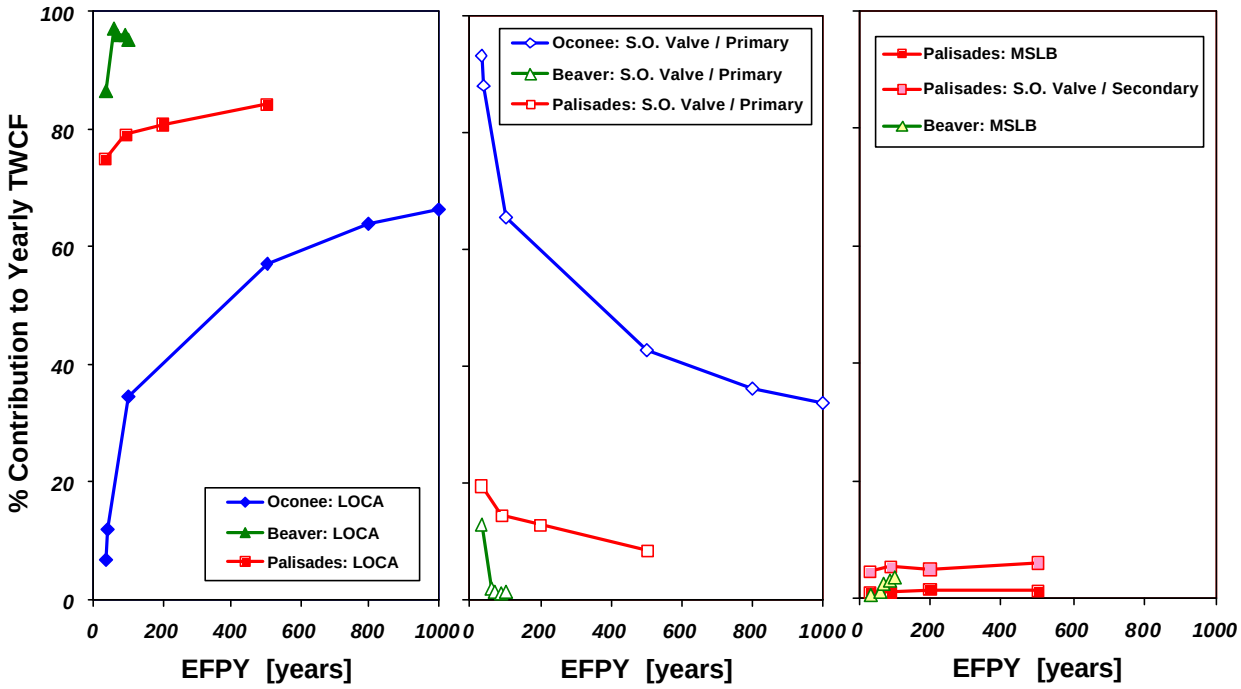

Figure 4.6. Percent contribution of various classes of transients to the total through wall cracking frequency.

4.3.2.1.1 Secondary Side Breaks

As illustrated in Figure 4.6, breaks in the primary system (either LOCAs or stuck open values) are responsible for 95% or more of the through wall cracking frequency in all three plants. This finding differs from the studies that provided the basis of the current PTS rule, wherein breaks in the secondary system, particularly main steam line breaks, constituted a significant portion of the total PTS risk. This difference from previous results occurs for the following reasons

1. In this investigation our representation of a group of different operational sequences by the same thermal-hydraulic pressure/temperature *vs*. time transient is

considerably more refined than in previous studies. For example, previous studies represented a full spectrum of secondary side breaks from small breaks and valve opening scenarios through a break of the main steam line using the pressure/temperature *vs*. time transient characteristic of a main steam line break. This significant conservatism, which over-emphasizes the importance of secondary side events, is removed in our analysis.

2. A break of the main steam line does not produce as severe a challenge to vessel integrity as do primary system LOCAs. As illustrated in Figure 4.7, at lower levels of embrittlement (top plot) the applied driving force to fracture for a MSLB fails to exceed the minimum initiation fracture toughness value (i.e., $K_{applied}/K_{Ic(min)} < 1$). In this situation the MSLB can make no contribution whatsoever to the through wall cracking frequency of the vessel. As the vessel embrittles (bottom plot) the MSLB transients are capable of initiating cracks (i.e., $K_{applied}/K_{Ic(min)} > 1$), but are not as severe as primary system LOCAs, which produce systematically higher values of $K_{applied}/K_{Ic(min)}$.
3. In our current analysis we provide realistic credit for operator actions, including uncertainties on human action probabilities. Such credits were not included in earlier analyses of PTS. We consider these credits appropriate for the following reasons:
   a. Overcooling prevention and control are an integral part of crew training today,
   b. Instrumentation is available and procedures are written to facilitate identification of a faulted steam generator (SG) and excessive steam demand. The information provided by this instrumentation enables plant operators to rapidly identify and address secondary side challenges.
   c. Standard operating procedures have steps that focus attention on control of RCS pressure, enabling operators to throttle/terminate safety injection when appropriate

   Simulator observations confirm that successful response to a secondary-side challenge is likely at the three plants studied here. Our judgments regarding operator response to secondary side challenges would have to be significantly different before the small contribution of these transients would approach the TWCFs associated with LOCAs. Moreover, as demonstrated in Figure 4.7, the variability in operator response to a MSLB that is considered likely hardly exerts any influence on the severity of the challenge to RPV integrity, certainly not enough to increase the severity of a MSLB enough to make it comparable to a LOCA.

4.3.2.1.2 Primary Side Breaks

Referring again to Figure 4.6, one observes that in both Beaver Valley and Palisades LOCA breaks alone contribute ≈80% or more of the total TWCF. Results from the Oconee plant differ in that at low embrittlement the challenge posed by stuck-open valves dominates the TWCF. As the RPV embrittles the importance of these transients diminishes and LOCA dominance returns. In the following two sub-sections we discuss first the reason for the significant contribution of stuck open values to the TWCF at Oconee, then we turn attention to the dominant role played by LOCAs at all three plants.

4.3.2.1.2.1 Stuck Open Valves

The Oconee plant differs from both Beaver Valley and Palisades due to the once-through steam generator design in B&W plants. This design has a smaller steam inventory produces a greater decoupling between the reactor coolant system (RCS) and the secondary side of the plant. Because there is less heat addition from steam generators into the RCS during and overcooling event in B&W plants, these events are more severe in B&W plants than in CE and Westinghouse designs.

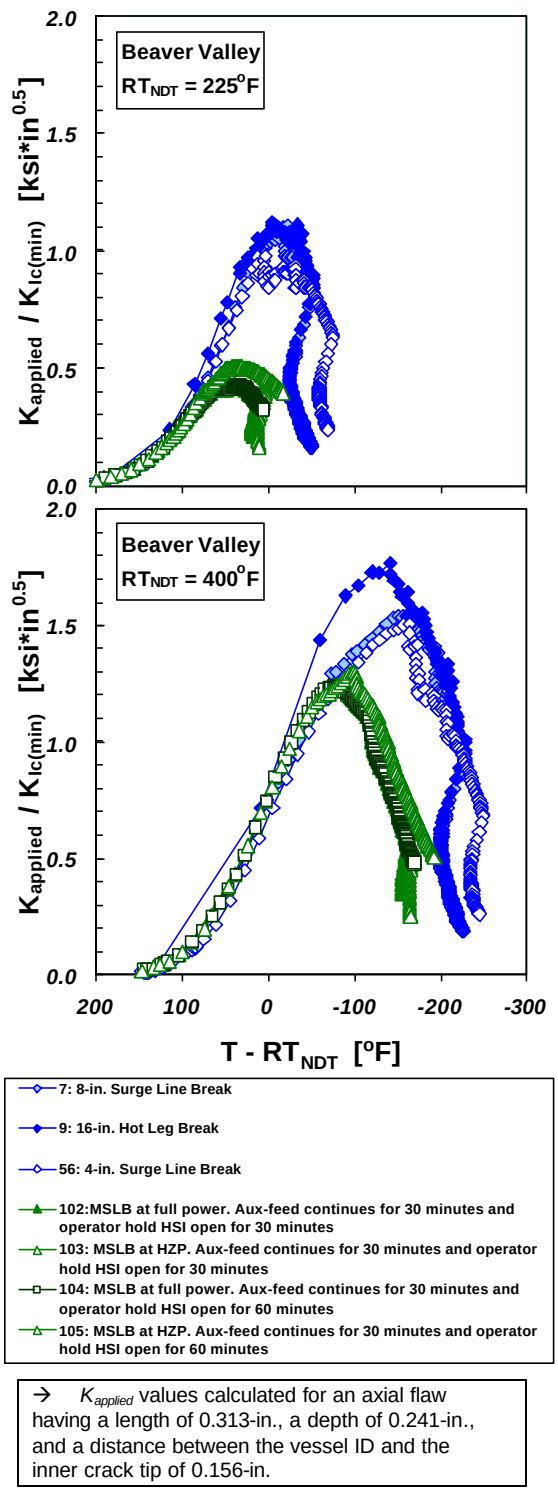

→ $K_{applied}$ values calculated for an axial flaw having a length of 0.313-in., a depth of 0.241-in., and a distance between the vessel ID and the inner crack tip of 0.156-in.

Figure 4.7. [§§]Comparison of the driving force to fracture produced by LOCAs and by main MSLBs in Beaver Valley.

The information presented in Figure 4.8 and Figure 4.9 helps to explain the reason why, in Oconee, stuck-open valves dominate the TWCF at low embrittlement levels yet LOCAs dominate the TWCF at high embrittlement levels. Figure 4.8 demonstrates that even though LOCAs dominate the TWCF only at high embrittlement levels they dominate the crack initiation frequency at all embrittlement levels. This agrees with Figure 4.9, which shows that LOCAs exhibit a higher crack initiation driving force than do stuck open valves. However, at lower embrittlement levels the late repressurization that results from valve closure elevates the $K_{applied}$ value sufficiently to re-initiate the crack and fail the vessel. At higher embrittlement levels the more severe stress state produced by the LOCA transients overcomes the crack driving force produced by re-pressurization, returning LOCAs to dominance.

We have addressed the key uncertainties in transients involving stuck-open valves quantitatively. These include the following factors:

- The degree of valve opening is modeled by a split fraction that reflects the fraction of valve opening size of interest to PTS. This model assumes any size opening is equally likely to occur.
- The timing for valve re-closure is modeled to occur at two discreet times, 50 minutes and 100 minutes, with equal probability.
- The speed with which the operator controls RCS re-pressurization is modeled by associating probabilities with different times at which throttling may occur. We adopted plant specific probabilities that reflect differences in operator training and procedures as well as our simulator observations.

[§§] Plots like Figure 4.7 illustrate the extent to which the driving force to fracture ($K_{applied}$) exceeds the fracture toughness ($K_{Ic(min)}$). Only when $K_{applied}$ exceeds $K_{Ic(min)}$ (i.e., $K_{applied}/K_{Ic(min)} > 1$) is there any probability of either crack initiation or through wall cracking. Since temperature normally decreases with time through a PTS transient, time increases as you move from left to right on the horizontal axis.

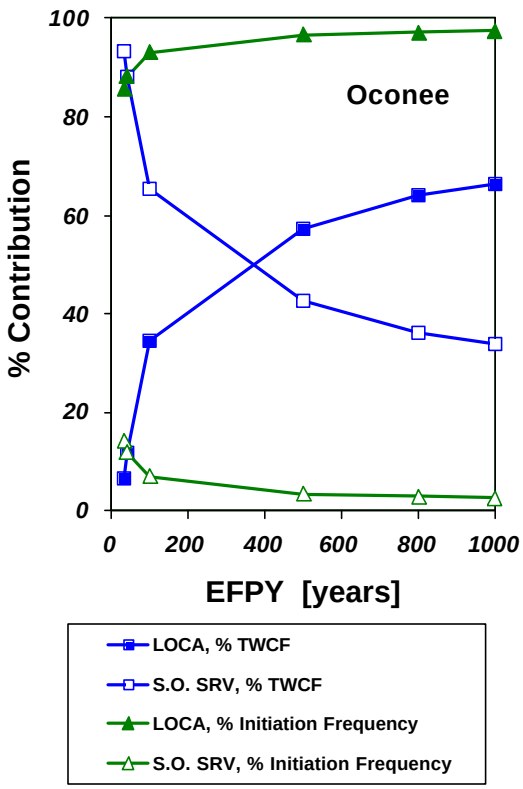

Figure 4.8. Comparison percentage contribution of both LOCAs and stuck open SRVs to both crack initiation and to through wall cracking frequency in Oconee.

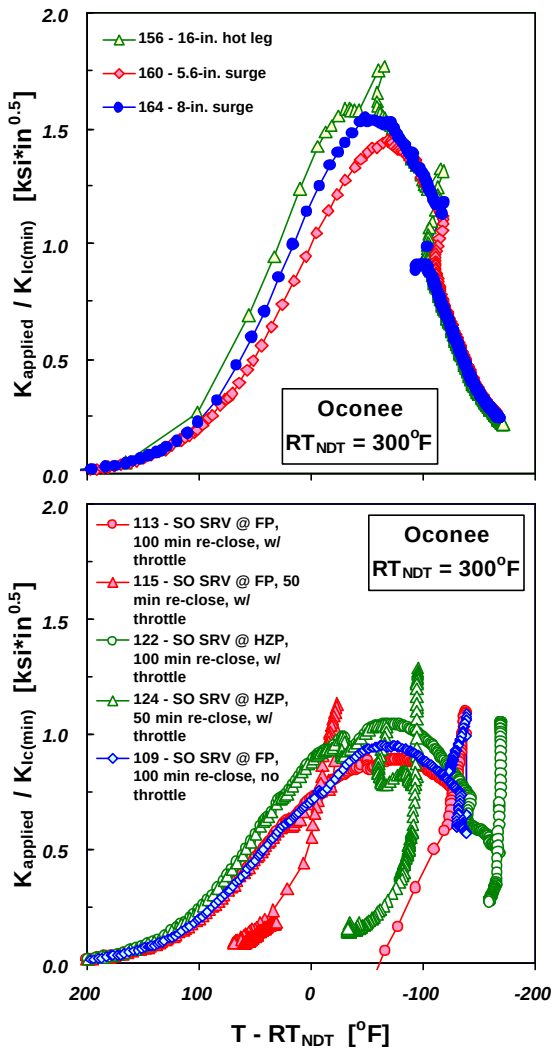

→ There is zero probability of crack initiation below a $K_{applied}/K_{Ic(min)}$ value of unity.
→ Time increases as the temperature falls below RT_{NDT} (i.e., proceeding from left to right on the horizontal axis).
→ $K_{applied}$ values calculated for an axial flaw having a length of 0.814-in., a depth of 0.169-in., and a distance between the vessel ID and the inner crack tip of 0.327-in.

Figure 4.9. Comparison of the driving force to fracture produced by loss of coolant accidents (top) and by stuck open safety release valves in Oconee.

4.3.2.1.2.2 LOCAs

Returning again to Figure 4.6, one notes that, accepting the affect that the B&W steam generator design has on stuck open valves, LOCAs dominate the risk of developing a through wall crack as the result of a pressurized thermal shock event. Here even large break LOCAs contribute to the TWCF whereas they never did in earlier studies [SECY-82-465, ORNL 85a, 86b, 86]. It should, however, be noted that in previous studies large break LOCAs could not have made any contribution to the through wall cracking frequency because they were excluded *a priori* from the probabilistic analysis.

Figure 4.15 shows the variation of the conditional probability of crack initiation and of through wall cracking for both Oconee and for Beaver Valley across the full spectrum of break size and of embrittlement. The trends in this graph suggest that there is a much more

pronounced effect of thermal gradient on both CPI and CPTWC than there is of system pressure. Figure 4.11 demonstrates that through wall cracking develops at a time after system pressure has stabilized while Figure 4.12 shows that system pressure drops systematically with increasing breaks size. Taken together, this information suggests that if pressure played a key role in defining crack initiation or through wall cracking frequencies then both CPI and CPTWC would reduce with increasing LOCA break diameter. Clearly this is not the trend in Figure 4.15. By way of example, Figure 4.13 illustrates the variation of pressure and temperature, and resultant variation in both the applied-K_I and in the minimum K_{Ic} value, for a 5.66-in. diameter LOCA break in Beaver Valley. Since toughness depends only on temperature it must track directly with it. Also, the behavior of the applied-K_I depends much more strongly on the time dependent changes in the crack tip temperature than it does on the pressure. Consequently, larger LOCA breaks generally pose a greater challenge to RPV integrity than do smaller LOCA breaks.

In closing it should be noted that there is little the operator can do in response to a medium or large break LOCA. The system pressure will blow-down as a consequence of the break. Both the severity of the thermal transient and the final system pressure depend only on the interaction of the break size and the capacity of the emergency core cooling system, which is an automatic function. Thus, operator actions, and HRA credits for operator actions, influence neither the plant response nor the calculated consequences to the plant. Since LOCA transients dominate the overall challenge posed by PTS the effect of HRA credits for operator actions on the calculated through wall cracking frequencies is quite small.

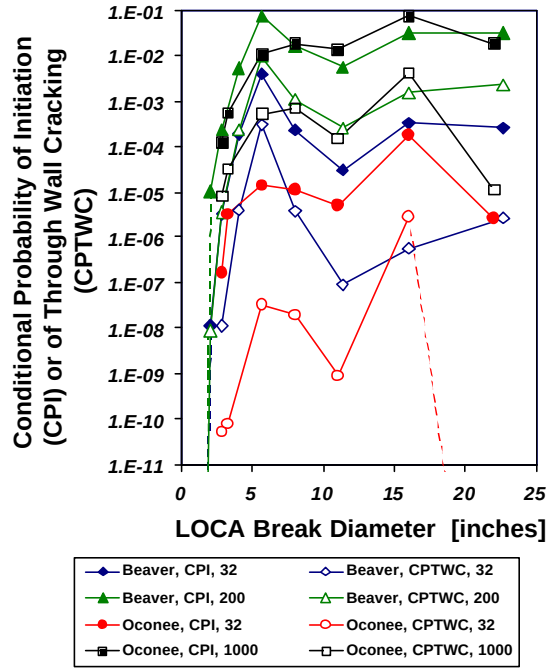

Figure 4.10. Variation in the conditional probability of crack initiation and of through wall cracking with LOCA break size (dashed lines connect to values of CPI and CPTWC = 0).

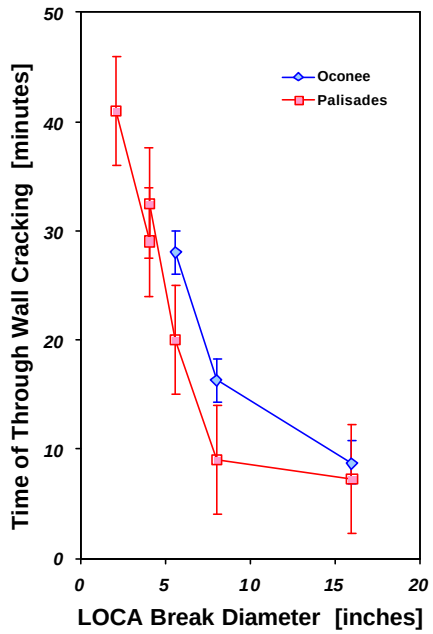

Figure 4.11. Effect of LOCA break diameter on the time at which through wall cracking occurs in for Oconee and Palisades.

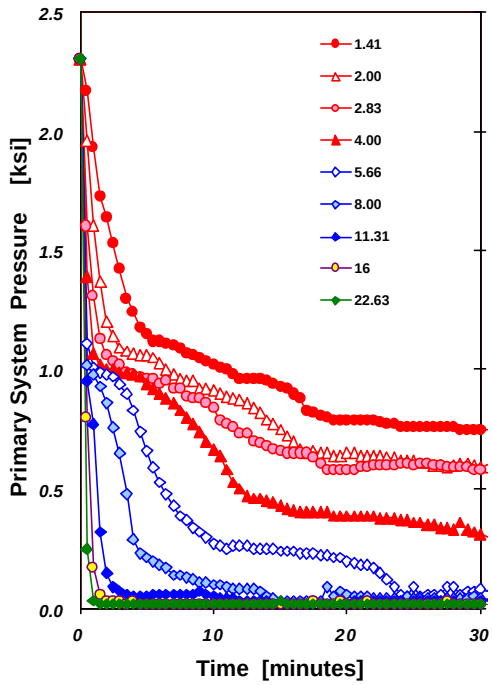

Figure 4.12. Variation of system pressure with LOCA break size for Beaver Valley.

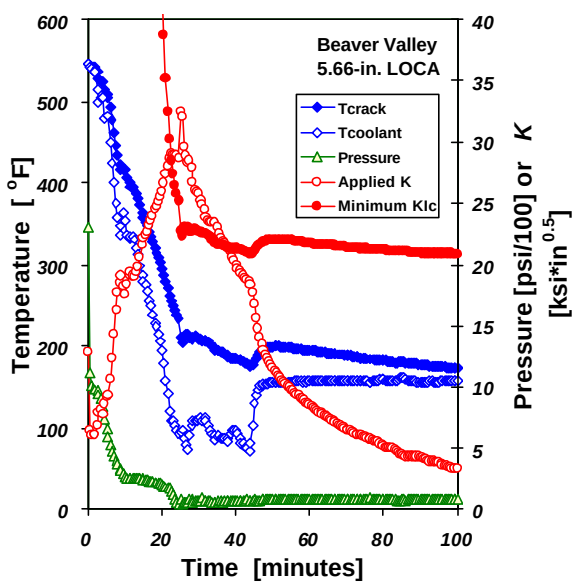

→ $K_{applied}$ values calculated for an axial flaw having a length of 0.313-in., a depth of 0.241-in., and a distance between the vessel ID and the inner crack tip of 0.156-in.

Figure 4.13. Variation of pressure, temperature, and K values with time for a 5.66-in. diameter LOCA break size in Beaver Valley.

4.3.2.2 Dominant Material Contributors

In this section we examine how different material regions and crack orientations contribute to the TWCF values reported in Figure 4.4. In the FAVOR PFM model cracks have prescribed orientations derived from a physical understanding of the mechanisms of their formations:

- Because buried weld cracks are invariably lack of fusion (LOF) defects (see Section 2.3.2.1) they are always oriented circumferentially in circumferential welds and axially in axial welds.
- Surface cracks through the stainless steel cladding are likewise LOF defects (see Section 2.3.2.3). Since weld overlay cladding is always laid down circumferentially these surface breaking defects, which in FAVOR can be associated with any of welds, plates, or forgings, are always oriented circumferentially.
- In plates no preferred orientation for flaws was discerned (see Section 2.3.2.2). Consequently FAVOR assumes a random and unbiased distribution of plate flaws orientations: half of the plate flaws simulated are oriented axially and half of the plate flaws simulated are oriented circumferentially.

The information in Figure 4.14 demonstrates that the TWCF values are dominated by flaws that are oriented axially in the vessel wall. This finding is consistent with past studies of PTS [ORNL 85a, 85b, 86]. Axial flaws dominate the TWCF because the driving force to fracture for an axial flaw under PTS loading continues to increase through nearly the entire vessel wall thickness. Conversely, the driving force to fracture for a circumferential flaw under PTS loading increases to a point between 50% and 60% of the way through the wall thickness. As an axial flaw progresses deeper into the vessel wall the driving force to fracture then begins to fall off. This reduction in fracture driving force coupled with the increase in material toughness (caused by the increased temperature and

reduced irradiation damage at these locations) as the flaw approaches the outer diameter makes stable crack arrest of circumferential cracks quite likely.

As discussed at the beginning of this section, circumferential welds contain no axial flaws. The finding from Figure 4.15 (bottom graph), i.e. that circumferential welds do not contribute much to the TWCF, is therefore expected. However, Figure 4.15 (top graph) also reveals that while axial welds are responsible for the great majority of the TWCF in Oconee and for all of the TWCF in Palisades they are only minor contributors to the TWCF in Beaver Valley. At Beaver Valley plates are responsible for 95% or more of the TWCF because the plates are much more embrittled than are the axial welds. Since the embedded axial weld flaws reside on the fusion line between the weld and the plate, FAVOR associates these flaws with the material properties of the more embrittled of the two surrounding materials (i.e., either the weld properties of the plate / forging properties)[***]. In Beaver Valley this almost invariably means that the larger embedded flaws from the axial weld flaw distribution are associated with the properties of the plate material.

In total, the information in Figure 4.14 and Figure 4.15, suggests that the axially oriented flaws that lie on the fusion line of the axial welds are responsible for the great majority (85% to 100%) of the through wall cracking frequency. The fracture resistance of flaws at these locations is governed by the more embrittled of the toughness properties of the materials that lie on either side of the fusion line (i.e. either plate and axial weld, or forging and axial weld). Consequently, even very embrittled circumferential welds are not expected to contribute significantly to the TWCF.

[***] This treatment is consistent with the physical understanding that a crack will tend to initiate and propagate towards the less-tough material. Appendix C provides a more detailed justification for this feature of the PFM model.

4.4 Applicability of these Results beyond the Three Study Plants

Before we can use the through wall cracking frequency values for Oconee, Beaver Valley, and Palisades reported in Section 4.3 we must first consider the potential effects of PRA external event initiators on our results. Additionally, a discussion is needed concerning how these three plant specific results can be applied to develop a screening limit generally applicable to all PWRs. We address these two topics in the following sub-sections.

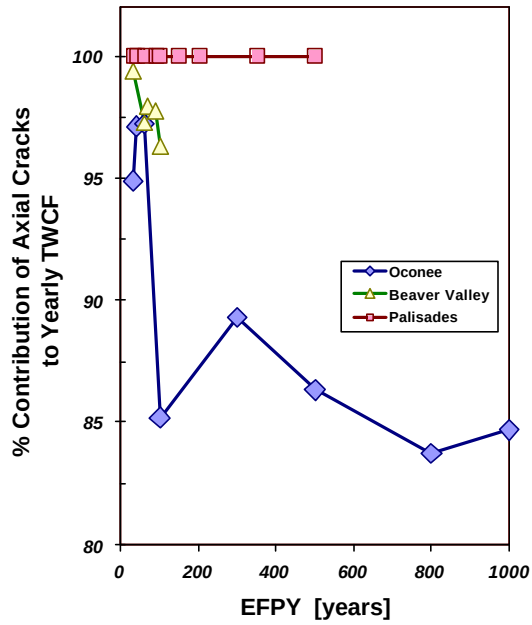

Figure 4.14. Contribution of axially oriented cracks to the total through wall cracking frequency (TWCF). The remainder of the TWCF contribution is entirely attributable to circumferentially oriented flaws.

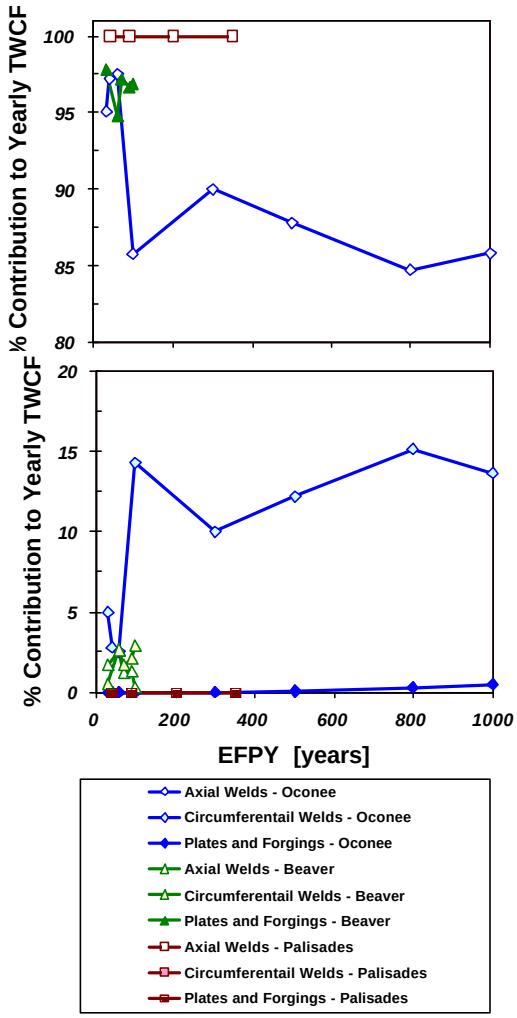

Figure 4.15. Contribution of the different major material regions to the total through wall cracking frequency (TWCF).

4.4.1 Consideration of External PTS Pre-Cursor Events

In examining the potential for a revised PTS screening criterion, it is important that the potential risk from external events also be considered. External events are those in which spatial interactions are crucial to the propagation of the accident sequence, and these can contribute to the PTS risk. External events include such scenarios as those involving fires, floods, high winds and tornados, seismic events, among others. As an example, a fire could start in an electrical cabinet causing the spurious opening of one or more secondary relief valves such as turbine bypass (steam dump) valves, which could induce a serious overcooling and a potential PTS concern depending on subsequent plant equipment and operator responses. Thus, while external events are generally less likely to occur relative to some other plant challenges, because they can affect multiple plant equipment and operator actions as well, they could be important to PTS.

Because (a) the specific effects of external events are very plant-specific (e.g., into which rooms the water from an internal flood propagates and thus what equipment is affected), and (b) since these analyses can be considerably resource intensive requiring the gathering of significant spatial information about each plant, it was not practical to perform plant-specific external event PTS analyses. Instead, a conservative analysis was performed with the goal of *enveloping* the potential PTS thru wall crack frequencies (TWCFs) from external events. This is in contrast to the internal event PTS analyses results reported in Section 7 above. The internal events analyses are generally "best-estimate" analyses meant to determine a realistic assessment of PTS TWCFs due to scenarios initiated by such events as turbine trips, loss of feedwater, etc. (i.e., internal events). As stated above, the contribution from external events was assessed by using a worse-case approach. This approach is based on using conservative assumptions to envelope the PTS TWCFs from external events and hopefully demonstrate that the TWCFs from external events are at least no higher than those estimated from the internal events analyses. The analysis results described here are based on such an approach.

As a result, the numerical results from the external events analyses (described in detail in XX[(Ref later)]) should not be taken as best-estimate or realistic values; they are intended to provide conservative screening bounds for the pertinent external scenarios. Also note that in following this approach, no particular plant was taken as a representative model for the analysis (with the exception of earthquake hazard, where H. B. Robinson and Diablo Canyon were used as surrogates). Therefore, because these results are intended to bound the worst situation that might

arise at virtually any plant, they may be extremely conservative for many plants. The degree of conservatism cannot be determined without performing plant-specific analyses.

4.4.1.1 Approach

A multi-faceted approach was used to gain insight as to the potential contribution of external events to the PTS TWCFs. This approach included the following:

A review was performed of the late 2001- early 2002 version of the Calvert Cliffs PRA model, with cooperation from the utility, which includes not only core damage scenarios, but also PTS scenarios. The model also includes contributions from both internal and external events for both core damage frequencies and PTS TWCFs and can offer insight into the potential importance of external events.
As further evidence of the potential importance of external events, a review of licensee event reports (LERs) was performed of actual overcooling events in U.S. plant operating experience covering approximately the past twenty years.
Further, a review was conducted of a sampling of (just two) Individual Plant Examinations for External Events (IPEEEs), one for Salem and one for Ginna, to determine what insights could be gained from those studies that might be applicable to PTS.
With all the above as background, it was nevertheless decided that additional analyses were necessary to be able to envelope the potential TWCFs from external event overcooling scenarios. This final step is summarized later in Section 8.2.4.

4.4.1.2 Preliminary Findings Based on the Reviews

The Calvert Cliffs PRA suggests that the TWCFs as a result of PTS caused by external events are low compared to that caused by internal events; i.e., less than 10%. The PRA shows fire as the external event of most concern. While this is an indicator of the potential relative contributions, it is only one plant's result and the finding is subject to potential modifications that may need to be made to the model so as to be better comparable to the three analyses conducted as part of this work. For instance, the Calvert Cliffs model may need modifications in the areas of the sequences being modeled and some human failure probabilities may need to be reconsidered during certain external events. Hence, while encouraging, the relative importance of external events and particularly fire to the PTS TWCFs cannot be generically ascertained based on this one input alone.

The LER review resulted in the identification of only three events that could be potentially categorized as involving an external event although only one, a switchgear fire, was clearly an external event (LER No. 26989002). Out of a total 128 "significant" events in the past twenty years from the LER review, this evidence suggests that external events are expected to be involved in no more than approximately 2% of all significant overcooling occurrences. While this is a valuable insight that again indicates that the importance of external events may be low, it still does not address the potential TWCFs from external events even if they do occur less frequently since the events could lead to more serious scenarios with resulting higher TWCFs.

The two IPEEE reviews were conducted to determine core damage frequencies as a result of under-cooling and not overcooling events; hence there were very limited insights from these reports applicable to PTS. Nevertheless, one general type of interaction between external events and effects of interest to PTS was noted to be included in both studies. This was a fire-induced opening of one or more power-operated relief valves (PORVs) on the pressurizer; a possible serious overcooling event. This indicates that any estimation of the external event contribution to PTS needs to include consideration of spurious actions such as that described due to fire scenarios. However, no other meaningful insights were gained from this review that would be applicable to this PTS work.

4.4.1.3 Additional Analyses

4.4.1.3.1 Overview

The above reviews provided some, but an incomplete set of insights with regard to how important external events may be to PTS. As a result, additional analyses were performed. These additional analyses involved high-level comparisons of (a) preliminary results from the internal events analyses for the three plant analyses, with (b) conservatively estimated corresponding external event sequence results. This comparative analysis was structured based on three *broad* types of overcooling scenarios analyzed in this PTS study. These include:

Category 1: Loss of Coolant Accidents (LOCAs). These are scenarios that involve primary system breaches such as pipe breaks and open pressurizer valves but without any secondary anomalies or faults.
Category 2: Secondary Anomalies or Faults. These are scenarios that involve such events as stuck-open secondary valves, main steam line breaks, and steam generator overfeeds but without any primary system anomalies or faults.
Category 3: Co-existing LOCA - Secondary Faults. These are scenarios that involve both primary system breaches and secondary faults at the same time.

As required, the analyses further divided these broad categories of scenarios into more specific types. In each case, conservative estimates were made with regard to the type of external event that could directly contribute to the cause of such a scenario. In addition, conservative estimates were made with regard to the applicable external event frequencies, plant equipment responses, and operator effects. With regard to operator actions, little or no credit was given in these analyses in response to the external events-induced PTS challenges. Finally, the resulting approximate TWCFs from both the internal events contribution and the conservatively assessed external events contribution were compared. The following is provided as just one example of such a comparison.

4.4.1.3.2 An Example

Category 1 - LOCAs; Scenario Type #3: A small LOCA (~1.5"-3" equivalent diameter) occurs and everything else functions as designed; i.e., High Pressure Injection (HPI) operates (so cold water is hitting the vessel downcomer) and the system likely stays on full since throttling criteria will not likely be met for most of this size range. The operator shuts off reactor coolant pumps (RCPs) as procedurally required (this is worse for PTS), and there are no secondary anomalies or operator errors.

A summary of the approximate internal event scenario frequencies and corresponding TWCFs is shown in Table 4.4.

POSSIBLE SEISMIC-SMALL LOCA SCENARIO:

For the small LOCA case, a 0.3g HCLPF (High Confidence of Low Probability of Failure) is conservatively assumed for piping and other components whose failure as a result of a seismic event could result in a small LOCA. This corresponds to the review level earthquake (RLE) peak ground acceleration for most plants in the IPEEE program. It is further assumed that both β_R and β_u that define the uncertainty in the HCLPF are 0.3, giving a median fragility of about 0.5g. Taking the H. B. Robinson site as a surrogate for Eastern plants, because it has the largest hazard (NUREG-1488)[(Ref later)] of any Eastern PWR, this corresponds to a mean accidence frequency of 1.6E-4/yr. An analysis was performed using SAPHIRE[(Ref later)] in order to convolve the above fragility for small LOCA with the revised Lawrence Livermore National Laboratory (LLNL) hazard curve for H. B. Robinson (NUREG-1488), giving a mean seismic-induced small LOCA frequency of 1.1E-4/yr.

As an additional sensitivity, the hazard curve for Diablo Canyon was also used as a surrogate for a high-seismicity site. A corresponding HCLPF for small LOCA at such a site was assumed to be 0.5g, because of the more rugged plant design (higher RLE). Maintaining β_R and β_u of 0.3, and

convolving this fragility for small LOCA with the mean hazard curve from the Diablo Canyon IPEEE(Ref later) gives a mean seismic-induced small LOCA frequency of 5.0E-4/yr[†††]. Using an approximate value of 0.02 (i.e., 2%) as the fraction of the year the plant is at hot zero power (HZP) conditions, as done in the internal events analysis, yields about 1E-5/yr as the highest estimated HZP condition frequency.

The approximate corresponding external event TWCFs are as shown in Table 8.2-1 and are derived by multiplying the above external event frequencies by the same conditional vessel failure probabilities derived from the internal events analyses (appropriate in this case).

POSSIBLE OTHER EXTERNAL EVENT - SMALL LOCA SCENARIOS:

No directly related cause and effect of significance has been identified relative to fires, floods, or high wind/tornado events causing small LOCAs. Hence these other external events under consideration should provide a negligible contribution to the TWCFs from small LOCAs as compared to the internal events contribution.

SMALL LOCA SCENARIOS:

Note that the external event contribution to the TWCFs for this type of accident are generally less than and certainly no greater than the internal event TWCFs.

4.4.1.4 Overall Findings

In spite of the conservative nature of the external event analyses, no external event scenarios were found where the TWCFs significantly exceed that of the worst internal event scenarios (medium and large LOCAs). Therefore, there is considerable assurance that the external event contribution to overall TWCF as a result of PTS is at least no greater than the contribution from internal events. In fact, given the conservative probabilities and dependencies assumed in the external event analyses, with the addition of little or no credit for any operator actions for the external event scenarios, it is more likely that the external event contribution to overall TWCF is realistically much less than the internal event contribution. It is therefore our view that the contribution of external initiating events to the overall TWCF due to PTS is well within the uncertainty associated with this analysis. Hence, it is recommended that the overall PTS TWCF can be estimated by neglecting the potential contribution from external events.

4.4.2 Generalization of These Results to All PWRs

The analyses presented thus far in this report provide perspectives as to the potential for serious overcooling events to lead to PTS and reactor vessel failure for three plants. At least one plant from each of the U.S. PWR nuclear steam supply system (NSSS) vendors has been studied from both plant design and operational characteristics (Oconee - Babcock & Wilcox; Beaver Valley - Westinghouse; Palisades - Combustion Engineering). Before considering the potential for changing the current PTS rule, it is important to gain some insight as to the applicability of the three plant results to a wider number of PWRs. This section provides the approach followed and the additional insights gained with regard to the broader applicability of the three plant results to PWRs in general.

[†††] The hazard curve in the Diablo Canyon IPEEE is given in terms of peak spectral acceleration in the range of 3.5-8Hz. This was converted to a zero-period peak ground acceleration by dividing the accelerations by a factor of 2.

Table 4.4. Results Summary for Small Pipe Break LOCA.

Scenario (@ Full Power)	Internal Frequency	Internal TWCF	External Frequency	External TWCF
Small LOCA	3E-4 to 3E-3	9E-8 to 2E-6	<5E-4	<5E-7
Scenario (@ HZP)	**Internal Frequency**	**Internal TWCF**	**External Frequency**	**External TWCF**
Small LOCA	6E-6 to 6E-5	~1E-7	1E-5	<5E-8

4.4.2.1 Approach

Given the non-feasibility of performing detailed examinations of all other PWRs in the U.S., it was decided that the best way to determine to what extent the three plant results might be generically applicable was to perform a comparison study. This comparison study reviews other PWR plant design and operational characteristics to those of the three plants to determine the similarities and differences in these plant features that matter most to the potential for PTS. Based on the extent of these similarities and differences, conclusions can be drawn with regard to the applicability of the three plant results to other PWRs.

4.4.2.1.1 Representative Plants for Comparison Study

In order to (a) limit the number of other representative plants to be compared as a resource savings, and (b) focus on those plants most likely susceptible to the PTS phenomenon, a select number of plants were chosen from those PWRs that have the highest RT_{NDT} associated with their reactor vessel. In determining the highest RT_{NDT} plants, those PWRs having circumferential welds with high degrees of embrittlement were eliminated since preliminary results indicated that while cracks may initiate in such welds, there is a lower likelihood of such cracks propagating all the way through the vessel wall as compared to other types of welds (axial, plate, forging). The resulting list of highest RT_{NDT} plants is shown in Table 4.5.

From the plants listed in Table 4.5, the following plants were chosen as representative of other PWRs to perform the plant feature comparisons. These representative plants were chosen on the basis of (a) being high on the list, (b) covering the NSSS vendors, and (c) including plants having different limiting materials (i.e., welds, plates, and forgings).

- Salem 1
- TMI 1
- Ft. Calhoun
- Diablo Canyon 1
- Sequoyah 1

4.4.2.1.2 Plant Features to be Compared

Based on the results of the three plant studies, a select set of plant design and operational features matter most to whether or not certain types of overcooling scenarios are important to PTS and what are the corresponding estimated thru-wall crack frequencies. Based on these insights, the following plant features were used to compare the five representative PWRs to the same features for the three plants studied.

One of the general types of scenarios that should not be of much concern (based on the 3 plant analyses thus far) is secondary breaches up to the size of even multiple steamline breaks. This is primarily dependent on the fact that if reasonable credit can be given for quickly isolating the breach (e.g., MSIVs close) and/or for operators to quickly identify and isolate the feed to a faulted SG(s), the amount of cooling is minimized and the resulting PTS risk is small. Additionally, guidance for ensuring proper steaming of good SGs is of some importance to avoid severe primary system repressurization.

In order to ensure this is generally true for other PWRs, there needs to be confidence that the capabilities to isolate, and the degree of operator credit to stop feeding a faulted SG(s) and properly steam with good SGs are similar for the other plants to what we have seen for the 3 plants analyzed. The following plant attributes should allow a determination as to whether such confidence is appropriate:

- Information on the number of MSIVs, and isolation capabilities to isolate other paths such as on ADV paths and steam dump/turbine bypass paths.
- Reactor trip and Excessive Steam Demand (or similar) procedures to ensure that the procedural directions and placement of appropriate steps in the procedures are such that identification and isolation of a faulted SG(s) are likely to lead to early and successful operator action like we have seen for the 3 plant analyses.
- Review of operator training, and EOP allowances to quickly isolate bad SGs even if not yet in the excessive steam demand procedure, that would further support a high likelihood for quick and successful operator action.

One of the general types of scenarios that should not be of much concern (based on the 3 plant analyses thus far) is secondary overfeeds such as a ramping up full of MFW during startup or an uncontrolled feed of AFW/EFW. This is primarily dependent on the fact that the rate of feed that can be achieved (relative to the normal inventory of the SGs) and the possible temperature of the feed are such that such scenarios simply cannot cause a severe overcooling event. In order to ensure this is generally true for other PWRs (seems very likely), there needs to be confidence that the ability to and rate of possible overfeed, and the temperature of the feed are similar to the 3 plants analyzed. Thus, the following plant attributes need to be compared:

- Information on the feed (MFW, AFW/EFW, condensate) capabilities and the normal inventories for the SGs
- Information on the possible feed temperatures for all feed sources (especially how cold they could be).

One of the general types of scenarios that tend to dominate the PTS risk is the general class of primary LOCAs (pipe breaks). Because the LOCA frequencies are “generic” in nature and would not vary from plant-to-plant, and since there is not much procedurally the operator can do to mitigate the effects of the event, the importance of these scenarios seem to be most dependent on the safety injection water temperature, the sump recirculation water temperature, and the time recirculation would likely occur. The latter item is probably most dependent on the size of the injection water tank(s), the flow rates for injection, and when containment spray pumps would also actuate and at what flow rate to get an idea as to how fast (or slow) the injection tanks may empty and hence recirculation begin. The following plant attributes are thus important to compare:

- Allowable range of safety injection water temperatures (especially how cold).
- Information that would allow a crude estimate of recirculation water temperature, noting for instance, if some plants cool (or don’t) the recirc water before re-entering the core in Safety injection tank(s) size
- Approximate safety injection flowrate vs. LOCA break size
- Actuation requirements for containment spray and flow rate once running

Scenarios involving stuck-open and possible subsequent reclosure of different numbers of PORVs or SRVs on the primary system pressurizer could be dominant depending on the sizes and numbers of valves and the ability of the operator to recognize when they are open and reclose, and procedures/training for addressing such events. Additionally, guidance with regard to terminating/throttling safety

injection to avoid severe repressurizations especially if/when these valves reclose is another critical characteristic. Therefore, the following plant features need to be compared:

- Numbers and sizes of PORVs and SRVs on the pressurizer and whether the plant operates with the PORV block valves normally shut.
- Instrumentation available (e.g. acoustic monitors...) to identify open PORVs or SRVs and that they may have reclosed.
- The EOPs for addressing such LOCAs as well as what to do (the procedures that are used or transferred to) should the valves reclose, along with any training information which may support the high likelihood the operators will take the correct actions quickly.
- Procedures for when to throttle/terminate safety injection so as to avoid severe primary system repressurization (especially if the valves were to reclose).
- Pressure - flow capabilities of high or intermediate pressure pumps (CVCS, SI...)

Scenarios involving total loss of all feed and therefore using "feed and bleed" can be of some importance mostly dependent on the degree of redundancy of feed capability and on the procedures for when to go to feed and bleed and the number of PORVs opened when in feed and bleed. Thus, the following plant information is important to compare:

- Number of AFW/EFW pumps/flowpaths vs. minimum success criteria for adequate feed to the SG(s).
- EOP criteria for when to go to "feed and bleed".
- Number of PORVs opened out of total number of available PORVs (or even SRVs if pumps can pump open SRVs, too) when in feed and bleed mode.

4.4.2.2 Results of Comparison Study

Detailed results from the comparison study outlined in Section 4.4.2.1 were not available in time for publication of this report December 2002). However, even absent this information several factors suggest that our current plant specific results from analysis of Oconee, Beaver Valley, and Palisades can be applied with confidence to discern a new PTS screening limit applicable to all PWRs. By any embrittlement metric (i.e., either **Error! Reference source not found.** or Eq. 2-5) Beaver Valley and Palisades contain some of the most embrittled materials in service today. Thus, all other conditions being equal, these two plants can be expected to exhibit TWCF values that represent more of a bound than they do central tendency values on the TWCF of all PWRs.

Table 4.5. Plant list for generalization study.

Tolerance to a PTS Challenge		Plant Name	Most Embrittled Material	$RT_{NDT(u)}$ + Irradiation Shift at 40 years [°F]	Manufacturer
The estimated tolerance to a PTS challenge increases as the number in the next column increases.	1	SALEM 1	PLATE	204	Combustion Engineering
	2	BEAVER VALLEY 1	PLATE	194	Combustion Engineering
	3	TMI-1	A-WELD	186	Babcock & Wilcox
	4	FORT CALHOUN	A-WELD	181	Combustion Engineering
	5	PALISADES	A-WELD	179	Combustion Engineering
	6	CALVERT CLIFFS 1	A-WELD	178	Combustion Engineering
	7	DIABLO CANYON 1	A-WELD	171	Combustion Engineering
	8	DIABLO CANYON 2	PLATE	170	Combustion Engineering
	9	SEQUOYAH 1	FORGING	167	Rotterdam Dockyard
	10	WATTS BAR 1	FORGING	164	Rotterdam Dockyard
	11	ST. LUCIE 1	A-WELD	164	Combustion Engineering
	12	SURRY 1	A-WELD	163	Babcock & Wilcox
	13	INDIAN POINT 2	PLATE	162	Combustion Engineering
	14	GINNA	FORGING	161	Babcock & Wilcox
	15	POINT BEACH 1	A-WELD	159	Babcock & Wilcox
	16	FARLEY 2	PLATE	158	Combustion Engineering
	17	MCGUIRE 1	A-WELD	158	Combustion Engineering
	18	OCONEE 1	A-WELD	157	Babcock & Wilcox
	19	NORTH ANNA 2	FORGING	155	Rotterdam Dockyard
	20	SHEARON HARRIS	PLATE	153	Chicago Bridge & Iron
	21	NORTH ANNA 1	FORGING	153	Rotterdam Dockyard
	22	COOK 2	PLATE	152	Chicago Bridge & Iron
	23	SALEM 2	A-WELD	148	Combustion Engineering
	24	CRYSTAL RIVER 3	A-WELD	141	Babcock & Wilcox
	25	CALVERT CLIFFS 2	PLATE	139	Combustion Engineering
	26	ROBINSON 2	PLATE	138	Combustion Engineering
	27	COOK 1	A-WELD	138	Combustion Engineering
	28	FARLEY 1	PLATE	133	Combustion Engineering
	29	ARKANSAS NUCLEAR 1	A-WELD	129	Babcock & Wilcox

Notes: (a) Plants analyzed in the PTS re-evaluation effort are shown with a shaded background. (b) Circ welds have been omitted because while circ cracks initiate they do not (usually) lead to vessel failure.

4.5 Summary of Findings

In this Chapter we have summarized the results of our assessment of the challenge to RPV integrity posed by PTS transients at three operating PWRs: Oconee, Beaver Valley, and Palisades. These results support the following conclusions:

1. Even at the end of license extension (60 operating years) we estimate the risk of through wall cracking posed by PTS challenges to be quite low, i.e. between $1x10^{-9}$/yr and $5x10^{-8}$/yr at the mean and 95th percentile[‡‡‡] in the three plants modeled.

[‡‡‡] Highly skewed TWCF distributions lead to mean and 95th percentile values that are very close.

2. The calculated distributions of TWCF are quite skewed toward zero, or very low, through wall cracking probabilities. Also they are very broad, spanning three or more orders of magnitude from minimum to maximum. These characteristics of the distributions do not arise due to an inadequate state of knowledge but rather are a natural and expected consequence of the underlying failure mechanism: cleavage fracture. The absolute lower bounds characteristic of both the cleavage crack initiation toughness and the cleavage crack arrest toughness distribution result in the great majority of the conditions simulated in our analysis having a zero (or a very very small) probability of crack initiation and through wall cracking. This situation produces TWCF distributions that are both skewed and broad.
3. By far the greatest contribution to PTS risk arises from LOCAs. The driving force to fracture in a LOCA depends primarily on how rapidly temperature changes with time, whereas the fracture resistance scales directly with temperature. Consequently larger breaks tend to produce a greater challenge to vessel integrity than do smaller breaks. Since the timing of events limits an operator's ability to respond to a LOCA, and since LOCA transients dominate the overall challenge posed by PTS, the total effect of HRA credits for operator actions on the calculated through wall cracking frequencies is limited.
4. The once-through steam generator design used in B&W plants make stuck-open valves in the primary system a dominant PTS event for these plants.
5. Transients initiated by secondary side events in general, and main steam line breaks in particular, do not contribute significantly to the PTS risk. Even without operator actions the transient conditions are not nearly as severe as those posed by LOCAs, resulting in small contributions to TWCF. In addition, probable operator actions mitigate the severity of these transients to the point that the challenge they pose is much less severe than primary side breaches.
6. The greater fracture driving force of axially oriented flaws (relative to circumferentially oriented flaws) makes them account for the great majority (≈85-90%, or more) of the estimated through wall cracking frequency. Since flaws of sufficient size to significantly challenge vessel integrity lie only along weld fusion lines, only axial welds contain axial flaws. The fracture resistance of flaws at these locations is governed by the more embrittled of the toughness properties of the materials that lie on either side of the fusion line (i.e. either plate or axial weld). Consequently, circumferential welds could be much more embrittled than axial welds and still not contribute significantly to the TWCF.
7. Flaws in plates account for very little (< ≈1%) of the TWCF owing to the much smaller size of plate flaws than weld flaws. Underclad cracks in forgings are reported to have flaw depths ranging from < 0.1 to 0.3-in. maximum [Bamford 00]. The similarity between these flaw depths and those used in this study for plates suggest that underclad cracks in forgings will behave similarly to plates (i.e., contribute minimally to TWCF). Thus, while not explicitly modeled in our investigation, it is expected that as long as the density of underclad cracks in forgings is comparable of the density of cracks in plates, the embrittlement of forgings should not control the fracture resistance of a vessel subjected to a PTS event.
8. The TWCF arising from transients initiated by external PTS events are expected to be much smaller than that arising from internal events. It is therefore our view that the contribution of external initiating events to the overall TWCF due to PTS is well within the uncertainty associated with this analysis.
9. While our comparison study aimed at generalizing these results from Oconee, Beaver Valley, and Palisades is to date incomplete, several factors suggest that these results can be applied with

confidence to discern a new PTS screening limit applicable to all PWRs. By any embrittlement metric Beaver Valley and Palisades contain some of the most embrittled materials in service today. Thus, all other conditions being equal, these two plants can be expected to exhibit TWCF values that represent more of a bound than they do central tendency values on the TWCF of all PWRs.

5 Risk-Informed Reactor Vessel Failure Frequency Acceptance Criterion

5.1 Introduction

As discussed in Chapter 1, the current PTS rule establishes a series of steps that PWR licensees must perform. The initial step involves a deterministic evaluation of the RPV's RT_{PTS} for welds and plate materials (Eq. 1-3 evaluated at EOL). If the computed RT_{PTS} values exceed the screening criteria established in 10 CFR 50.61, licensees are directed to accomplish reasonably practicable neutron flux reduction to avoid exceeding the screening criteria during the RPV's licensed life. Plants for which the computed RT_{PTS} values, even with neutron flux reduction, will still exceed the screening criteria are required, at least three years before exceeding the criteria, to submit a plant-specific safety analysis demonstrating that the risk associated with PTS events is acceptably low. NRC Regulatory Guide (RG) 1.154 [RG 1.154], describes one acceptable method for performing such safety analyses.

Two key parts of the PTS safety analysis approach described in RG 1.154 are the estimation of RPV through-wall crack frequency (TWCF) and the comparison of the estimated TWCF with an acceptance criterion of 5 x 10^{-6} per reactor year (ry). Neither RG 1.154 nor Enclosure A to SECY-82-465 [SECY-82-465] provides a detailed discussion regarding this specific value, although the Enclosure A does argue that an even higher TWCF value (i.e., 1 x 10^{-5}/ry) is consistent with the then-proposed Safety Goal Policy guidelines on "core melt frequency" and the desire that the core melt frequency ascribable to "one sequence" (such as PTS) should be a small fraction of the overall core melt frequency. Based on the assessed likelihood of potential PTS challenges, the predicted thermal-hydraulic response of the plant, and the predicted behavior of the RPV, the RTNDT screening criteria recommended by the staff in 1982 and subsequently incorporated in 10 CFR 50.61 were determined to be consistent with a TWCF of around 5 x 10^{-6}/ry.

The NRC has established a considerable amount of guidance on the use of risk information in regulation since it issued SECY-82-465 and published the original PTS Rule. In light of this more recent guidance, the staff has, as part of the PTS technical basis re-evaluation project, identified and assessed options for a risk-informed criterion for the reactor vessel failure frequency (RVFF) associated with PTS (currently specified in RG 1.154 in terms of TWCF). The assessment includes a scoping study of the issue of containment performance during PTS accidents, which has implications to the specification of the acceptance criterion. The resulting conclusions and their basis are provided in this chapter.

5.2 Current Guidance on Risk-Informed Regulation

Key documents published since the issuance of the original PTS rule include the Commission's Safety Goal Policy Statement (issued in 1986); a June 1990 Staff Requirements Memorandum (SRM); and RG 1.174 (and the associated revision to Standard Review Plan Chapter 19).

The Safety Goal Policy Statement [NRC FR 86] defines qualitative goals and quantitative health objectives (QHOs) for the acceptable risk of nuclear power plant operations. The QHOs address the prompt fatality risk to individuals, and the cancer fatality risk to society. For both

the individual and societal risks, the QHOs are defined to ensure that the public health and safety risk arising from nuclear power plant operations is a very small (0.1 percent or less) fraction of the total risk to the public.

The June 1990 SRM [USNRC 1990] discusses subsequent Commission decisions with respect to the policy statement. Of particular interest, the SRM establishes a subsidiary core damage frequency (CDF) goal of $1x10^{-4}$/ry. At the time it was developed, this subsidiary goal, as well as the qualitative safety goals and QHOs, was intended for use in generic agency decisions such as rulemakings. It was not aimed at plant-specific applications.

RG 1.174 [RG 1.174] and Standard Review Plan Chapter 19 [USNRC 1998b] describe a risk-informed process by which licensee-proposed license amendments which act to change regulatory requirements can be submitted, reviewed, and, if appropriate, approved. RG 1.174:

- describes a set of general principles for this process;
- extends the policies established in the Safety Goal Policy Statement, in that a large early release frequency (LERF) subsidiary objective is provided, and makes use of the QHOs in plant-specific decision-making; and
- provides a set of probabilistic guidelines defining acceptable changes in CDF and LERF associated with proposed reductions in regulatory requirements.

RG 1.174 is aimed at voluntary changes to a plant's licensing basis. However, it provides a general template for improving consistency in regulatory decisions in areas in which the results of risk analyses are used to help justify regulatory action. The principles of integrated, risk-informed decision-making (involving consideration of risk information, defense-in-depth, safety margins, and uncertainties) discussed in that RG broadly apply to risk-informed regulatory activities. RG 1.174 provides acceptance guidelines for changes in CDF and LERF. These guidelines were developed to provide assurance that proposed increases in CDF and LERF are small and consistent with the intent of the Safety Goal Policy Statement. If the baseline risk can be shown to be acceptable (as indicated by a total mean CDF of less than 1×10^{-4}/ry and a total mean LERF less than 1×10^{-5}/ry), applications for plant changes leading to small increases in mean CDF (up to 1×10^{-5}/ry) and mean LERF (up to 1×10^{-6}/ry) will be considered for regulatory approval.

The relationship between the RG 1.174 LERF criterion and the QHOs is discussed in Appendix A of NUREG/CR-6595 [Pratt 99]. In particular, that appendix argues that, for certain large early releases (involving the release of 2.5% to 3% of the reactor's iodine and/or tellurium inventory within 4 hours of accident initiation), a LERF of 1×10^{-5}/ry roughly corresponds to the prompt fatality QHO (currently around 5×10^{-7}/yr). The calculations supporting NUREG/CR-6094 [Hanson 94] and SECY-93-138 [SECY-93-138] are cited as the basis for these conclusions.

The staff's current activities on Option 3 for risk-informing 10 CFR Part 50, as described in SECY-00-0198 [USNRC 2000], take advantage of the groundwork laid by RG 1.174. The Option 3 framework being developed employs the total mean CDF and mean LERF guidelines mentioned above (1×10^{-4}/ry and 1×10^{-5}/ry, respectively). The framework also provides guidelines to limit the CDF and LERF associated with any single accident type from being a large fraction of the plant's total CDF and LERF.

5.3 Containment Performance During PTS Accidents

As discussed in Section 5.1, the current TWCF criterion of 5×10^{-6}/ry provided in RG 1.154 is aimed at ensuring that the risk associated with PTS is a small fraction of the risk level established by the Safety Goals and is consistent with the philosophy of distributing risk among accident types. However, the relationship between this criterion and the CDF and LERF guidelines established in RG 1.174 and those

proposed in the draft Option 3 framework is not clear because there currently is an incomplete understanding regarding the progression of an accident following a postulated PTS-induced RPV failure.

5.3.1 Previous Research Results

A number of research efforts have addressed potential PTS-induced RPV failure modes and their effects on core cooling and containment integrity. In the late 1970s and 1980s, large-scale experiments on prototypic RPVs subjected to pressure and temperature transients characteristic of PTS loadings were conducted as part of the NRC-sponsored Heavy Steel Section Technology (HSST) research program. These experiments demonstrated three potential outcomes of a PTS event (depending on the particulars of the transient, material embrittlement, etc.):

- No cracks initiate and the vessel remains intact.
- A crack initiates, propagates to some depth into the vessel wall, and stops. The vessel remains intact with little additional deformation.
- A crack initiates and propagates entirely through the vessel wall. In addition to large openings in the reactor vessel, this outcome involves significant additional deformation of the vessel.

In the context of RPVs, the third outcome presents a potentially significant challenge to core cooling and containment integrity.

In the mid-1980's, following the promulgation of the initial versions of 10 CFR 50.61 and RG 1.154, the NRC sponsored a number of studies on the risk associated with PTS . One such study, documented in NUREG/CR-4483 [Simonen 86], evaluated the current state of knowledge regarding post-vessel failure accident progression. The study considered such issues as the axial and azimuthal extent of crack propagation, the depressurization of the reactor coolant system, RPV vertical movement due to postulated full circumferential breaks of the vessel wall, and the possibility of missiles generated during the RPV failure. From the perspective of an RVFF acceptance criterion, two key findings of NUREG/CR-4483 are: a) the possibility of axial cracks propagating into embrittled circumferential welds and then propagating along these welds cannot be neglected; and b) the effects of PTS-induced missiles (including, in extreme cases, the RPV), are likely to be contained within the concrete barriers surrounding the RPV.

In 2001, the NRC sponsored a study on the potential structural consequences of PTS events. This study [Theofanous 2001] assumed the instantaneous opening of a very large (4m x 0.4m, ~2480 in^2) axially oriented hole in the RPV as a postulated result of PTS. Under these conditions and given the relatively low energy of the fluid, the impulse on the RPV and piping resulting from the blowdown was predicted to be within the bounds of a design basis Safe Shutdown Earthquake (SSE). However, the effects of internal structures (fuel supports, fuel assemblies, etc.) on the blowdown loads and the possible effects of blowdown on the internal structures themselves were not modeled.

The study also explored a simplified crack opening model that predicts a small hole (~110 in^2) resulting from a postulated 4m long axial crack rather than the very large hole (~2480 in^2) assumed in the analysis of blowdown loads. The study found that emergency core cooling system (ECCS) injection would not be challenged by a crack (and predicted hole area) of this size. The study did not address the possibility of more extensive axial crack propagation and the possibility of circumferential cracks that could challenge the ECCS. The staff's evaluation, summarized in Section 5.3.2, addresses these issues.

In July 2002, the Advisory Committee on Reactor Safeguards (ACRS) wrote a letter on the issue of PTS acceptance criteria [USNRC 2002]. The letter noted that the LERF criterion provided in RG 1.174 is not a proper starting point for PTS considerations, since the "...source terms used to develop the current goal do not

reflect the air-oxidation phenomena that would be a likely outcome of a PTS event."

The concern with air-oxidation events is associated with potential scenarios where fuel cooling has been lost and the fuel rods are exposed to air (as opposed to steam). Should such a situation arise, some portion of the reactor fuel will eventually be oxidized in an air environment. Based upon currently available information, it is expected that this oxidation will result in release fractions for key volatiles (ruthenium being of primary concern) that may be significantly (e.g., a factor of 20) larger than those associated with fuel oxidation in steam environments, and that these larger release fractions could lead to larger number of prompt fatalities than predicted for non-PTS risk significant scenarios.

5.3.2 Post-RPV Failure Scenarios Scoping Study

In order to support the assessment of options for a RVFF acceptance criterion (see Section 5.4 for a description of the options considered), the staff conducted a limited scoping study of PTS-induced post-RPV failure scenarios. The specific aim of the study was to develop an initial qualitative assessment of the potential impact (both positive and negative) of the unique characteristics of such scenarios on the likelihood of severe source terms, especially source terms beyond those typically assessed for non-PTS associated risk-significant scenarios.

The study involved the structured identification of technical issues underlying the assessment of the margins to core damage and large early release following potentially significant PTS-induced RPV failure scenarios (dominant scenarios for the pilot plants addressed by the PTS re-evaluation project are discussed in Chapter 4 of this report), and the collection and evaluation of currently available information relevant to these issues. Of particular interest was the identification of PTS-unique physical mechanisms that could lead to dependent failures of accident mitigation features. To better inform the evaluation, a small number of limited-scope thermal hydraulic and structural calculations were performed.

The scoping study focused on differences between post-PTS induced RPV failure accident progression and accident progression associated with non-PTS core damage events. Thus, in addition to the air-oxidation issue mentioned earlier, the scoping study addressed issues associated with the development and characteristics of the postulated opening in the RPV, the resulting blowdown forces, the effect on key structural components (e.g., the RPV, containment penetrations), and the potential for damaging missiles.

A list of the issues addressed, including a short description of each issue, is provided in Table 5.1.

To support the identification and semi-quantitative analysis of the issues, an accident progression event tree (APET) was developed. This tree, shown in Figure 5.1, identifies potentially important phenomena and possible scenarios following PTS-induced RPV failure.§§§

In general, the APET explicitly addresses the issues listed in Table 5.1. Two notable exceptions are associated with the issue of missiles and the issue of early overpressure. Regarding missiles, activities performed under the scoping study indicate that the possibility of a PTS-induced RPV failure leading to energetic missiles that could affect important top events in the APET (i.e., those associated with containment isolation, sprays, and ECCS) is sufficiently remote to allow exclusion of this issue from the APET. The activities included a review of NUREG/CR-4483 in light of currently available information on missile generation and penetration potential, a review of the reactor

§§§ Note that the APET includes branches for issues whose uncertainties are more epistemic in character (e.g., the blowdown forces associated with a given break size) as well as branches associated with issues whose uncertainties are more aleatory in character (e.g., the availability of ECCS).

Table 5.1. Post-RPV Failure Technical Issues.

Dominant PTS scenarios	This issue concerns the relative likelihood and characteristics of the scenarios predicted to contribute most to PTS-induced RPV failure. The characteristics of the PTS scenario (e.g., pressure, temperature, timing) directly affects the following issues (see below): crack propagation, blowdown forces, and ECCS status.
Relative contribution of axial and circumferential welds	This issue concerns the relative frequencies of PTS-induced RPV failures due to flaws in axial welds vs. flaws in circumferential welds. The orientation of the crack affects crack propagation and the characteristics of the resulting hole.
Crack propagation, hole size, hole location	This issue concerns the characteristics of the crack and the resulting hole in the RPV (including the rate of opening and the shape of the hole). This issue directly affects the following issues: blowdown forces, fuel coolability, and fuel environment.
Blowdown forces	This issue concerns the pressure differential driving fluid out of the RPV and the associated forces on the RPV, its internals, and connected piping. This issue directly affects the following issues: containment isolation, missiles, ECCS status, core status, and fuel dispersal.
Containment isolation	Early failure of containment isolation (e.g., by the failure of containment penetrations) is a contributing factor to the occurrence of a large early release.
Missiles	This issue concerns the possibility of a PTS-induced RPV failure leading to energetic missiles that could affect accident progression. This issue directly affects the following issues: ECCS status and containment spray status.
ECCS status (injection, recirculation)	This issue concerns the reliability of ECCS (given that ECCS was working prior to RPV failure). Potential contributors to ECCS failure include random hardware failure, failure to properly switchover to recirculation, failure of ECCS piping, and containment sump clogging.
Containment spray status	Early failure of containment spray is a contributing factor to the occurrence of a large early release. This issue concerns the reliability of containment spray (given that ECCS was working prior to RPV failure). Potential contributors to failure include random hardware failure, failure of piping (due to missiles), and containment sump clogging.
Core status (intact, distorted, disrupted)	This issue concerns whether the fuel geometry is distorted or severely disrupted due to the blowdown forces associated with a PTS-induced RPV failure.
Fuel dispersal	This issue concerns the location of fuel, should it be dispersed from the core as a consequence of a PTS-induced RPV failure.
Fuel coolability	This issue concerns whether the fuel, given its location and the core status, can be cooled.
RPV water level	This issue concerns the availability of water to cool the fuel (even should ECCS not be working). It is affected by a number of factors, including the characteristics of the RPV cavity and the inventory of water available.
Fuel environment (steam, air)	This issue concerns whether large-scale air oxidation can occur. It is strongly dependent on the development of the accident scenario.
Early overpressure	This issue concerns the possibility of early containment failure due to: 1) overpressures resulting from PTS-induced RPV failure events, and 2) overpressure due to other mechanisms (e.g., hydrogen combustion).

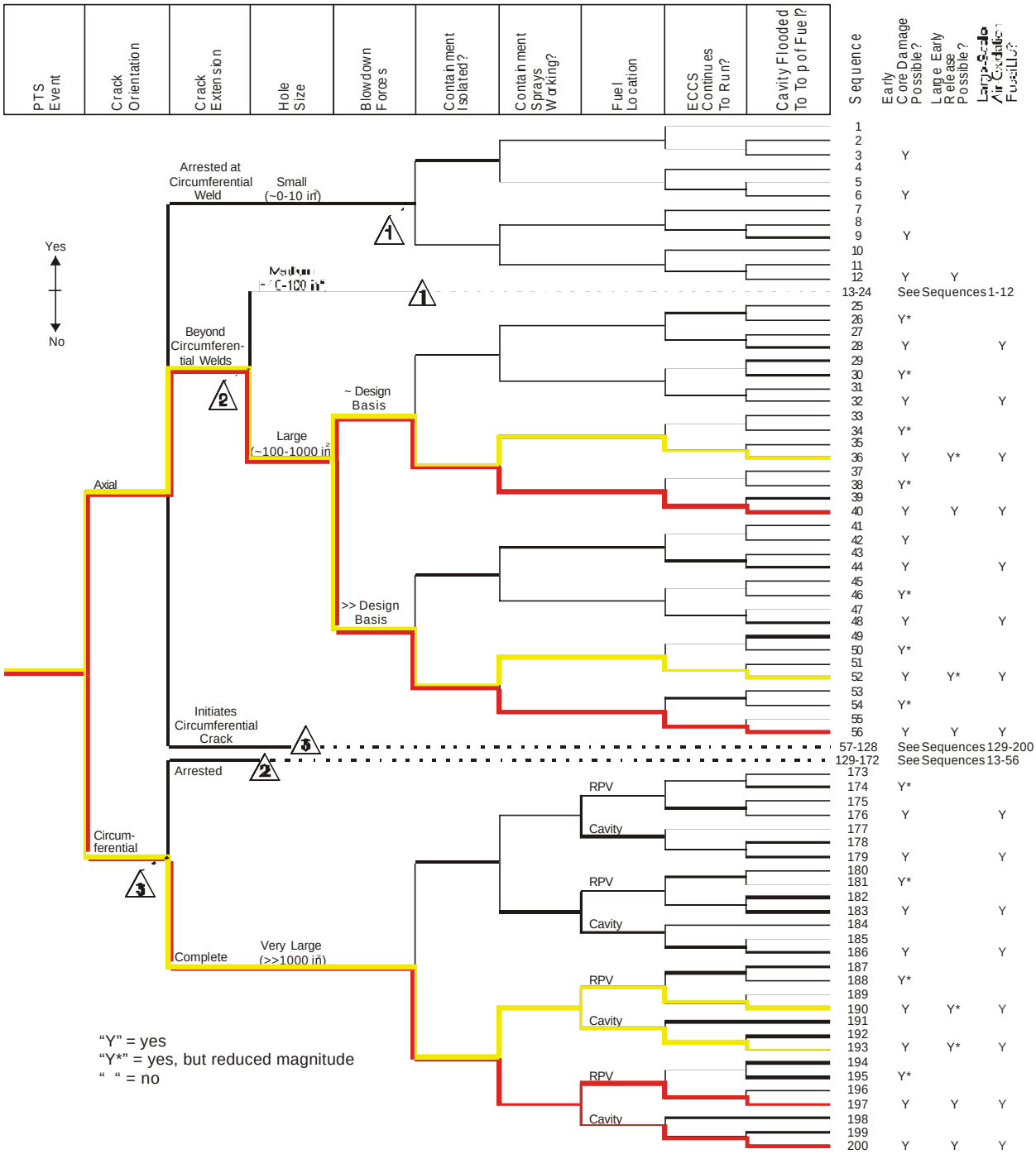

Figure 5.1. Post RPV failure accident progression tree.

cavity designs of the plants considered in this study, and the performance of limited calculations to estimate plastic strains associated with a postulated, instantaneous large (~4 m x 0.3 m, 1728 in^2) hole in the side of a representative RPV.

Regarding early overpressure, limited scope RELAP5 calculations (performed for a representative plant) indicate that the initial containment pressure rise associated with a range of PTS-induced RPV failures should be small, relative to the containment design pressure. PTS-initiated scenarios involving large amounts of hydrogen generation are possible (e.g., see Scenario 56 in the APET), but are not likely to lead to failure of either large, dry containments or ice condenser containments. The former are designed to withstand the overpressures associated with 100% clad reaction, and the principal failure mode of the hydrogen igniters for the latter is a loss of station power, which is not a concern for PTS scenarios. (Loss of power is, of course, an issue for core overheating scenarios typically addressed by PRAs, in which possible RPV failures occur after core damage.)

Figure 5.1 identifies scenarios that have the potential to lead to source terms significantly worse than those associated with risk significant, non-PTS related accident scenarios. Scenarios that are judged to have a possibility of leading to an early (i.e., less than 4 hours after RPV failure) release with a severe source term (i.e., a source term associated with large-scale air-oxidation of fuel) are highlighted in red. Scenarios that are judged to have a possibility of leading to an early release with a containment-spray scrubbed, air-oxidation source term are highlighted in yellow.

Table 5.2 provides a summary of the key characteristics associated with each of the highlighted scenarios. The common characteristics of these scenarios are also shared with risk-significant non-PTS scenarios: they require the loss of fuel cooling (either from ECCS or from water in the reactor cavity), the loss of containment isolation, and, in the case of the most severe scenarios, the loss of containment spray. Table 5.2 also provides a summary assessment of the conditional likelihood of each scenario, given the occurrence of a PTS event.

The discussion in Table 5.2 identifies two classes of plants: (a) those for which it is expected that, following a PTS-initiated RPV failure, the reactor cavity will be flooded above the top of the active fuel, and (b) all other plants. For the first class, it is believed that for all scenarios identified by the APET, the conditional probability of PTS-induced fuel damage and subsequent large early release is extremely small (i.e., much less than 0.01).

For the second class of plants, the most important APET scenarios appear to be Scenarios 96, 100, 118, and 125. These postulated scenarios all involve:

- an initial crack in an axial weld that propagates to the circumferential weld, and then initiates a circumferential crack;
- blowdown forces above those anticipated for design basis events;
- the possibility of containment penetration failures due to RPV movement; and
- the possibility of ECCS failure due to RPV movement.

Table 5.3 identifies the key differences between the four scenarios and the assessed likelihoods of the scenarios.

In Table 5.3, a likelihood rating of “extremely small” corresponds to a conditional probability much less than 0.01, a rating of “very small” corresponds to a conditional probability less than 0.01, and a rating of “small” corresponds to a conditional probability less than 0.1.

Table 5.2. Potentially Risk Significant Post-RPV Failure Accident Progression Scenarios.

Scenario[a]	Characteristics	Potential Consequential Failures[b]	Independent Failures[c]	Conditional Probability Rating[d,e]
36	**- Axial crack that extends beyond circumferential weld - Medium-to-Large (~100-1000 in^2) hole in RPV - Blowdown forces within design basis - Failed containment isolation - Operating containment spray - Loss of fuel cooling**		**- Containment Isolation - ECCS**	**Extremely small**
40	**- Axial crack that extends beyond circumferential weld - Medium-to-Large (~100-1000 in^2) hole in RPV - Blowdown forces within design basis - Failed containment isolation - Failed containment spray - Loss of fuel cooling**		**- Containment Isolation - Containment Spray - ECCS**	**Extremely small**
52	**- Axial crack that extends beyond circumferential weld - Medium-to-Large (~100-1000 in^2) hole in RPV - Blowdown forces greater than design basis - Failed containment isolation - Operating containment spray - Loss of fuel cooling**	**- Containment Penetration - ECCS piping**		**- Extremely small for plants where cavity flooding above the top of the fuel is expected - May be very small for other plants, depending on effect of blowdown forces**
56	**- Axial crack that extends beyond circumferential weld - Medium-to-Large (~100-1000 in^2) hole in RPV - Blowdown forces greater than design basis - Failed containment isolation - Failed containment spray - Loss of fuel cooling**	**- Containment Penetration - ECCS piping**	**- Containment Spray**	**Extremely small**
80	- Axial crack that initiates a circumferential crack that arrests after limited propagation - Medium-to-Large (~100-1000 in^2) hole in RPV - Blowdown forces within design basis - Failed containment isolation - Operating containment spray - Loss of fuel cooling		- Containment Isolation - ECCS	Extremely small
84	- Axial crack that initiates a circumferential crack that arrests after limited propagation - Medium-to-Large (~100-1000 in2) hole in RPV - Blowdown forces within design basis		- Containment Isolation - Containment Spray	Extremely small

	- Failed containment isolation - Failed containment spray - Loss of fuel cooling		- ECCS	
96	- Axial crack that initiates a circumferential crack that arrests after limited propagation - Medium-to-Large (~100-1000 in2) hole in RPV - Blowdown forces greater than design basis - Failed containment isolation - Operating containment spray - Loss of fuel cooling	- Containment Penetration - ECCS piping		- Extremely small for plants where cavity flooding above the top of the fuel is expected - May be small to very small for other plants, depending on effect of blowdown forces
100	- Axial crack that initiates a circumferential crack that arrests after limited propagation - Medium-to-Large (~100-1000 in2) hole in RPV - Blowdown forces greater than design basis - Failed containment isolation - Failed containment spray - Loss of fuel cooling	- Containment Penetration - ECCS piping	- Containment Spray	- Extremely small for plants where cavity flooding above the top of the fuel is expected - May be very small to extremely small for other plants, depending on effect of blowdown forces
118	- Axial crack that initiates a circumferential crack that subsequently progresses around the entire RPV - Very Large (>>1000 in2) hole - Blowdown forces greater than design basis - Failed containment isolation - Operating containment spray - Majority of fuel retained in RPV - Loss of fuel cooling	- Containment Penetration - ECCS piping		- Extremely small for plants where cavity flooding above the top of the fuel is expected - May be small to very small for other plants, depending on effect of blowdown forces
121	- Axial crack that initiates a circumferential crack that subsequently progresses around the entire RPV - Very Large (>>1000 in2) hole - Blowdown forces greater than design basis - Failed containment isolation - Operating containment spray - Majority of fuel dispersed into reactor cavity - Loss of fuel cooling	- Containment Penetration - ECCS piping		- Extremely small for plants where cavity flooding above the top of the fuel is expected - May be very small to extremely small for other plants, depending on effect of blowdown forces
125	- Axial crack that initiates a circumferential crack that subsequently progresses around the entire RPV - Very Large (>>1000 in2) hole - Blowdown forces greater than design basis - Failed containment isolation - Failed containment spray - Majority of fuel retained in RPV - Loss of fuel cooling	- Containment Penetration - ECCS piping	- Containment Spray	- Extremely small for plants where cavity flooding above the top of the fuel is expected - May be very small to extremely small for other plants, depending on effect of blowdown forces
128	- Axial crack that initiates a circumferential crack that	- Containment	- Containment	Extremely small

	subsequently progresses around the entire RPV - Very Large (>>1000 in2) hole - Blowdown forces greater than design basis - Failed containment isolation - Failed containment spray - Majority of fuel dispersed into reactor cavity - Loss of fuel cooling	Penetration - ECCS piping	Spray	
152	- Circumferential crack that arrests - Medium-to-Large (~100-1000 in2) hole in RPV - Blowdown forces within design basis - Failed containment isolation - Operating containment spray - Loss of fuel cooling		- Containment Isolation - ECCS	Extremely small
156	- Circumferential crack that arrests - Medium-to-Large (~100-1000 in2) hole in RPV - Blowdown forces within design basis - Failed containment isolation - Failed containment spray - Loss of fuel cooling		- Containment Isolation - Containment Spray - ECCS	Extremely small
168	- Circumferential crack that arrests - Medium-to-Large (~100-1000 in2) hole in RPV - Blowdown forces greater than design basis - Failed containment isolation - Operating containment spray - Loss of fuel cooling	- Containment Penetration - ECCS piping		- Extremely small for plants where cavity flooding above the top of the fuel is expected - May be very small to extremely small for other plants, depending on effect of blowdown forces
172	- Circumferential crack that arrests - Medium-to-Large (~100-1000 in2) hole in RPV - Blowdown forces greater than design basis - Failed containment isolation - Failed containment spray - Loss of fuel cooling	- Containment Penetration - ECCS piping	- Containment Spray	Extremely small
190	**- Circumferential crack that progresses around the entire RPV - Very Large (>>1000 in2) hole - Blowdown forces greater than design basis - Failed containment isolation - Operating containment spray - Majority of fuel retained in RPV - Loss of fuel cooling**	**- Containment Penetration - ECCS piping**		**- Extremely small for plants where cavity flooding above the top of the fuel is expected - May be very small to extremely small for other plants, depending on effect of blowdown forces**
193	**- Axial crack that initiates a circumferential crack that subsequently progresses around the entire**	**- Containment Penetration**		**Extremely small**

	RPV **- Very Large (>>1000 in2) hole** **- Blowdown forces greater than design basis** **- Failed containment isolation** **- Operating containment spray** **- Majority of fuel dispersed into reactor cavity** **- Loss of fuel cooling**	**- ECCS piping**		
197	**- Axial crack that initiates a circumferential crack that subsequently progresses around the entire RPV** **- Very Large (>>1000 in2) hole** **- Blowdown forces greater than design basis** **- Failed containment isolation** **- Failed containment spray** **- Majority of fuel retained in RPV** **- Loss of fuel cooling**	**- Containment Penetration** **- ECCS piping**	**- Containment Spray**	**Extremely small**
200	**- Axial crack that initiates a circumferential crack that subsequently progresses around the entire RPV** **- Very Large (>>1000 in2) hole** **- Blowdown forces greater than design basis** **- Failed containment isolation** **- Failed containment spray** **- Majority of fuel dispersed into reactor cavity** **- Loss of fuel cooling**	**- Containment Penetration** **- ECCS piping**	**- Containment Spray**	**Extremely small**

Notes:

a) **Bolded scenarios are shown explicitly in Figure 5.1.**

b) Identifies failures that might be caused by scenario phenomena (e.g., blowdown forces). This column does not include the possibility of loss of ECCS and containment sprays in recirculation mode due to containment sump clogging. The issue of sump clogging is being addressed under Generic Safety Issue 191.

c) Identifies failures believed to be independent of, or at least not enhanced by, scenario phenomena. (Rigorous estimates of system failure probabilities could lead to lower values, due to the operation of support systems during the event.)

d) Conditional probability ratings are conditioned on the occurrence of a PTS-induced RPV failure.

e) Ratings scale:

extremely small: probability is much less than 0.01
very small: probability is less than 0.01
small: probability is less than 0.1

Table 5.3. Key APET Scenarios.

Scenario	Circumferential Crack Arrested?	Containment Spray Status	Likelihood Rating
96	Yes	Operating	Very small to small
100	Yes	Failed	Extremely small to very small
118	No	Operating	Very small to small
125	No	Failed	Extremely small to very small

The ratings are based largely on the following considerations:

- Containment spray operation is not expected to be adversely affected by the occurrence of a PTS event. In fact, its reliability may be higher than for non-PTS risk-significant scenarios, since support system availability is not generally a concern for PTS scenarios.[****]
- As shown in Chapter 4, PTS scenarios generally involve situations where the reactor coolant system (RCS) is at relatively low temperature. Consequently, the stored energy in the RCS is relatively low and there is little driving force to directly cause the damage postulated in the scenarios.
- An initial assessment of the RPV deformation associated with a (conservatively assumed) instantaneous hole opening in the RPV indicates that substantial deformations will not occur, and that, therefore, the movement of the pipes connected to the RPV will be limited by the gap between the RPV and the cavity wall.

Table 5.3 is based upon currently available information. Key uncertainties whose resolution could affect the assessment involve:

- the likelihood that an axial crack will indeed initiate a propagating circumferential crack;
- the likelihood of blowdown forces that lead to damage of both ECCS piping and containment penetrations;
- the potential effect of "external events" (e.g., earthquakes) and other environmental hazards (e.g., internal fires) that were not addressed in the scoping study.

[****] This assessment is based on an assumption that any potential recirculation sump clogging issues, as identified under GSI-191, are addressed.

5.4 Acceptance Criteria Options

The staff has developed two sets of options for PTS-associated RVFF acceptance guidelines. The first set of options concerns the specific definition of RPV failure to be used. The second concerns possible quantitative acceptance limits for that metric. Note that any potential changes to the RT_{NDT} screening limits discussed in Chapter 6 may affect RVFF but are not likely to affect the conditional probability of core damage (given a PTS-induced RPV failure) or the conditional probability of large, early release (given a PTS-induced core damage event). Thus, they will likely have little effect on the level of defense-in-depth against PTS challenges already provided by the current rule.

The two options considered for defining RPV failure are as follows:

1. RPV failure occurs when a PTS-induced crack penetrates the RPV wall (i.e., RVFF = TWCF).
2. RPV failure occurs when a PTS event initiates a crack in the RPV wall (i.e., RVFF = Vessel Crack Initiation Frequency, or VCIF).

The first option uses the current definition of RPV failure. The second definition reflects the position adopted by non-U.S. regulatory bodies.

Regarding the possible quantitative acceptance limits for RVFF (denoted by RVFF*), the staff considered the following four options:

A. RVFF* = 5×10^{-6}/ry
B. RVFF* = 1×10^{-5}/ry
C. RVFF* = 1×10^{-6}/ry
D. RVFF* << 1×10^{-6}/ry

Option A is suggested by the current value in RG 1.154. Option B is suggested by current guidelines on CDF provided by RG 1.174 and the Option 3 framework for risk-informing 10 CFR Part 50. Option C is suggested by current guidelines on LERF. Option D is suggested by the possibility of significantly worse consequences for PTS events (as opposed to other risk-significant scenarios), as discussed by the ACRS' July 2002 letter [USNRC 2002].

5.5 Conclusions

The staff's analysis has led to the following conclusions regarding the establishment of a criterion for RVFF.

1) The analysis supports a definition of RVFF as being equivalent to TWCF (i.e, for PTS considerations, RPV "failure" can be defined as an occurrence of a through-wall crack.) This conclusion is based on the following two factors:

   a) TWCF is a more direct measure than VCIF of the likelihood of events with potentially significant public health consequences. This is desirable from a risk-informed decision-making perspective.
   b) The uncertainties associated with the prediction of a through-wall crack (under PTS conditions) are only slightly larger than those associated with the prediction of crack initiation (also under PTS conditions). For example, at the 10CFR50.61 RT_{PTS} screening limit the separation between the 50th and 95th percentiles in the distribution of *VCIF* ranges from 0.8 to 1.8 orders of magnitude, while the separation between the 50th and 95th percentiles in the distribution of *TWCF* ranges from 0.9 to 2.6 orders of magnitude. This slight increase in uncertainty is a natural and expected consequence of a cleavage failure mechanism and does not reflect a state of knowledge limitation regarding crack arrest (see Section 2.3.1.5 and Appendix A for details of the crack arrest model).

2) The analysis supports an acceptance criterion for *RVFF*, *RVFF**, of 1x10^{-6}/ry. This recommendation is based on the following observations:

   a) The conditional probability of an unscrubbed, large early release with a large air-oxidation source term (given a PTS-induced RPV failure) appears to be very small (i.e., much less than 0.01). It is particularly small for plants where water in the reactor cavity (following a PTS-induced RPV failure) will cover the fuel. For plants with larger cavities, the low probability of the scenario is largely due to the independence and reliability of containment sprays.
   b) The assessment underlying the above observation does not account for potential dependencies associated with PTS-events initiated by "external events" (e.g., earthquakes) or internal fires.
   c) For plants with cavities such that fuel cooling is not assured following a PTS-induced RPV failure, the APET (Figure 5.1) identifies credible scenarios where limited fuel damage might occur, even if ECCS operates as designed.

   Observation (a), taken in isolation, supports the use of an *RVFF** based on considerations of core damage consistent with those proposed in current activities for risk-informing 10 CFR Part 50 [SECY-00-0198]. However, Observation (b) identifies a potentially significant uncertainty regarding the margin between PTS-induced RPV failure and large early release, and Observation (c) raises a potential concern regarding defense-in-depth. Consequently, it is judged that an acceptance criterion based on considerations of LERF is more defensible given currently available information.

3) When assessing the acceptability of the PTS-associated risk at a given plant, the mean value of the plant's PTS-induced *RVFF* (i.e., the mean *TWCF*) should be compared with *RVFF**.

This conclusion is based on how other NRC risk-informed are using risk information (e.g., see RG 1.174).

4) Should additional work be performed to address the key post-RPV failure accident progression uncertainties identified in this study, the following issues are of principle importance:

   a) the likelihood that a PTS-induced axial crack will, upon reaching a circumferential weld, turn and progress along the circumferential weld;
   b) the likelihood of PTS-induced containment isolation failure (especially failures associated with failure of containment penetrations) and ECCS failure (especially ECCS piping failures);
   c) the impact of external events on PTS-induced LERF; and
   d) the magnitude of potential source terms and consequences associated with PTS events.

   It is anticipated that state-of-knowledge improvements in any of these areas will strengthen this study's conclusions regarding the margin between a PTS-induced RPV failure and consequent large early releases.

6 PTS Screening Limit

6.1 Introduction

As discussed in Chapter 1, the PTS screening limits specified in 10CFR50.61 were based on information available in the early 1980's regarding the likelihood and potential aftermath of PTS-induced RPV failures. Our results suggest that these screening limits can be revisited in two ways. First, it appears that, from a risk-informed perspective, there may be better metrics (other than the value of RT_{PTS} (i.e., RT_{NDT} at EOL) defined by 10CFR50.61) for characterizing RPV embrittlement. Should a different metric be used, this would naturally lead to a different PTS screening criterion. Second, it appears that a numerical value for the screening criterion might be derivable from the plant-specific results summarized in Chapter 4 and the *RVFF* criterion discussion of Chapter 5.

In this Chapter we begin (Section 6.2) with a discussion of material embrittlement metrics that can be used to "normalize" differences in chemical composition, fluence, and un-irradiated toughness properties. In Section 6.3 we discuss one possible PTS screening criterion and the technical issues that need to be addressed when establishing an actual screening criterion.

6.2 Material Embrittlement Metrics

In 10CFR50.61 an embrittlement metric called RT_{PTS} is adopted. This metric, defined by Eq. 1-2, Eq. 1-3, and Eq. 1-4, is used as the abscissa of a plot of TWCF results from Chapter 4 in Figure 6.1. This figure provides an indication of the TWCF that has heretofore been implicitly accepted at the current 10CFR50.61 screening limits of 270°F for axial welds, plates, and forgings and 300°F for circumferential welds. The data in Figure 6.1 suggest that these screening limits correspond to a TWCF of around 1×10^{-8}/ry, a value considerably below the RG 1.154 limit of 5×10^{-6}.

The RT_{PTS} embrittlement metric, defined by Eq. 1-2, Eq. 1-3, and Eq. 1-4, suggests that the embrittlement of the RPV, and by implication its TWCF, is controlled by the following factors:

1. The material (be it an axial weld, circumferential weld, plate, or forging) having the highest transition temperature.
2. The peak fluence in any particular weld, plate, or forging.

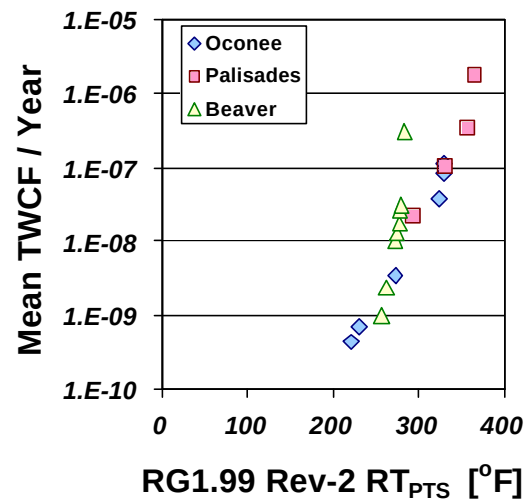

Figure 6.1. Plant-specific TWCF results combined with the Reg. Guide 1.99 Revision 2 / 10CFR50.61 embrittlement metric RT_{PTS}.

However, as shown by the results presented in Section 4.3.2.2, the dominant contributors to PTS-induced RPV failure are not necessarily those materials with the highest transition temperature, nor are the dominant contributors necessarily subjected to a uniform fluence (let alone the highest fluence for that material). The observation from Section 4.3.2.2 that axial flaws in welds are the dominant (85% to 90%, or

greater) contributors to the TWCF suggest that an improved embrittlement metric that more directly addresses factors affecting the likelihood and consequences of PTS-induced RPV failure can be defined. Such a metric should have the following characteristics:

1. It should reflect the embrittlement level of the most irradiation sensitive material in the vessel that can have weld fusion line axial flaws associated with it. Therefore, the embrittlement characteristics of axial welds and plates should be of primary importance in constructing the embrittlement metric.
2. It should reflect the maximum fluence that can occur on the fusion line of an axial weld.
3. It should reflect the total length of weld fusion line in the active core region. Thus, both the length of the active core and the number of axial welds in the active core region need to be considered.

The following embrittlement metric, which accounts for all of these considerations, is therefore proposed:

Eq. 6-1 $$RT_{NDT}{*} \equiv W_{P-F-CW} \cdot RT_{P-F-CW} + W_{P-AW} \cdot RT_{P-AW}$$

where

$W_{P\text{-}F\text{-}CW}$	is the plate / forging / circumferential weld weighting factor. It has a value of $0.033 \cdot n_{circ}$, where n_{circ} is the number of circumferential welds in the vessel.
$W_{P\text{-}AW}$	is the plate / axial weld weighting factor. It has a value of (1 - $W_{P\text{-}F\text{-}CW}$).
$RT_{P\text{-}F\text{-}CW}$	is the reference temperature for the plate / forging / circumferential weld. It is defined as follows: $$RT_{P-F-CW} \equiv MAX\left[\left(RT_{NDT(u)}^{P-F} + \Delta T_{30}^{P-F}\left(f_{\max}^{CW}\right)\right), \left(RT_{NDT(u)}^{CW} + \Delta T_{30}^{CW}\left(f_{\max}^{CW}\right)\right)\right]$$
$RT_{NDT(u)}^{P\text{-}F}$	is the unirradiated RT_{NDT} of the plate or forging on either side of the circumferential weld having the highest irradiated RT_{NDT} of all circumferential welds in the vessel.
$RT_{NDT(u)}^{CW}$	is the unirradiated RT_{NDT} of the circumferential weld.
$DT_{30}^{P\text{-}F}(f_{max}^{CW})$	is the Charpy irradiation shift values calculated using Eq. 2-5, the Cu, Ni, and P appropriate to the plate of forging, and the maximum fluence that occurs along the circumferential weld fusion line (f_{max}^{CW}).
$DT_{30}^{CW}(f_{max}^{CW})$	is the Charpy irradiation shift values calculated using Eq. 2-5, the Cu, Ni, and P appropriate to the circumferential weld, and the maximum fluence that occurs along the circumferential weld fusion line (f_{max}^{CW}).
$RT_{P\text{-}AW}$	is the reference temperature for the plate / axial weld. It is defined as follows: $$RT_{P-AW} \equiv \frac{\sum_{i=1}^{n}\left\{L_i \cdot MAX\left[\left(RT_{NDT(u)}^{P} + \Delta T_{30}^{P}\left(f_{\max}^{AW}\right)\right), \left(RT_{NDT(u)}^{AW} + \Delta T_{30}^{AW}\left(f_{\max}^{AW}\right)\right)\right]\right\}}{\sum_{i=1}^{n} L_i}$$
n	is the total number of axial weld fusion lines in the vessel,
i	denotes a particular axial weld fusion line,
L_i	is the total length of an axial weld fusion line measured from a position extending from 1-ft. above the top to 1-ft. below the bottom of the active core,
$RT_{NDT(u)}^{P}$	is the unirradiated RT_{NDT} of the plate on either side of the axial weld fusion line,
$RT_{NDT(u)}^{AW}$	is the unirradiated RT_{NDT} of the axial weld.
$DT_{30}^{P}(f_{max}^{AW})$	is the Charpy irradiation shift values calculated using Eq. 2-5, the Cu, Ni, and P appropriate to the plate, and the maximum fluence that occurs along the axial weld fusion line (f_{max}^{AW}).

$DT_{30}^{AW}(f_{max}^{AW})$ is the Charpy irradiation shift values calculated using Eq. 2-5, the Cu, Ni, and P appropriate to the axial weld, and the maximum fluence that occurs along the axial weld fusion line (f_{max}^{AW}).

While the explanation of Eq. 6-1 is somewhat lengthy, RT_{NDT}* is simply a weighted average that accounts for the combined effects of material composition, unirradiated fracture toughness transition temperature, flaw density, flaw location, flaw orientation, and irradiation damage in the region of the vessel where PTS challenging flaws reside. The weighting factors employed make RT_{NDT}* depend mostly (90% or more) on the embrittlement characteristics of materials associated with axial flaws. However, there is a minor contribution (10% or less) from the embrittlement characteristics of materials associated with circumferential flaws.

RT_{NDT}* can be determined based on only the following routinely available information:

1. The best-estimate chemical compositions (Cu, Ni, and P) of the various welds, plates, and forgings that make up the beltline region of the RPV. All of this information has already been docketed by the licensees, and is available in the RVID database [RVID].
2. A fluence map that details the axial and azimuthal variation of fast neutron fluence on the inner diameter of the RPV.
3. The dimensions of the various welds, plates, and forgings that make up the beltline region of the RPV. This information is available in plant construction records.

The information in Items 1 and 2 are already needed to determine RT_{PTS}; the only additionally information needed to determine RT_{NDT}* is that in Item 3.

Unlike RT_{PTS}, RT_{NDT}* does not include a materials margin term (Eq. 1-4 expresses the materials margin term for RT_{PTS}). A materials margin term is inappropriate for RT_{NDT}* because uncertainty in all input variables and models has already been considered in calculation of the TWCF values reported in Chapter 4.

6.3 Possible Screening Limit

In Figure 6.2 we combine the mean TWCF values from Chapter 4 with RT_{NDT}* values estimated using Eq. 6-1. While further examination is warranted, the close agreement of TWCF data from three different operating plants suggests that the combined effects of material composition, fluence, and flaw distribution accounted for by RT_{NDT}* appear to exert a stronger influence on the TWCF than the total effect of the many operational and design differences not accounted for by this embrittlement metric. A relationship curve fit to these data using the method of least squares, i.e.:

Eq. 6-2 $$TWCF = 8\times10^{-32} \cdot RT_{NDT}^{*\ 10.18}$$

suggests a PTS screening limit on RT_{NDT}* of (about) 290°F at the 1x10^{-6} events / reactor year criterion suggested in Chapter 5. Since this RT_{NDT}* value is a mean value (i.e., it contains no margin term) that is weighted to account for the different embrittlement levels that can exist throughout the vessel, the suggested RT_{NDT}* screening limit is considerably higher than the 10CFR50.61 screening limits on RT_{PTS}. As illustrated in Figure 6.3, RT_{NDT}* is, on average, about 90°F below RT_{PTS}, making the possible PTS screening limit of 290°F on RT_{NDT}* equivalent to a RT_{PTS} value of (about) 380°F. Thus, a PTS screening limit of 290°F on RT_{NDT}* is between 80°F and 110°F higher than the current 10CFR50.61 PTS screening limits on RT_{PTS} of , respectively, 300°F and 270°F.

While the results in Figure 6.2 and Figure 6.3 suggest that embrittlement to levels beyond those allowed by the current 10CFR50.61 screening criteria can be permitted while still maintaining the RVFF at an acceptably low value, some additional work is warranted to support a definitive a RT_{NDT}*-based screening criterion. Specifically, we need to establish the

extent to which the relationship shown in Figure 6.2 applies to other than the three pilot plants considered in this study. Additionally, adoption of an RT_{NDT}* screening limit of 290°F, which corresponds to a RT_{PTS} value of approximately 380°F, may make it difficult or impossible to start a plant in compliance with current 10CFR50 Appendix G rules due to conservatisms in the 10CFR50 Appendix G procedures (assumption of a ¼-T flaw, for example). This outcome, that limits associated with an accident (PTS) may be less restrictive than the limits associated with normal operation (plant startup and shutdown), suggests that the basis for the 10CFR50 Appendix G rules may need to be revisited.

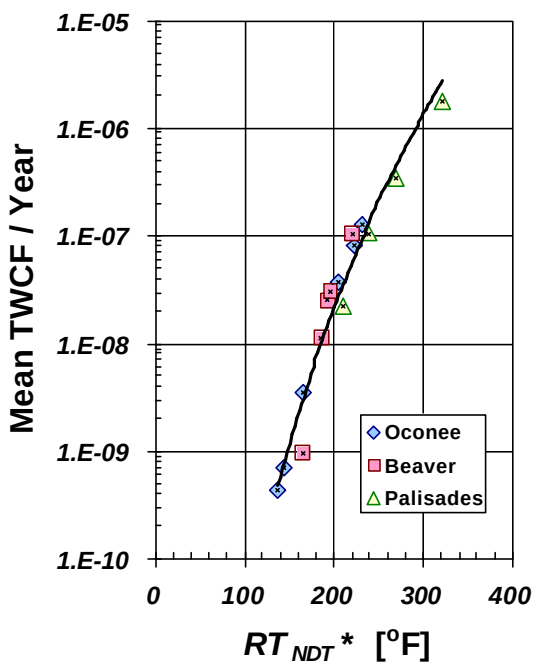

Figure 6.2. Variation of the mean through wall cracking frequency with RT_{NDT}* (see Eq. 6-1) for the three plants analyzed in this study.

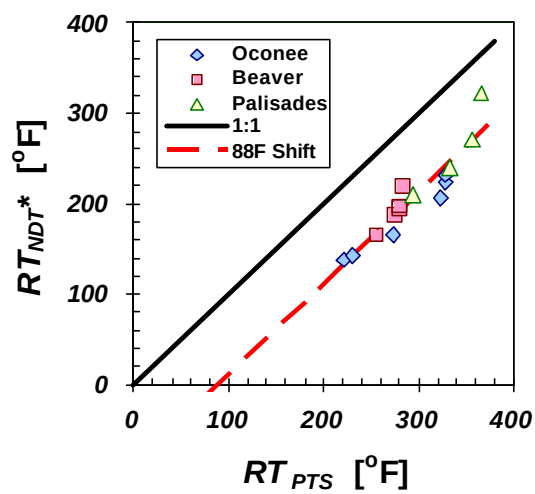

Figure 6.3. A comparison of the 10CFR50.61 embrittlement metric (RT_{PTS}) and the embrittlement metric suggested by this study (RT_{NDT}*) for the three plants analyzed in this study illustrating that RT_{NDT}* is about 90°F lower than RT_{PTS}.

7 Findings and Considerations for Rulemaking

The investigation reported herein represents a comprehensive re-evaluation of the technical basis of the pressurized thermal shock (PTS) rule and its associated screening criteria. Our approach considers the factors that influence the risk of vessel failure during a PTS event while accounting for uncertainties as an integrated part of a quantitative probabilistic risk analysis. Two central features of our approach are a focus on the use of realistic input values and models (wherever possible), and an *explicit* treatment of uncertainties (to the greatest extent practicable). Thus, our approach differs markedly from that employed in the development 10CFR50.61 wherein intentional and un-quantified conservatisms were included in the many aspects of the analysis, and where uncertainties were treated *implicitly* by incorporating them into the models.

In this Chapter we summarize results of our analysis of the likelihood of PTS-induced RPV failure at three plants (Oconee 1, Beaver Valley, and Palisades) and of our reassessment of the reactor vessel failure frequency acceptance criterion.

7.1 Findings

1. Even at the end of a hypothesized license extension to 60 operating years we estimate that the frequency of through wall cracking posed by PTS challenges is extremely, i.e. between $1x10^{-9}$/yr and $5x10^{-8}$/yr at the mean and 95th percentile[††††] in the three plants modeled. If, for illustrative purposes, the embrittlement in these plants is artificially advanced to equal the 10CFR50.61 RT_{PTS} screening limit the estimated mean TWCF is about $1x10^{-8}$. Thus, by any measure, the likelihood of PTS induced RPV failure is low, and falls considerably below the RG 1.154 risk limit of $5x10^{-6}$.
2. The calculated distributions of TWCF are quite skewed toward zero, or very low, through wall cracking probabilities. Also they are very broad, spanning three or more orders of magnitude from minimum to maximum.
3. By far the greatest contribution to PTS risk arises from LOCAs.
4. The once-through steam generator design used in B&W plants make stuck-open valves in the primary system a dominant PTS event for these plants.
5. Transients initiated by secondary side events in general, and main steam line breaks in particular, do not contribute significantly to the PTS risk.
6. Axially oriented flaws account for the great majority (≈85-90%, or more) of the estimated through wall cracking frequency.
7. Flaws in plates account for very little (< ≈1%) of the TWCF owing to the much smaller size of plate flaws than weld flaws.
8. The TWCF arising from transients initiated by external events (e.g., earthquakes, fires, floods) are expected to be much smaller than that arising from the initiators addressed in this study. It is therefore our view that the contribution of external events to the overall TWCF due to PTS is well within the uncertainty associated with this analysis.
9. One potentially appealing metric of RPV embrittlement, termed RT_{NDT}*, is introduced. This metric is designed to reflect the principal contributors to PTS-induced RPV failure. A PTS screening limit of about 290°F on a mean value of RT_{NDT}* will maintain the yearly risk of

[††††] Highly skewed TWCF distributions lead to mean and 95th percentile values that are very close.

developing a through wall crack as a consequence of PTS challenges at or below $1x10^{-6}$ events per reactor operating year, a limit that is consistent with agency policy. This RT_{NDT}* screening limit represents, a considerable (80°F to 110°) increase relative to the current 10CFR50.61 screening limits on RT_{PTS}.

7.2 Considerations for Rulemaking

As indicated in Section 7.1, the risk of vessel failure associated with PTS events appears to be extremely small. There appears to be considerable safety margin associated with the screening criteria embodied in the current PTS rule. These margins would appear to justify consideration of rulemaking.

Should rulemaking proceed, it appears feasible to use improved (i.e., more risk-informed) metrics for representing RPV embrittlement. One potentially appealing metric, termed RT_{NDT}*, is discussed in Chapter 6. This metric is designed to reflect the principal contributors to PTS-induced RPV failure. A numeric value for a RT_{NDT}*-based screening criteria can be established based on considerations of risk that are current with NRC guidance in other, non-PTS, related risk-informed regulatory activities.

8 References

10CFR50.61	Code of Federal Regulation 10CFR50.61, "Fracture Toughness Requirements for Protection Against Pressurized Thermal Shock Events," promulgated 06/26/84.
10CFR50 App. G	Code of Federal Regulation 10CFR50 Appendix G, "Fracture Toughness Requirements {for Normal Operation}."
10CFR50 App. H.	Code of Federal Regulation 10CFR50 Appendix H, "Reactor Vessel Material Surveillance Program Requirements"
ASME NB2331	ASME NB-2331, 1998 ASME Boiler and Pressure Vessel Code, Rules for Construction of Nuclear Power Plants, Division 1, Subsection NB, Class 1 Components
ASTM E23	ASTM E23, "Standard test Methods for Notched Bar Impact Testing of Metallic Materials," ASTM, 1998.
ASTM E185	ASTM E185-94, "Standard Practice for Conducting Surveillance Tests for Light-Water Cooled Nuclear Power Reactor Vessels," ASTM, 1998.
ASTM E208	ASTM E208, "Standard Test Method for Conducting Drop-Weight Test to Determine Nil-Ductility Transition Temperature of Ferritic Steels," ASTM 1998.
ASTM E399	ASTM E399, "Test Method for Plane-Strain Fracture Toughness Testing of Metallic Materials," ASTM, 1998.
ATHENA	U.S. Nuclear Regulatory Commission, Technical Basis and Implementation Guidelines for A Technique for Human Event Analysis (ATHEANA). NUREG-1624, Rev. 1, Washington, DC, May 2000.
Bamford 00	Bamford, W., and Rishel, R.D., "A Review of Cracking Associated with Weld Deposited Cladding in Operating PWR Plants, Westinghouse Electric Company LLC, Nuclear Services Division, WCAP-15338, March 2000.
Beaton 02a	Beaton, R. and Arcieri, W., RELAP5 Model Development for Oconee PTS Applications, (in preparation).
Beaton 02b	Beaton, R. and Fletcher, C.D., RELAP5 Input Model Development for Beaver Valley PTS Application, (in preparation).
Brothers 63	Brothers, A.J. and Yukawa, S., "The Effect of Warm Prestressing on Notch Fracture Strength," *Journal of Basic Engineering*, March 1963, p. 97.
Bryan 75	Bryan, R. H. et al., Test of 6-inch-Thick Pressure Vessels. Series 2: Intermediate Test Vessels V-3, V-4, and V-6, Report ORNL-5059, Oak Ridge National Laboratory, November 1975.
Bryan 78a	Bryan, R. H. et al., Test of 6-Inch-Thick Pressure Vessels. Series 3: Intermediate Test Vessel V-7B, Report NUREG/CR-0309 (ORNL/NUREG-38), Oak Ridge National Laboratory, October 1978.

Bryan 78b	Bryan, R. H. et al., Test of 6-Inch-Thick Pressure Vessels. Series 3: Intermediate Test Vessel V-7A Under Sustained Loading, ORNL/NUREG-9, Oak Ridge National Laboratory, February 1978.
Bryan 79	Bryan, R. H. et al., Test of 6-Inch-Thick Pressure Vessels, Series 3: Intermediate Test Vessel V-8, Report NUREG/CR-0675 (ORNL/NUREG-58), Oak Ridge National Laboratory, December 1979.
Bryan 85	Bryan, R. H. et al., Pressurized Thermal Shock Test of 6-in.-Thick Pressure Vessels. PTSE-1: Investigation of Warm-Prestressing and Upper-Shelf Arrest, Report NUREG/CR-4106 (ORNL-6135), Oak Ridge National Laboratory, April 1985.
Bryan 87a	Bryan, R. H. et al., Pressurized Thermal Shock Test of 6-in.-Thick Pressure Vessels. PTSE-2: Investigation of Low-Tearing Resistance and Warm-Prestressing, Report NUREG/CR-4888 (ORNL-6377), Oak Ridge National Laboratory, April 1987.
Bryan 87b	Bryan, R. H. et al., Test of 6-Inch-Thick Pressure Vessels. Series 3: Intermediate Test Vessel V-8A Tearing Behavior of Low Upper-Shelf Material, Report NUREG/CR-4760 (ORNL-6187), Oak Ridge National Laboratory, May 1987.
Cheverton 76	Cheverton, R. D., Pressure Vessel Fracture Studies Pertaining to a PWR LOCA-ECC Thermal Shock: Experiments TSE-1 and TSE-2, Report ORNL/NUREG/TM-31, Oak Ridge National Laboratory, September 1976.
Cheverton 77	Cheverton, R. D. and Bolt, S. E., Pressure Vessel Fracture Studies Pertaining to a PWR LOCA-ECC Thermal Shock: Experiments TSE-3 and TSE-4 and Update of TSE-1 and TSE-2 Analysis, Report ORNL/NUREG-22, Oak Ridge National Laboratory, December 1977.
Cheverton 84	Cheverton, R. D., Ball, D. G., A Deterministic and Probabilistic Fracture Mechanics Code for Applications to Pressure Vessels, Report NUREG/CR-3618 (ORNL-5991), Oak Ridge National Laboratory, May 1984.
Cheverton 85a	Cheverton, R. D. et al., Pressure Vessel Fracture Studies Pertaining to the PWR Thermal-Shock Issue: Experiments TSE-5, TSE-5A, and TSE-6, NUREG/CR-4249 (ORNL-6163), Oak Ridge National Laboratory, June 1985.
Cheverton 85b	Cheverton, R. D. et al., Pressure Vessel Fracture Studies Pertaining to the PWR Thermal-Shock Issue: Experiment TSE-7, Report NUREG/CR-4303 (ORNL-6177), Oak Ridge National Laboratory, August 1985.
Cheverton 86	Cheverton, R. D., Iskander, S. K., and Ball, D. G., "Review of Pressurized-Water-Reactor-Related Thermal Shock Studies," pp.752-766 in Fracture Mechanics: Nineteenth Symposium, ASTM 969, Ed. Thomas A. Cruse, July 1986.
Derby 74	Derby, R. W. et al., Test of 6-Inch-Thick Pressure Vessels. Series 1: Intermediate Test Vessels V-1 and V-2, Report ORNL-4895, Oak Ridge National Laboratory, February 1974.
Dixon 02a	Dixon, T.L., and Simonen, F.A., "The Impact of an Improved Flaw Model on a Pressurized Thermal Shock Evaluation," Proceedings of the 2002 ASME Pressure Vessel and Piping Conference, August 2002, Vancouver, Canada.
Dickson 02b	Dickson, T. L. et al., "Status of the United States Nuclear Regulatory Commission Pressurized Thermal Shock Rule Re-Evaluation Project,"

Proceeding of ICONE10, Paper ICONE10-22656, International Conference on Nuclear Engineering, Arlington, Virginia, April 14-18, 2002.

DORT — "DORT, Two-Dimensional Discrete Ordinates Transport Code," RSIC Computer Code Collection, CCC-484, Oak Ridge National Laboratory, 1988.

FAVOR 02 — Williams, P.T., and Dickson, T.L., "Fracture Analysis of Vessels, Oak Ridge: FAVOR V02.4 Computer Code, Theory and Implementation of Algorithms, Methods, and Correlations, NUREG/CR-xxxx (in Review), December 2002.

Fletcher 84 — Fletcher, C. Don, et al., RELAP5 Thermal Hydraulic Analysis of Pressurized Thermal Shock Sequence for the Oconee-1 Pressurized Water Reactor, NUREG/CR-3761, June, 1984.

Fletcher 02a — Fletcher, C.D. et al., Palisades RELAP5 Model Revisions for Pressurized Thermal Shock Calculations, Revision 1, June 3, 2002 (in preparation).

Fletcher 02b — Fletcher, C.D and Palazov, V., Palisades RELAP5 PTS Calculation Transient Results, Revision 1 (in preparation)

Fletcher 02c — Fletcher, C.D. and Arcieri, W.C., Palisades RELAP5 PTS Calculations for Rerun and Additional Cases, Revision 2 (in preparation)

Habib 91 — Habib, T.F, et al., Multiloop Integral System Test (MIST): MIST Facility Functional Specification, NUREG/ CR-5670, April, 1991

Hanson 94 — A.L. Hanson, R.E. Davis, and V. Mubayi, "Calculations in Support of a Potential Definition of Large Release," NUREG/CR-6094, BNL-NUREG-52387, May 1994.

Iskander 81 — Iskander, S. K., Cheverton, R. D. and Ball, D. G., OCA-I, A Code for Ingersoll 95 (Flu2) D. T. Ingersoll, J. E. White, R. Q. Wright, H. T. Hunter, C. O. Slater, N. M. Greene, R. E. MacFarlane, R. W. Roussin, "Production and Testing of the VITAMIN-B6 Fine-Group and the BUGLE-93 Broad-Group Neutron/Photon Cross-section Libraries Derived from ENDF/B-VI Nuclear Data," ORNL-6795, NUREG/CR-6214, January 1995.

INEEL 99 — Idaho National Engineering and Environmental Laboratory, Rates of Initiating Events at U.S. Nuclear Power Plants: 1987 – 1995, NUREG/CR-5750, INEEL/EXT-98-00401, February 1999.

INEEL 00a — INEEL staff review of LERs for the Oconee PTS analysis conducted during March-April, 2000 based on keywords "overcooling," "thermal shock," and "excessive cooling." This includes a draft letter report, "Human Performance Insights for Overcooling Events in Support of PTS," D. Gertman and M. Parrish, INEEL, March 7, 2000.

INEEL 00b — Idaho National Engineering and Environmental Laboratory, Rates of Initiating Events at U.S. Nuclear Power Plants: 1987 – 1998, Draft, NUREG/CR-5750, INEEL/EXT-2000-00153, March 2000.

Jackson 00 — Jackson, D.A., Abramson, L., "Report on the Preliminary Results of the Expert Judgment Process for the Development of a Methodology for a Generalized Flaw Size and Density Distribution for Domestic Reactor Pressure Vessels", USNRC MEB-00-01, September 2000

Kirk 01a — Kirk, M.T., Natishan, M.A.E., M. Wagenhofer, "Microstructural Limits of Applicability of the Master Curve," *32nd Volume, ASTM STP-1406,* R. Chona, Ed., American Society for Testing and Materials, Philadelphia, PA 2001.

Kirk 01b	Kirk, M., and Natishan, M.E., "Shift in Toughness Transition Temperature Due to Irradiation: DT_o *vs.* DT_{41J}, A Comparison and Rationalization of Differences," Proceedings of the IAEA Specialists Meeting on Master Curve Technology, Prague, Chech Republic, September 2001
Kirk 02a	Kirk, M. T., Natishan, M. E., and Wagenhofer, M., "A Physics-Based Model for the Crack Arrest Toughness of Ferritic Steels," Fatigue and Fracture Mechanics, 33rd Volume, ASTM STP-1417, W. G. Reuter, and R. S. Piascik, Eds., American Society for Testing and Materials, West Conshohocken, PA, 2002.
Kuo 99	Kuo, Han-Hsiung, Assessment of the RELAP5-3D Code Using the Upper Plenum Test Facility Downcomer Countercurrent Flow Test No. 6, Run 131, Presented at the RELAP5 International Users Seminar, July 28-30, 1999
Marshall 82	Marshall Committee, 1982, An Assessment of the Integrity of PWR Vessels, Second Report by a Study Group under the Chairmanship of D. W. Marshall, published by the U.K. Atomic Energy Commission.
Merkle 75	Merkle, J. G., An Evaluation of the HSST Program Intermediate Pressure Vessel Tests in Terms of Light-Water-Reactor Pressure Vessel Safety, Report ORNL-TM-5090, Oak Ridge National Laboratory, November 1975.
Merkle 76	Merkle, J. G. et al., Test of 6-Inch-Thick Pressure Vessels. Series 3: Intermediate Test Vessel V-7, Report ORNL/NUREG-1, Oak Ridge National Laboratory, August 1976.
Merkle 77	Merkle, J. G. et al., Test of 6-Inch-Thick Pressure Vessels. Series 4: Intermediate Test Vessels V-5 and V-6, with Inside Nozzle Corner Cracks, Report ORNL/NUREG-7, Oak Ridge National Laboratory, August 1977.
MESH	"MESH - A Code for Determining the DORT Fixed Neutron Source," BNL-Memorandum, M. D. Zentner to J. F. Carew, August 25, 1981
Natishan 02	"Evaluation and Characterization of Uncertainty in Fracture Toughness Models for Ferritic Reactor Pressure Vessel Steels," WRC Bulliten, in preparation.
NRC 86	U.S. Nuclear Regulatory Commission, "Safety Goals for the Operation of Nuclear Power Plants; Policy Statement; Correction and Republication," Federal Register, Vol. 51, p. 30028 (51 FR 30028), August 21, 1986.
NRC FR 95	"Use of Probabilistic Risk Assessment Methods in Nuclear Activities: Final Policy Statement," Federal Register, Vol. 60, p. 42622 (60 FR 42622), August 16, 1995
NRC MEMO 82	Memorandum dated August 30 1982 from M. Vagans to S. Hanauer (DST/NRR).
NRC MTEB 5.2	METB 5-2, Branch Technical Position, Fracture Toughness Requirements, Rev. 1 – July 1981.
NRC LTR 02	Memorandum from Thadani to Collins on "Transmittal of Technical work to Support Possible Rulemaking on a Risk-Informed Alternative to 10 CFR 50.46/GDC 35," dated July 31, 2002 (Accession number ML022120660).
NUREG 1624 R1	
ORNL 84	Calculating the Behavior of Flaws on the Inner Surface of a Pressure Vessel, Report ORNL/NUREG-84, Oak Ridge National Laboratory, August 1981.
ORNL 85a	Oak Ridge National Laboratory, Pressurized Thermal Shock Evaluation of the Calvert Cliffs Unit 1 Nuclear Power Plant, NUREG/CR-4022,

ORNL/TM-9408, for the U.S. Nuclear Regulatory Commission, September 1985.

ORNL 85b — Oak Ridge National Laboratory, Pressurized Thermal Shock Evaluation of the H.B. Robinson Unit 2 Nuclear Power Plant, NUREG/CR-4183, ORNL/TM-9567, for the U.S. Nuclear Regulatory Commission, September 1985.

ORNL 86 — Oak Ridge National Laboratory, Preliminary Development of an Integrated Approach to the Evaluation of Pressurized Thermal Shock as Applied to the Oconee Unit 1 Nuclear Power Plant, NUREG/CR-3770, ORNL/TM-9176, for the U.S. Nuclear Regulatory Commission, May 1986.

PAL PRA

Randall 87 — Randall, P.N., "Basis for Revision 2 of the U.S. Nuclear Regulatory Commission's Regulatory Guide 1.99," Radiation Embrittlement in Nuclear Pressure Vessel Steels: An International Review (Second Volume), ASTM STP-909, L.E. Steele, Ed., 1987.

RELAP — RELAP5/MOD3.3 Code Manual – Vol III: Developmental Assessment Problems, December 2001

RELAP — RELAP5/MOD3 Code Manual, Volume IV: Models and Correlations, June 1999.

RVID — Nuclear Regulatory Commission Reactor Vessel Integrity Database, Version 2.1.1, July 6, 2000.

Pratt 1999 — W.T. Pratt, et al., "An Approach for Estimating the Frequencies of Various Containment Failure Modes and Bypass Events," NUREG/CR-6595, BNL-NUREG-52539, January 1999.

RG 1.154 — U.S. Nuclear Regulatory Commission, "Format and Content of Plant-Specific Pressurized Thermal Shock Safety Analysis Reports for Pressurized Water Reactors," Regulatory Guide 1.154, 1987.

RG 1.174 — U.S. Nuclear Regulatory Commission, "An Approach for Using Probabilistic Risk Assessment in Risk-Informed Decisions on Plant-Specific Changes to the Licensing Basis," Regulatory Guide 1.174, July 1998.

RG 1.190 — Office of Nuclear Regulatory Research, "Calculational and Dosimetry Methods for Determining Pressure Vessel Neutron Fluence," Regulatory Guide 1.190, U.S. Nuclear Regulatory Commission, March 2001.

SECY-82-465 — U.S. Nuclear Regulatory Commission, "Pressurized Thermal Shock," SECY-82-465, November 23, 1982.

SECY-93-138 — U.S. Nuclear Regulatory Commission, "Recommendation on Large Release Definition," SECY-93-138, May 19, 1993.

SECY-00-0198 — U.S. Nuclear Regulatory Commission, "Status Report On Study Of Risk-Informed Changes To The Technical Requirements Of 10 Cfr Part 50 (Option 3) And Recommendations On Risk-Informed Changes To 10 Cfr 50.44 (Combustible Gas Control)," SECY-00-0198, September 14, 2000.

SECY-02-0092 — U.S. Nuclear Regulatory Commission, "Status Report: Risk Metrics and Criteria for Pressurized Thermal Shock," SECY-02-0092, May 30, 2002.

SAPHIRE

Simonen 1986 — F.A. Simonen, et al., "Reactor Pressure Vessel Failure Probability Following Through-Wall Cracks Due to Pressurized Thermal Shock Events," NUREG/CR-4483, PNL-5727, April 1986.

Simonen 02 — F.A. Simonen, S.R. Doctor, G.J. Schuster, and P.G. Heasler, "A Generalized Procedure for Generating Flaw Related Inputs for the FAVOR Code," NUREG/CR-????, ???? 2002.

Siu 99 — "Uncertainty Analysis and Pressurized Thermal Shock, An Opinion," United States Nuclear Regulatory Commission, 1999.

Siu 01 — Siu, N., Malik, S., Bessette, D., Woods, R., Mosleh, A. and Modarres, M. "Treating Aleatory and Epistemic Uncertainties in Analyses of Pressurized Thermal Shock," Proceedings of PSAM 5, International Conference on Probabilistic Safety Assessment and Management, Osaka, Japan, November 27-December 1, 2000, pp. 377-382.

Theofanous 2001 — T.G. Theofanous, et al, "Consequences of Postulated PTS-Induced Brittle Failure of a Pressurized Water Reactor Vessel," CRSS-SA-01/4, Center for Risk Studies and Safety, University of California, Santa Barbara, April 5, 2001.

Wallin 93a — Wallin, K., "Irradiation Damage Effects on the Fracture Toughness Transition Curve Shape for Reactor Vessel Steels," Int. J. Pres. Ves. & Piping, 55, pp. 61-79, 1993

WRC 175 — PVRC Ad Hoc Group on Toughness Requirements, "PVRC Recommendations on Toughness Requirements for Ferritic Materials." Welding Research Council Bulletin No. 175, August 1972.

Westinghouse 99 — Westinghouse Electric Company LLC, Nuclear Services Division, WOG Pilot-Plant Application of the EPRI Alternative Method for Reactor Vessel PTS, WCAP-15156, June 1999.

Whitman 86 — Whitman, G. D., Historical Summary of the Heavy-Section Steel Technology Program and Some Related Activities in Light-Water Reactor Pressure Vessel Safety Research, Report NUREG/CR-4489 (ORNL-6259), Oak Ridge National Laboratory, March 1986.

Woods 01 — Woods, R., Siu, N., Kolaczkowski, A., and Galyean, W., "Selection of Pressurized Thermal Shock Transients to Include in PTS Risk Analysis," *IJPVP*, 78 (2001) 179-183.

Appendix A – Toughness and Embrittlement Model

INSERT *APPENDIX A.DOC* HERE

Appendix B – Warm Pre-Stress Model

INSERT *APPENDIX B.DOC* HERE

Appendix C – Transient List and Initiating Event Frequency Values

Oconee

Case	Type	Primary Side Failure	Secondary Side Failure	Operator Action	Initiating Event Frequency		
					Mean	Min.	Max.
1	LOCA	2.54 cm (1 inch) surge line break	None	None	Not in base case		
2	LOCA	3.59 cm (1.414 in) surge line break	None	None	Not in base case		
3	LOCA	5.08 cm (2 in) surge line break	None	None	Not in base case		
4	LOCA	7.183 cm (2.828 in) surge line break	None	None	Not in base case		
5	LOCA	10.16 cm (4 inch) surge line break	None	None	Not in base case		
6	LOCA	3.59 cm (1.414 in) cold leg break	None	None	Not in base case		
7	LOCA	5.08 cm (2 inch) cold leg break	None	None	Not in base case		
8	LOCA	2.54 cm (1 inch) surge line break	1 stuck open safety valve in SG-A	None	9.7E-08	2.7E-13	4.2E-06
9	LOCA	2.54 cm (1 inch) surge line break	2 stuck open safety valves in SG-A	None	Not in base case		
10	LOCA	3.59 cm (1.414 inches) surge line break	2 stuck open safety valves in SG-A	None	Not in base case		

11	LOCA	2.54 cm (1 inch) surge line break	1 stuck open safety valve in SG-A	HPI terminated when subcooling margin exceeds 55.6 K (100° F)	Not in base case		
12	LOCA	2.54 cm (1 inch) surge line break	1 stuck open safety valve in SG-A	HPI throttled to maintain 27.8 K (50° F) subcooling margin	9.2E-07	2.8E-12	3.1E-05
13	LOCA	2.54 cm (1 inch) surge line break	2 stuck open safety valves in SG-A	HPI terminated when subcooling margin exceeds 55.6 K (100° F)	Not in base case		
14	LOCA	3.59 cm (1.414 in) surge line break	None	Operator is assumed to trip the reactor coolant pumps at 2.778 K (5° F) subcooling.	Not in base case		
15	LOCA	2.54 cm (1 in) surge line break with HPI Failure	None	At 15 minutes after transient initiation, operator opens all TBVs to lower primary system pressure and allow CFT and LPI injection.	3.4E-08	6.3E-15	7.2E-07
16	LOCA - HZP	2.54 cm (1 in) surge line break	None	None	Not in base case		
17	LOCA - HZP	2.54 cm (1 in) surge line break	1 stuck open safety valve in SG-A	None	Not in base case		

18	TT/RT	None	SG level control system failure causes SG overfill.	Operator is assumed to shut off the emergency feedwater system when the level reaches 96% operating range.	Not in base case		
19	TT/RT	None	SG level control system failure causes SG overfill. EFW continues running and the SGs flood and remain flooded.	Operator throttles EFW, maintaining flooded SGs without flooding the steam lines.	Not in base case		
20	TT/RT	None	One stuck open TBV in SG-A	Operator throttles HPI to maintain a level of 5.59 m (220 in) in the pressurizer	Not in base case		
21	TT/RT	None	None	None	Not in base case		
22	TT/RT	Stuck open PORV	TBVs kept closed to force PORV to open.	None	Not in base case		
23	TT/RT	None	SG level control system failure causes SG overfill. EFW continues running and the SGs flood and remain flooded.	Operator trips MFW and turbine driven EFW. Motor driven EFW remains running.	Not in base case		

24	TT/RT	None	SG level control system failure causes SG overfill. MFW continues running and the SGs flood.	Operator trips MFW when water enters the steam lines.	Not in base case		
25	MSLB	None	MSLB with trip of turbine driven emergency feedwater by the MSLB circuitry.	None	Not in base case		
26	MSLB	None	MSLB without trip of turbine driven emergency feedwater	None	Not in base case		
27	MSLB	None	MSLB without trip of turbine driven emergency feedwater.	Operator throttles HPI to maintain 27.8 K (50° F) subcooling margin.	2.1E-06	2.5E-08	9.2E-05
28	TT/RT	None	1 stuck open safety valve in SG-A	None	7.5E-08	1.6E-14	6.4E-06
29	TT/RT	None	1 stuck open safety valve in SG-A and a second stuck open safety valve in SG-B	None	3.1E-07	1.1E-10	4.2E-05
30	TT/RT - HZP	None	1 stuck open safety valve in SG-A	None	1.5E-07	1.9E-13	4.4E-05
31	TT/RT - HZP	None	1 stuck open safety valve in SG-A and a second stuck open safety valve in SG-B	None	8.4E-09	0.0E+00	1.1E-06

32	TT/RT	None	SG level control system failure causes SG overfill. MFW continues running and the SGs flood.	Operator trips MFW when water enters the steam lines. Operator also throttles HPI (throttling criteria is 27.8 K (50°F) subcooling and 300 cm (120") pressurizer level)	Not in base case		
33	TT/RT	None	One stuck open TBV in SG-A. Valve recloses in 10 minutes.	Operator throttles HPI to maintain a level of 559 cm (220 in) in the pressurizer	Not in base case		
34	TT/RT	Stuck open pressurizer safety valve	None	None	Not in base case		
35	TT/RT	None	1 stuck open safety valve in SG-A	Operator throttles HPI to maintain 27.8 K (50° F) subcooling and 304.8 cm (120 in) pressurizer level.	Not in base case		
36	TT/RT	None	1 stuck open safety valve in SG-A and a second stuck open safety valve in SG-B	Operator throttles HPI to maintain 27.8 K (50° F) subcooling and 304.8 cm (120 in) pressurizer level.	1.4E-05	1.5E-07	3.8E-04
37	TT/RT - HZP	None	1 stuck open safety valve in SG-A	Operator throttles HPI to maintain 27.8 K (50° F)) subcooling and 304.8 cm (120 in) pressurizer level.	1.4E-06	4.2E-13	8.6E-05

38	TT/RT-HZP	None	1 stuck open safety valve in SG-A and a second stuck open safety valve in SG-B	Operator throttles HPI to maintain 27.8 K (50° F) subcooling and 304.8 cm (120 in) pressurizer level.	2.6E-06	1.4E-08	7.7E-05
39	SGTR	None	SGTR with a stuck open SRV in SG-A. A reactor trip is assumed to occur at the time of the tube rupture.	None.	Not in base case		
40	SGTR	SGTR with PORV stuck open.	A reactor trip is assumed to occur at the time of the tube rupture.		Not in base case		
41	TT/RT	Stuck open pressurizer safety valve. Valve recloses at 6000 secs (RCS low pressure point).	None	None	Not in base case		
42	TT/RT - HZP	Stuck open pressurizer safety valve. Valve recloses at 6000 secs.	None	None	Not in base case		
43	TT/RT	Stuck open PORV. Valve recloses at 400 sec (RCS low pressure point)	None	None	Not in base case		

44	LOCA	2.54 cm (1 in) surge line break with HPI Failure	None.	At 15 minutes after initiation, operators open all TBVs to depressurize the system to the CFT setpoint. When the CFTs are 50 percent discharged, HPI is assumed to be recovered. The TBVs are assumed remain open for the duration of the transient.	2.7E-07	1.8E-15	1.8E-05
45	TT/RT	None	Loss of MFW and EFW. At 30 minutes after operator starts HPI and opens the PORV, EFW is restored. Normal EFW level control is assumed.	Operator starts primary system "feed and bleed" cooling by starting the HPI and opening the PORV at RCS pressure > 2275 psia. Operator also trips one RCP in each steam generator loop (if 0.27 K (0.5° F) subcooling margin is reached, the remaining two RCPs	Not in base case		

46	TT/RT	None	Loss of MFW and EFW. At 30 minutes after operator starts HPI and opens the PORV, EFW is restored. Normal EFW level control is assumed.	Operator starts primary system "feed and bleed" cooling by starting the HPI and opening the PORV at RCS pressure > 2275 psia. Operator also trips one RCP in each steam generator loop (if 0.27 K (0.5° F) subcooling margin is reached, the remaining two RCPs	Not in base case		
47	TT/RT	None	Loss of MFW and EFW. At 30 minutes after operator starts HPI and opens the PORV, EFW is restored. EFW level control fails where the steam generators are overfilled and remain overfilled but water does not enter the steam lines.	Operator starts primary system "feed and bleed" cooling by starting the HPI and opening the PORV at RCS pressure > 2275 psia. Operator also trips one RCP in each steam generator loop (if 0.27 K (0.5° F) subcooling margin is reached, the remaining two RCPs	Not in base case		

48	TT/RT	None	Loss of MFW and EFW. At 30 minutes after operator starts HPI and opens the PORV, EFW is restored. Normal EFW level control is assumed.	Operator starts primary system "feed and bleed" cooling by starting the HPI and opening the PORV at RCS pressure > 2275 psia. Operator also trips one RCP in each steam generator loop when 2.7 K (5° F) subcooling margin is reached, the remaining two RCPs a	Not in base case		
49	TT/RT	None	Loss of MFW and EFW.	Operator opens the TBV to depressurize the secondary side to below the condensate booster pump shutoff head so that these pumps feed the steam generators. Booster pumps are assumed to be uncontrolled so that the steam generators are overfilled. Booster p	Not in base case		

50	TT/RT	None	Loss of MFW and EFW.	Operator opens all TBVs to depressurize the secondary side to below the condensate booster pump shutoff head so that these pumps feed the steam generators. Booster pumps are assumed to be uncontrolled so that the steam generators are filled to the top. B	Not in base case		
51	TT/RT - HZP	None	Loss of MFW and EFW.	Operator opens the TBVs to depressurize the secondary side to below the condensate booster pump shutoff head so that these pumps feed the steam generators. Booster pumps are assumed to be uncontrolled so that the steam generators are filled to the top. B	Not in base case		
52	LOCA	14.37 cm (5.656 in) surge line break	None	None	Not in base case		

53	LOCA	20.32 cm (8 inch) surge line break	None	None	Not in base case		
54	LOCA-Hi K	5.08 cm (2 in) surge line break	None	None	Not in base case		
55	LOCA-Hi K	7.183 cm (2.828 in) surge line break	None	None	Not in base case		
56	TT/RT-Hi K	Stuck open pressurizer safety valve.	None	None	Not in base case		
57	TT/RT	None	Two stuck open safety valves in SG-A.	Operator isolates EFW in SG-A.	Not in base case		
58	LOCA-Hi K	10.16 cm (4 inch) surge line break	None	None	Not in base case		
59	TT/RT	None	2 stuck open safety valves in SG-A	Operator throttles HPI to maintain 27.8 K (50oF) subcooling and pressurizer level of 304 cm (120 inches). The operator stops emergency feedwater flow to SG-A at 15 minutes after accident initiation.	Not in base case		

60	TT/RT - HZP	None	2 stuck open safety valves in SG-A	Operator throttles HPI to maintain 27.8 K (50° F) subcooling and pressurizer level of 304 cm (120 inches). The operator stops emergency feedwater flow to SG-A at 15 minutes after accident initiation.	Not in base case		
61	MSLB	None	MSLB with shutdown of the MFW and the turbine driven EFW pumps by the MSLB circuitry.	Operator stops motor driven EFW flow to the affected steam generator after 10 minutes.	Not in base case		
62	MSLB	None	MSLB with shutdown of the MFW and the turbine driven EFW pumps by the MSLB circuitry. Break occurs in the containment so that RCP trip occurs due to a containment isolation signal at 1 minute after break initiation.	None	Not in base case		

63	LOCA-S	5.08 cm (2 in) surge line break. Core flood tank temperature of 294 K (70°F). Nominal temperature is 300 K (80° F)	None	None	Not in base case		
64	LOCA-S	5.08 cm (2 in) surge line break. Core flood tank temperature of 310 K (100°F). Nominal temperature is 300 K (80° F)	None	None	Not in base case		
65	LOCA-S	5.08 cm (2 in) surge line break. HPI temperature of 278 K (40° F). Nominal temperature is 294 K (70° F)	None	None	Not in base case		
66	LOCA-S	5.08 cm (2 in) surge line break. HPI temperature of 300 K (80° F). Nominal temperature is 294 K (70° F).	None	None	Not in base case		
67	LOCA-S	5.08 cm (2 in) surge line break. Increased effective heat transfer coefficient used (1.3 x HTC).	None	None	Not in base case		

68	LOCA-S	5.08 cm (2 in) surge line break. Decreased effective heat transfer coefficient used (0.7 x HTC).	None	None	Not in base case		
69	LOCA-S	5.08 cm (2 in) surge line break. Increased loop flow resistance to reduce natural circulation (100 % increase).	None	None	Not in base case		
70	LOCA-HZP	5.08 cm (2 inch) surge line break	None	None	Not in base case		
71	LOCA-S	5.08 cm (2 in) surge line break. Reduced vent valve delta-P required to open by a factor of 0.5.	None	None	Not in base case		
72	LOCA-S	5.08 cm (2 in) surge line break. No vent valve function.	None	None	Not in base case		
73	LOCA-HZP	14.366 cm (5.656 in) surge line break	None	None	Not in base case		
74	LOCA-HZP	2.54 cm (1 in) surge line break with HPI Failure	None	At 15 minutes after transient initiation, the operator opens all TBVs to lower primary system pressure and allow core flood tank and LPI injection.	Not in base case		

75	LOCA-HZP	2.54 cm (1 in) surge line break with HPI Failure	None	At 15 minutes after sequence initiation, operators open all TBVs to depressurize the system to the CFT setpoint. When the CFTs are 50 percent discharged, HPI is assumed to be recovered. The TBVs are assumed remain opened for the duration of the transien	Not in base case		
76	LOCA	3.81 cm (1.5 in) surge line break	None	None	Not in base case		
77	TT/RT	None	One stuck open TBV in SG-A. Valve recloses in 20 minutes.	Operator throttles HPI to maintain 558 cm (220 in) level in the pressurizer.	Not in base case		
78	LOCA-S	5.08 cm (2 in) surge line break. No heat structures.	None	None	Not in base case		
79	LOCA-S	5.08 cm (2 in) surge line break. No heat structures and no vent valve function.	None	None	Not in base case		
80	LOCA-S	5.08 cm (2 in) surge line break. No vent valve function.	None	None	Not in base case		

81	LOCA	5.08 cm (2 inch) surge line break with HPI Failure	None	At 15 minutes after transient initiation, operator opens all TBVs to lower primary system pressure and allow CFT and LPI injection.	Not in base case		
82	LOCA	2.54 cm (1 in) surge line break with HPI Failure	None	At 15 minutes after initiation, operator opens all TBVs to lower primary pressure and allow CFT and LPI injection. When the CFTs are 50% discharged, HPI is recovered. At 3000 seconds after initiation, operator starts throttling HPI to 55 K (100°F) subco	Not in base case		

83	TT/RT	Stuck open pressurizer safety valve. Valve recloses at 6000 secs.	None	After valve recloses, operator throttles HPI 1 minute after 2.7 K (5°F) subcooling and 254 cm (100") pressurizer level is reached (throttling criteria is 27.8 K (50°F) subcooling)	Not in base case		
84	TT/RT	Stuck open pressurizer safety valve. Valve recloses at 6000 secs.	None	After valve recloses, operator throttles HPI 10 minutes after 2.7 K (5°F) subcooling and 254 cm (100") pressurizer level is reached (throttling criteria is 27.8 K (50°F) subcooling)	Not in base case		
85	TT/RT	Stuck open pressurizer safety valve. Valve recloses at 3000 secs.	None	After valve recloses, operator throttles HPI 1 minute after 2.7 K (5°F) subcooling and 254 cm (100") pressurizer level is reached (throttling criteria is 27.8 K (50°F) subcooling)	Not in base case		

86	TT/RT	Stuck open pressurizer safety valve. Valve recloses at 3000 secs.	None	After valve recloses, operator throttles HPI 10 minutes after 2.7 K (5°F) subcooling and 254 cm (100") pressurizer level is reached (throttling criteria is 27.8 K (50°F) subcooling)	Not in base case		
87	TT/RT	Stuck open pressurizer SRV and HPI Failure	None	At 15 minutes after initiation, operator opens all TBVs to lower primary pressure and allow CFT and LPI injection. When the CFTs are 50% discharged, HPI is recovered. The HPI is throttled 20 minutes after 5°F subcooling and 254 cm (100") pressurizer lev	Not in base case		

88	TT/RT	Stuck open pressurizer safety valve and HPI Failure	None	At 15 minutes after initiation, operator opens all TBVs to lower primary pressure and allow CFT and LPI injection. When the CFTs are 50% discharged, HPI is recovered. The SRV is closed 5 minutes after HPI recovered. HPI is throttled at 1 minute after 2	Not in base case		
89	TT/RT	None	Loss of MFW and EFW.	Operator opens all TBVs to depressurize the secondary side to below the condensate booster pump shutoff head so that these pumps feed the steam generators. Booster pumps are assumed to be initially uncontrolled so that the steam generators are overfilled	5.4E-07	2.3E-15	1.3E-04

90	TT/RT	None	2 stuck open safety valves in SG-A	Operator throttles HPI 20 minutes after 2.7 K (5°F) subcooling and 254 cm (100") pressurizer level is reached (throttling criteria is 27.8 K (50°F) subcooling).	6.3E-07	7.6E-12	3.7E-05
91	SGTR	None	SGTR with a stuck open SRV in SG-B. A reactor trip is assumed to occur at the time of the tube rupture. Stuck safety relief valve is assumed to reclose 10 minutes after initiation.	Operator trips RCP's 1 minute after initiation. Operator also throttles HPI 10 minutes after 2.7 K (5°F) subcooling and 254 cm (100") pressurizer level is reached (assumed throttling criteria is 27.8 K (50°F) subcooling).	6.1E-06	9.0E-12	1.9E-04
92	TT/RT-HZP	Stuck open pressurizer safety valve. Valve recloses at 6000 secs .	None	After valve recloses, operator throttles HPI at 1 minute after 2.7 K (5°F) subcooling and 254 cm (100") pressurizer level is reached (throttling criteria is 27.8 K (50°F) subcooling).	Not in base case		

93	TT/RT-HZP	Stuck open pressurizer safety valve. Valve recloses at 6000 secs.	None	After valve recloses, operator throttles HPI at 10 minutes after 2.7 K (5°F) subcooling and 254 cm (100") pressurizer level is reached (throttling criteria is 27.8 K (50°F) subcooling).	Not in base case		
94	TT/RT-HZP	Stuck open pressurizer safety valve. Valve recloses at 3000 secs.	None	After valve recloses, operator throttles HPI at 1 minute after 2.7 K (5°F) subcooling and 254 cm (100") pressurizer level is reached (throttling criteria is 27.8 K (50°F) subcooling).	Not in base case		
95	TT/RT-HZP	Stuck open pressurizer safety valve. Valve recloses at 3000 secs.	None	After valve recloses, operator throttles HPI at 10 minutes after 2.7 K (5°F) subcooling and 254 cm (100") pressurizer level is reached (throttling criteria is 27.8 K (50°F) subcooling).	Not in base case		

96	TT/RT-HZP	Stuck open pressurizer safety valve and HPI Failure	None	At 15 minutes after initiation, operator opens all TBVs to lower primary pressure and allow CFT and LPI injection. When the CFTs are 50% discharged, HPI is recovered. HPI is throttled 20 minutes after 2.7 K (5°F) subcooling and 254 cm (100") pressurize	Not in base case		
97	TT/RT-HZP	Stuck open pressurizer SRV and HPI Failure	None	At 15 minutes after initiation, operator opens all TBVs to lower primary pressure and allow CFT and LPI injection. When the CFTs are 50% discharged, HPI is recovered. SRV is closed at 5 minutes after HPI is recovered. HPI is throttled at 1 minute after	Not in base case		

98	TT/RT-HZP	None	Loss of MFW and EFW.	Operator opens all TBVs to depressurize the secondary side to below the condensate booster pump shutoff head so that these pumps feed the steam generators. Booster pumps are assumed to be initially uncontrolled so that the steam generators are overfilled	1.0E-07	1.1E-14	1.5E-05
99	MSLB	None	MSLB with trip of turbine driven EFW by MSLB Circuitry.	HPI is throttled 20 minutes after 2.7 K (5°F) subcooling and 254 cm (100") pressurizer level is reached (throttling criteria is 27.8 K (50°F) subcooling).	2.4E-07	1.0E-09	9.4E-06
100	MSLB-HZP	None	MSLB with trip of turbine driven EFW by MSLB Circuitry	Operator throttles HPI 20 minutes after 2.7 K (5°F) subcooling and 254 cm (100") pressurizer level is reached (throttling criteria is 27.8 K (50°F) subcooling).	5.1E-08	6.6E-11	4.3E-06

101	MSLB-HZP	None	MSLB without trip of turbine driven EFW by MSLB Circuitry	Operator throttles HPI to maintain 27.8 K (50° F) subcooling margin (throttling criteria is 27.8 K (50°F) subcooling).	3.9E-07	3.1E-09	1.2E-05
102	TT/RT-HZP	None	2 stuck open safety valves in SG-A	Operator throttles HPI 20 minutes after 2.77 K (5°F) subcooling and 254 cm (100 in) pressurizer level is reached (throttling criteria is 27 K (50°F) subcooling).	2.0E-07	4.2E-11	2.8E-05
103	SGTR-HZP	None	SGTR with a stuck open SRV in SG-B. A reactor trip is assumed to occur at the time of the tube rupture. Stuck safety relief valve is assumed to reclose 10 minutes after initiation.	Operator trips RCP's 1 minute after initiation. Operator also throttles HPI 10 minutes after 2.77 K (5° F) subcooling and 254 cm (100 in) pressurizer level is reached (throttling criteria is 27 K (50°F) subcooling).	Not in base case		
104	LOCA-HZP	3.59 cm (1.414 in) surge line break	None	None	Not in base case		

105	LOCA-HZP	5.08 cm (2 inch) surge line break with HPI failure.	None	At 15 minutes after initiation, operator opens all TBVs to lower primary pressure and allow CFT and LPI injection.	Not in base case		
106	LOCA-HZP	7.18 cm (2.828 in) surge line break	None	None	Not in base case		
107	LOCA-Hi K	2.54 cm (1 inch) surge line break	2 stuck open safety valves in SG-A	HPI terminated when subcooling margin exceeds 55.6 K (100o F)	Not in base case		
108	TT/RT-Hi K	Stuck open pressurizer safety valve	None	None	Not in base case		
109	TT/RT-Hi K	Stuck open pressurizer safety valve. Valve recloses at 6000 secs (RCS low pressure point).	None	None	9.6E-06	4.2E-09	3.9E-04
110	LOCA-Hi K		None	At 15 minutes after transient initiation, operator opens both TBV to lower primary system pressure and allow CFT and LPI injection.	3.4E-06	9.5E-10	4.6E-05

111	LOCA-Hi K		None	At 15 minutes after initiation, operator opens all TBVs to lower primary pressure and allow CFT and LPI injection. When the CFTs are 50% discharged, HPI is recovered. At 3000 seconds after initiation, operator starts throttling HPI to 55 K (100°F) subco	4.2E-07	1.6E-14	1.1E-05
112	TT/RT-Hi K	Stuck open pressurizer safety valve. Valve recloses at 6000 secs.	None	After valve recloses, operator throttles HPI 1 minute after 2.7 K (5°F) subcooling and 254 cm (100") pressurizer level is reached (throttling criteria is 27 K (50°F) subcooling)	1.2E-04	4.6E-06	9.2E-04

113	TT/RT-Hi K	Stuck open pressurizer safety valve. Valve recloses at 6000 secs.	None	After valve recloses, operator throttles HPI 10 minutes after 2.7 K (5°F) subcooling and 254 cm (100") pressurizer level is reached (throttling criteria is 27.8 K (50°F) subcooling)	5.1E-05	3.9E-08	1.8E-03
114	TT/RT-Hi K	Stuck open pressurizer safety valve. Valve recloses at 3000 secs.	None	After valve recloses, operator throttles HPI 1 minute after 2.7 K (5°F) subcooling and 254 cm (100") pressurizer level is reached (throttling criteria is 50°F subcooling)	1.2E-04	4.6E-06	9.2E-04
115	TT/RT-Hi K		None	After valve recloses, operator throttles HPI 10 minutes after 2.7 K (5°F) subcooling and 254 cm (100") pressurizer level is reached (throttling criteria is 50°F subcooling)	5.1E-05	3.9E-08	1.8E-03

116	TT/RT-Hi K		None	At 15 minutes after initiation, operator opens all TBVs to lower primary pressure and allow CFT and LPI injection. When the CFTs are 50% discharged, HPI is recovered. The HPI is throttled 20 minutes after 2.7 K (5°F) subcooling and 254 cm (100") pressur	2.6E-07	4.6E-16	9.3E-06
117	TT/RT-Hi K		None	At 15 minutes after initiation, operator opens all TBV to lower primary pressure and allow CFT and LPI injection. When the CFTs are 50% discharged, HPI is recovered. The SRV is closed 5 minutes after HPI recovered. HPI is throttled at 1 minute after 2.	5.4E-07	1.6E-14	2.4E-05
118	LOCA-Hi K	5.08 cm (2 inch) surge line break	None	None	Not in base case		

119	LOCA-Hi K	2.54 cm (1 in) surge line break with HPI Failure	None	At 15 minutes after transient initiation, the operator opens all turbine bypass valves to lower primary system pressure and allow core flood tank and LPI injection.	4.4E-07	4.4E-11	1.2E-05
120	LOCA-Hi K	2.54 cm (1 in) surge line break with HPI Failure	None	At 15 minutes after sequence initiation, operators open all TBVs to depressurize the system to the CFT setpoint. When the CFTs are 50 percent discharged, HPI is assumed to be recovered. The TBVs are assumed remain opened for the duration of the transien	4.2E-08	2.9E-17	1.2E-06

121	TT/RT-Hi K	Stuck open pressurizer safety valve. Valve recloses at 6000 secs .	None	Operator throttles HPI at 1 minute after 2.7 K (5°F) subcooling and 254 cm (100") pressurizer level is reached (throttling criteria is 27.8 K (50°F) subcooling).	2.3E-05	4.1E-07	1.9E-04
122	TT/RT-Hi K	Stuck open pressurizer safety valve. Valve recloses at 6000 secs.	None	Operator throttles HPI at 10 minutes after 2.7 K (5°F) subcooling and 254 cm (100") pressurizer level is reached (throttling criteria is 27.8 K (50°F) subcooling).	7.6E-06	3.5E-09	8.3E-05
123	TT/RT-Hi K	Stuck open pressurizer safety valve. Valve recloses at 3000 secs.	None	Operator throttles HPI at 1 minute after 2.7 K (5°F) subcooling and 254 cm (100") pressurizer level is reached (throttling criteria is 27.8 K (50°F) subcooling).	2.3E-05	4.1E-07	1.9E-04

124	TT/RT-Hi K	Stuck open pressurizer safety valve. Valve recloses at 3000 secs.	None	Operator throttles HPI at 10 minutes after 2.7 K (5°F) subcooling and 254 cm (100") pressurizer level is reached (throttling criteria is 27.8 K (50°F) subcooling).	7.6E-06	3.5E-09	8.3E-05
125	TT/RT-Hi K	Stuck open pressurizer safety valve and HPI Failure	None	At 15 minutes after initiation, operator opens all TBVs to lower primary pressure and allow CFT and LPI injection. When the CFTs are 50% discharged, HPI is recovered. HPI is throttled 20 minutes after 2.7 K (5°F) subcooling and 254 cm (100") pressurize	4.6E-08	0.0E+00	1.1E-06

126	TT/RT-Hi K	Stuck open pressurizer safety valve and HPI Failure	None	At 15 minutes after initiation, operator opens all TBVs to lower primary pressure and allow CFT and LPI injection. When the CFTs are 50% discharged, HPI is recovered. SRV is closed at 5 minutes after HPI is recovered. HPI is throttled at 1 minute after	8.4E-08	3.3E-15	2.7E-06
127	SGTR-HiK	None	SGTR with a stuck open SRV in SG-B. A reactor trip is assumed to occur at the time of the tube rupture. Stuck safety relief valve is assumed to reclose 10 minutes after initiation.	Operator trips RCP's 1 minute after initiation. Operator also throttles HPI 10 minutes after 2.77 K (5° F) subcooling and 254 cm (100 in) pressurizer level is reached (assumed throttling criteria is 27 K (50°F) subcooling).	1.3E-07	7.9E-14	6.2E-06
128	LOCA-HiK	7.18 cm (2.828 in) surge line break	None	None	Not in base case		
129	LOCA	10.16 cm (4 inch) cold leg break	None	None	Not in base case		
130	LOCA	14.37 cm (5.656 in) cold leg break	None	None	Not in base case		

131	LOCA-HZP	10.16 cm (4 inch) surge line break	None	None	Not in base case		
132	LOCA-HZP	20.32 cm (8 inch) surge line break	None	None	Not in base case		
133	LOCA-HZP & HiK	10.16 cm (4 inch) surge line break	None	None	Not in base case		
134	LOCA-HZP & HiK	20.32 cm (8 inch) surge line break	None	None	Not in base case		
135	LOCA-S	8.53 cm (3.35 in) surge line break (Break flow area reduced by 30% from 10.16 cm (4 in) break). Vent valves do not function.	None	None	Not in base case		
136	LOCA-S	4.34 cm (1.71 in) surge line break (Break flow area increased by 30% from 3.81 cm (1.5 in) break). Winter conditions assumed (HPI, LPI temp = 277 K (40° F) and CFT temp = 294 K (70° F)).	None	None	Not in base case		

137	TT/RT-S	TT/RT with stuck open pzr SRV (valve flow area reduced by 30 percent). Summer conditions assumed (HPI, LPI temp = 302 K (85° F) and CFT temp = 310 K (100° F)). Vent valves do not function.	None	None	Not in base case		
138	TT/RT-S	TT/RT with stuck open pzr SRV. Summer conditions assumed (HPI, LPI temp = 302 K (85° F) and CFT temp = 310 K (100° F)).	None	None	Not in base case		
139	TT/RT-S	TT/RT with partially stuck open pzr SRV (flow area equivalent to 1.5 in diameter opening). HTC coefficients increased by 1.3.	None	None	Not in base case		
140	TT/RT-S	TT/RT with stuck open pzr SRV. SRV assumed to reclose at 3000 secs. Operator does not throttle HPI.	None	None	Not in base case		

141	LOCA-HiK	8.19 cm (3.22 in) surge line break (Break flow area increased by 30% from 7.18 cm (2.828 in) break).	None	None	1.1E-04	1.0E-05	6.7E-04
142	LOCA-HiK	6.01 cm (2.37 in) surge line break (Break flow area decreased by 30% from 7.18 cm (2.828 in) break).	None	None	1.1E-04	1.0E-05	6.7E-04
143	LOCA-HiK	7.18 cm (2.828 in) cold leg break.	None	None	Not in base case		
144	LOCA-HiK	8.53 cm (3.35 in) surge line break (Break flow area reduced by 30% from 10.16 cm (4 in) break). Vent valves do not function.	None	None	Not in base case		
145	LOCA-HiK	4.34 cm (1.71 in) surge line break (Break flow area increased by 30% from 3.81 cm (1.5 in) break). Winter conditions assumed (HPI, LPI temp = 277 K (40° F) and CFT temp = 294 K (70° F)).	None	None	1.3E-04	1.3E-05	8.4E-04

146	TT/RT-HiK	TT/RT with stuck open pzr SRV (valve flow area reduced by 30 percent). Summer conditions assumed (HPI, LPI temp = 302 K (85° F) and CFT temp = 310 K (100° F)). Vent valves do not function.	None	None	4.2E-05	6.7E-07	2.4E-04
147	TT/RT-Hi K	TT/RT with stuck open pzr SRV. Summer conditions assumed (HPI, LPI temp = 302 K (85° F) and CFT temp = 310 K (100° F)).	None	None	3.6E-05	5.8E-07	2.1E-04
148	TT/RT-Hi K	TT/RT with partially stuck open pzr SRV (flow area equivalent to 1.5 in diameter opening). HTC coefficients increased by 1.3.	None	None	4.2E-05	6.7E-07	2.4E-04
149	TT/RT-Hi K	TT/RT with stuck open pzr SRV. SRV assumed to reclose at 3000 secs. Operator does not throttle HPI.	None	None	9.6E-06	4.2E-09	3.9E-04

150	LOCA	14.37 cm (5.656 in) surge line break. ECC suction switch to the containment sump included in the analysis.	None	None	Not in base case		
151	LOCA	20.32 cm (8 inch) surge line break. ECC suction switch to the containment sump included in the analysis.	None	None	Not in base case		
152	LOCA-Hi K	7.183 cm (2.828 in) surge line break. ECC suction switch to the containment sump included in the analysis.	None	None	Not in base case		
153	LOCA-HiK	8.19 cm (3.22 in) surge line break (Break flow area increased by 30% from 7.18 cm (2.828 in) break). ECC suction switch to the containment sump included in the analysis.	None	None	Not in base case		

154	LOCA-HiK	8.53 cm (3.36 in) surge line break (Break flow area reduced by 30% from 10.16 cm (4 in) break). Vent valves do not function. ECC suction switch to the containment sump included in the analysis.	None	None	1.3E-04	1.3E-05	8.4E-04
155	LOCA-HiK	28.738 cm (11.314 in) hot leg break. ECC suction switch to the containment sump included in the analysis.	None	None	Not in base case		
156	LOCA-HiK	40.64 cm (16 in) hot leg break. ECC suction switch to the containment sump included in the analysis.	None	None	7.0E-06	3.1E-08	3.4E-04
157	LOCA-HiK	57.48 cm (22.63 in) hot leg break. ECC suction switch to the containment sump included in the analysis.	None	None	Not in base case		
158	LOCA-HiK	40.64 cm (16 in) cold leg break. ECC suction switch to the containment sump included in the analysis.	None	None	Not in base case		

159	LOCA-HiK	14.37 cm (5.656 in) surge line break	None	None	Not in base case		
160	LOCA-HiK	14.37 cm (5.656 in) surge line break. ECC suction switch to the containment sump included in the analysis.	None	None	1.8E-05	4.9E-08	6.6E-04
161	LOCA-HZP & HiK	14.366 cm (5.656 in) surge line break	None	None	Not in base case		
162	LOCA-HZP & HiK	14.366 cm (5.656 in) surge line break. ECC suction switch to the containment sump included in the analysis.	None	None	Not in base case		
163	LOCA-HiK	20.32 cm (8 inch) surge line break	None	None	Not in base case		
164	LOCA-HiK	20.32 cm (8 inch) surge line break. ECC suction switch to the containment sump included in the analysis.	None	None	2.1E-05	5.8E-08	7.7E-04
165	TT/RT-HZP & Hi K	Stuck open pressurizer safety valve. Valve recloses at 6000 secs (RCS low pressure point).	None	None	1.8E-06	2.2E-10	4.6E-05

166	TT/RT-HZP & Hi K	Stuck open pressurizer safety valve. Valve recloses at 6000 secs.	None	After valve recloses, operator throttles HPI 1 minute after 2.7 K (5°F) subcooling and 254 cm (100") pressurizer level is reached (throttling criteria is 50°F subcooling)	Not in base case		
167	TT/RT-HZP & Hi K	Stuck open pressurizer safety valve. Valve recloses at 6000 secs.	None	After valve recloses, operator throttles HPI 10 minutes after 2.7 K (5°F) subcooling and 254 cm (100") pressurizer level is reached (throttling criteria is 50°F subcooling)	Not in base case		
168	TT/RT-Hi K	TT/RT with stuck open pzr SRV. SRV assumed to reclose at 3000 secs. Operator does not throttle HPI.	None	None	1.8E-06	2.2E-10	4.6E-05

169	LOCA-HiK	TT/RT with stuck open pzr SRV (valve flow area reduced by 30 percent). Summer conditions assumed (HPI, LPI temp = 302 K (85° F) and CFT temp = 310 K (100° F)). Vent valves do not function.	None	None	7.3E-06	1.3E-07	7.9E-05
170	TT/RT-Hi K	TT/RT with stuck open pzr SRV. Summer conditions assumed (HPI, LPI temp = 302 K (85° F) and CFT temp = 310 K (100° F)).	None	None	6.3E-06	1.1E-07	6.8E-05
171	TT/RT-Hi K	TT/RT with partially stuck open pzr SRV (flow area equivalent to 1.5 in diameter opening). HTC coefficients increased by 1.3.	None	None	7.3E-06	1.3E-07	7.9E-05
172	LOCA-HiK	10.16 cm (4 in) cold leg break. ECC suction switch to the containment sump included in the analysis.	None	None	1.1E-04	1.0E-05	6.7E-04

173	MSLB-HZP	No primary side failure. Decay power set to 0.007 of full power and held constant (17.98 MW).	MSLB with trip of turbine driven EFW by MSLB Circuitry	Operator throttles HPI 20 minutes after 2.7 K (5°F) subcooling and 254 cm (100") pressurizer level is reached (throttling criteria is 27.8 K (50°F) subcooling).	Not in base case		
174	MSLB-HZP	No primary side failure. Decay power set to 0.003 of full power and held constant (7.70 MW).	MSLB with trip of turbine driven EFW by MSLB Circuitry	Operator throttles HPI 20 minutes after 2.7 K (5°F) subcooling and 254 cm (100") pressurizer level is reached (throttling criteria is 27.8 K (50°F) subcooling).	Not in base case		
175	TT/RT-Hi K	Stuck open pressurizer safety valve. Valve recloses at 6000 secs. Decay power set to 0.007 of full power and held constant (17.98 MW).	None	Operator throttles HPI at 10 minutes after 2.7 K (5°F) subcooling and 254 cm (100") pressurizer level is reached (throttling criteria is 27.8 K (50°F) subcooling).	Not in base case		

176	TT/RT-Hi K	Stuck open pressurizer safety valve. Valve recloses at 6000 secs. Decay power set to 0.003 of full power and held constant (7.70 MW).	None	Operator throttles HPI at 10 minutes after 2.7 K (5°F) subcooling and 254 cm (100") pressurizer level is reached (throttling criteria is 27.8 K (50°F) subcooling).	Not in base case		
177	LOCA-HiK	10.16 cm (4 in) surge line break. ECC suction switch to the containment sump included in the analysis.	None.	None.	Not in base case		

Beaver Valley

Case	Type	Primary Side Failure	Secondary Side Failure	Operator Action	Initiating Event Frequency		
					Mean	Min.	Max.
1	LOCA	2.54 cm (1.0 in) surge line break	None	None	Not in base case		
2	LOCA	3.59 cm (1.414 in) surge line break	None	None	1.2E-04	1.2E-05	1.2E-03
3	LOCA	5.08 cm (2.0 in) surge line break	None	None	9.8E-05	9.7E-06	9.6E-04
4	LOCA	7.18 cm (2.828 in) surge line break	None	None	Not in base case		
5	LOCA	10.16 cm (4.0 in) surge line break	None	None	Not in base case		
6	LOCA	14.37 cm (5.657 in) surge line break	None	None	Not in base case		
7	LOCA	20.32 cm (8.0 in) surge line break	None	None	2.1E-05	9.4E-08	1.0E-03
8	LOCA	28.74 cm (11.314 in) hot leg break	None	None	Not in base case		
9	LOCA	40.64 cm (16.0 in) hot leg break	None	None	7.0E-06	1.8E-08	3.3E-04
10	LOCA	57.47 cm (22.63 in) hot leg break	None	None	Not in base case		

11	RT/TT	None	None	None	Not in base case		
12	RT/TT	One stuck open pressurizer PORV	None	None	Not in base case		
13	RT/TT	One stuck open pressurizer PORV (isolated at 20 minutes)	None	None	Not in base case		
14	RT/TT	One stuck open pressurizer SRV	None	None	2.2E-04	7.7E-06	1.1E-03
15	RT/TT	None	One stuck open SDV	None	Not in base case		
16	RT/TT	None	Two stuck open SDVs	None	Not in base case		
17	RT/TT	None	One stuck open SDV	Close all MSIVs at 20 minutes	Not in base case		
18	RT/TT	None	Three stuck open ASDVs (one/SG)	None	Not in base case		
19	RT/TT	None	Two stuck open ASDVs (SG's A and B)	None	Not in base case		
20	RT/TT	None	One stuck open ASDV (SG A)	None	Not in base case		
21	RT/TT	None	One stuck open ASDV (SG A)	Close all MSIVs at 20 minutes	Not in base case		
22	RT/TT	One stuck open pressurizer PORV	One stuck open ASDV (SG A)	None	Not in base case		
23	RT/TT	One stuck open pressurizer SRV	One stuck open ASDV (SG A)	None	Not in base case		
24	RT/TT	None	Three stuck open MS-SRVs (one/SG)	None	Not in base case		
25	RT/TT	None	Two stuck open MS-SRVs (SG's A and B)	None	Not in base case		
26	RT/TT	None	One stuck open MS-SRV (SG A)	None	Not in base case		
27	RT/TT	None	One stuck open MS-SRV (SG A)	Close all MSIVs at 20 minutes	Not in base case		
28	RT/TT	None	MFW overfeed of all SGs	Trips MFW when water enters steam line	Not in base case		
29	RT/TT	None	MFW overfeed of SGs A and B	Trips MFW when water enters steam line	Not in base case		

30	RT/TT	None	MFW overfeed of SG A	Trips MFW when water enters steam line	Not in base case		
31	RT/TT	None	Loss of all feedwater	Opens all pressurizer PORVs and uses all HPI pumps	3.1E-07	1.2E-10	3.2E-06
32	MSLB	None	Double ended guillotine break of steam line A	Operator terminates feedwater to SG A upon break	Not in base case		
33	RT/TT	Two stuck open pressurizer PORVs	None	None	Not in base case		
34	RT/TT	Two stuck open pressurizer SRVs	None	None	4.9E-07	1.8E-08	2.8E-06
35	RT/TT	One stuck open pressurizer SRV	None	None	Not in base case		
36	RT/TT	None	Three stuck open SDVs	None	Not in base case		
37	SGTR	Steam generator tube rupture (SG A)	None	None	Not in base case		
38	SGTR	Steam generator tube rupture (SG A)	Stuck open SDV	None	Not in base case		
39	RT/TT	One stuck open pressurizer PORV	One stuck open SDV	None	Not in base case		
40	RT/TT	One stuck open pressurizer SRV	One stuck open SDV	None	Not in base case		
41	RT/TT	One stuck open pressurizer SRV	One stuck open MS-SRV (SG A)	None	Not in base case		
42	RT/TT	None	One stuck open MS-SRV (SG A)	MS-SRV isolated at 7000 seconds	Not in base case		
43	RT/TT	One stuck open pressurizer SRV	None	None	Not in base case		
44	RT/TT, HZP	None	MFW overfeed of all SGs	MFW tripped when water in steamline	Not in base case		
45	RT/TT	None	MFW overfeed of all SGs	None	Not in base case		
46	RT/TT	None	MFW overfeed of SG's A and B	None	Not in base case		
47	RT/TT	None	MFW overfeed of SG A	None	Not in base case		
48	RT/TT	None	MFW overfeed of all SGs	None	Not in base case		

49	MSLB	None	Double ended guillotine break of steam line A, no MSIV closure	None	Not in base case		
50	SGTR	Steam generator tube rupture (SG A)	None	RCP's are tripped	Not in base case		
51	SGTR	Steam generator tube rupture (SG A), one stuck open pressurizer PORV	One stuck open ASDV (SG A)	RCP's are tripped	Not in base case		
52	LOCA, HZP	2.54 cm (1.0 in) surge line break	None	None	Not in base case		
53	LOCA, HZP	3.59 cm (1.414 in) surge line break	None	None	Not in base case		
54	LOCA, HZP	5.08 cm (2.0 in) surge line break	None	None	Not in base case		
55	LOCA, HZP	7.18 cm (2.828 in) surge line break	None	None	Not in base case		
56	LOCA, HZP	10.16 cm (4.0 in) surge line break	None	None	1.2E-04	1.2E-05	1.2E-03
57	LOCA, HZP	14.37 cm (5.657 in) surge line break	None	None	Not in base case		
58	LOCA, HZP	20.32 cm (8.0 in) surge line break	None	None	Not in base case		
59	RT/TT	One stuck open pressurizer SRV	None	None	3.5E-04	1.3E-05	2.1E-03
60	RT/TT	One stuck open pressurizer SRV	None	None	2.2E-05	1.4E-07	3.3E-04
61	RT/TT	Two stuck open pressurizer SRVs	None	None	1.8E-06	3.8E-08	1.1E-05
62	RT/TT	Two stuck open pressurizer SRVs	None	None	1.1E-07	2.0E-10	1.3E-06
63	LOCA	40.64 cm (16.0 in) cold leg break	None	None	Not in base case		
64	RT/TT, HZP	Two stuck open pressurizer SRVs	None	None	8.7E-08	2.1E-09	4.5E-07
65	RT/TT	Two stuck open pressurizer SRVs, no HPI	None	Open all ASDVs 5 minutes after HPI would have come on	1.0E-09	5.0E-12	1.6E-08
66	RT/TT	Two stuck open pressurizer SRVs	None	None	1.2E-06	3.8E-08	8.0E-06
67	RT/TT	Two stuck open pressurizer SRVs	None	None	1.2E-06	3.8E-08	8.0E-06
68	RT/TT	Two stuck open pressurizer SRVs, no HPI	None	Open all ASDVs 5 minutes after HPI would have come on	1.3E-08	8.3E-11	2.4E-07
69	RT/TT, HZP	Two stuck open pressurizer SRVs	None	None	2.1E-08	3.5E-11	5.3E-07
70	RT/TT, HZP	Two stuck open pressurizer SRVs	None	None	2.1E-08	3.5E-11	5.3E-07
71	RT/TT, HZP	One stuck open pressurizer SRV	None	None	3.7E-06	2.3E-08	8.6E-05
72	RT/TT	One stuck open pressurizer SRV, no HPI	None	Open all ASDVs 5 minutes after HPI would have come on	5.1E-07	1.0E-08	1.3E-05

73	RT/TT, HZP	One stuck open pressurizer SRV, no HPI	None	Open all ASDVs 5 minutes after HPI would have come on	6.6E-08	2.9E-10	1.4E-06
74	MSLB	None	Double ended guillotine break of steam line A	None	1.5E-06	5.2E-09	1.8E-04
75	RT/TT	None	MFW overfeed of all SGs	RCP's are tripped	Not in base case		
76	RT/TT, HZP	None	MFW overfeed of all SGs	RCP's are tripped	3.0E-04	1.7E-07	7.5E-03
77	RT/TT, HZP	None	Loss of all feedwater	Opens all pressurizer PORVs and uses all HPI pumps	Not in base case		
78	RT/TT	None	Loss of MFW and AFW	Open all ASDVs	1.1E-04	4.9E-08	4.9E-03
79	MSLB	None	Double ended guillotine break of steam line A	RCP's are tripped	Not in base case		
80	MSLB, HZP	None	Double ended guillotine break of steam line A	RCP's are tripped	Not in base case		
81	MSLB	Initial HPI failure	Double ended guillotine break of steam line A	Open ASDVs on SG A	3.3E-08	2.7E-12	8.5E-07
82	RT/TT	One stuck open pressurizer SRV, no HPI	None	Open all ASDVs 5 minutes after HPI would have come on	2.6E-06	1.4E-13	1.2E-04
83	LOCA	2.54 cm (1.0 in) surge line break, no HPI	no motor AFW, overfeed of SGs with turbine AFW	RCP's are tripped, MFW tripped, open all ASDVs 5 minutes after HPI would have come on	1.5E-06	8.5E-09	2.1E-05
84	LOCA, HZP	14.37 cm (5.657 in) surge line break	None	None	Not in base case		
85	LOCA	14.37 cm (5.657 in) surge line break	None	None	Not in base case		
86	RT/TT	Two stuck open pressurizer SRVs	None	Controls HPI 1 minute after allowed	3.5E-06	3.5E-10	1.5E-04
87	RT/TT	Two stuck open pressurizer SRVs	None	Controls HPI 10 minutes after allowed	6.8E-07	2.2E-08	4.2E-06
88	RT/TT, HZP	Two stuck open pressurizer SRVs	None	Controls HPI 1 minutes after allowed	1.0E-06	1.7E-08	6.1E-06
89	RT/TT, HZP	Two stuck open pressurizer SRVs	None	Controls HPI 1 minutes after allowed	1.3E-07	1.8E-09	8.6E-07
90	RT/TT, HZP	Two stuck open pressurizer SRVs	None	Controls HPI 10 minutes after allowed	1.3E-07	1.8E-09	8.6E-07
91	RT/TT, HZP	Two stuck open pressurizer SRVs	None	Controls HPI 10 minutes after allowed	1.7E-07	3.1E-09	1.4E-06
92	RT/TT, HZP	Two stuck open pressurizer SRVs	None	None	1.7E-07	3.1E-09	1.4E-06
93	RT/TT, HZP	Two stuck open pressurizer SRVs	None	None	2.1E-07	3.0E-09	2.6E-06
94	RT/TT, HZP	One stuck open pressurizer SRV	None	None	2.1E-07	3.0E-09	2.6E-06
95	RT/TT	One stuck open pressurizer SRV	None	Controls HPI 1 minutes after allowed	4.1E-05	9.3E-07	3.9E-04
96	RT/TT	One stuck open pressurizer SRV	None	Controls HPI 10 minutes after allowed	1.3E-04	6.2E-06	7.6E-04
97	RT/TT, HZP	One stuck open pressurizer SRV	None	None	1.9E-04	3.0E-06	1.1E-03
98	RT/TT, HZP	One stuck open pressurizer SRV	None	Controls HPI 1 minutes after allowed	3.7E-06	2.3E-08	8.6E-05
99	RT/TT, HZP	One stuck open pressurizer SRV	None	Controls HPI 1 minutes after allowed	2.6E-05	8.9E-07	1.9E-04

100	RT/TT, HZP	One stuck open pressurizer SRV	None	Controls HPI 10 minutes after allowed	2.6E-05	8.9E-07	1.9E-04
101	RT/TT, HZP	One stuck open pressurizer SRV	None	Controls HPI 10 minutes after allowed	3.1E-05	2.4E-07	2.3E-04
102	MSLB	None	Double ended guillotine break of steam line A	RCP's are tripped. Controls HPI 30 minutes after allowed	3.1E-05	2.4E-07	2.3E-04
103	MSLB, HZP	None	Double ended guillotine break of steam line A	RCP's are tripped. Controls HPI 30 minutes after allowed	1.0E-04	2.8E-07	9.9E-04
104	MSLB	None	Double ended guillotine break of steam line A	RCP's are tripped. Controls HPI 60 minutes after allowed	1.1E-05	3.3E-07	4.5E-05
105	MSLB, HZP	None	Double ended guillotine break of steam line A	RCP's are tripped. Controls HPI 60 minutes after allowed	1.1E-04	5.2E-08	1.6E-03
106	MSLB	None	Double ended guillotine break of steam line A	RCP's are tripped. Controls HPI 30 minutes after allowed	1.1E-05	2.4E-07	5.4E-05
107	MSLB, HZP	None	Double ended guillotine break of steam line A	RCP's are tripped. Controls HPI 30 minutes after allowed	2.2E-06	1.3E-08	1.4E-04
108	MSLB	None	All MS-SRVs on SG A stuck open	Controls HPI 30 minutes after allowed	4.3E-07	1.5E-09	1.1E-05
109	MSLB, HZP	None	All MS-SRVs on SG A stuck open	RCP's are tripped. Controls HPI 30 minutes after allowed	6.5E-04	1.8E-06	6.3E-03
110	MSLB	None	All MS-SRVs on SG A stuck open	Controls HPI 60 minutes after allowed	6.8E-05	2.1E-06	2.9E-04
111	MSLB, HZP	None	All MS-SRVs on SG A stuck open	RCP's are tripped. Controls HPI 60 minutes after allowed	6.9E-04	3.3E-07	1.0E-02
112	MSLB	None	All MS-SRVs on SG A stuck open	RCP's are tripped. Controls HPI 30 minutes after allowed	6.8E-05	1.5E-06	3.4E-04
113	MSLB, HZP	None	All MS-SRVs on SG A stuck open	RCP's are tripped. Controls HPI 30 minutes after allowed	1.4E-05	8.3E-08	9.2E-04
114	LOCA	7.18 cm (2.828 in) surge line break	None	None	2.7E-06	9.8E-09	7.2E-05
115	LOCA	7.18 cm (2.828 in) cold leg break	None	None	9.8E-05	9.7E-06	9.6E-04
116	LOCA	16.38 cm (6.45 in) cold leg break	None	None	9.8E-05	9.7E-06	9.6E-04
117	LOCA	14.37 cm (5.657 in) cold leg break	None	None	1.8E-05	8.0E-08	8.7E-04
118	MSLB	None	All MS-SRVs on SG A stuck open	None	2.1E-05	9.4E-08	1.0E-03

Palisades

Case	Type	Primary Side Failure	Secondary Side Failure	Operator Action	Initiating Event Frequency		
					Mean	Min.	Max.
1	LOCA-HiK	2.54 cm (1 inch) surge line break. Containment sump recirculation included in the analysis.	None	None	Not in base case		
2	LOCA-HiK	3.59 cm (1.414 in) surge line break. Containment sump recirculation included in the analysis.	None	None	2.7E-04	4.0E-05	1.7E-03

3	LOCA-HiK	5.08 cm (2 in) surge line break. Containment sump recirculation included in the analysis.	None	None	Not in base case		
4	LOCA-HiK	7.183 cm (2.828 in) surge line break. Containment sump recirculation included in the analysis.	None	Operator assumed to throttle HPI if auxiliary feedwater is running with SG wide range level > -84% and RCS subcooling > 25 F. HPI is throttled to maintain pressurizer level between 40 and 60 %.	Not in base case		
5	LOCA-HiK	10.16 cm (4 inch) surge line break. Containment sump recirculation included in the analysis.	None	Operator assumed to throttle HPI if auxiliary feedwater is running with SG wide range level > -84% and RCS subcooling > 25 F. HPI is throttled to maintain pressurizer level between 40 and 60 %.	Not in base case		
6	LOCA-HiK	14.366 cm (5.656 inch) surge line break. Containment sump recirculation included in the analysis.	None	Operator assumed to throttle HPI if auxiliary feedwater is running with SG wide range level > -84% and RCS subcooling > 25 F. HPI is throttled to maintain pressurizer level between 40 and 60 %.	Not in base case		
7	LOCA-HiK	20.32 cm (8 inch) surge line break. Containment sump recirculation included in the analysis.	None	Operator does not throttle HPI.	Not in base case		
8	LOCA-HiK	5.08 cm (2 in) surge line break. Containment sump recirculation included in the analysis.	1 stuck-open ADV on SG-A. No AFW isolation.	Operator assumed to throttle HPI if auxiliary feedwater is running with SG wide range level > -84% and RCS subcooling > 25 F. HPI is throttled to maintain pressurizer level between 40 and 60 %.	Not in base case		
9	LOCA-HiK	5.08 cm (2 in) surge line break. Containment sump recirculation included in the analysis.	1 stuck-open ADV on SG-A. Normal MFW/AFW function.	Operator isolates AFW to affected SG at 15 minutes after initiation. Operator assumed to throttle HPI if auxiliary feedwater is running with SG wide range level > -84% and RCS subcooling > 25 F. HPI is throttled to maintain pressurizer level between 4	Not in base case		

10	LOCA-HiK	5.08 cm (2 in) surge line break. Containment sump recirculation included in the analysis.	1 stuck-open ADV on SG-A. Normal MFW/AFW function.	Operator isolates AFW to affected SG at 30 minutes after initiation. Operator assumed to throttle HPI if auxiliary feedwater is running with SG wide range level > -84% and RCS subcooling > 25 F. HPI is throttled to maintain pressurizer level between 40	Not in base case		
11	LOCA-HiK	5.08 cm (2 in) surge line break. Containment sump recirculation included in the analysis.	1 stuck-open ADV on SG-A. Failure to isolate MFW and condensate feed system.	None.	Not in base case		
12	LOCA-HiK	5.08 cm (2 in) surge line break. Containment sump recirculation included in the analysis.	1 stuck-open ADV on SG-A. Failure of both MSIVs (SG-A and SG-B) to close.	Operator does not isolate AFW on affected SG. Operator assumed to throttle HPI if auxiliary feedwater is running with SG wide range level > -84% and RCS subcooling > 25 F. HPI is throttled to maintain pressurizer level between 40 and 60 %.	Not in base case		
13	TT/RT	One stuck open pressurizer SRV. Containment spray is assumed not to actuate.	None.	Operator assumed to throttle HPI if auxiliary feedwater is running with SG wide range level > -84% and RCS subcooling > 25 F. HPI is throttled to maintain pressurizer level between 40 and 60 %.	Not in base case		
14	TT/RT	None.	2 stuck-open ADVs on SG-A	Operator assumed to throttle HPI if auxiliary feedwater is running with SG wide range level > -84% and RCS subcooling > 25 F. HPI is throttled to maintain pressurizer level between 40 and 60 %.	Not in base case		
15	TT/RT	None.	2 stuck-open ADVs on SG-A combined with controller failure resulting in the flow from two AFW pumps into affected steam generator.	Operator starts second AFW pump. Operator isolates AFW to affected SG at 15 minutes after initiation. Operator assumed to throttle HPI if auxiliary feedwater is running with SG wide range level > -84% and RCS subcooling > 25 F. HPI is throttled to main	Not in base case		

16	TT/RT	None.	2 stuck-open ADVs on SG-A combined with controller failure resulting in the flow from two AFW pumps into affected steam generator.	Operator starts second AFW pump. Operator isolates AFW to affected SG at 30 minutes after initiation. Operator assumed to throttle HPI if auxiliary feedwater is running with SG wide range level > -84% and RCS subcooling > 25 F. HPI is throttled to main	1.2E-04	5.8E-08	5.4E-03
17	TT/RT	None.	2 stuck-open ADVs on SG-A combined with controller failure resulting in the flow from two AFW pumps into affected steam generator.	Operator starts second AFW pump. Operator assumed to throttle HPI if auxiliary feedwater is running with SG wide range level > -84% and RCS subcooling > 25 F. HPI is throttled to maintain pressurizer level between 40 and 60 %.	Not in base case		
18	TT/RT	None	1 stuck-open ADV on SG-A. Failure of both MSIVs (SG-A and SG-B) to close.	Operator does not isolate AFW on affected SG. Normal AFW flow assumed (200 gpm). Operator assumed to throttle HPI if auxiliary feedwater is running with SG wide range level > -84% and RCS subcooling > 25 F. HPI is throttled to maintain pressurizer lev	4.7E-03	2.2E-06	1.6E-01
19	RT	None.	1 stuck-open ADV on SG-A	None. Operator does not throttle HPI.	2.3E-03	2.5E-06	1.2E-01
20	TT/RT	None	SG level control system failure causes SG overfill. MFW continues running and the SGs flood.	Operator terminates MFW when either water flows to the steam line or 75,000 gallons is pumped into the steam generators. Operator assumed to throttle HPI if auxiliary feedwater is running with SG wide range level > -84% and RCS subcooling > 25 F. HPI is	Not in base case		
21	RT	None	SG level control system failure causes SG overfill. MFW continues running and the SGs flood.	Operator terminates MFW when either water flows to the steam line or 75,000 gallons is pumped into the steam generators. Operator does not throttle HPI.	Not in base case		
22	TT/RT	None.	Loss of MFW and AFW.	Operator depressurizes through ADVs and feeds SG's using condensate booster pumps. Operators maintain a cooldown rate within technical specification limits and throttle condensate flow at 84 % level in the steam generator.	6.7E-05	9.4E-06	1.0E-03

23	TT/RT	Two stuck-open pressurizer SRVs that reclose at 6000 sec after initiation. Containment spray is assumed not to actuate.	None.	Operator assumed to throttle HPI if auxiliary feedwater is running with SG wide range level > -84% and RCS subcooling > 25 F. HPI is throttled to maintain pressurizer level between 40 and 60 %.	Not in base case		
24	MSLB	None	Break assumed to be inside containment causing containment spray actuation.	None	2.4E-06	5.6E-09	4.2E-05
25	MSLB	None	Break assumed to be inside containment causing containment spray actuation.	Operator isolates AFW to affected SG at 15 minutes after initiation.	Not in base case		
26	MSLB	None	Break assumed to be inside containment causing containment spray actuation.	Operator isolates AFW to affected SG at 30 minutes after initiation.	5.7E-04	2.9E-04	2.8E-03
27	MSLB	None	Controller failure resulting in the flow from two AFW pumps into affected steam generator. Break assumed to be inside containment causing containment spray actuation.	Operator starts second AFW pump.	3.7E-05	6.8E-06	3.6E-04
28	MSLB	None	Failure of both MSIVs to close. Break assumed to be inside containment causing containment spray actuation.	Operator does not isolate AFW on affected SG.	Not in base case		
29	MSLB	None	None. Break assumed to be inside containment causing containment spray actuation.	None. Operator does not throttle HPI.	4.2E-08	1.2E-10	8.2E-07
30	LOCA-HiK	5.08 cm (2 in) surge line break	None.	None. Operator does not throttle HPI.	Not in base case		
31	TT/RT	None.	Failure of MFW and AFW. Containment spray actuation assumed due to PORV discharge.	Operator maintains core cooling by "feed and bleed" using HPI to feed and two PORVs to bleed.	1.3E-05	1.2E-06	1.9E-04
32	TT/RT	None.	Failure of MFW and AFW. Containment spray actuation assumed due to PORV discharge.	Operator maintains core cooling by "feed and bleed" using HPI to feed and two PORV to bleed. AFW is recovered 15 minutes after initiation of "feed and bleed" cooling. Operator closes PORVs when SG level reaches 60 percent.	1.1E-06	1.1E-07	7.6E-05

33	TT/RT	None.	Failure of MFW and AFW. Containment spray actuation assumed due to PORV discharge.	Operator maintains core cooling by "feed and bleed" using HPI to feed and PORV to bleed. AFW is recovered 30 minutes after initiation of "feed and bleed" cooling. Operator closes PORV when SG level reaches 60 percent.	Not in base case		
34	MSLB/ SGTR	Single tube fails in SG-A due to MSLB vibration.	None.	Operator isolates AFW to affected SG at 15 minutes after initiation. Operator trips RCPs assuming that they do not trip as a result of the event. Operator assumed to throttle HPI if auxiliary feedwater is running with SG wide range level > -84% and RCS	1.5E-05	4.2E-06	7.3E-05
35	MSLB/ SGTR	Ten tubes assumed to fail in SG-A due to MSLB vibration.	None.	Operator isolates AFW to affected SG at 15 minutes after initiation. Operator trips RCPs assuming that they do not trip as a result of the event. Operator assumed to throttle HPI if auxiliary feedwater is running with SG wide range level > -84% and RCS	Not in base case		
36	MSLB	None	Controller failure resulting in the flow from two AFW pumps into affected steam generator. Break assumed to be inside containment causing containment spray actuation.	Operator starts second AFW pump. Operator isolates AFW to affected SG at 15 minutes after initiation.	Not in base case		
37	MSLB	None	Controller failure resulting in the flow from two AFW pumps into affected steam generator. Break assumed to be inside containment causing containment spray actuation.	Operator starts second AFW pump. Operator isolates AFW to affected SG at 30 minutes after initiation.	Not in base case		
38	TT/RT	None.	Loss of MFW and AFW.	Operator depressurizes through ADVs and feeds SG's using condensate booster pumps. Feed is terminated once SG's are filled.	Not in base case		
39	LOCA-HiK	27.94 cm (11 in) hot leg break. Containment sump recirculation included in the analysis.	None.	None. Operator does not throttle HPI.	Not in base case		

40	LOCA-HiK	40.64 cm (16 in) hot leg break. Containment sump recirculation included in the analysis.	None.	None. Operator does not throttle HPI.	3.2E-05	8.1E-07	9.0E-04
41	LOCA-HiK	55.88 cm (22 in) hot leg break. Containment sump recirculation included in the analysis.	None.	None. Operator does not throttle HPI.	Not in base case		
42	TT/RT	Two stuck open pressurizer SRVs. Containment spray is assumed not to actuate.	None.	Operator assumed to throttle HPI if auxiliary feedwater is running with SG wide range level > -84% and RCS subcooling > 25 F. HPI is throttled to maintain pressurizer level between 40 and 60 %.	7.7E-07	1.2E-07	2.2E-06
43	TT/RT	None.	Failure of MFW and AFW.	Operator maintains core cooling by "feed and bleed" using HPI to feed and two PORVs to bleed.	Not in base case		
44	TT/RT	None.	Failure of MFW and AFW.	Operator maintains core cooling by "feed and bleed" using HPI to feed and two PORV to bleed. AFW is recovered 15 minutes after initiation of "feed and bleed" cooling. Operator closes PORVs when SG level reaches 60 percent.	Not in base case		
45	LOCA	5.08 cm (2 in) surge line break. Containment sump recirculation included in the analysis.	None	None	Not in base case		
46	LOCA	10.16 cm (4 inch) surge line break. Containment sump recirculation included in the analysis.	None	Operator assumed to throttle HPI if auxiliary feedwater is running with SG wide range level > -84% and RCS subcooling > 25 F. HPI is throttled to maintain pressurizer level between 40 and 60 %.	Not in base case		
47	LOCA	40.64 cm (16 in) hot leg break. Containment sump recirculation included in the analysis.	None.	None. Operator does not throttle HPI.	Not in base case		
48	RT	Two stuck-open pressurizer SRVs that reclose at 6000 sec after initiation. Containment spray is assumed not to actuate.	None.	None. Operator does not throttle HPI.	7.7E-07	1.1E-07	2.2E-06

49	MSLB	None	Break assumed to be inside containment causing containment spray actuation.	Operator isolates AFW to affected SG at 30 minutes after initiation. Operator does not throttle HPI.	1.0E-05	2.2E-06	4.5E-05
50	MSLB	None	Controller failure resulting in the flow from two AFW pumps into affected steam generator. Break assumed to be inside containment causing containment spray actuation.	Operator starts second AFW pump. Operator does not throttle HPI.	5.8E-07	8.0E-08	7.2E-06
51	MSLB	None	Failure of both MSIVs to close. Break assumed to be inside containment causing containment spray actuation.	Operator does not isolate AFW on affected SG. Operator does not throttle HPI.	7.5E-08	2.8E-10	1.0E-05
52	RT	None	1 stuck-open ADV on SG-A. Failure of both MSIVs (SG-A and SG-B) to close.	Operator does not isolate AFW on affected SG. Normal AFW flow assumed (200 gpm). Operator does not throttle HPI.	6.4E-04	4.0E-07	2.7E-02
53	TT/RT	Two stuck-open pressurizer SRVs that reclose at 6000 sec after initiation. Containment spray is assumed not to actuate.	None.	None. Operator does not throttle HPI.	1.1E-03	3.9E-04	2.4E-03
54	MSLB	None	Failure of both MSIVs to close. Break assumed to be inside containment causing containment spray actuation.	Operator does not isolate AFW on affected SG. Operator does not throttle HPI.	4.3E-06	1.0E-07	2.4E-04
55	TT/RT	None.	2 stuck-open ADVs on SG-A combined with controller failure resulting in the flow from two AFW pumps into affected steam generator.	Operator starts second AFW pump.	2.7E-03	1.6E-06	1.4E-01
56	LOCA-HiK	2.54 cm (1 inch) surge line break. Containment sump recirculation included in the analysis. Both HPI and charging are assumed to fail.	None.	Operator initiates emergency depressurization by opening all TBV's ADVs and one pressurizer PORV. Operator trips two of the four reactor coolant pumps. When temperature and pressure start to level off, HPI and charging are restored. The operator is ass	Not in base case		
57	LOCA-HiK (RELAP5/MOD3.3)	40.64 cm (16 in) hot leg break. Containment sump recirculation included in the analysis.	None.	None.	Not in base case		

58	LOCA-HiK	10.16 cm (4 in) cold leg break. Winter conditions assumed (HPI and LPI injection temp = 40 F, Accumulator temp = 60 F)	None.	None. Operator does not throttle HPI.	2.7E-04	4.0E-05	1.7E-03
59	LOCA-HiK	10.16 cm (4 in) cold leg break. Summer conditions assumed (HPI and LPI injection temp = 100 F, Accumulator temp = 90 F)	None.	None. Operator does not throttle HPI.	2.1E-04	3.1E-05	1.4E-03
60	LOCA-HiK	5.08 cm (2 in) surge line break. Winter conditions assumed (HPI and LPI injection temp = 40 F, Accumulator temp = 60 F)	None.	None. Operator does not throttle HPI.	2.1E-04	3.1E-05	1.4E-03
61	LOCA-HiK	7.18 cm (2.8 in) cold leg break. Summer conditions assumed (HPI and LPI injection temp = 100 F, Accumulator temp = 90 F)	None.	None. Operator does not throttle HPI.	2.1E-04	3.1E-05	1.4E-03
62	LOCA-HiK	20.32 cm (8 in) cold leg break. Winter conditions assumed (HPI and LPI injection temp = 40 F, Accumulator temp = 60 F)	None.	None. Operator does not throttle HPI.	7.1E-06	1.5E-07	2.3E-04
63	LOCA-HiK	14.37 cm (5.656 in) cold leg break. Winter conditions assumed (HPI and LPI injection temp = 40 F, Accumulator temp = 60 F)	None.	None. Operator does not throttle HPI.	6.1E-06	1.3E-07	2.0E-04
64	LOCA-HiK	10.16 cm (4 in) surge line break. Summer conditions assumed (HPI and LPI injection temp = 100 F, Accumulator temp = 90 F)	None.	None. Operator does not throttle HPI.	7.1E-06	1.5E-07	2.3E-04

Appendix D – RELAP Results for all Three Plants

INSERT *APPENDIX D1.DOC*, *APPENDIX D2.DOC*, AND *APPENDIX D3.DOC*, HERE

Appendix E – Uncertainty Analysis

INSERT *APPENDIX E.PDF* HERE